ABSTRACT

Title of Dissertation: DETERMINATION OF DYNAMIC MODULI AND PERMANENT DEFORMATION OF MARYLAND ASPHALT MIXTURES USING AMPT

Intikhab Haider, Doctor of Philosophy, 2017

Dissertation directed by: Professor Schwartz, Charles W.
Department of Civil and Environmental Engineering

Full implementation of the mechanistic-empirical pavement design guide (MEPDG) in Maryland requires Level 1 (measured) material properties to characterize asphalt mixtures commonly used in the state. Specifically, these proprieties are the dynamic modulus (DM) and the repeated load permanent deformation (RLPD) properties. To achieve this goal, 28 asphalt mixtures were collected from construction sites/asphalt plants and tested in the Maryland State Highway Administration Office of Materials Technology Asphalt Technology Division laboratory. The DM and RLPD testing was performed on all 28 asphalt mixtures following the AASHTO PP 60, AASHTO PP 61 and AASHTO TP 79 protocols. In addition to the 28 asphalt mixtures from Maryland, DM and RLPD data for 18 asphalt mixtures tested in NCHRP Project 9-30A were also included in parts of this study. In addition to developing a catalog of typical Level 1 material properties for common Maryland asphalt mixtures, this study produced several other important results

and findings. These include: (1) The L-1 inputs (measured E* and G* and recalibrated coefficients of rut model, K_1, K_2, K_3) consistently give lesser predicted distresses than L-3 inputs (predicted E* values, default G* values, and default coefficients of rut model) in MEPDG software. (2) The average percentage differences for each predicted distress at all levels of traffic are highest for L-1 versus L-3 inputs and lowest for L-1 versus L-1A (measured E* and G* data and default coefficients of rut model) inputs. (3) The recalibration of Witczak E* model removes the bias toward underprediction in the original Witczak model. The distresses predicted using L-3 (CWM-Calibrated Witczak Model based on Maryland mixes) inputs are closest to the distresses predicted using the measured L-1 inputs. (4) The total number of samples required for complete characterization of one asphalt mixtures as per AASHTO PP 61 and AASHTO TP 79 can be reduced from 12 to 3. The reduction in total specimen preparation (from 60 to 15 hours) and testing time (from 30 to 10 hours) represents substantial economies in structural characterization of asphalt mixtures and motivates state agencies to perform DM and RLPD testing on routine basis to develop performance based specification.

DETERMINATION OF DYNAMIC MODULI AND PERMANENT DEFORMATION OF MARYLAND ASPHALT MIXTURES USING AMPT

By

Intikhab Haider

Dissertation submitted to the Faculty of the Graduate School of the
University of Maryland, College Park in partial fulfillment
of the requirements for the degree of
Doctor of Philosophy
2017

Advisory Committee:

Professor Schwartz, Charles W., Chair
Professor Aggour, M. Sherif
Professor Aydilek, Ahmet H.
Associate Professor Chang, Peter C.
Professor McCluskey, F. Patrick

ACKNOWLEDGEMENT

First and foremost, I would like to thank my advisor, Professor, Charles W. Schwartz, for his enthusiasm and guidance throughout my graduate studies at the University of Maryland – College Park. Thanks also to Professors: Ahmet H. Aydilek, Muhammad S. Aggour, Peter C. Chang, and Patrick F. McCluskey, for being part of my committee. I am grateful to Maryland State Highway Administration, particularly members of Asphalt Technology Division (Ron, Kevin, Bob, and Jasmine), for their help in performing testing at their laboratory and to provide necessary information about highway construction practices being used in State of Maryland. Thanks to my wife for her dedicated support throughout my graduate studies. I am also thankful to my mother for her nonstop prayers for me.

TABLE OF CONTENTS

LIST OF FIGURES V

LIST OF TABLES VIII

ABBREVIATION AND ACRONYMS X

CHAPTER 1: INTRODUCTION 1

1.1 BACKGROUND 1
1.2 OBJECTIVE OF RESEARCH STUDY 6

CHAPTER 2: PROJECT EXPERIMENTAL PLAN 7

2.1 SELECTION OF ASPHALT MIXTURES 7
2.1.1. Factorial of Testing 7
2.2 LABORATORY TEST METHODS 10
2.2.1 Specimen Fabrication 11
2.2.1.1 Heating and Compaction 12
2.2.1.2 Target Air Voids 14
2.2.1.3 Coring and Cutting Procedure 15
2.2.1.4 LVDT Installation 15
2.2.1.5 Temperature Control and Conditioning of Specimens 16
2.3 ASPHALT MIXTURE PERFORMANCE TESTER (AMPT) 17
2.4 DYNAMIC MODULUS TESTING 18
2.5 REPEATED LOAD PERMANENT DEFORMATION (RLPD) TEST 20

CHAPTER: 3 DYNAMIC MODULUS TEST DATA AND ANALYSES 22

3.1 MIXTURE CHARACTERIZATION 22
3.2 VOLUMETRIC PROPERTIES AND GRADATIONS OF ASPHALT MIXTURES 25
3.3 DEVELOPMENT OF DYNAMIC MODULUS MASTER CURVES 29
3.3.1 Fitting Parameter of Master Curves 35
3.4 COMPARISON OF MEASURED E* VALUES OF MIXTURES 39
3.4.1 Ranking and Effect of Variables on E* Values of Asphalt Mixtures 42

CHAPTER 4: PERMANENT DEFORMATION TEST DATA AND ANALYSIS 50

4.1 RLPD TEST RESULTS 50
4.2 CALIBRATION OF MEPDG RUT MODEL 64
4.3 RLPD TEST DATA FROM NCHRP PROJECT 9-30A 69

CHAPTER 5: EXPEDITED TESTING PROGRAM 72
5.1 First Approach: Reduction in Dynamic Modulus Testing Time 74
5.2 Second Approach: Reduction in RLPD Specimens 81
5.3 Third Approach: Time-Temperature Superposition for RLPD Testing 91
CHAPTER 6: SENSITIVE ANALYSIS OF DM AND RLPD PROPERTIES IN MEPDG 109
6.1 Variables and Fixed Inputs Used in Sensitivity Analyses 109
6.2 Insights from the Sensitivity Analyses 118
CHAPTER 7: RECALIBRATION OF WITCZAK E* PREDICTIVE MODEL 119
7.1 Recalibration of Witczak E* Predictive Model 119
7.2 MEPDG Sensitivity Analyses of Recalibrated E* Predicted Model 124
CHAPTER 8: PREDICTIVE MODELS FOR RLPD PROPERTIES 131
8.1 Predictive Models for RLPD Properties 131
8.2 Data Set 1 - MDSHA Mixtures Only 133
8.2.1 Correlation Matrices 133
8.3 Second Set of Data (NCHRP 9-30A Project) 141
8.3.1 Correlation Matrices 141
8.4 Combined Data Set (MDSHA and NCHRP 9-30A Project Data – Set 1) 148
8.4.1 Correlation Matrices 148
8.5 Combined Data (MDSHA and NCHRP 9-30A Project Data – Set 2) 155
8.5.1 Stepwise Multiple Linear Regression Models. 155
8.6 Summary of Modeling 155
CHAPTER 9: SUMMARY AND CONCLUSIONS 157
9.1 Dynamic Modulus Data 158
9.3 Expedited Testing 160
9.4 Predicted Pavement Performance Using MEPDG 161
APPENDIX A 163
APPENDIX B 164
APPENDIX C 181
REFERENCES 186

LIST OF FIGURES

Figure 1: Equipment Used in Preparation of Specimens 12
Figure 2: Gyratory Compactor 13
Figure 3: Stepwise Procedure for Preparation of DM and RLPD Specimens 14
Figure 4: Asphalt Mixture Performance Tester 18
Figure 5: Haversine Loading in DM Testing 19
Figure 6: Typical Curve of RLPD Test 21
Figure 7: Gradations of A) Dense Graded Mixtures B) Gap Graded Mixtures 25
Figure 8: Box and Whisker Plots Representing Variations in Volumetric Properties and Asphalt Contents of Asphalt Mixtures 28
Figure 9: Typical Development of DM Master Curve of an Asphalt Mixture 30
Figure 10: DM Master Curves of All Asphalt Mixtures 33
Figure 11: Shift Factors of Asphalt Mixtures Used in Development of Master Curves 34
Figure 12: Phase Angles of Asphalt Mixtures 35
Figure 13: Box and Whisker Plots of Fitting Parameters of Master Curves of Mixtures 38
Figure 14: Comparison of E* Values of All Mixtures (Orange Bars Represents High RAP Dense Graded, High RAP/Shingles Dense Graded and Warm Mixes) 41
Figure 15: Comparison of Average E* Values of Gap Graded Mixes, Dense Graded (Low RAP) Mixes, and Dense Graded (High RAP and Warm Mixtures) 43
Figure 16: Box and Whisker Plots Representing Variability in E* Values in All Mixtures 44
Figure 17: Comparison of Level 3 and Level 1 Dynamic Moduli in MEPDG 46
Figure 18: Variability in Errors in 9mm, 12mm and 19mm NMAS Mixtures 47
Figure 19: Comparison of Master Curves Developed by Level 1 and Level 3 E* Input (a) "Best" Agreement (b) "Worst" Agreement 49
Figure 20: Accumulated Permanent Microstrains of All Mixtures at 20^{o}C, 40^{o}C and 58^{o}C 53
Figure 21: Comparison of Permanent Deformations of All Mixtures at 40^{o}C (Orange Represents the High RAP Dense Graded (HRDG), High RAP/Shingle Dense Graded (HRSDG) and Warm Mixes (WM), Purple Line Represents Virgin Dense Graded (VDG) 55
Figure 22: Average Accumulated Microstrains of Different Type of Asphalt Mixtures at 40^{o}C 56
Figure 23: Variation in Permanent Deformation with Respect to Mixtures Properties 58
Figure 24: Variation in RLPD Test Results of All Mixtures at 20^{o}C, 40^{o}C, 58^{o}C 59
Figure 25: Secondary Portion of RLPD Test Results of All Mixtures at 20^{o}C, 40^{o}C, and 58^{o}C 61
Figure 26: Average Slope of the Secondary Portion of the Permanent Deformation Response 63
Figure 27: Predicted vs. Measured ϵ_{per} Values 68
Figure 28: Comparison of Coefficients Obtained by MDSHA Lab Data and NCHRP 9-30A Data 70
Figure 29: Master Curves Developed by E* Data Obtained at Two and Three Temperature a) Overlapping Scenario b) Non-Overlapping Scenario 76

Figure 30: Variation in % Difference of E* Values of Twelve Asphalt Mixtures Obtained by 3T and 2T Master Curves 77
Figure 31: Predicted Distresses using E* Data Obtained from 2T and 3T Master Curves at Low Traffic (LT), Medium Traffic (MT) and Heavy Traffic (HT) 79
Figure 32: Percentage Differences in Predicted Distresses using E* Values Predicted by 2T and 3T Master Curves at Low Traffic (LT), Medium Traffic (MT) and Heavy Traffic (HT) 80
Figure 33: Sequence of Repeated DM Testing on a Specimen 83
Figure 34: Dynamic Moduli of Re-Tested Specimens of H161A12R4F01 Mixture at 4^0C, 20^0C, and 40^0C 84
Figure 35: Variation in CV Between and Within the DM Tested Specimens 85
Figure 36: RLPD Test Results of Fresh and Reused Specimens 87
Figure 37: Comparison of Cumulative Strains of Fresh and Reused Specimens at 1000 and 10000 Cycles of Loading at Three Temperatures (20°C, 40°C and 58°C) 88
Figure 38: The Average (A) Intercept and (B) Slope of the Line of the Secondary Phase of RLPD Tests. The Error Bars Represent One Standard Deviation. 89
Figure 39: (A) Schematic of the Three Main Stages of the RLPD Behavior and the Slope and Intercept of the Secondary Stage; (B) The Process of Shifting the RLPD Data at Different Temperatures to Obtain the RLPD Master Curve at the Reference Temperature. 96
Figure 40: The RLPD Test Results at Three Different Temperatures (A) Before Shifting and (B) After Shifting 100
Figure 41: Average Prediction Errors for All Temperatures using the RLPD Master Curve (MC_{all}); Error Bars Show One Standard Deviation 102
Figure 42: Predicted Versus Measured Plastic Axial Cumulative Strains at Various Temperatures at 5000 Cycles. Prediction Master Curve Coefficients Obtained using: (A) Data at All Temperatures; (B) Low Temperature Data Only; (C) Intermediate Temperature Data Only; (D) High Temperature Data Only 103
Figure 43: Distribution of MC_{high} Relative Error of Prediction in Low and Intermediate Temperatures 106
Figure 44: Variations in Predicted Distresses due to L-1, L-1-A, and L-1 Input Levels 115
Figure 45: Average Percentage Differences from L-3 versus L-1-A, L-3 versus L-1, and L-1 versus L-1-A Inputs 117
Figure 46: Comparison of Level 3 (Predicted using Original Witczak Model) versus Level 1 (Measured) Dynamic Moduli 120
Figure 47: Comparison of Level 3 (Predicted using Recalibrated Witczak Model) versus Level 1 (Measured) Dynamic Moduli 122
Figure 48: Ranges of Errors for Predicted versus Measured E* Values at Different Temperatures and Loading Frequencies. (A) Original Witczak Model (B) Recalibrated Witczak Model 123
Figure 49: Master Curves Developed using E* Values Predicted by Original Witczak Model (Level 3), Recalibrated Witczak Model (Level 3 CWM), and Measured Level 1 Values. 125
Figure 50: Predicted Distresses for Different MEPDG Input Scenarios for Five Asphalt Mixtures. (A) Heavy Traffic (HT), (B) Medium Traffic (MT), (C) Low Traffic (LT). . 128

Figure 51: Predicted Distresses for Different MEPDG Input Scenarios for Five Asphalt Mixtures. (A) Heavy Traffic (HT), (B) Medium Traffic (MT), (C) Low Traffic (LT). . 129
Figure 52: Percentage Differences for Different Input Scenarios at Low, Medium, and Heavy Traffic. 130
Figure B-53: Naming Convention for MDSHA Asphalt Mixtures 164
Figure B-54a: Master Curves Developed using Level 1 and Level 3 E* Values 168
Figure C-55a: Master Curves Developed from Tests at Two and Three Temperatures . 181

LIST OF TABLES

Table 1: Factorial of Testing (Priority 1-Asphalt Mixtures)..... 9
Table 2: Temperatures and Loading Frequencies for DM Testing..... 19
Table 3: Criteria for Acceptance of DM Test Result as Per AASHTO TP 79 20
Table 4: Characteristics of All Asphalt Mixtures 24
Table 5: Volumetric Properties and Gradations of All Asphalt Mixtures 27
Table 6: Fitting Parameters of Master Curves of the Mixtures 37
Table 7: Measured E* Values of Asphalt Mixtures..... 40
Table 8: Ranking of Mixtures Based on Their E* Values at 4^{o}C@10Hz..... 42
Table 9: Average Accumulated Microstrains for All Asphalt Mixtures at 1000, 5000 And 10,000 Loading Cycles at 20^{o}C, 40^{o}C, 58^{o}C 54
Table 10: Coefficients of Power Model Fitted for Secondary Portion of RLPD Tests at 20^{o}C, 40^{o}C and 58^{o}C..... 62
Table 11: Recalibrated Coefficients of the MEPDG Rut Model 67
Table 12: Coefficients of MEPDG Rut Model Based on NCHRP 9-30A RLPD Data 69
Table 13: Volumetric Properties and RLPD Test Temperatures of Asphalt Mixtures of NCHRP 9-30A Project..... 71
Table 14: T-Tests for E* Values Obtained by 2T and 3T Master Curves of Mixtures 78
Table 15: t-Test on E* Values of Repeatedly Tested Specimens of a Mixture 85
Table 16: Two Tailed t-Test to Evaluate the Differences Between Fresh and Reused RLPD Specimens..... 90
Table 17: NCHRP 9-30A Asphalt Mixture Properties 93
Table 18: Average Coefficients of RLPD Power Law Model before and after Shifting 101
Table 19: Average Relative Error from Each Master Curve Model..... 104
Table 20: Recalibrated Coefficients of the MEPDG Rut Model 111
Table 21: Fixed Inputs Used in MEPDG Software for Sensitivity Analyses 112
Table 22: Input Values for Sensitivity Analyses 113
Table 23: Design Distress Limits as per MDSHA PAGD..... 113
Table 24: Percentage Differences of Predicted Distresses Due to L-3, L-1-A, and L-1 Input Levels at Three Volumes of Traffic 116
Table 25: Correlation Coefficient (R Values) Matrices of Dependent and Independent Variables (MDSHA Data)..... 136
Table 26: Regression Statistics for the Predictive Models for the Rut Model Coefficients (MDSHA Data)..... 138
Table 27: Summary of Predictive Models along with Their Regression Statistics (MDSHA Data)..... 140
Table 28: Correlation Coefficient (R Values) Matrices of Dependent and Independent Variables (NCHRP 9-30A Data) 143
Table 29: Regression Statistics of Predictive Models for Rut Model Coefficients..... 145
Table 30: Regression Statistics of Modified Predictive Models for Rut Model Coefficients (NCHRP 9-30A Data) 146
Table 31: Summary of Predictive Models and Their Regression Statistics (NCHRP 9-30A Data)..... 147

Table 32: Correlation Coefficient (R Values) Matrices of Dependent and Independent Variables (Combined MDSHA and NCHRP 9-30A Data – Set 1) 149
Table 33: Regression Statistics of Models for Rut Model Coefficients (Combined MDSHA and NCHRP 9-30A Data – Set 1)..... 151
Table 34: Regression Statistics of Modified Predictive Models for Rut Model Coefficients (Combined MDSHA and NCHRP 9-30A Data – Set 1) 152
Table 35: Summary of Predictive Models with Regression Statistics (Combined MDSHA and NCHRP 9-30A Data) 154
Table 36: Regression Statistics Of Stepwise Multivariate Linear Regression Analyses 156
Table A-37: JMF and Verification Data of Asphalt Mixtures..... 163
Table B-38: Predicted E* Values from Master Curves of Asphalt Mixtures 165
Table B-39: Phase Angles and Shift Factors of Asphalt Mixtures 166
Table B-40: Measured E* Values for All Mixtures..... 167

ABBREVIATION AND ACRONYMS

AASHTO	American Association of State Highways and Transportation Officials
ATD	Asphalt Technology Division
BU-FC	Bottom Up Fatigue Cracking
DM	Dynamic Modulus
E*	Dynamic Modulus
G*	Dynamic Shear Modulus
HP	High Polish
HRDG	High RAP Dense Graded
HRSDG	High RAP Shingle Dense Graded
IRI	International Roughness Index
LRDG	Low RAP Dense Graded
LRG	Low RAP Gap
MDSHA	Maryland State Highway Administration
η	Viscosity
NCHRP	National Cooperative Highway Research Program
NMAS	Nominal Maximum Aggregate Size
OMT	Office of Material Technology
PD	Permanent Deformation
RAP	Reclaimed Asphalt Pavement
RAS	Reclaimed Asphalt Shingle
RLPD	Repeated Load Permanent Deformation
TD-FC	Top Down Fatigue Cracking
V_a	Air Voids

VDG	Virgin Dense Graded
VFA	Voids Filled with Asphalt
VG	Virgin Gap
VMA	Voids in Mineral Aggregate
WM	Warm Mixes
α	Shift Factor
ω	Frequency
ω_r	Reduced Frequency
ϵ_p	Permanent Strain
ϵ_r	Resilient Strain

CHAPTER 1: INTRODUCTION

1.1 Background

Most pavements in United States have been designed using different versions of the empirical American Association of State Highway and Transportation Officials (AASHTO) Pavement Design Guide. The original 1960 AASHTO Interim Pavement Design Guide and the several updates since then are all based empirically on data collected at the AASHO Road Test in the late 1950s. The empirical approach embodied in these pavement design guide made them increasingly difficult to apply to new materials, different vehicle types, and vastly larger design traffic volumes.

These and other limitations of the empirical design approach provided the impetus for the development of mechanistic-empirical (ME) alternatives. One of the first of these was the SHELL pavement design manual presented at the 4th International Conference on Structural Design of Asphalt Pavements (Claussen et al., 1977; SHELL, 1978). AASHTO's interest in ME design initiated in the mid-1980s. The 1986 AASHTO Pavement Design Guide for the first time included in Part IV a section entitled "Mechanistic-Empirical Design Procedures" that stated "For purpose of this guide, the use of analytical methods refers to the numerical capability to calculate the stress, strain, or deflection in a multi-layers system, such as a pavement, when subjected to external loads, or the effects of temperature or moisture. Mechanistic procedures will refer to the ability to translate the analytical calculations of pavement response to performance. Performance, for the majority of procedures used, refers to physical distress such as cracking or rutting. However, researchers recognize that pavement performance will likely be influenced by a number of factors which will not be precisely modeled by mechanistic methods. It is,

therefore, necessary to calibrate the models with the observations of performance i.e. empirical correlations. Thus, the procedure is referred to in the Guide as a mechanistic-empirical design procedure."

In order to develop a ME design procedure, AASHTO launched a research project, National Cooperative Highway Research Program (NCHRP) Project 1-26 "Calibrated Mechanistic Structural Analysis Procedures for Pavements" (NCHRP, 1996). The ME principles and concepts stated in 1986 AASHTO Guide were included in the NCHRP Project 1-26 project statement. This project assessed and evaluated the best available ME technology (pavement structural models and computer codes for mechanistic analysis) and proposed procedures/processes for ME design. The major components of the ME model were identified as: inputs (material characterization, traffic, and climate), structural models, transfer functions, and reliability. The NCHRP 1-26 approach recognized that pavement structural responses change with time, climate, material properties, and loading throughout the design life. Pavement performance calculated via transfer functions depends on the structural responses to loading; it also changes throughout the design life. The NCHRP 1-26 study concluded that the transfer functions are the weak links in the ME design approach. Extensive field and lab calibration are required to establish reliable distress prediction models.

Although the NCHRP 1-26 study laid important groundwork, it did not produce a usable ME design procedure. A follow up project, NCHRP 1-37A (ARA, Inc., ERES Consultants Division, 2004), "Development of the 2002 Guide for the Design of New and Rehabilitated Pavement Structures," was initiated in February, 1998. The key goal of this project was the development of a ME design guide that utilized existing mechanistic based

models and data reflecting the current state-of-the-art in pavement design. The Mechanistic-Empirical Pavement Design Guide (MEPDG) was completed and released to the public for review and evaluation in 2004. A formal review performed under NCHRP Project 1-40A (Brown et al., 2006) resulted in a number of improvements.

The complexity of the calculations in the MEPDG required computer software for solution. This software calculates pavement responses in term of stresses, strain, and deflections using a mechanistic approach. These responses are used as input in the empirical distress prediction models (transfer functions). The various distress prediction models used in the MEPDG software include International Roughness Index (IRI), thermal and reflective cracking, top down and bottom up fatigue cracking, rutting in each layer and total rutting. These empirical distress prediction models were calibrated using national data from the Long Term Pavement Performance (LTPP) database managed by Federal Highway Administration (FHWA). The collected data in LTPP program include information on seven modules: Inventory, Maintenance, Monitoring (Deflection, distress and profile), Rehabilitation, Materials Testing, Traffic and Climatic.

Nationally calibrated distress models may not provide good predictions for all local conditions—e.g., local subgrades, materials, and traffic. The MEPDG software, therefore, included the capability for local calibration of the empirical distress prediction models. Local calibration of predicted models eliminates potential biases and increases the accuracy of performance prediction. To locally calibrate the distress predicted models and implement the MEPDG/Pavement ME software in Maryland, there is a need to measure engineering properties of locally available materials, asphalt mixtures, granular bases and subgrades. The most sensitive property related to predictive performance of pavement

structure is dynamic modulus of asphalt mixture (Li, 2013). In addition to dynamic moduli of local asphalt mixtures, permanent deformation's characteristics of asphalt mixtures are also very important to understand the rutting behavior of flexible pavement structure.

Modeling techniques (statistical, Artificial Neural Network etc.) have also been used for predicting dynamic modulus of asphalt layers and the resilient moduli of unbound base layers and subgrades however no prediction model is available to predict permanent deformation properties of asphalt layer. These material properties are required to calculate the responses, stress, strain, deflections of pavement structure used as inputs to the empirical performance prediction models. The expense and time required to measure many of these properties in the laboratory led to development of predictive models that take as inputs more easily measured material characteristics.

Witczak's dynamic modulus prediction model (Andrei et al. 1999; Bari and Witczak, 2006) and Artificial Neural Network for Asphalt Concrete Dynamic Modulus Prediction (Ceylan et al. 2007) are examples of material property prediction models. These models are based on volumetric properties of the asphalt mixture and the properties of binder.

The rut transfer function (Kaloush and Witczak, 2000) provided in the MEPDG needs local calibration to accurately predict rutting performance of locally available asphalt mixtures in Maryland. The calibration of MEPDG rut transfer function includes two parts: measurement of material properties in the laboratory and measured pavement performance data from the field. The coefficients of the rut transfer function can be obtained from laboratory testing, however these coefficients are modified based on the actual field performance data. One of the objectives of this research study is to calibrate the rut transfer

function based on laboratory testing of locally available asphalt mixtures and provides these coefficients to Maryland Department of Transportation, State Highway Administration (MDOT, SHA) pavement design section for implementation of MEPDG.

Although much work has been done on predictive models for dynamic modulus of asphalt mixtures, there is no model available for prediction of repeated load permanent deformation (RLPD) properties of asphalt mixtures. In order to perform one RLPD test, nine samples (3 replicates for three temperatures) are required to characterize one HMA mixture according to AASHTO TP-79, "Determining the Dynamic Modulus and Flow Number for Hot Mix Asphalt Using the Asphalt Mixture Performance Tester." One to two weeks (40 to 60 hours) are required to complete testing on one mixture. Therefore, it is not practical for an agency to characterize each and every HMA mixtures in the laboratory. A statistical model based on easily measured mixture characteristics (e.g., binder content, volumetric properties, gradation) is desirable to predict the permanent deformation properties of HMA mixtures.

1.2 Objective of Research Study

An extensive study is proposed to evaluate the dynamic modulus and RLPD properties of asphalt mixtures commonly used in Maryland. The main objectives of this research study are outlined below.

1. Development of database of Maryland asphalt mixtures' properties to use in MEPDG design.
2. Development of an expedited testing program for performance characterization of asphalt mixtures on a routine basis.
3. Comparison of predicted pavement performance using Level 1 (measured properties) vs. Level 3 (predicted properties) of asphalt mixtures.
4. Evaluation of the sensitivity of predicted pavement performance to dynamic modulus (E*) and RLPD property inputs in the MEPDG software.
5. Recalibration of the existing E* predictive model in MEPDG software based on Maryland asphalt mixture properties.
6. Calibration of rut transfer function included in the MEPDG software for Maryland asphalt mixtures.

CHAPTER 2: PROJECT EXPERIMENTAL PLAN

After an extensive literature review, the project experimental plan was developed. The key components of this experimental plan were the selection of materials to be characterized and the identification of the test methods to be used in this characterization.

2.1 Selection of Asphalt Mixtures

2.1.1. Factorial of Testing

The selection of asphalt mixtures for testing was based on the following considerations:

1. **District.** The Maryland State Highway Administration (MDSHA) divides the state into seven districts.
2. **Binder Grade.** Based on weather conditions and traffic, there are two types of performance grade (PG) binders being used in asphalt mixtures in Maryland: PG 64-22 and PG 76-22.
3. **Mix Aggregate Size:** The three nominal maximum aggregate sizes (NMAS) used most commonly in Maryland are 9mm, 12mm and 19mm. Surface asphalt mixtures include 9mm or 12mm NMAS and the base mixtures are 12mm or 19mm NMAS mixtures. Asphalt mixtures with 25mm NMAS are rarely used in Maryland.
4. **Gradation.** Two types of aggregate gradations are used in Maryland asphalt mixtures: dense graded and gap graded.
5. **RAP.** Most asphalt mixtures in Maryland have reclaimed asphalt pavement (RAP) materials varying from 10% to 40%. The asphalt mixtures with less than 20% RAP are categorized as low RAP asphalt mixtures. In addition to RAP, some asphalt

mixtures include recycled asphalt shingles (RAS). Virgin mixtures (i.e., no RAP or shingles) are increasingly rare in Maryland pavement construction.

Overall, there are five variables involved in the asphalt mixtures: district (7), binder (2), NMAS (3), gradation type (2), and recycled material content (3—virgin, Low RAP, high RAP/RAS). The source of aggregates (limestone, basalt, gneiss, serpentine etc.) does not have significant effect on the engineering properties of asphalt mixtures (King et al., 2005 and Tran and Hall, 2005), so it was not included in the testing factorial. Based on these considerations, the initial testing factorial required 252 (7x2x3x2x3) asphalt mixtures.

The time required to completely characterize one asphalt mixture is almost three working weeks. It was therefore not feasible to perform laboratory testing on all 252 mixtures in the initial testing factorial within practical time limits. Consequently, the testing factorial cells were prioritized based on the preceding two years' production (2012 and 2013) and on recommendations from the Pavement and Geotechnical Division (PAGD) of MDSHA. The first priority was given to those asphalt mixtures with more than 25 thousand tons of production in last two years and which were most frequently recommended by PAGD. Out of 252 asphalt mixture, 26 asphalt mixtures were categorized as first priority mixtures and the rest were categorized as priority 2 and priority 3. The final factorial of testing includes only priority 1 asphalt mixtures is shown below in Table 1.

Table 1: Factorial of Testing (Priority 1-Asphalt Mixtures)

Mix Type	NMAS	Binder	District 1	District 2	District 3	District 4	District 5	District 6	District 7
Low RAP Dense Graded	9.5	64-22							
		76-22							
	12.5	64-22							
		76-22							
	19	64-22							
Low RAP GAP Graded	12.5	76-22							
High RAP/RAS/ HP Dense Graded	9.5	64-22							
	12.5	64-22							
	19	64-22							
Virgin GAP Graded	12.5	76-22							
	19.5	76-22							
Virgin/HP Dense Graded	12.5	64-22							
	12.5	76-22							

NMAS: Nominal Maximum Aggregate Size, RAP: Reclaimed Asphalt Pavement, RAS, Reclaimed Asphalt Shingle, HP: High Polish

Before starting the testing on selected priority-1 asphalt mixtures, two additional asphalt mixtures were tested to go through the whole testing procedure to see the critical areas of testing. Overall, twenty eight (28) asphalt mixtures were tested for this study. All testing was performed at the MDSHA Office of Materials Technology (OMT), Asphalt Technology Division (ATD) Laboratory.

2.2 Laboratory Test Methods

Dynamic modulus (DM) and repeated load permanent deformation (RLPD) testing was performed on all mixtures following AASHTO TP 79, "Determining The Dynamic Modulus and Flow Number for HMA Using the Asphalt Mixture Performance Tester (AMPT)" The main testing was performed in the ATD laboratory in Hanover, MD.

Twelve (12) specimens meeting the quality metrics of AASHTO PP 60 "Standard Practice for Preparation of Cylindrical Performance Test Specimens Using the Superpave Gyratory Compactor (SGC)" are required to completely characterize one mixture following AASHTO TP 79. The preparation and testing of 12 specimens of one mixture required two to three working business weeks (60 to 90 hours). In order to get twelve acceptable specimens that meet the quality requirements of AASHTO PP 60, fourteen (14) to eighteen (18) specimens were prepared for each mixture. For asphalt mixtures having nominal maximum aggregate size (NMAS) of 19mm or above, the success rate for achieving acceptable specimens reduced to 50% percent, which added even more labor and time costs. Three specimens out of twelve were used for DM (also denoted as E*) testing and rest of nine specimens were used for RLPD testing. The time required to perform the DM loading sequence at 0.01Hz, the lowest frequency, was forty five minutes while the testing time at the other frequencies was less than 10 minutes. The RLPD test requires

almost three hours at each temperature. Additional temperature equilibration time is also required each time the test temperature is changed. Overall, twenty seven hours of machine time were required to complete testing on three replicates at three temperatures. This time does not include specimen preparation.

2.2.1 Specimen Fabrication

The asphalt mixtures used in this research study were collected from construction sites and asphalt plants throughout Maryland. Ten boxes (10-inch x 12-inch x 8-inch) of each asphalt mixture were brought to the ATD laboratory for testing. The MDSHA approved job mix formula (JMF) of each asphalt mixture was obtained from the ATD. In order to verify if the received asphalt mixtures met the criteria defined in the JMFs, specimens were prepared according to AASHTO T 166 "Bulk Specific Gravity of Compacted Asphalt Mixtures Using Saturated Surface-Dry Specimens" and tested in the laboratory to measure the bulk specific gravity (G_{mb}). Maximum specific gravity (G_{mm}) tests were also performed in the laboratory according to AASHTO T 209 "Theoretical Maximum Specific Gravity and Density of Hot Mix Asphalt". The asphalt contents and aggregate gradations were measured using AASHTO T 308 "Determining the Asphalt Binder Content of Hot Mix Asphalt by the Ignition Method" and AASHTO T 27 "Sieve Analysis of Fine and Coarse Aggregates" respectively. The results of verification testing along with job mix formula (JMF) values are tabulated in APPENDIX A (Table A-37). All mixtures met the criteria specified in their respective JMFs.

After verification testing of the asphalt mixtures, the specimens for DM and RLPD testing were prepared according to AASHTO PP 60. The following steps were followed to

get sufficiently high quality specimens for the testing in this research study. The equipment used in preparation of specimens is shown in Figure 1.

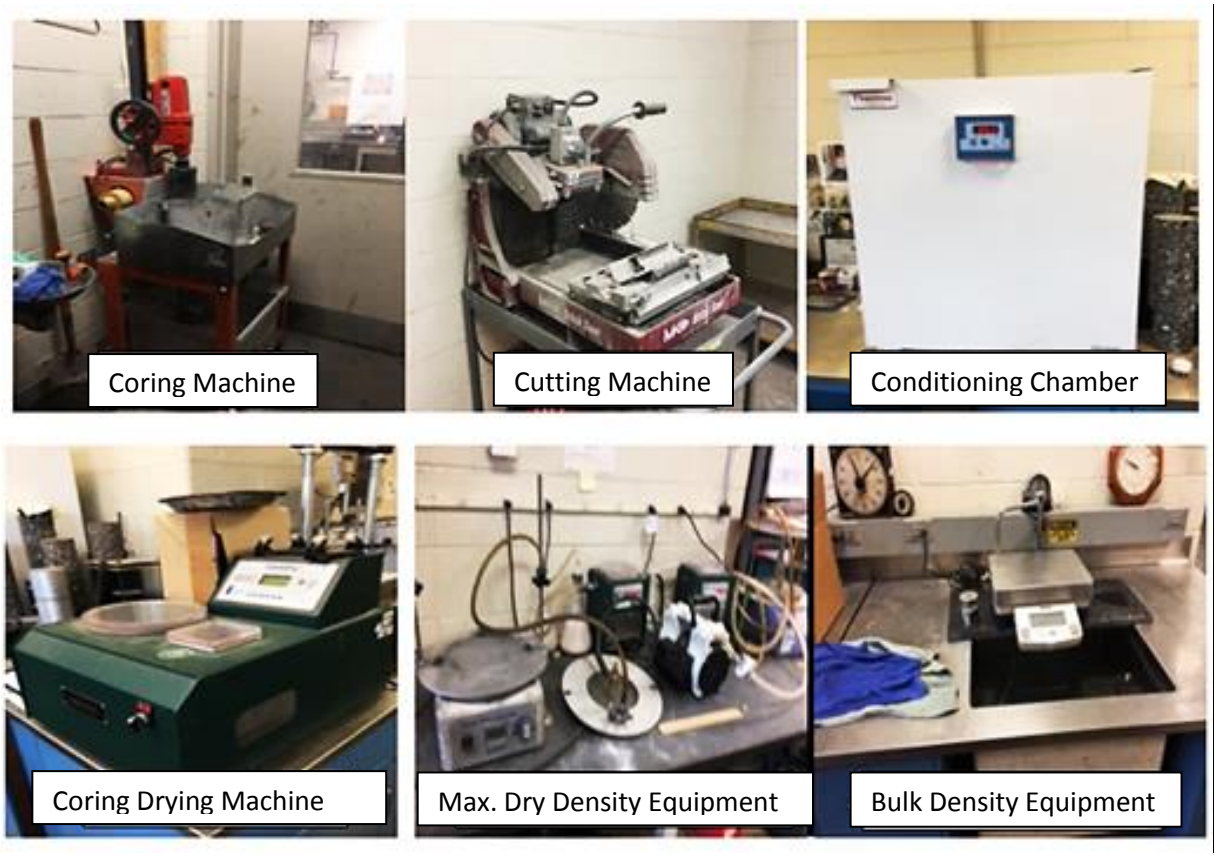

Figure 1: Equipment Used in Preparation of Specimens

2.2.1.1 Heating and Compaction

The asphalt mixtures having PG 64-22 and PG 76-22 binder grades were heated in the oven for 3 hours at 145 C^0 and 154 C^0 temperatures, respectively. The heated mixtures were compacted in the gyratory compactor shown in Figure 2. The initial height and diameter of the specimens were 150mm and 178mm respectively as shown in Figure 3a. They were subsequently cored and cut to cylindrical specimens of 100mm diameter and

150mm height. This can also be seen in Figure 3a. Both ends were cut to ensure more consistent air void distribution along the height of the test specimens.

Figure 2: Gyratory Compactor

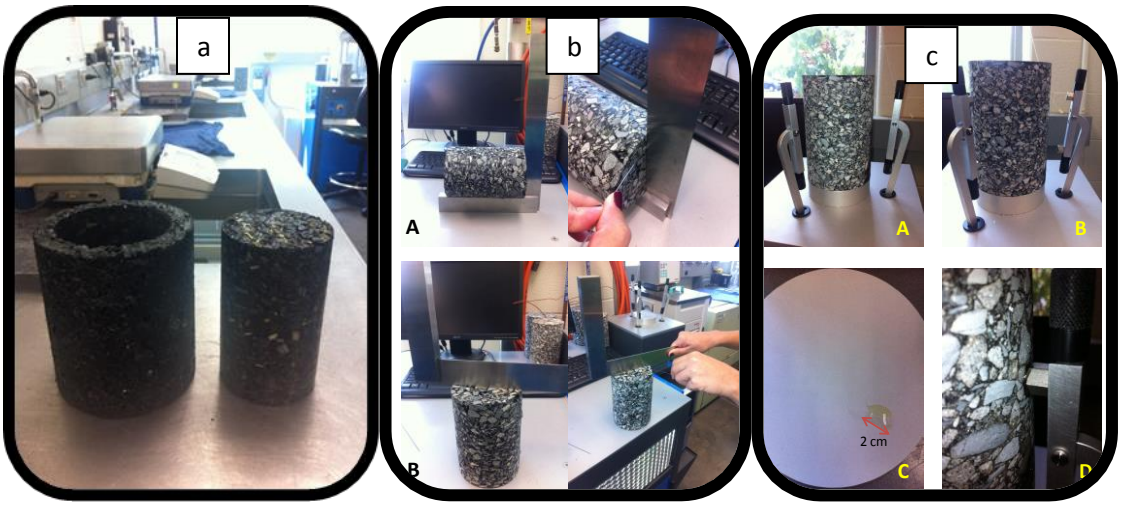

Figure 3: Stepwise Procedure for Preparation of DM and RLPD Specimens

2.2.1.2 Target Air Voids

As per AASHTO TP 79, the target air voids in all specimens for DM and RLPD testing was 7% ± 0.5%. In order to achieve the target air voids in the specimens, an iterative trial method was used as defined in AASHTO TP 79. Normally, two to three trials were enough to achieve the target air voids. However, in the case of 19mm or above NMAS mixtures, more trials were required. Higher variability in air voids within the specimens for 19mm or above NMAS mixtures was also noticed.

The gyratory compactor plugs before coring and cutting had 8% ± 0.5% air voids. The reason for 0.5% to 1.5% higher air voids in the gyratory compacted material was the variation in density throughout the specimen. The specimens were denser in the center than on the surface. The core of the initial specimens (100mm x 178mm) had more uniform air voids. Trimming the ends to achieve a 150mm height further increased air void uniformity. The difference between the target air voids of specimens before and after the coring and

cutting process increases as the NMAS increases. (Chehab et al., 2000). This was also observed in this research study.

Air voids were measured using the Corelok vacuum sealing device (Figure 1) following ASTM D 6752, "Standard Test Method for Bulk Specific Gravity and Density of Compacted Bituminous Mixtures Using Automatic Vacuum Sealing Method."

2.2.1.3 Coring and Cutting Procedure

The coring and cutting procedure is very important for achieving high quality test specimens for DM and RLPD testing, the tolerances for end flatness and perpendicularity of the specimen are 0.5mm and 1mm respectively as per AASHTO PP 60. Achieving high quality specimens for 19mm or coarser mixtures was very difficult. The success rate for 9mm and 12mm asphalt mixtures were almost 70% while the success rate for 19mm mixtures dropped to about 50%. The method to measure the end flatness and perpendicularity of specimens is shown in Figure 3b. The final height and diameter of all specimens were within the range of 147.5mm to 152.5mm and 98mm to 102mm respectively as per AASHTO PP 60. The standard deviation of the diameter of specimens was less than 0.5mm.

2.2.1.4 LVDT Installation

For DM testing, the studs (gauge points) required to hold the three linear variable differential transducers (LVDTs) for displacement measurement under loading were glued on the specimens at an angle of 120 degrees. The equipment used to glue the LVDT studs on the specimens is shown in Figure 3c. Four steps (A, B, C and D as shown in Figure 3c) are required to properly install the studs on the specimen. In step A, the specimen is placed

in the middle of the frame. In step B, the studs are inserted in the hinges provided on the frame. In step C, an epoxy is mixed and applied on the studs, and then in step D the frame is pushed and attached with the specimen for 5 minutes. After curing, the LVDT are mounted on the glued studs. The AMPT uses spring loaded linear variable differential transformers (LVDT's) that fit between clips on the gauge points. The gauge length between the studs is 70mm.

For RLPD testing, the glued stud LVDT system is not used. Instead, the loading actuator LVDT is used to measure permanent deformations of the specimens under the applied repeated loading.

2.2.1.5 Temperature Control and Conditioning of Specimens

Before performing DM and RLPD testing in the AMPT, all specimens were conditioned as per requirement of AASHTO PP 61, "Developing Dynamic Modulus Master Curves for asphalt mixtures using AMPT." The conditioning chambers used in this research study are shown in Figure 1. All specimens for DM testing were conditioned at 4^oC, 20^oC and 40^oC as per AASHTO PP 61. For RLPD testing, the specimens were conditioned at 4^oC, 20^oC and 58^oC as per recommendation of NCHRP 9-30A project (Von Quintus et al., 2011). To monitor the temperature of the specimens during the conditioning process, thermocouple wires were inserted into two dummy specimens at the center of the specimens. The AMPT has its own conditioning chamber to control the temperature of specimens within ± 0.5^oC of the target temperature during testing. All specimens were conditioned overnight for 4^oC and 20^oC temperatures and 2 to 4 hours for 40^oC and 58^oC temperatures. The maximum time required for taking a specimen from the conditioning chamber to placement in the temperature control chamber of the AMPT was 5 minutes.

2.3 Asphalt Mixture Performance Tester (AMPT)

The major components of AMPT machine shown in Figure 4 are the computer control and data acquisition system, test chamber, hydraulic loading system, confining pressure system, temperature control system, actuator deformation measuring system, specimen mounted deformation measuring system, and gauge point gluing fixture. The loading system uses 21MPa (3,000 psi) hydraulic pressure that is generated by the hydraulic power supply unit and controlled by a servo valve. Load is applied to the test specimen by hydraulic actuator from the bottom. The maximum load that can be applied by the machine is 13.5KN (3000 lb.). The loading system can apply ramp, constant, pulse and sinusoidal loadings. The frequency range of the sinusoidal loading is from 0.01Hz to 25Hz. Axial load is measured by a load cell that is mounted inside the testing chamber. There are two configurations for the loading platens. In the DM test, the upper loading platen is allowed to rotate via a ball placed between the upper loading platen and the load cell. For the flow test, the upper loading platen is not allowed to rotate. The position of loading actuator is monitored with an LVDT deformation sensor in the actuator. This sensor also measures the permanent deformations in the RLPD test. The AMPT can apply a confining pressure up to 30 psi. For confined tests, the specimens are encased in a latex membrane. A bubble chamber is used to detect leaks in the membrane. The AMPT has a temperature control system that is capable of maintaining the test chamber to within ± 0.5^{o}C of the set point over a range from 4 to 70^{o}C.

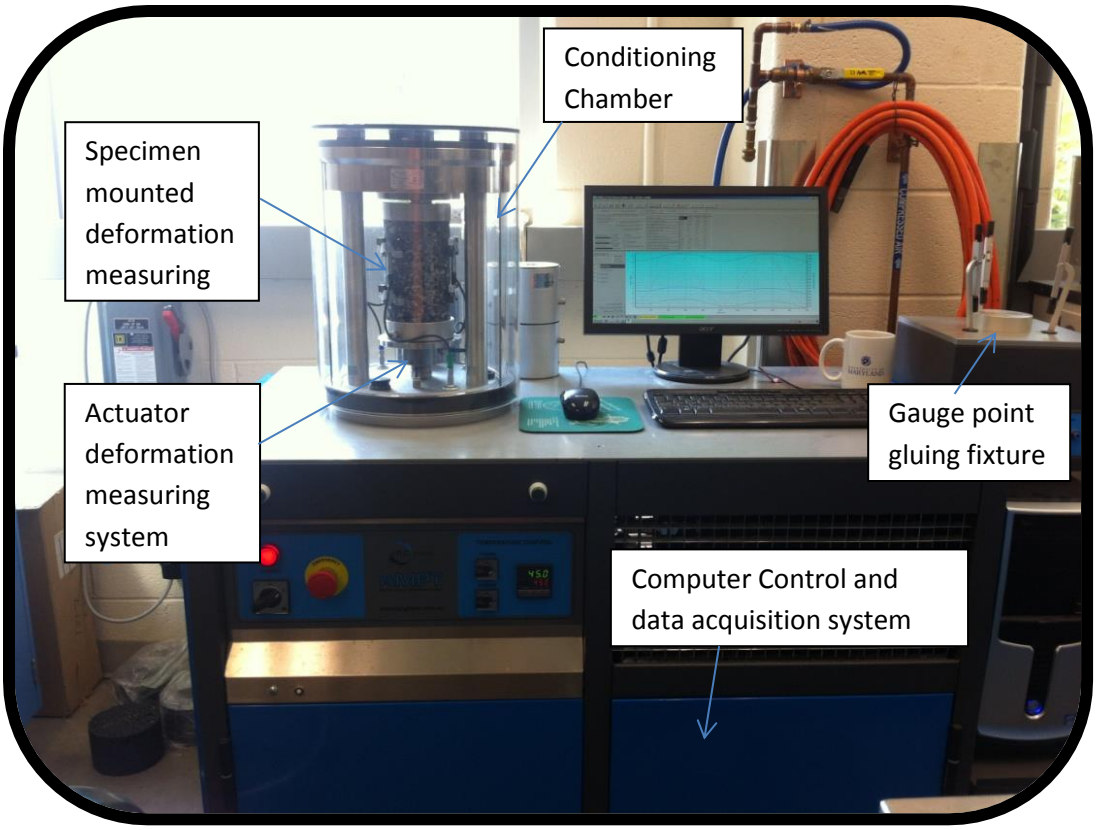

Figure 4: Asphalt Mixture Performance Tester

2.4 Dynamic Modulus Testing

The DM test characterizes the viscoelastic behavior of asphalt mixtures as a function of loading time (or loading frequency) and temperature. The testing temperatures and loading frequencies used for DM tests as per AASHTO PP 61 are given in Table 2. In the DM test, the specimen is subjected to controlled sinusoidal (haversine) compressive stress as shown in Figure 5. The applied stress is kept small to avoid damaging the specimen. The applied stresses and resulting axial strains are measured as a function of time and used to calculate the dynamic modulus, E*. The dynamic modulus is the peak

stress divided by the peak strain and the phase angle (ϕ) is the lag between stress and strain peaks (Figure 5). Phase angle measures the viscous behavior of the mixture.

The DM master curve is developed from the laboratory measured E* values by following AASHTO PP 61.

Table 2: Temperatures and Loading Frequencies for DM Testing

Temperature (C°)	Loading Frequencies (Hz)
4	10, 1, 0.1
20	10,1,0.1
40	10,1,0.1, 0.01

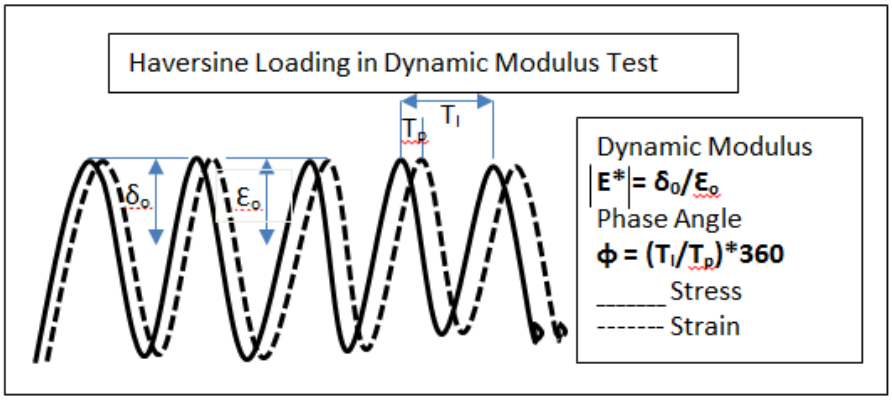

Figure 5: Haversine Loading in DM Testing

An unconfined dynamic modulus master curve is the required material input for HMA in the MEPDG. Consequently, all DM testing in this study was performed under unconfined condition.

The criteria for accepting DM test results are defined in AASHTO TP 79. These are tabulated in Table 3. Specimens which do not meet the acceptance criteria of AASHTO TP 79 were discarded and not included in the analysis.

Table 3: Criteria for Acceptance of DM Test Result as Per AASHTO TP 79

Data Quality Statistic	Limit
Deformation Drift	In direction of applied load
Peak to Peak Strain	75 to 125 micro strain for unconfined tests 85 to 115 micro strain for confined tests
Load Standard Error	10%
Deformation Standard Error	10%
Deformation Uniformity	30%
Phase Uniformity	3 degree

2.5 Repeated Load Permanent Deformation (RLPD) Test

The RLPD test characterizes the rutting susceptibility of asphalt mixtures by applying a pulse load for numerous cycles and observing the cumulative plastic strain versus loading cycles. The RLPD testing was performed according to AASHTO TP 79 at the low (20^{o}C), intermediate (40^{o}C), and high (58^{o}C) temperatures recommended by NCHRP Project 9-30A (Von Quintus et al., 2011). Three replicate specimens were tested at each temperature. A cyclic haversine pulse having a 0.1 second load duration and 0.9 second rest period shown in Figure 6 was applied for 10,000 cycles or until 5%, cumulative axial plastic strain was reached. Following the recommendations from NCHRP Report 719 (Von Quintus et al., 2011), a constant confining pressure of 10 psi (68.9 KPa) and a cyclic deviator stress of 70 Psi (482.6 KPa) are applied to the specimens in RLPD test. The cumulative axial plastic strain is measured by the axial LVDT mounted on the actuator.

As shown in Figure 6, the typical cumulative plastic strain curve in RLPD test consists of three stages defined as (1) primary, (2) secondary, and (3) tertiary. The primary stage is defined as the initial rapid permanent deformation with a high but decreasing

permanent strain per cycle and is mainly due to densification of asphalt mixture. In the secondary stage, the slope of the line slowly decreases with increase of number of cycles of loading. This stage of the RLPD test best simulates the rutting phenomenon of asphalt layers over service life in typical pavement structure. The permanent deformation per cycle in the secondary stage is mainly due to stable shear deformation in the asphalt mixture. The tertiary stage, if present, develops when the rate of permanent deformation increases, leading to an unstable shear failure or flow in the material. The tertiary stage is usually not observed in confined RLPD tests.

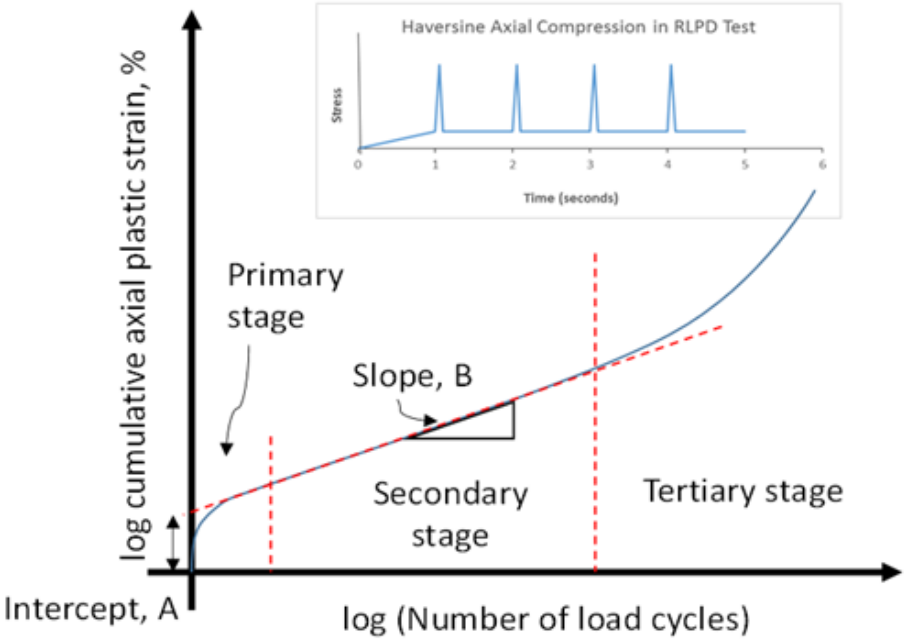

Figure 6: Typical Curve of RLPD Test

CHAPTER: 3 DYNAMIC MODULUS TEST DATA AND ANALYSES

DM and RLPD tests were performed on twenty eight (28) asphalt mixtures, (hereafter, the mixtures) collected from the seven MDSHA districts, as per standard test method AASHTO TP 79.

3.1 Mixture Characterization

The mixtures are named based on the MDSHA standard coding system which is explained below. In order to explain the coding system, an example is used: H123A12V2C01.

1. All mixtures are designated with letter 'H'(Hanover). In this research study all mixtures are designed based on Superpave specification and tested at MDSHA, Hanover office so all mixtures have same 'H' letter in the start of the name.
2. The number '123' represents the plant number.
3. The letter 'A' represents the mixing process. There are four mixing processes commonly used in Maryland: A (Hot Mix), B (Warm Mix- Plant Processed - Mechanical Water Injection), C (Warm Mix - Plant Processed - Additive), D (Warm Mix - Refinery Processed - Additive).
4. The number '12' represents the NMAS of the mix.
5. The letter 'V' represents the mix type: V (Virgin), R (RAP), H (High Polish), G (Gap Graded), S (Shingles), D (Shingles/High Polish), A (RAP/High Polish), B (RAP/GAP), C (RAP/Shingles).

6. The number ‘2’ represents the ESAL Level: 1 (<0.3), 2 (0.3 to < 3), 3 (3 to < 10), 4 (10 to 30), 5 (>30). The numbers given in parenthesis are ESALs in millions.
7. The letter ‘C’ represents the binder type: C (PG 64-22), F (PG 76-22).
8. The number ‘01’ represents the mix number. It varies from 0 to 99.

A complete copy of MDSHA mix design coding is included in APPENDIX B (Figure B-53). There are nine categories of the mixtures tested in this research study: Low RAP Dense Graded (LRDG - 9 mixtures), Warm Mix Low RAP Dense Graded (WM-LRDG – 3 mixtures), High RAP Dense Graded (HRDG – 2 mixtures), RAP-RAS (Shingle) Dense Graded (RSDG – 1 mixture), High RAP-RAS (Shingle) Dense Graded (HRSDG – 3 mixtures), Warm Mix High RAP Dense Graded (WM-HRSDG - 1 mixture), Low RAP Gap Graded (LRG - 4 mixtures), Virgin Gap Graded (VGG - 3 mixtures), and Virgin Dense Graded (VDG - 2 mixtures). Five mixtures out of the twenty-eight are warm mix asphalt mixtures (WMA) and rest are hot mix asphalt mixtures (HMA). All mixtures have RAP except the five virgin asphalt mixtures (three gap and two dense graded virgin mixtures). The NMAS varies from 9mm to 19mm. Two binders, PG 64-22 and PG 76-22, are used in the mixtures. The characteristics of all mixtures are summarized in Table 4.

Table 4: Characteristics of All Asphalt Mixtures

Type	Mixture	NMAS	PG Binder	RAP (%)	RAS (%)	Remarks
Low RAP Dense Graded						
LRDG-9-C	H077A09A2C03	9.5	64-22	15	0	
	H168A09R2C02			15	0	
	H176A09R2C01			10	0	
	H160A09R1C03			15	0	
WM-LRDG-9-F	H116C09A2F02	9.5	76-22	15	0	WM-Additive at Plant
LRDG-12-C	H127A12R2C02	12.5	64-22	19	0	
	H168A12R2C02			19	0	
	H040A12R2C12			19	0	
WM-LRDG-12-C	H138B12R2C05			15	0	WM-PlantWater Injection
LRDG-12-F	H161A12R4F01	12.5	76-22	10	0	
WM-LRDG-19-C	H151B19R2C02	19	64-22	15	0	WM-PlantWater Injection
LRDG-19-C	H176A19R2C01			10	0	
High RAP-RAS-HP-Dense Graded						
RSDG-9-C	H077A09C2C01	9.5	64-22	14	5	
WM-HRDG-9-C	H158B09R2C60			40	0	WM-PlantWater Injection
HRDG-9-C	H131A09A4C01			28	0	
HRSDG-12-C	H083A12C2C02	12.5	64-22	14	5	
HRDG-12-C	H177A12R2C50			25	0	
HRSDG-19-C	H187A19C2C02	19	64-22	17	5	
	H083A19C2C02			18	5	
Low RAP-GAP Graded						
LRG-12-F	H128A12B4F02	12.5	76-22	15	0	
	H051A12B4F01			10	0	
	H186D12B4F01			12	0	WM-Additive at Refinery
	H169A12B4F03			15	0	
Virgin GAP Graded						
VG-12-F	H138A12G4F05	12.5	76-22	0	0	
	H135A12G4F01			0	0	
VG-19-F	H135A19G4F01	19	76-22	0	0	
HP Virgin Dense Graded						
VDG-12-C	H135A12H2C03	12.5	64-22	0	0	
VDG-12-F	H160A12H2F01	12.5	76-22	0	0	

LRDG : Low Rap Dense Graded, WM-LRDG: Warm Mix Low Rap Dense Graded, HRDG: High Rap Dense Graded, RSDG: Rap Shingle Dense Graded, HRSDG: High Rap Shingle Dense Graded, LRG: Low Rap Gap, VG: Virgin Gap, VDG: Virgin Dense Graded, RAP: Recclaimed Asphalt Pavement, RAS: Reclaimed Asphalt Shingle, NMAS: Nomimal Maximum Aggregate Size

3.2 Volumetric Properties and Gradations of Asphalt Mixtures

The gradations of all mixtures are shown in Figure 7. The volumetric properties and asphalt contents of all mixtures at 7% ± 0.5% air voids are tabulated in Table 5.

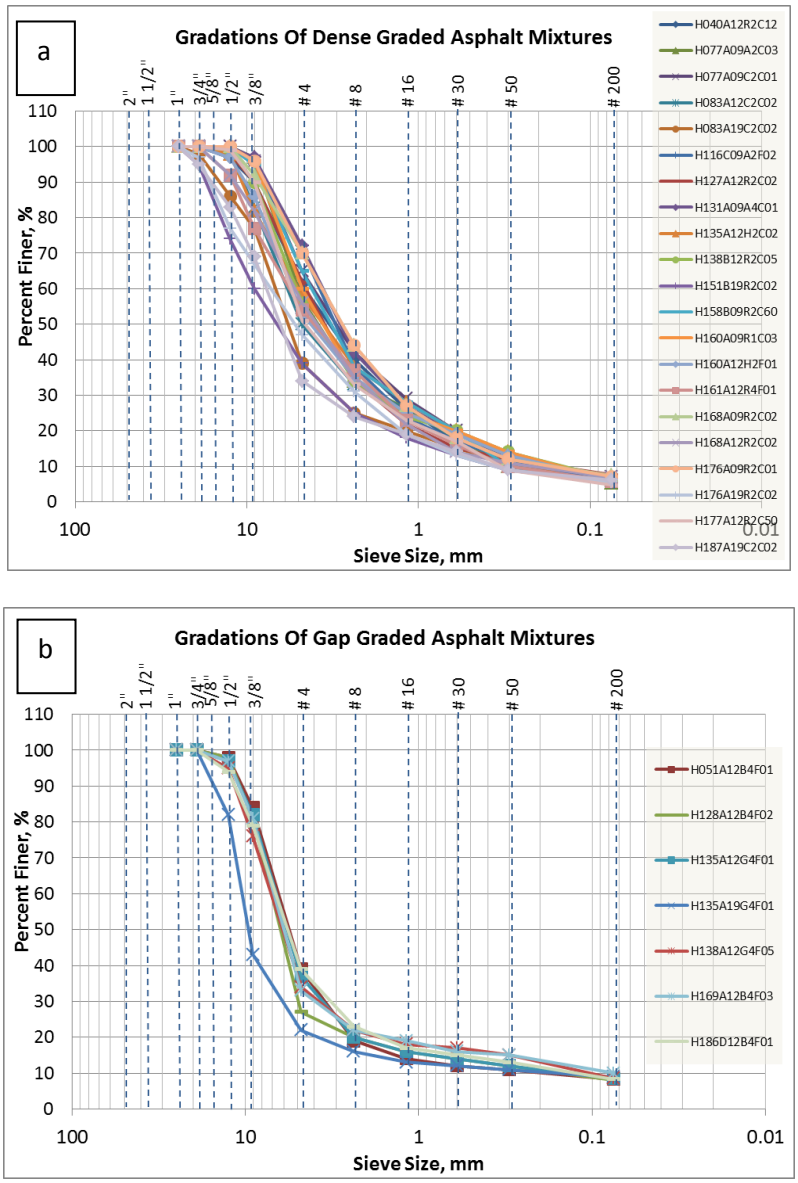

Figure 7: Gradations of A) Dense Graded Mixtures B) Gap Graded Mixtures

The box and whisker plots in Figure 8 show the variability among mixtures of the following volumetric properties: maximum specific gravity (G_{mm}), bulk specific gravity (G_{mb}), combined aggregate specific gravity (G_{sb}), voids in mineral aggregate (VMA) and voids filled with asphalt (VFA). The box and whisker plots show the minimum and maximum values of these variables along with the 25^{th}, 50^{th} and 75^{th} percentiles.

Table 5: Volumetric Properties and Gradations of All Asphalt Mixtures

No	Mixture	Gmm	Gmb	Pb	Gsb	VMA	VFA	Passing Percentage (%)						
				%		%	%	3/8"	#4	#8	#16	#30	#50	#200
1	H040A12R2C12	2.566	2.389	4.8	2.751	17.2	60.7	90	61	40	26	17	13	6.3
2	H051A12B4F01	2.528	2.352	6.5	2.766	20.4	66.5	84	39	19	14	12	11	8.3
3	H077A09A2C03	2.567	2.389	5.2	2.741	17.5	60.1	97	57	34	26	18	10	5.3
4	H077A09C2C01	2.539	2.36	5.3	2.747	18.7	62	96	65	42	29	20	12	7
5	H083A12C2C02	2.583	2.399	4.8	2.764	17.2	59.9	83	50	33	26	18	12	5.7
6	H083A19C2C02	2.579	2.397	4.3	2.765	16.9	59.7	77	39	25	20	15	11	6.2
7	H116C09A2F02	2.589	2.407	5.3	2.78	18.1	61.2	95	71	38	24	17	12	5.5
8	H127A12R2C02	2.578	2.398	5.3	2.76	17.6	59.9	90	62	34	22	15	12	7.5
9	H128A12B4F02	2.589	2.409	6.5	2.848	21.1	66.1	81	27	20	16	14	12	8.0
10	H131A09A4C01	2.496	2.318	5.2	2.668	17.5	60.1	97	72	42	27	19	13	6.8
11	H135A12G4F01	2.445	2.27	6.7	2.666	20.4	66	82	37	20	16	14	12	8.5
12	H135A12H2C02	2.492	2.318	5	2.65	17	58.5	82	58	38	28	20	14	6.3
13	H135A19G4F01	2.435	2.252	6.5	2.68	21.2	66.9	43	22	16	13	12	11	9
14	H138A12G4F05	2.624	2.444	6.5	2.82	19.1	63.3	76	34	22	18	17	15	8.5
15	H138B12R2C05	2.609	2.425	4.4	2.792	16.6	59.9	90	56	34	24	20	14	6.5
16	H151B19R2C02	2.57	2.388	4	2.731	16.2	55.4	60	39	25	18	13	9	5.3
17	H158B09R2C60	2.548	2.369	5.2	2.771	18.9	63.1	95	65	38	28	20	10	5.2
18	H160A09R1C03	2.53	2.354	5.2	2.722	18.1	61.3	96	60	35	25	20	14	6
19	H160A12H2F01	2.545	2.367	5.2	2.721	17.4	60.9	86	53	35	25	19	13	6
20	H161A12R4F01	2.532	2.356	5	2.716	17.8	60	77	54	37	23	16	10	5.8
21	H168A09R2C02	2.53	2.352	5.9	2.684	17.3	61.3	92	70	44	27	18	12	7.4
22	H168A12R2C02	2.52	2.344	5.6	2.708	18	63.3	82	56	35	22	14	11	6.9
23	H169A12B4F03	2.549	2.37	6.5	2.775	20.4	64.3	81	33	22	19	16	15	10
24	H176A09R2C01	2.48	2.306	6.1	2.645	18	61.8	96	70	44	27	18	12	7.1
25	H176A19R2C02	2.503	2.328	5.3	2.668	17.5	59.1	67	47	31	19	13	9	5.4
26	H177A12R2C50	2.542	2.362	4.9	2.722	17.3	60	90	51	33	23	17	9	4.7
27	H186D12B4F01	2.592	2.409	6.5	2.891	22	68.6	79	39	23	17	15	13	8.3
28	H187A19C2C02	2.611	2.426	4.2	2.77	15.4	56	69	34	24	19	14	9	6.1

Gmm: Maximum Specific Gravity, Gmb: Bulk Specific Gravity, Pb: Effective Binder Content, Gsb: Combined Aggregate Specific Gravity
VMA: Void in Mineral Aggregates, VFA: Void filled with asphalt,

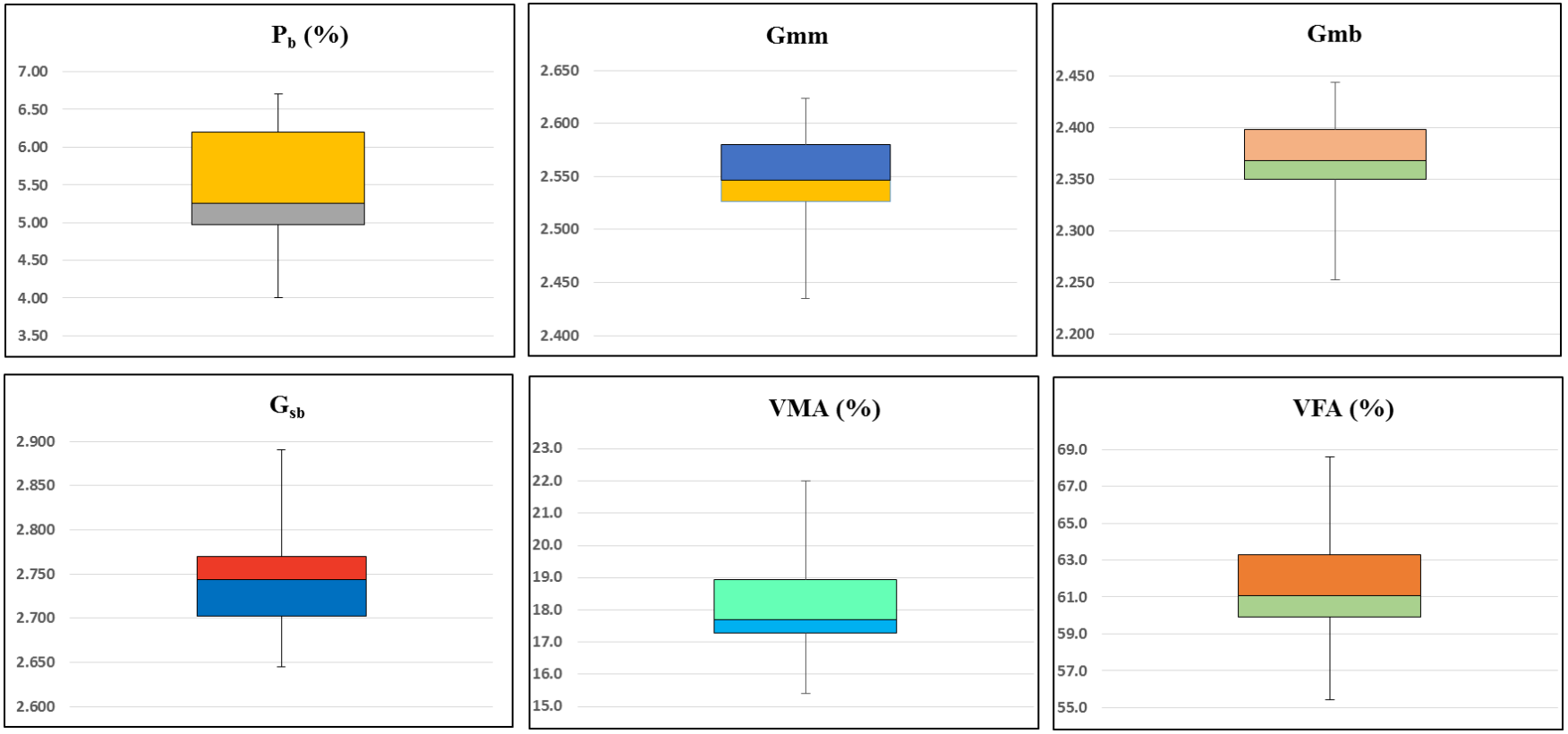

Figure 8: Box and Whisker Plots Representing Variations in Volumetric Properties and Asphalt Contents of Asphalt Mixtures

3.3 Development of Dynamic Modulus Master Curves

In the DM test, an asphalt mixture behaves as a linear viscoelastic (LVE) material. The dynamic modulus (E*) measures the elastic behavior of the mixture and is equal to the peak stress divided by the peak strain under sinusoidal (haversine) compressive loading. The viscous behavior of the mixture is governed by the phase angle. The phase angle (ϕ) is proportional to the period of the loading cycle divided by lag time between stress and strain peaks (Figure 5). The dynamic modulus (E*) and phase angle (ϕ) determined in the DM test characterize the LVE behavior of the mixture. E* and ϕ are the function of temperature and loading time/frequency. Within the viscoelastic range, the time-temperature superposition principle can be applied to shift E* in the frequency (or, conversely, loading time) domain. The new shifted frequency, which is a combined function of temperature and time, is called the reduced frequency. All DM testing on asphalt mixtures were performed according to the AASHTO TP 79 and AASHTO PP 61 protocols.

The E* values of the asphalt mixture are key inputs to the Mechanistic-Empirical Pavement Design Guide (MEPDG). The MEPDG uses DM to calculate the stresses, strains and deflections in the asphalt layers. These responses are inputs to the empirical distress models for predicting the performance of the pavement structure. The pavement structure goes through different climate and loading conditions throughout of its design life so it is important to have E* values at all temperatures and loading frequencies. This is accomplished by using the time-temperature superposition concept to create a master curve

for the dynamic modulus of the mixture. A master curve of asphalt material is based on two components.

A. A temperature shift function in the frequency domain to convert frequency values to a reference temperature (normally 20°C). These shifted frequencies at the reference temperature are termed as reduced frequencies.

B. A master curve function (commonly a sigmoidal curve) relating the temperature-shifted E* values to the reduced frequency at the reference temperature.

A typical development of master curve is shown in Figure 9.

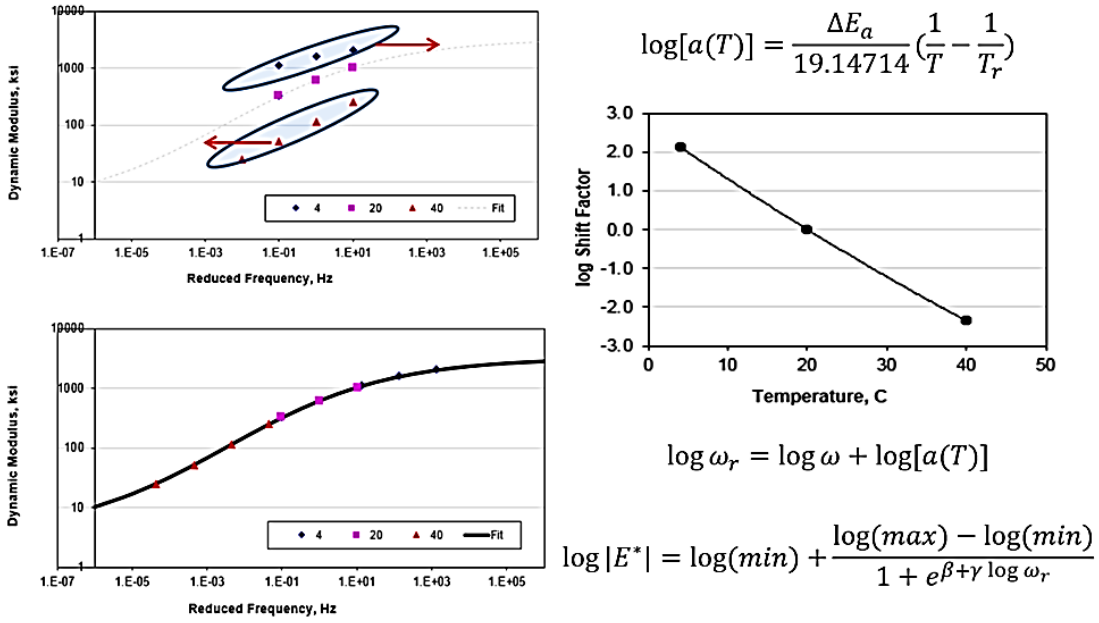

Figure 9: Typical Development of DM Master Curve of an Asphalt Mixture

A standard procedure to develop a DM master curve of asphalt mixture based on measured E* values is explained in AASHTO PP 61. Currently, the MEPDG uses a symmetric sigmoidal function fitted in logarithmic space as given in Equation 1.

$$\log E^* = \log(E^*_{min}) + \frac{\log(E^*_{max}) - \log(E^*_{min})}{\left(1 + e^{\beta + \gamma \log \omega_r}\right)} \quad \text{Equation (1)}$$

in which

E^* = Dynamic modulus, ksi

ω_r = Reduced frequency at reference temperature, Hz

E^*_{max} = Limiting maximum dynamic modulus, calculated from Hirsch model, ksi

E^*_{min} = Limiting minimum dynamic modulus, a fitting parameter, ksi

β, γ = Fitting parameters

The reduced frequency is computed as:

$$\log \omega_r = \log \omega + \log[a(T)] \quad \text{Equation (2)}$$

in which

ω= frequency at the test temperature

a(T) = the temperature shift factor at the test temperature, which equals to ratio of reduced frequency to original frequency.

The Arrhenius equation was used to define the temperature shift function:

$$\log[a(T)] = \frac{\Delta E_a}{19.14714}\left(\frac{1}{T} - \frac{1}{T_r}\right) \quad \text{Equation (3)}$$

in which

T_r = Reference temperature, K

T = Test temperature, K

ΔE_a = Activation energy (treated as a fitting parameter)

As per AASHTO PP 61, the maximum value of the dynamic modulus is calculated using the Hirsch model (Christensen *et al.*, 2003) and a limiting binder modulus of 1 GPa:

$$E^*_{max} = P_c\left[4200000\left(1 - \frac{VMA}{100}\right) + 435000\left(\frac{VMA \times VFA}{10000}\right) + \frac{1 - P_c}{\left[\frac{1 - \frac{VMA}{100}}{4200000} + \frac{VMA}{435000(VFA)}\right]}\right] \quad \text{Equation (4)}$$

in which

$$P_c = \frac{\left(20 + \frac{435000 \times VFA}{VMA}\right)^{0.58}}{650 + \left(\frac{435000 \times VFA}{VMA}\right)^{0.58}} \quad \text{Equation (5)}$$

in which

E^*_{max} = Limiting maximum mixture dynamic modulus

VMA = Voids in mineral aggregate, %

VFA = Voids filled with asphalt, %

The Solver tool in Microsoft Excel is used to calculate the temperature shift function parameters and E* values based on numerical minimization of the squared errors between measured and predicted E* values in log space. The initial or "seed" values of the

parameters for the numerical optimization are log (min) = -0.5, β=-1, γ=-0.5, and ΔE_a = 200000.

E* values are measured at three temperatures (4°C, 20°C and 40°C) as per AASHTO PP 61. At 4°C and 20°C, E* is measured at three frequencies (10Hz, 1Hz and 0.1Hz) and at four frequencies (10Hz, 1Hz, 0.1Hz and 0.01Hz) at 40°C. The DM test is performed on three replicate specimens and the E* average values at each temperature and frequency from the three specimens are used to develop the master curve. As per AASHTO TP 79, individual specimen E* values varying by more than 13% from the mean value of three specimens are discarded. A 20°C reference temperature was used to calculate the shift factors and to develop the master curves for all mixtures. Dynamic modulus master curves for all 28 asphalt mixtures are shown in Figure 10. The predicted E* values obtained from the master curves for each individual mixture are tabulated in APPENDIX B (Table B-38).

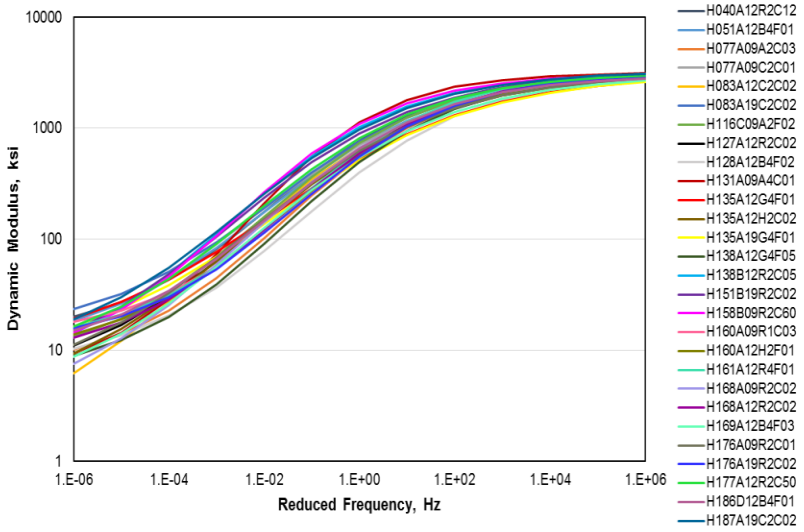

Figure 10: DM Master Curves of All Asphalt Mixtures

The shift factors used in the development of the master curves for all mixtures are shown in Figure 11. The calculated shift factors for each individual mixture are tabulated in APPENDIX B (Table B-39).

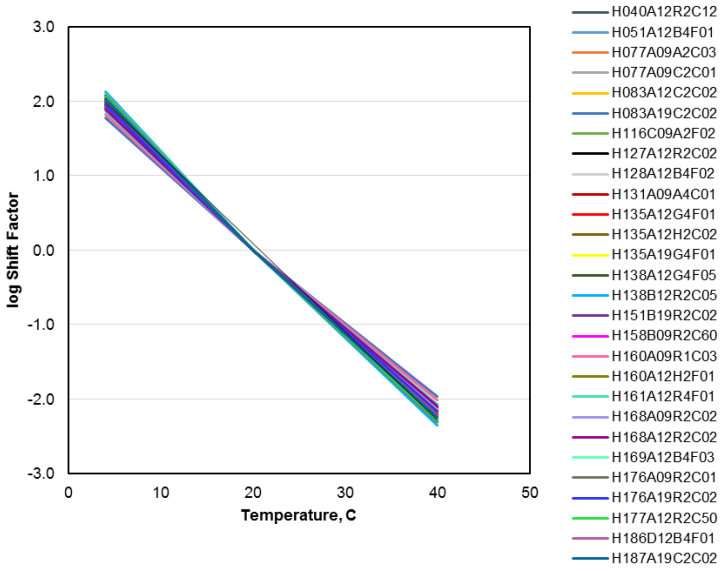

Figure 11: Shift Factors of Asphalt Mixtures Used in Development of Master Curves

In general, the stiffer binder (PG 76-22 - F binder code) produces higher shift factors than for the soft binder (PG 64-22 - C binder code). However, it is difficult to see the difference in shift factors in Figure 11 because most of the mixtures contain RAP. For RAP mixtures, the binder is a blend of the virgin binder and the aged binder from the RAP. The performance grade of this blended binder is unknown for the tested mixtures.

The phase angles representing the viscous behavior of the mixtures are shown in Figure 12.

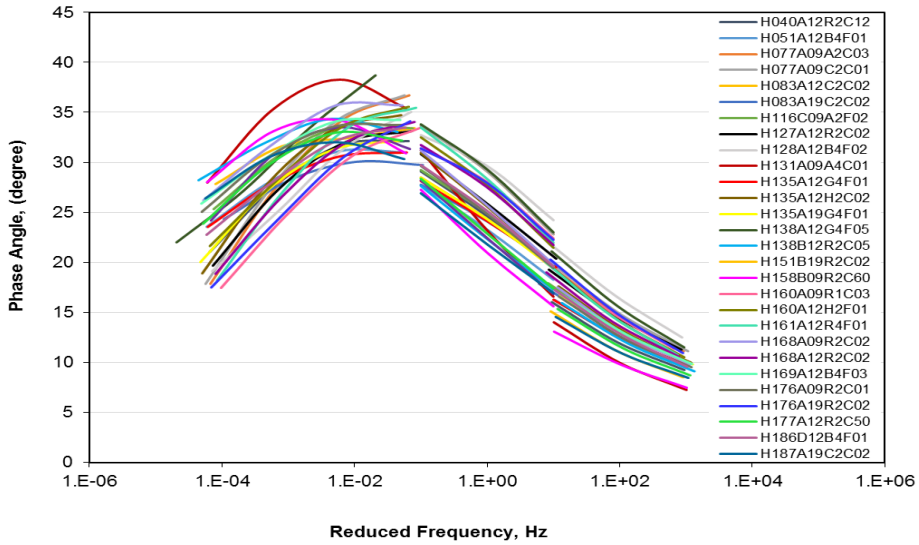

Figure 12: Phase Angles of Asphalt Mixtures

The phase angles are measured at all testing temperatures and frequencies and plotted against reduced frequencies. The measured phase angle values at all test temperatures and frequencies for each individual mixture are tabulated in APPENDIX B (Table B-39).

3.3.1 Fitting Parameter of Master Curves

The master curve fitting parameters along with goodness of fit statistics (R^2 and S_e/S_y) are shown in Table 6 for all twenty-eight mixtures. The variations in the fitting parameters are represented in the box and whisker plots in Figure 13. The variations in fitting parameters are due to different types of binders, asphalt contents, gradations, and

volumetric properties of the asphalt mixtures. The variation in fitting parameters indicates different viscoelastic characteristics of the mixtures.

The coefficient of determination (R^2) for all master curves equals or exceeds 0.99 and S_e/S_y (standard deviation of errors/standard deviation of predicted E* values) is less than 0.06; both of these statistics indicate very high accuracy of the E* predictions at all temperatures and frequencies.

The MEPDG software requires E* values at five temperatures and six frequencies as inputs. The measured E* data per AASHTO TP 79 and AASHTO PP 61 are insufficient for MEPDG inputs. However, the required MEPDG E* inputs can be extracted from the master curve for the mixture. This incompatibility between AASHTO TP 79, AASHTO PP 61 and the MEPDG software needs to be addressed in future.

Table 6: Fitting Parameters of Master Curves of the Mixtures

No	Mixtures	Max E* (Ksi)	Min E* (Ksi)	Beta (β)	Gamma (γ)	ΔEa	R2	Se/Sy
1	H040A12R2C12	3185.38	12.63	-1.06	-0.58	192091.78	0.99	0.06
2	H051A12B4F01	3061.00	9.77	-1.07	-0.53	196026.44	1.00	0.02
3	H077A09A2C03	3169.34	6.29	-0.93	-0.57	191154.24	1.00	0.04
4	H077A09C2C01	3118.79	5.24	-1.19	-0.47	197456.15	1.00	0.02
5	H083A12C2C02	3181.53	1.14	-1.40	-0.45	184298.59	1.00	0.02
6	H083A19C2C02	3196.31	13.84	-1.02	-0.54	173266.50	0.99	0.05
7	H116C09A2F02	3142.21	7.15	-1.15	-0.56	186773.60	1.00	0.04
8	H127A12R2C02	3160.10	5.10	-1.11	-0.52	187829.60	1.00	0.02
9	H128A12B4F02	3024.38	6.82	-0.69	-0.55	188717.51	1.00	0.03
10	H131A09A4C01	3165.93	5.46	-1.64	-0.67	195202.79	1.00	0.05
11	H135A12G4F01	3058.39	9.32	-0.83	-0.46	194569.01	0.99	0.05
12	H135A12H2C02	3182.57	3.25	-1.15	-0.48	201914.81	1.00	0.02
13	H135A19G4F01	3027.26	7.57	-0.86	-0.46	204311.52	1.00	0.03
14	H138A12G4F05	3107.33	5.45	-0.90	-0.57	191828.45	1.00	0.02
15	H138B12R2C05	3214.58	5.46	-1.51	-0.54	206829.27	1.00	0.04
16	H151B19R2C02	3206.44	5.25	-1.39	-0.51	190399.19	1.00	0.02
17	H158B09R2C60	3115.14	6.68	-1.58	-0.59	195496.72	1.00	0.05
18	H160A09R1C03	3144.96	13.01	-0.75	-0.59	176994.88	1.00	0.04
19	H160A12H2F01	3177.87	8.29	-0.90	-0.54	191874.87	1.00	0.02
20	H161A12R4F01	3154.29	11.61	-0.90	-0.61	182215.43	1.00	0.03
21	H168A09R2C02	3184.40	2.65	-1.25	-0.50	200388.21	1.00	0.02
22	H168A12R2C02	3161.32	8.06	-0.94	-0.56	184183.88	1.00	0.04
23	H169A12B4F03	3050.87	3.25	-1.09	-0.48	203163.51	1.00	0.02
24	H176A09R2C01	3149.81	4.28	-1.12	-0.48	202467.89	1.00	0.02
25	H176A19R2C02	3161.20	10.96	-0.81	-0.58	190008.82	1.00	0.02
26	H177A12R2C50	3178.96	7.96	-1.22	-0.54	200685.81	1.00	0.02
27	H186D12B4F01	2997.98	8.96	-1.03	-0.56	196228.59	1.00	0.02
28	H187A19C2C02	3253.85	8.56	-1.37	-0.54	197924.83	1.00	0.04
Minimum value		**2997.98**	**1.14**	**-1.64**	**-0.67**	**173266.50**	**0.99**	**0.02**
Maximum value		**3253.85**	**13.84**	**-0.69**	**-0.45**	**206829.27**	**1.00**	**0.06**
Mean Value		**3140.43**	**7.29**	**-1.10**	**-0.54**	**193010.82**	**1.00**	**0.03**
Standard Deviation		**63.54**	**3.21**	**0.25**	**0.05**	**8174.60**	**0.00**	**0.01**

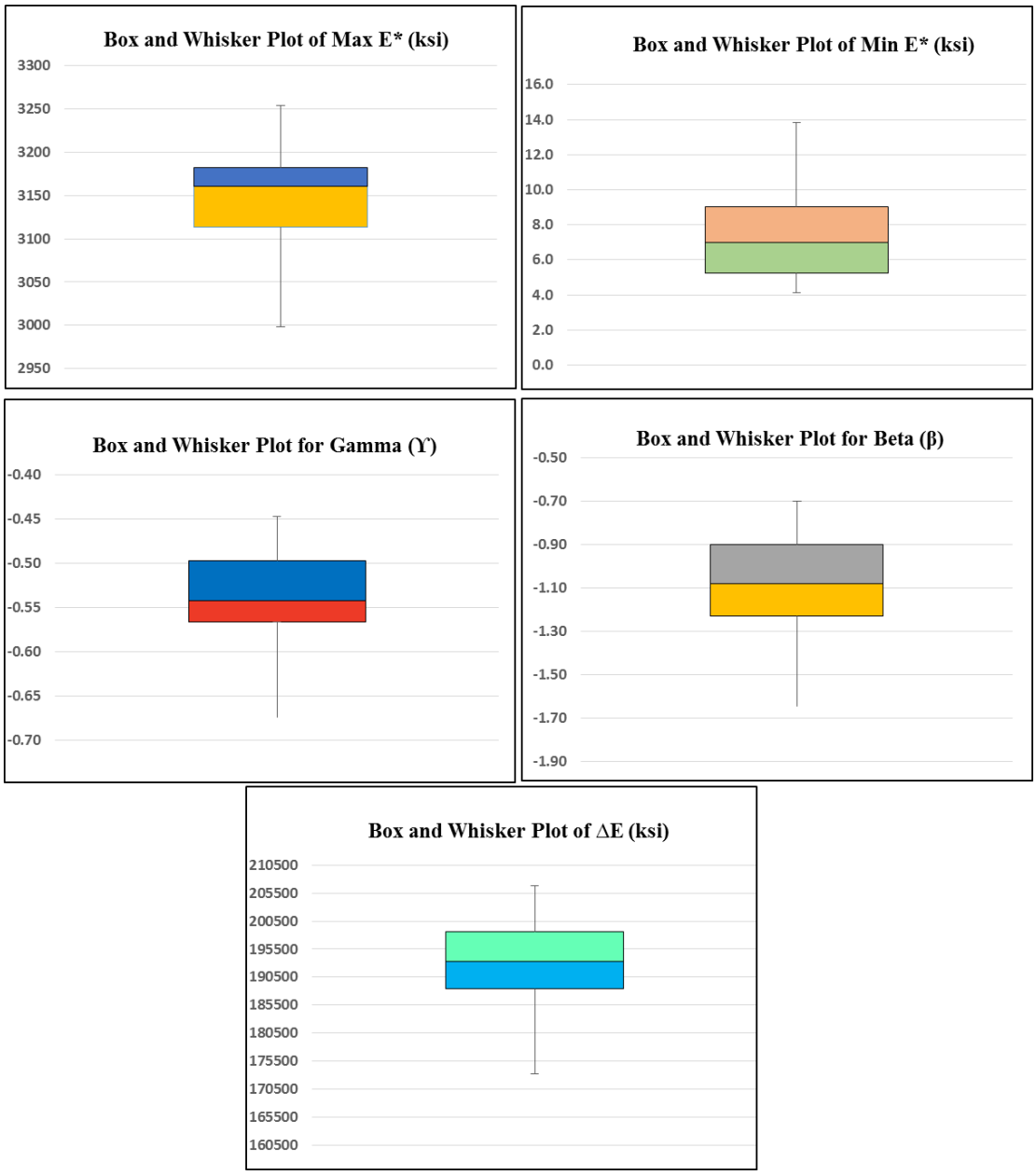

Figure 13: Box and Whisker Plots of Fitting Parameters of Master Curves of Mixtures

3.4 Comparison of Measured E* Values of Mixtures

The E* values are measured in the laboratory at three temperatures and three frequencies with one additional frequency at 40^{o}C. All measured E* are provided in APPENDIX B (Table B-40). However, for comparison purpose and discussion, the E* values of all mixtures measured at 4^{o}C@10Hz, 20^{o}C@10Hz and 40^{o}C@1Hz are shown in Table 7 and compared in Figure 14. These three E* conditions roughly correspond to the upper shelf, middle of the transition region, and lower shelf of the master curve.

The key mixture variable is binder type—i.e., PG 64-22 (C binder) or PG 76-22 (F binder). It can be seen from the Figure 14 that low RAP mixtures and virgin mixtures having C or F binder give similar E* values. However, a high RAP content (more than 20%) in the mixture changes the stiffness of the blended binder and, consequently, the mixture stiffness increases. The high RAP and warm mixes (HRDG and WM) show higher E* values at upper, middle and lower regions of the master curves as shown in Figure 14 and highlighted in orange even though they have C binder (less stiff than F binder).

Mixtures having high stiffness are good for hot weather conditions (lower rutting potential) but not good for cold weather (higher cracking potential). Therefore, it is recommended that the true performance grade of the blended binder in high RAP mixtures be determined in order to accurately assess the predicted performance of the mixture. In summary, percentage of RAP and mix process, hot mix or warm mix, have significant effects on the E* values of the mixtures.

Table 7: Measured E* Values of Asphalt Mixtures

Type	Mixture	NMAS	PG Binder	RAP (%)	RAS (%)	4C@10Hz	20C@10Hz	40C@1Hz	Remarks
Low RAP Dense Graded									
LRDG-9-C	H077A09A2C03	9.5	64-22	15	0	2178.83	936.27	89.57	
	H168A09R2C02			15	0	2209.46	1085.57	112.09	
	H176A09R2C01			10	0	2059.67	994.81	119.34	
	H160A09R1C03			15	0	2050.64	934.96	115.53	
WM-LRDG-9-F	H116C09A2F02	9.5	76-22	15	0	2390.25	1153.69	145.75	WM-Additive at Plant
LRDG-12-C	H127A12R2C02	12.5	64-22	19	0	2169.59	1078.17	130.29	
	H168A12R2C02			19	0	2148.37	989.53	114.34	
	H040A12R2C12			19	0	2510.29	1169.23	159.38	
WM-LRDG-12-C	H138B12R2C05			15	0	2825.28	1530.72	195.75	WM-PlantWater Injection
LRDG-12-F	H161A12R4F01	12.5	76-22	10	0	2267.21	1076.27	116.18	
WM-LRDG-19-C	H151B19R2C02	19	64-22	15	0	2370.37	1344.52	209.33	WM-PlantWater Injection
LRDG-19-C	H176A19R2C01			10	0	2101.05	993.06	98.41	
High RAP-RAS-HP-Dense Graded									
RSDG-9-C	H077A09C2C01	9.5	64-22	14	5	2119.08	1078.66	159.26	
WM-HRDG-9-C	H158B09R2C60			40	0	2821.80	1553.68	222.33	WM-PlantWater Injection
HRDG-9-C	H131A09A4C01			28	0	3118.76	1689.06	172.94	
HRSDG-12-C	H083A12C2C02	12.5	64-22	14	5	2026.13	1050.19	146.36	
HRDG-12-C	H177A12R2C50			25	0	2390.23	1267.20	159.83	
HRSDG-19-C	H187A19C2C02	19	64-22	17	5	2656.93	1427.86	216.34	
	H083A19C2C02			18	5	2313.14	1149.85	202.81	
Low RAP-GAP Graded									
LRG-12-F	H128A12B4F02	12.5	76-22	15	0	1749.50	737.83	68.09	
	H051A12B4F01			10	0	2162.77	1127.42	147.32	
	H186D12B4F01			12	0	2169.68	1072.71	120.47	WM-Additive at Refinery
	H169A12B4F03			15	0	1872.05	913.74	95.93	
Virgin GAP Graded									
VG-12-F	H138A12G4F05	12.5	76-22	0	0	2050.30	907.85	49.64	
	H135A12G4F01			0	0	1782.05	857.29	130.08	
VG-19-F	H135A19G4F01	19	76-22	0	0	1724.46	817.44	108.95	
HP Virgin Dense Graded									
VDG-12-C	H135A12H2C03	12.5	64-22	0	0	2002.67	1012.55	111.48	
VDG-12-F	H160A12H2F01	12.5	76-22	0	0	2031.44	992.97	104.06	

LRDG : Low Rap Dense Graded, WM-LRDG: Warm Mix Low Rap Dense Graded, HRDG: High Rap Dense Graded, RSDG: Rap Shingle Dense Graded, HRSDG: High Rap Shingle Dense Graded, LRG: Low Rap Gap, VG: Virgin Gap, VDG: Virgin Dense Graded, RAP: Recclaimed Asphalt Pavement, RAS: Reclaimed Asphalt Shingle, NMAS: Nomimal Maximum Aggregate Size

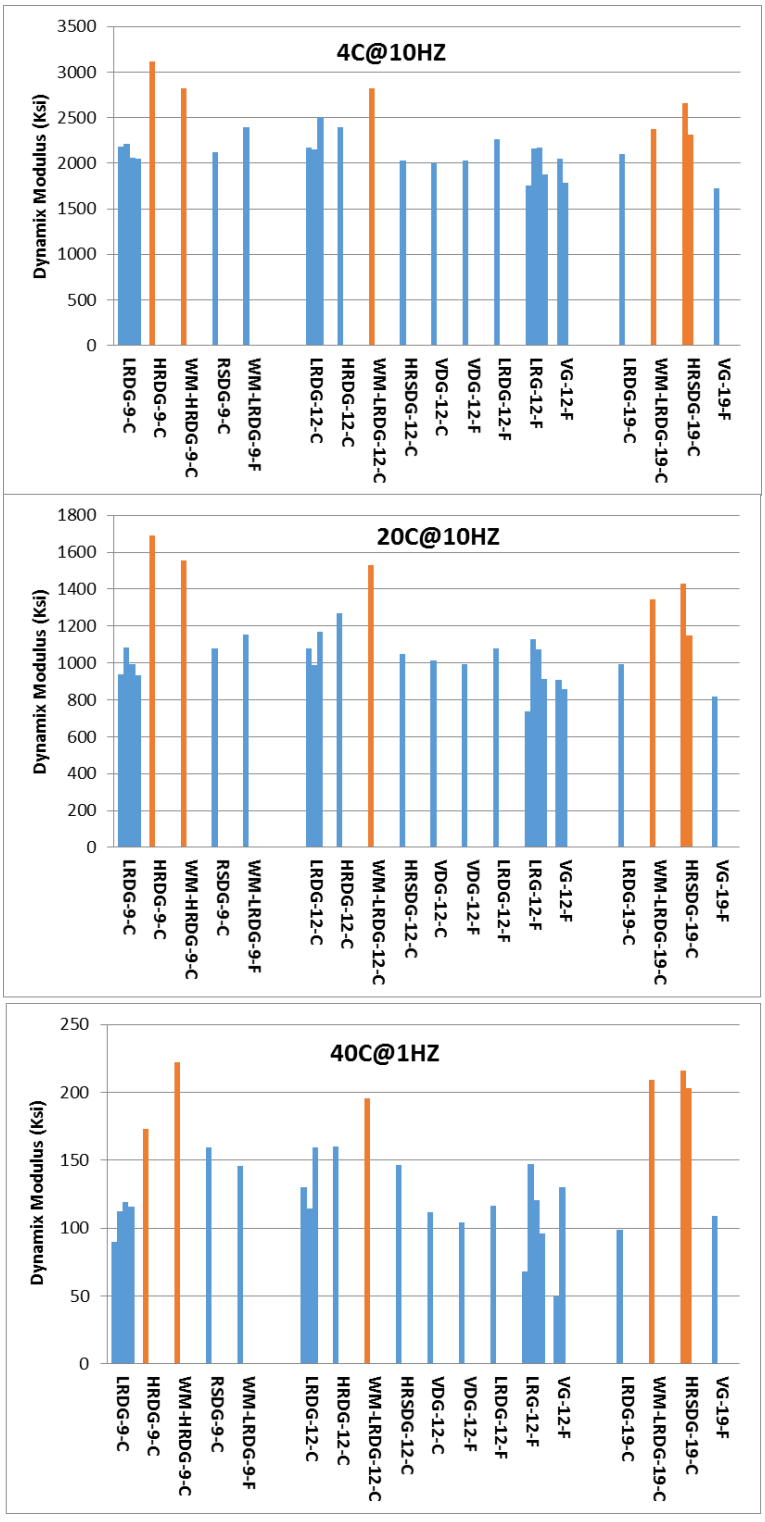

Figure 14: Comparison of E* Values of All Mixtures (Orange Bars Represents High RAP Dense Graded, High RAP/Shingles Dense Graded and Warm Mixes)

3.4.1 Ranking and Effect of Variables on E* Values of Asphalt Mixtures

As per Figure 14, the asphalt mixtures can be ranked based on their E* values measured at 4^{o}C@10Hz. Ranking of the mixtures is given in Table 8. The same ranking of the mixtures can be observed in E* values at 20^{o}C@10Hz and 40^{o}C@1Hz with one exception: the WM-HRDG-9-C mixture behaves comparatively better than HRDG-9-C at 40C@1Hz. This ranking can be used by Pavement and Geotechnical Division (PAGD) of MDSHA to select mixture type for pavement design in different climate conditions.

Table 8: Ranking of Mixtures Based on Their E* Values at 4^{o}C@10Hz

Ranking of Asphalt Mixtures		
Rank	**Type of Mixture**	**E* at 4C@10Hz**
1	HRDG-9-C	> 3000
2	WM-HRDG-9C, WM-LRDG-12-C, HRSDG-19-C	2500< E* <3000
3	WM-LRDG-9-F,HRDG-12-C, LRDG-12-F WM-LRDG-19-C	2250 < E* <2500
4	All other mixtures	< 2250

Based on previous studies (King et al., 2004, Tran and Hall, 2005), the aggregate source does not have a significant effect on E*. Subsequently, the quarry location/aggregate type used in the mixtures should not affect E*.

There are two types of gradations used in the mixtures: dense graded and gap graded. The average E* values of gap graded mixtures, and Low RAP (LR) dense graded mixtures, High RAP/WM (HR/WM) dense graded mixtures are shown in Figure 15. It can be seen from Figure 15 that the mixtures having gap gradation have lower average E* values at all loading frequencies and temperatures as compared to the dense graded mixtures (LR and HR/WM). The average E* values of HR/WM dense graded mixtures are significantly larger than average E* of gap graded mixtures by 32%, 43%, and 58% at

4ºC@10Hz, 20ºC@10Hz and 40C@1Hz, respectively. It is likely that both the mixture gradation and the presence of RAP contribute to these differences.

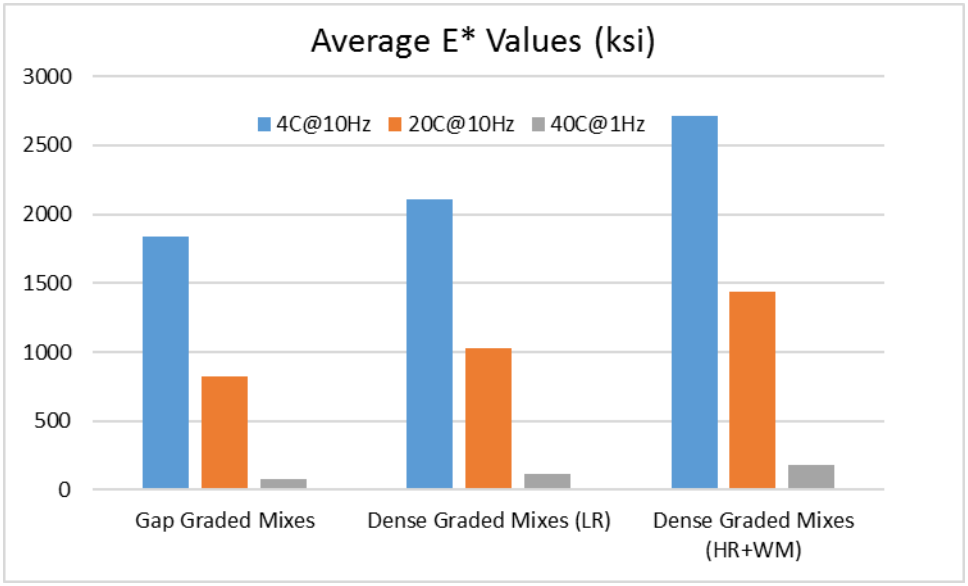

Figure 15: Comparison of Average E* Values of Gap Graded Mixes, Dense Graded (Low RAP) Mixes, and Dense Graded (High RAP and Warm Mixtures)

Box and whisker plots in Figure 16 summarize the variability in measured E* values segregated by NMAS (9mm, 12mm and 19mm). The error bars in the box and whisker plots show the minimum and maximum E* values while the boxes show the 25th, 50th, and 75th percentiles. The 12mm NMAS mixtures have the lowest variability as compared to the 9mm and 19mm NMAS mixtures. Within each NMAS category, the variability in E* decreases with decreasing frequency and increasing temperature. At high temperatures and low frequencies, the mixture behavior approaches that of a granular material as the viscosity of the binder becomes negligibly small.

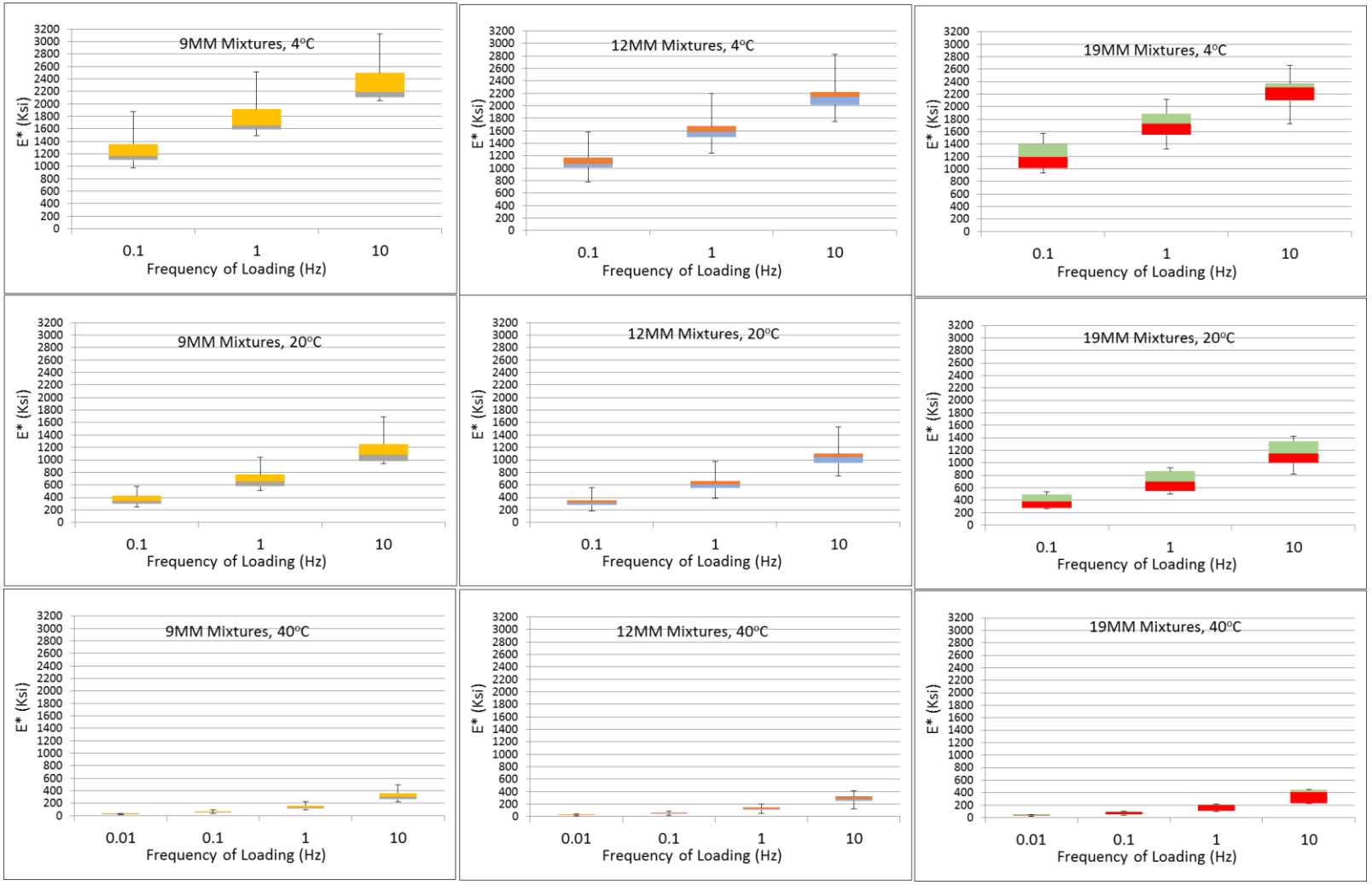

Figure 16: Box and Whisker Plots Representing Variability in E* Values in All Mixtures

3.4 Comparison of Measured E* Values with Predicted E* Values of Mixtures

The measured dynamic modulus values are defined as Level 1 inputs in the MEPDG software. In the absence of Level 1 inputs, Level 3 inputs consisting of predicted E* values calculated using the Witczak E* prediction model (Witczak and Fonseca, 1996) can be used:

$$\log E^* = 3.750063 + 0.029\rho_{200} - 0.0018{\rho_{200}}^2 - 0.0028\rho_4 - 0.058V_a - 0.822\frac{V_{eff}}{V_{eff}+V_a} + \frac{3.872-0.0021\rho_4+0.004\rho_{38}-0.000017({\rho_{38}}^2)+0.0055\rho_{34}}{1+e^{(-0.603313-0.313351\log f-0.393532\log \eta)}} \quad \text{Equation (6)}$$

in which

E* = Dynamic modulus of mix, 10^5 psi

η = Viscosity of binder, 10^6 Poise

f = Loading frequency, Hz

ρ_{200} = % passing #200 (0.075mm) sieve

ρ_4 = Cumulative % retained on #4 (4.75mm) sieve

ρ_{38} = Cumulative % retained on 3/8 inch (9.5mm) sieve

$\rho_{3/4}$ = Cumulative % retained on 3/4 inch (19mm) sieve

V_a = Air void, % by volume

V_{beff} = Effective binder content, % by volume.

Equation 6 was used to predict E* values for all mixtures tested in this study. Figure 17 plots the predicted (MEDPG Level 3) vs. measured (MEDPG Level 1) E* values for all mixtures. It is clear from Figure 17 that the Witczak E* prediction model tends to underpredict the E* values, as most of the data points are either on or below the line of

equality. This underprediction of E* may result in over or under prediction of the distresses in the pavement structure over its design life.

Figure 18 depicts the ranges in prediction errors for different NMAS mixtures at 4°C@10Hz, 20°C@10Hz and 40°C@1Hz. It can be seen that the prediction errors increase as the frequency of loading increases and decrease as the temperature increases. The range of errors is high in the 9mm NMAS mixtures at all three temperatures/loading rate combinations as compared to the 12mm and 19mm NMAS mixtures. The range of errors in the 12mm NMAS mixture is the smallest among the three types of mixtures.

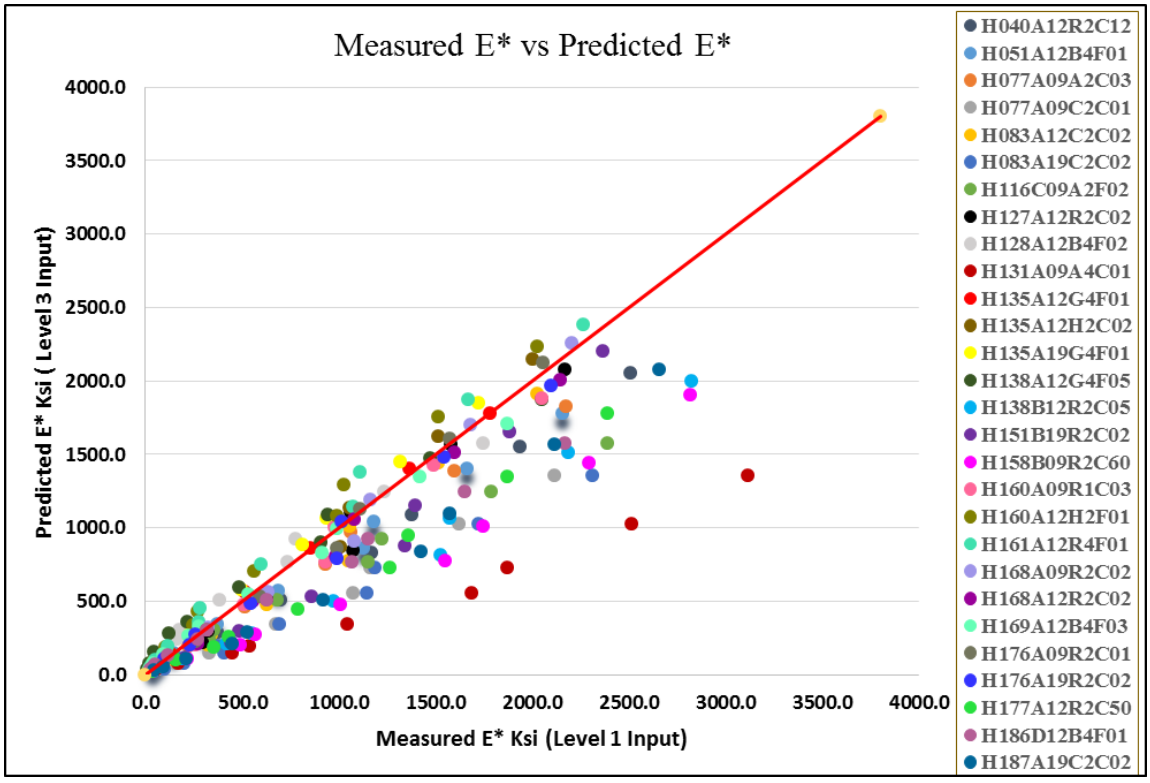

Figure 17: Comparison of Level 3 and Level 1 Dynamic Moduli in MEPDG

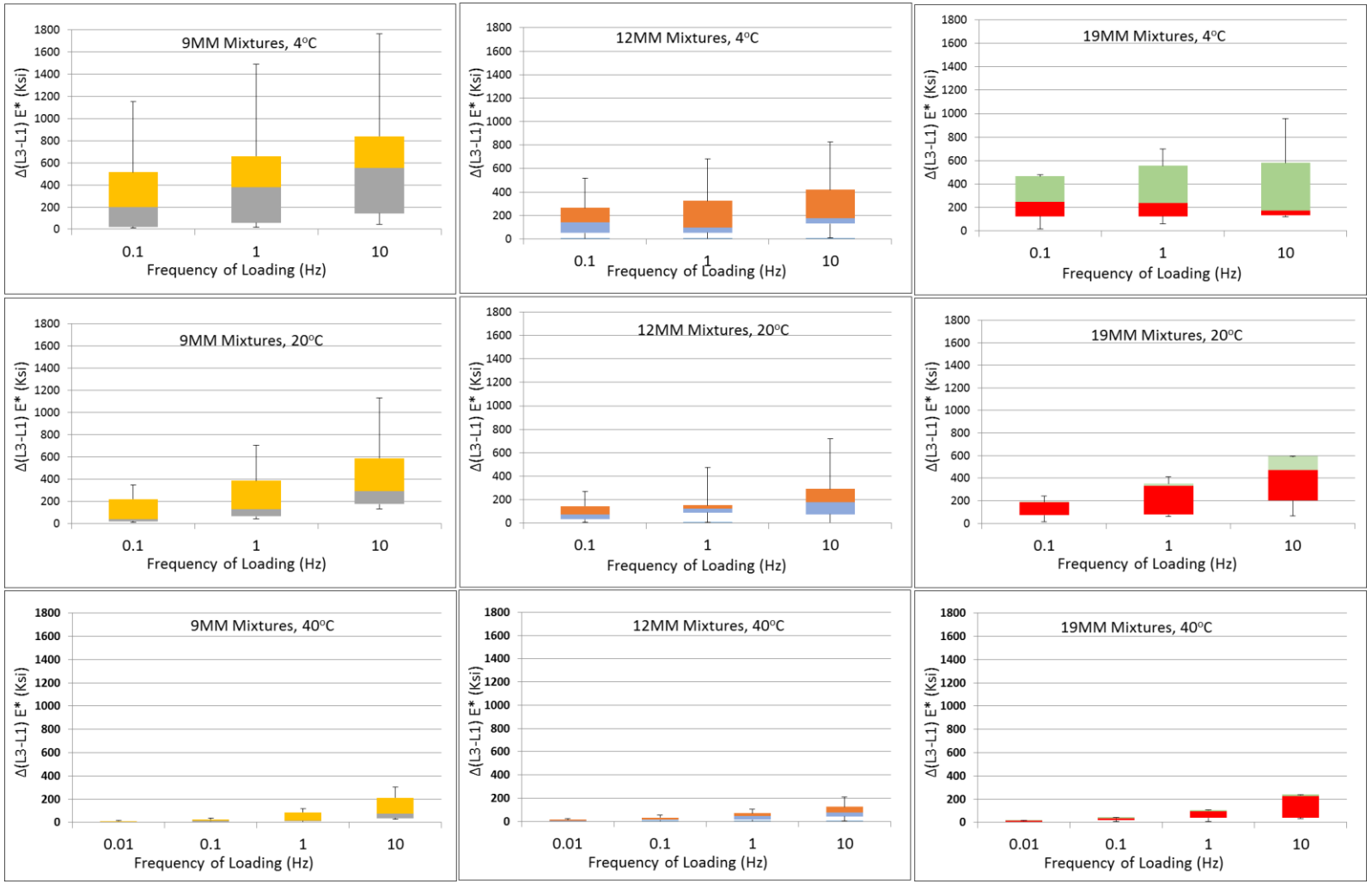

Figure 18: Variability in Errors in 9mm, 12mm and 19mm NMAS Mixtures

The MEPDG software develops master curve internally once the measured Level 1 or predicted Level 3 E* data is input. Example comparisons of master curves based on predicted E* values versus measured E* values are shown in Figure 19. Only two cases are shown here for the limiting cases of "best" (Figure 19a) and "worst" agreement (Figure 19b). Comparisons for all mixtures are given in APPENDIX B (Figure B-54 a to m). These differences in the master curves, particularly in the case of poor agreement, could have a significant effect on the prediction of distresses in the pavement structure.

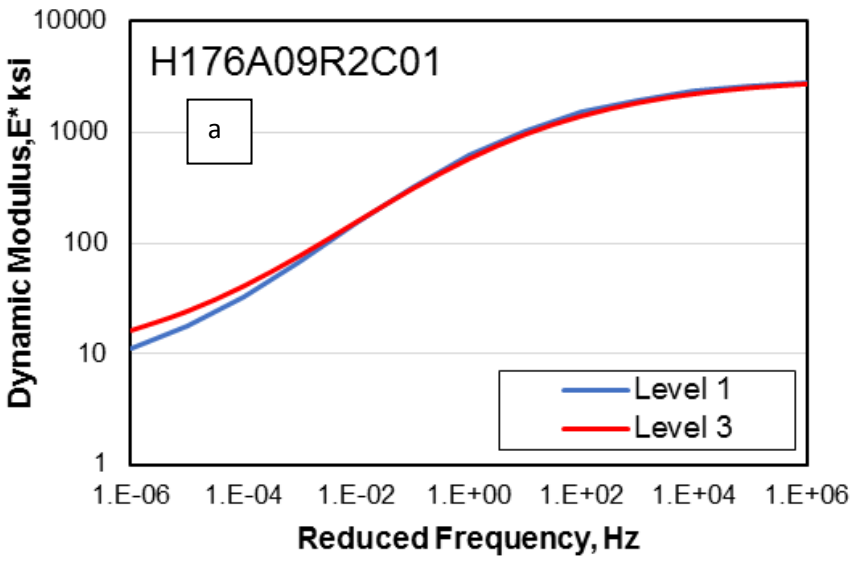

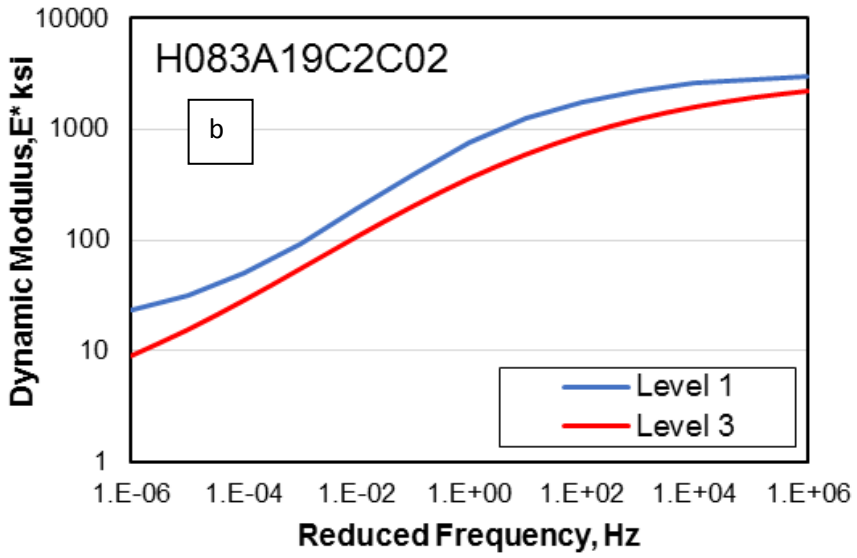

Figure 19: Comparison of Master Curves Developed by Level 1 and Level 3 E* Input (a) "Best" Agreement (b) "Worst" Agreement

CHAPTER 4: PERMANENT DEFORMATION TEST DATA AND ANALYSIS

4.1 RLPD Test Results

Permanent deformation (rutting) distress in flexible pavements is related to loading and temperature. Rutting normally occurs under the wheel paths and negatively affects the ride quality of the pavement. Ruts filled with water can cause hydroplaning, a situation where tires become separated from the pavement surface by a layer of water, which can cause the vehicle to skid.

Rutting is a combination of two phenomena: densification and shear flow. Densification is associated with mixture volume changes and usually occurs early in the pavement life. Shear flow is plastic flow with little or no volume change. Shear flow starts when the aggregate structure of the mixture cannot withstand traffic loads, especially at high temperatures when the stiffness of the binder and therefore the mixture drops. It is mainly shear flow that causes deep ruts that lead to the eventual failure of the pavement.

In the RLPD test, repeated load cycles are applied to a cylindrical asphalt concrete specimen and the cumulative permanent deformation as a function of the number of load cycles is recorded. A single load cycle consists of a 0.1-second haversine pulse load followed by a 0.9-second rest period; typically, about 10,000 load cycles are applied in each test. As recommended in the NCHRP Project 9-30A (Von Quintus et al., 2011), a deviator stress of 70 psi and a confining stress of 10 psi are applied throughout the 10,000 cycles of loading at low (20^{o}C), medium (40^{o}C) and high (58^{o}C) temperatures. All RLPD testing in this study were performed under confined conditions. RLPD test results are usually presented in terms of the cumulative permanent strain (ϵ_r) versus the number of

loading cycles (*N*) in log-log space. A typical RLPD permanent strain versus number of loading cycles relationship was shown in Figure 6 (Chapter 2). The cumulative permanent strain curve is divided into the following three stages:

- Primary stage: Most material densification (volume change) occurs in this stage. This stage corresponds to the initial rutting typically observed in the field during the first year or two of pavement life.
- Secondary Stage: The secondary stage of the RLPD response is of main concern. This is a stable shear flow stage in which permanent deformations (rutting) accumulate at a constant rate in log-log space. In log space the slope is flat, but the derivative in arithmetic space is negative (exponent on N is less than 1), meaning that rutting per cycle decreases during the secondary stage. Good performing pavements are expected to stay within the secondary stage for their entire service life. Therefore, the data from the secondary stage of the RLPD test is used to characterize the permanent deformation behavior of asphalt mixtures and to calibrate the MEPDG rutting model. As per NCHRP Project 9-30A (Von Quintus et al., 2011), this portion of the test starts when the slope of accumulated permanent strain vs. number of loading cycles becomes almost constant in log-log space. Based on the test data collected in this study, the secondary stage of the RLPD test was defined as starting after 2000 cycles of loading in all mixtures.
- Tertiary stage. Rutting during this stage is caused mainly by unstable shear deformation to failure. The number of cycles that corresponds to the beginning of this stage is referred to as the *Flow Number* (FN).

The results of the RLPD tests for all 28 mixtures included in this research work are presented in Figure 20. All mixtures were tested at air voids of 7.0 ± 0.5% per AASHTO TP 79 at the NCHRP Project 9-30A recommended test temperatures of 20°C, 40°C and 58°C. Two to three test replicates were tested for each set of test conditions; the curves in Figure 20 represent the averages of the replicates. None of the mixtures went into the tertiary stage during the tests and therefore the flow number (FN) values are greater than 10,000 cycles, indicating that these mixes are acceptable in terms of rutting performance.

The average accumulated permanent microstrains of all asphalt mixtures at 1000, 5000, and 10,000 cycles are tabulated in Table 9 and compared at 40°C in Figure 21. Only results for 40°C are shown since nearly all rutting in pavements occurs at high temperatures. As can be seen from Figure 21, High RAP and WM asphalt mixtures regardless of their NMAS (highlighted in orange) have lower accumulated permanent microstrains at 1000, 5000 and 10,000 cycles of loading as compared to the all other mixtures with the exception of virgin dense graded mixture (highlighted in purple). This finding is consistent with the ranking of mixtures based on their E* values, as given earlier in Table 8. The same ranking (best to worst) of mixtures based on E* shown in Table 8 is generally consistent with the rankings based on accumulated permanent microstrains of mixtures.

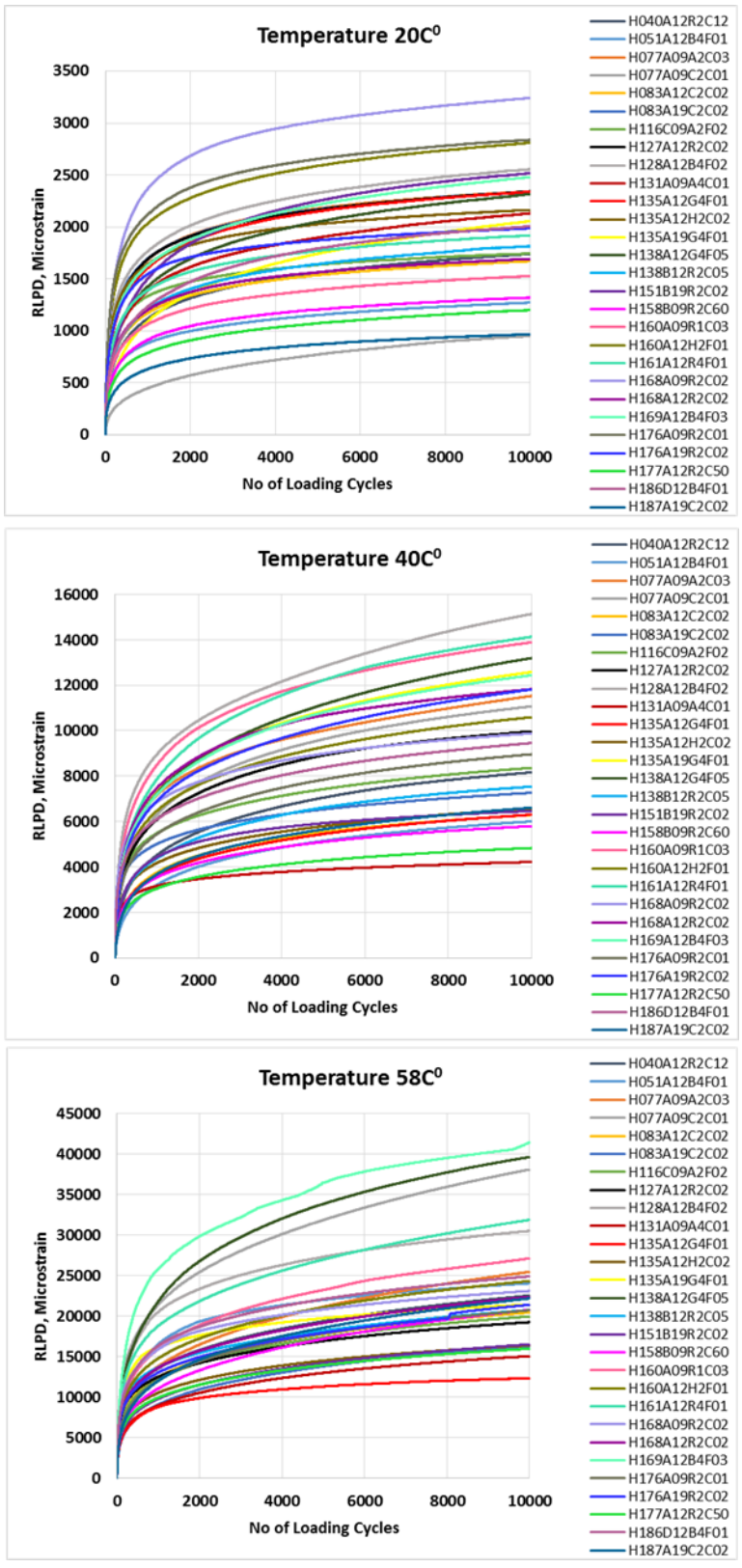

Figure 20: Accumulated Permanent Microstrains of All Mixtures at 20ºC, 40ºC and 58ºC

Table 9: Average Accumulated Microstrains for All Asphalt Mixtures at 1000, 5000 And 10,000 Loading Cycles at 20°C, 40°C, 58°C

Type	Mixture	NMAS	PG Binder	RAP (%)	RAS (%)	Microstrain @ 20C°			Microstrain @ 40C°			Microstrain @ 58C°		
						1000 Cycles	5000 cycles	10000 Cycles	1000 Cycles	5000 cycles	10000 Cycles	1000 Cycles	5000 cycles	10000 Cycles
Low RAP Dense Graded														
LRDG-9-C	H077A09A2C03	9.5	64-22	15	0	1688	2179	2342	7172	10007	11529	13801	21139	25437
	H168A09R2C02			15	0	2371	3019	3241	6861	8985	9879	15910	20823	23091
	H176A09R2C01			10	0	2121	2654	2838	5451	7843	8960	12074	17840	20710
	H160A09R1C03			15	0	1065	1395	1528	8497	12226	13888	15953	23209	27109
WM-LRDG-9-F	H116C09A2F02	9.5	76-22	15	0	1336	1636	1744	5487	7423	8361	12173	17376	19939
LRDG-12-C	H127A12R2C02	12.5	64-22	19	0	1693	2163	2342	6094	8916	9961	12490	16920	19234
	H168A12R2C02			19	0	1203	1563	1691	7478	10674	11827	13611	19155	22347
	H040A12R2C12			19	0	1119	1559	1741	4521	7050	8164	13560	19350	22526
WM-LRDG-12-C	H138B12R2C05	12.5	64-22	15	0	1211	1641	1815	4385	6613	7535	13678	18175	20743
LRDG-12-F	H161A12R4F01	12.5	76-22	10	0	1392	1770	1918	7870	12220	14133	18787	26973	31861
WM-LRDG-19-C	H151B19R2C02	19	64-22	15	0	1506	2250	2516	4430	5925	6465	9787	14195	16496
LRDG-19-C	H176A19R2C01			10	0	1548	1871	1987	6913	10170	11813	13020	17933	21375
High RAP-RAS-HP-Dense Graded														
RSDG-9-C	H077A09C2C01	9.5	64-22	14	5	448	771	950	6305	9623	11070	21394	31847	38073
WM-HRDG-9-C	H158B09R2C60			40	0	915	1204	1319	3551	5104	5792	11063	17169	20756
HRDG-9-C	H131A09A4C01			28	0	1392	1896	2131	3164	3883	4216	8958	12981	15040
HRSDG-12-C	H083A12C2C02	12.5	64-22	14	5	1173	1537	1670	3753	5535	6290	12442	17777	20428
HRDG-12-C	H177A12R2C50			25	0	789	1072	1200	3053	4284	4835	9928	13940	15962
HRSDG-19-C	H187A19C2C02	19	64-22	17	5	633	870	967	3680	5654	6606	12004	18549	22167
	H083A19C2C02			18	5	1697	2167	2336	5008	6535	7264	9074	13785	16309
Low RAP-GAP Graded														
LRG-12-F	H128A12B4F02	12.5	76-22	15	0	1768	2326	2555	8958	12815	15136	20520	27291	30495
	H051A12B4F01			10	0	884	1151	1271	3208	5146	6010	16528	21983	24029
	H186D12B4F01			12	0	1236	1793	2006	6111	8379	9454	16347	22079	24886
	H169A12B4F03			15	0	1632	2214	2479	7196	10808	12437	25796	36453	41423
Virgin GAP Graded														
VG-12-F	H138A12G4F05	12.5	76-22	0	0	1429	2049	2315	7247	11154	13196	21798	33830	39617
	H135A12G4F01			0	0	1609	2150	2339	3647	5453	6301	8780	11300	12325
VG-19-F	H135A19G4F01	19	76-22	0	0	1095	1742	2055	7294	10867	12583	16144	19728	21407
HP Virgin Dense Graded														
VDG-12-C	H135A12H2C03	12.5	64-22	0	0	1645	2027	2163	4173	5793	6517	10529	14492	16369
VDG-12-F	H160A12H2F01	12.5	76-22	0	0	2036	2587	2809	6475	9278	10589	14769	21065	24312

LRDG : Low Rap Dense Graded, WM-LRDG: Warm Mix Low Rap Dense Graded, HRDG: High Rap Dense Graded, RSDG: Rap Shingle Dense Graded, HRSDG: High Rap Shingle Dense Graded, LRG: Low Rap Gap, VG: Virgin Gap, VDG: Virgin Dense Graded, RAP: Recclaimed Asphalt Pavement, RAS: Reclaimed Asphalt Shingle, NMAS: Nomimal Maximum Aggregate Size

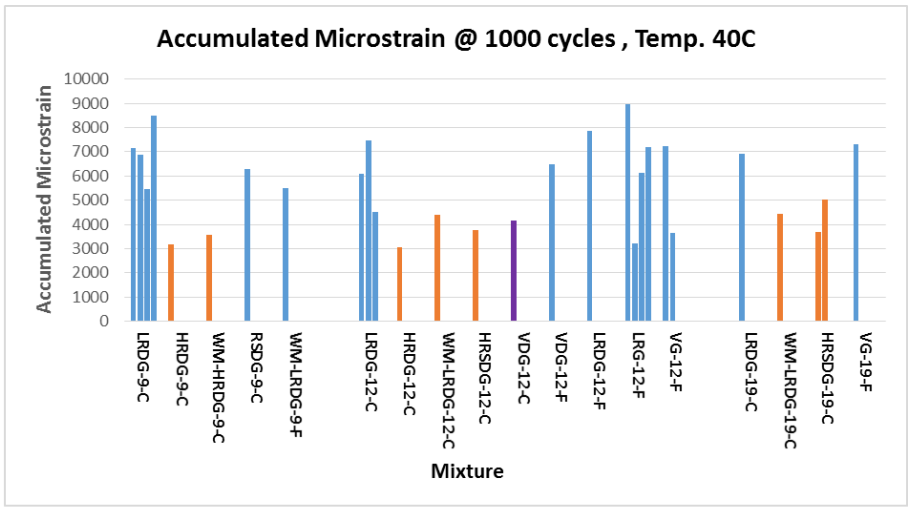

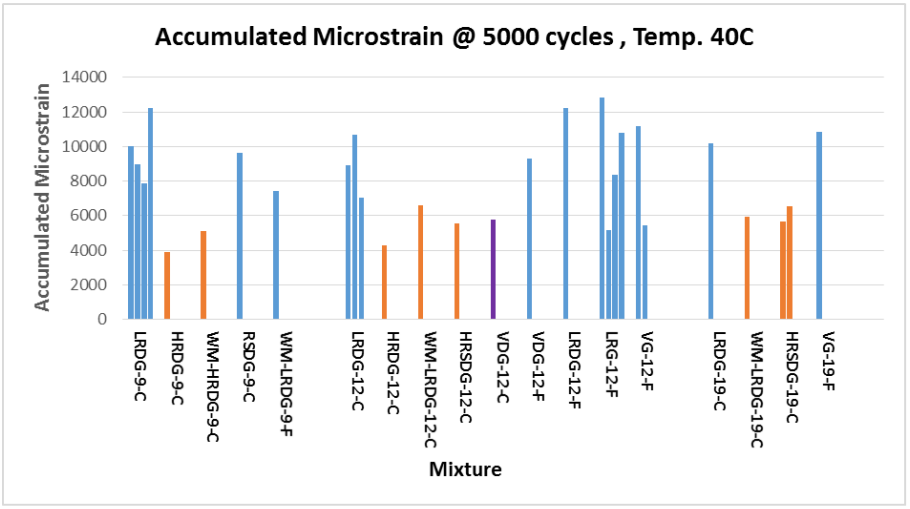

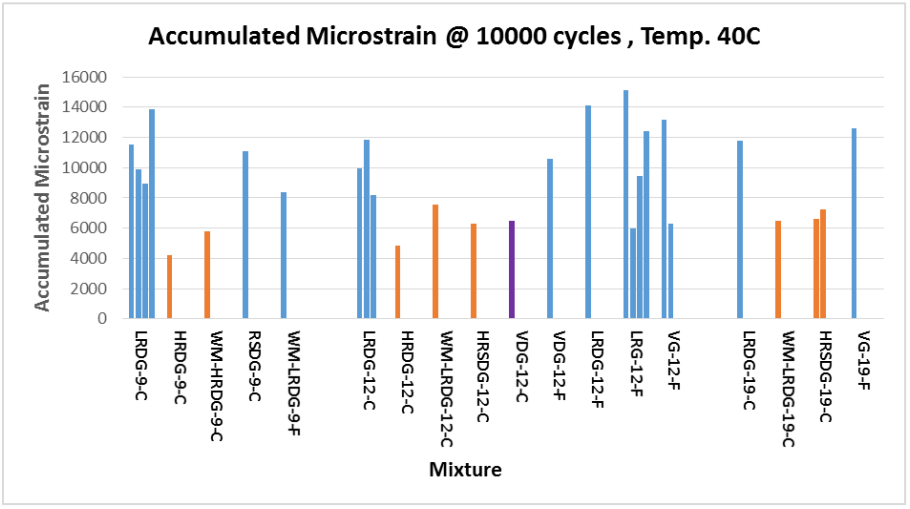

Figure 21: Comparison of Permanent Deformations of All Mixtures at 40ºC (Orange Represents the High RAP Dense Graded (HRDG), High RAP/Shingle Dense Graded (HRSDG) and Warm Mixes (WM), Purple Line Represents Virgin Dense Graded (VDG)

The type of mix such as high RAP or low RAP or virgin mix or warm mix, has significant effect on the permanent deformation of the mixture which can be seen from Figure 22.The mixtures having high RAP and warm mixes have less permanent deformation as compared to other mixtures. The performance grade of the virgin binder in the mixture changes with the addition of RAP in it because the binder coming from the RAP material in the mix is aged binder and consequently, increases the stiffness of the virgin binder in the mixture. This increase in the stiffness of the binder results into more resistance to permanent deformation at high temperatures. This could be a reason that high RAP and warm mixtures with RAP get less permanent deformations at high temperatures as compared to other mixtures.

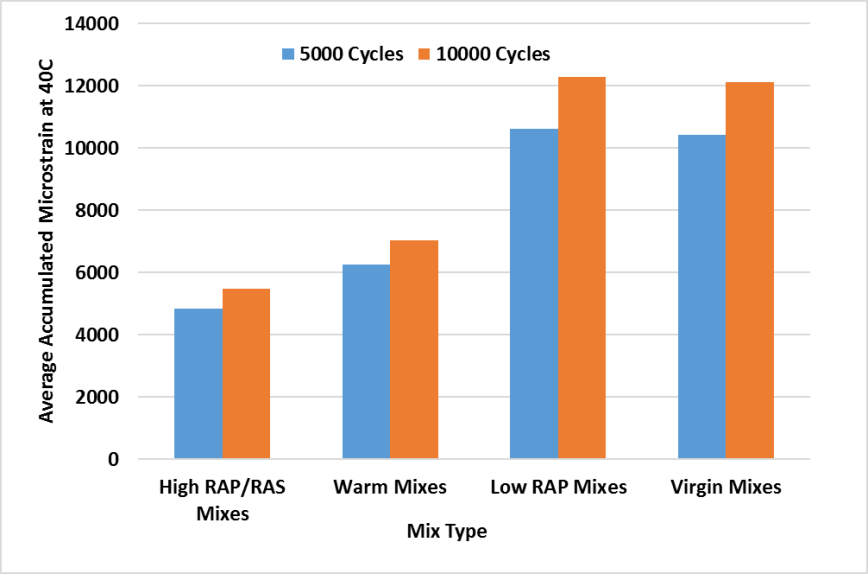

Figure 22: Average Accumulated Microstrains of Different Type of Asphalt Mixtures at 40ºC

In order to see the variation of permanent deformations with respect to mixture properties, the accumulated permanent microstrains of all mixtures at 5000 cycles of loading at three temperatures (20^{o}C, 40^{o}C, 58^{o}C) are plotted against mixture volumetric properties, gradation parameters, and asphalt binder contents in Figure 23. The coefficient of determination (R^2) values are very low in all graphs ($R^2 < 0.25$), indicating that the variations in permanent deformation is not well correlated with mixture properties. The volumetric properties, gradation and binder contents of the mixtures have little systematic effect on the permanent deformation of the mixtures included in this research study.

The box and whisker plots are shown in Figure 24 summarize the variability in the accumulated permanent microstrains with respect to the NMAS of mixtures at three temperatures. The following observations can be drawn from Figure 24.

- The 19mm mixtures have less accumulated permanent microstrains at all temperatures than the 12mm and 9mm mixtures.
- The accumulated permanent microstrains of the mixtures are more variable at 40^{o}C as compared to 20^{o}C and 58^{o}C. The least variability is observed in the accumulated permanent microstrains of mixtures at 58^{o}C.
- The 9mm mixtures have higher variability in accumulated permanent microstrains at 20^{o}C as compared to 12mm and 19mm mixtures at the same temperature.
- The variability in accumulated permanent microstrains of 19mm mixtures is comparatively less at 58^{o}C as compared to 9mm and 12mm mixtures.

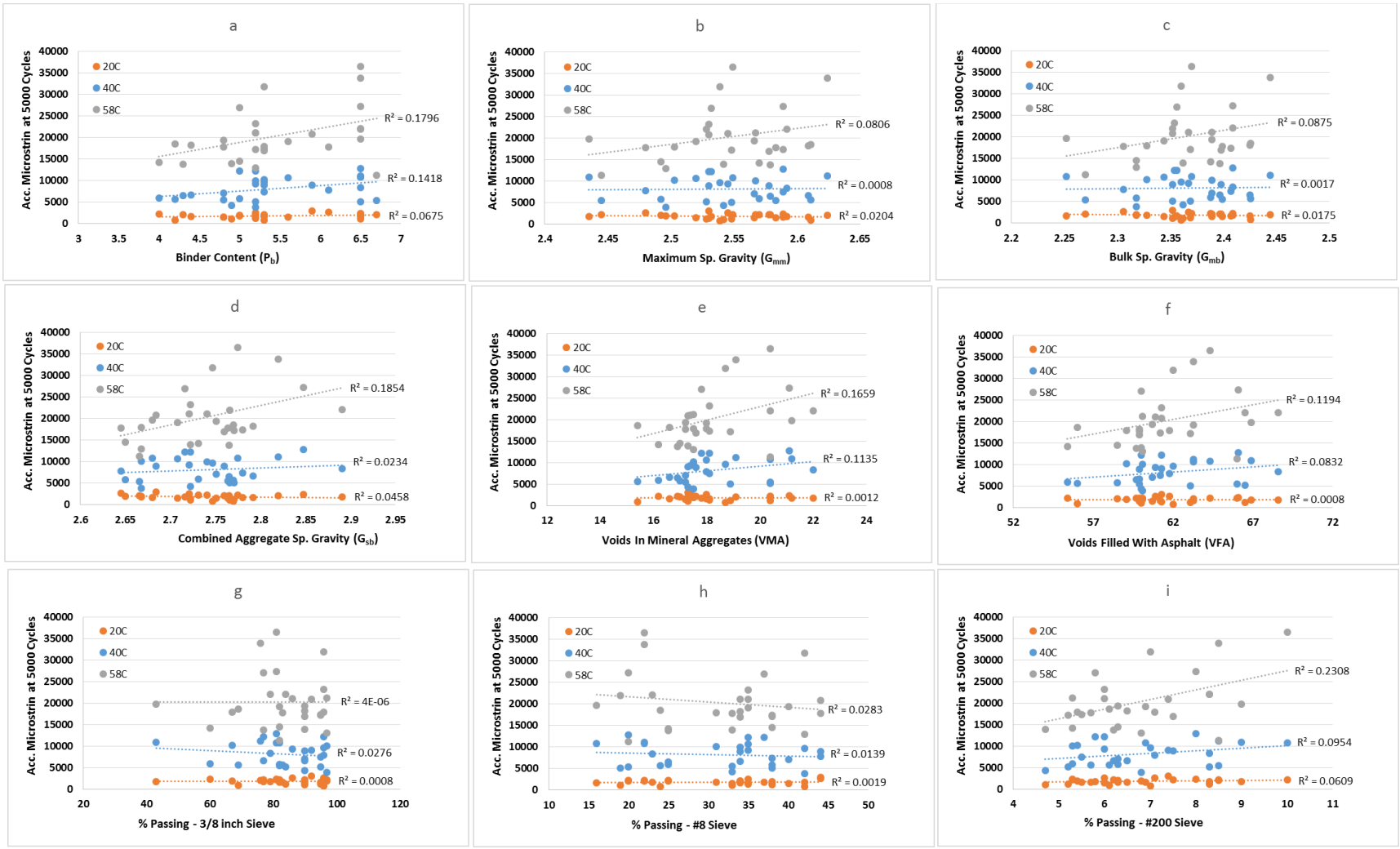

Figure 23: Variation in Permanent Deformation with Respect to Mixtures Properties

Figure 24: Variation in RLPD Test Results of All Mixtures at 20ºC, 40ºC, 58ºC

The secondary stage of the RLPD test is most important for characterizing the permanent deformation behavior of the mixtures. Accumulated permanent microstrains in the secondary stage are plotted against numbers of cycles of loading in log-log space in Figure 25 for all mixtures at 20^{o}C, 40^{o}C and 58^{o}C. The relationship between the accumulated permanent microstrains and number of loading cycles can be represented by the following power model:

$$\epsilon_p = aN^b \qquad \text{Equation (7)}$$

in which

ϵ_p = Accumulated permanent microstrains

N = Number of loading cycles

a,b = Model coefficients (fitting parameters)

The "a" and "b" coefficients of the model at 20^{o}C, 40^{o}C and 58^{o}C along with the corresponding R^2 values are shown in Table 10. The coefficient "a" represents the intercept and coefficient "b" represents the slope of the linear representation of the power model in log-log space. The average slope of mixtures at 20^{o}C is twenty-five percent less than that average slope at 40^{o}C and 58^{o}C, as shown in Figure 26. The average slope of the mixtures at 40^{o}C is same as at 58^{o}C.

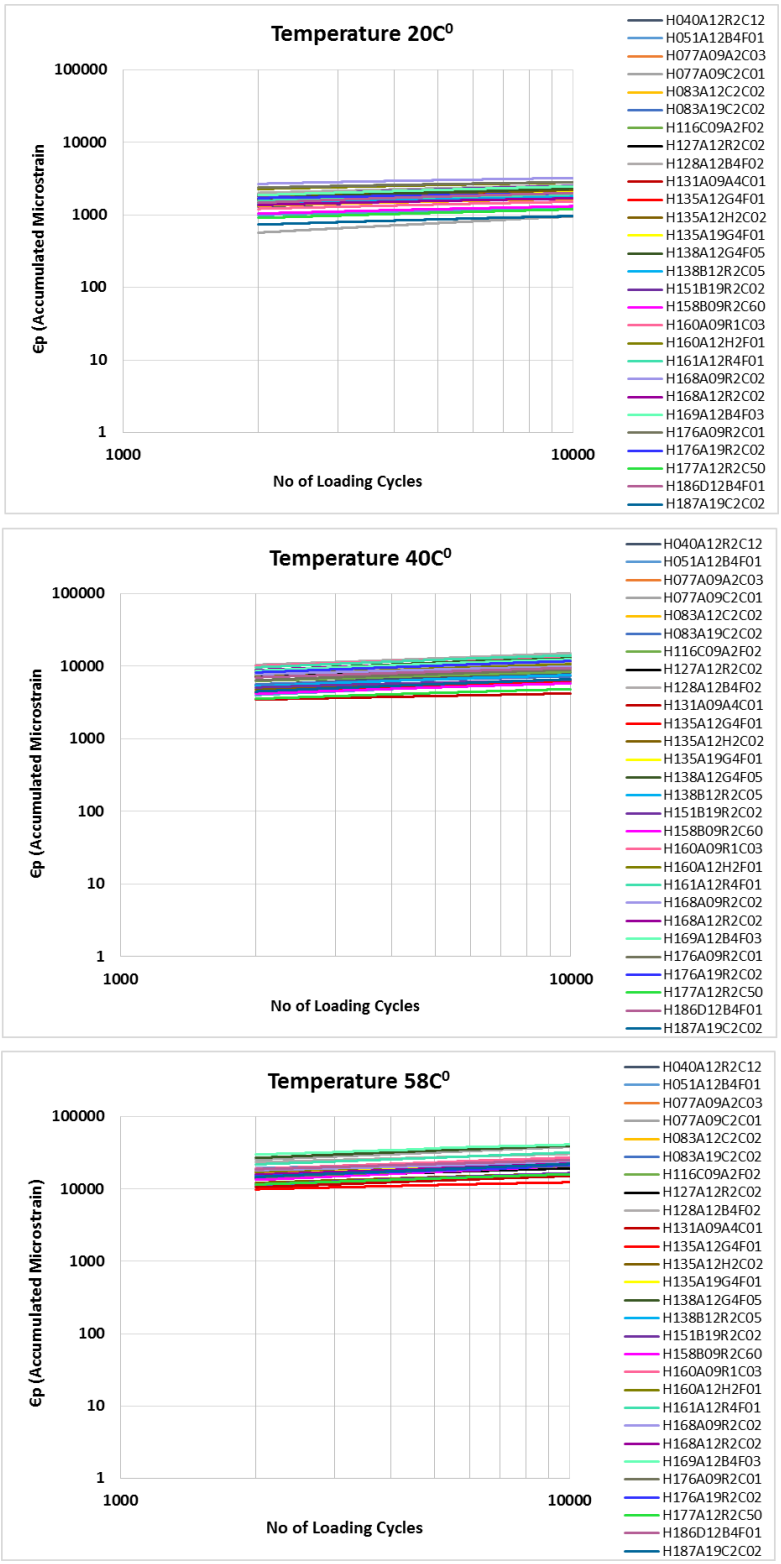

Figure 25: Secondary Portion of RLPD Test Results of All Mixtures at 20°C, 40°C, and 58°C

Table 10: Coefficients of Power Model Fitted for Secondary Portion of RLPD Tests at 20ºC, 40ºC and 58ºC

Type	Mixture	NMAS	PG Binder	RAP (%)	RAS (%)	20C			40C			58C		
						a	b	R^2	a	b	R^2	a	b	R^2
Low RAP Dense Graded														
LRDG-9-C	H077A09A2C03	9.5	64-22	15	0	793.44	0.12	0.99	1893.6	0.2	0.99	2088.7	0,27	0.99
	H168A09R2C02			15	0	1166.1	0.11	0.99	2508.5	0.15	0.99	5803.3	0.15	0.99
	H176A09R2C01			10	0	1071.3	0.11	0.99	1337.2	0.21	0.99	2644.4	0.22	0.99
	H160A09R1C03			15	0	359.88	0.14	0.99	915.9	0.2	0.99	3449.6	0.22	0.99
WM-LRDG-9-F	H116C09A2F02	9.5	76-22	15	0	679.23	0.1	0.99	1611.3	0.18	0.99	2947.6	0.21	0.99
LRDG-12-C	H127A12R2C02	12.5	64-22	19	0	754.46	0.12	0.99	1710.2	0.19	0.99	3378.1	0.19	0.99
	H168A12R2C02			19	0	537.49	0.12	0.99	2458.4	0.17	0.99	2924.5	0.22	0.99
	H040A12R2C12			19	0	366.11	0.17	0.99	921.03	0.23	0.99	2952.6	0.22	0.99
WM-LRDG-12-C	H138B12R2C05	12.5	64-22	15	0	434.73	0.16	0.99	1031.8	0.22	0.99	3742.7	0.19	0.99
LRDG-12-F	H161A12R4F01	12.5	76-22	10	0	623.31	0.12	0.99	1652.7	0.23	0.99	3598.1	0.23	0.99
WM-LRDG-19-C	H151B19R2C02	19	64-22	15	0	448.3	0.19	0.99	1778.3	0.14	0.99	2119.3	0.22	0.99
LRDG-19-C	H176A19R2C01			10	0	855.24	0.09	0.99	1499.4	0.22	0.99	2717.8	0.22	0.99
High RAP-RAS-HP-Dense Graded														
RSDG-9-C	H077A09C2C01	9.5	64-22	14	5	51.48	0.32	0.99	1464	0.22	0.99	3705.5	0.25	0.99
WM-HRDG-9-C	H158B09R2C60			40	0	359.88	0.14	0.99	915.9	0.2	0.99	1602.1	0.28	0.99
HRDG-9-C	H131A09A4C01			28	0	447.28	0.17	0.99	1387	0.12	0.99	1957.6	0.22	0.99
HRSDG-12-C	H083A12C2C02	12.5	64-22	14	5	492.51	0.13	0.99	981.83	0.2	0.99	2961.8	0.21	0.99
HRDG-12-C	H177A12R2C50			25	0	252.54	0.17	0.99	867.2	0.19	0.99	2572.3	0.2	0.99
HRSDG-19-C	H187A19C2C02	19	64-22	17	5	208.95	0.17	0.99	741.92	0.24	0.99	2060.8	0.26	0.99
	H083A19C2C02			18	5	781.69	0.12	0.99	1722.9	0.16	0.99	1651.7	o.25	0.99
Low RAP-GAP Graded														
LRG-12-F	H128A12B4F02	12.5	76-22	15	0	675.82	0.14	0.99	1755.8	0.23	0.99	6680.1	0.17	0.99
	H051A12B4F01			10	0	319.93	0.15	0.99	626.05	0.25	0.99	7048.1	0.13	0.99
	H186D12B4F01			12	0	365.39	0.19	0.99	1736.7	0.18	0.99	4831.4	0.18	0.99
	H169A12B4F03			15	0	519.06	0.17	0.99	1620.8	0.22	0.99	6391.5	0.2	0.99
Virgin GAP Graded														
VG-12-F	H138A12G4F05	12.5	76-22	0	0	406.08	0.19	0.99	1297.8	0.25	0.99	4307.5	0.24	0.99
	H135A12G4F01			0	0	660.49	0.14	0.99	779.69	0.23	0.99	3523.9	0.14	0.99
VG-19-F	H135A19G4F01	19	76-22	0	0	203.89	0.25	0.99	1622.6	0.22	0.99	6990.2	0.12	0.99
HP Virgin Dense Graded														
VDG-12-C	H135A12H2C03	12.5	64-22	0	0	840.87	0.1	0.99	1146.8	0.19	0.99	2947.9	0.19	0.99
VDG-12-F	H160A12H2F01	12.5	76-22	0	0	869.85	0.13	0.99	1639.8	0.2	0.99	3402	0.21	0.99

LRDG : Low Rap Dense Graded, WM-LRDG: Warm Mix Low Rap Dense Graded, HRDG: High Rap Dense Graded, RSDG: Rap Shingle Dense Graded, HRSDG: High Rap Shingle Dense Graded, LRG: Low Rap Gap, VG: Virgin Gap, VDG: Virgin Dense Graded, RAP: Recclaimed Asphalt Pavement, RAS: Reclaimed Asphalt Shingle, NMAS: Nomimal Maximum Aggregate Size

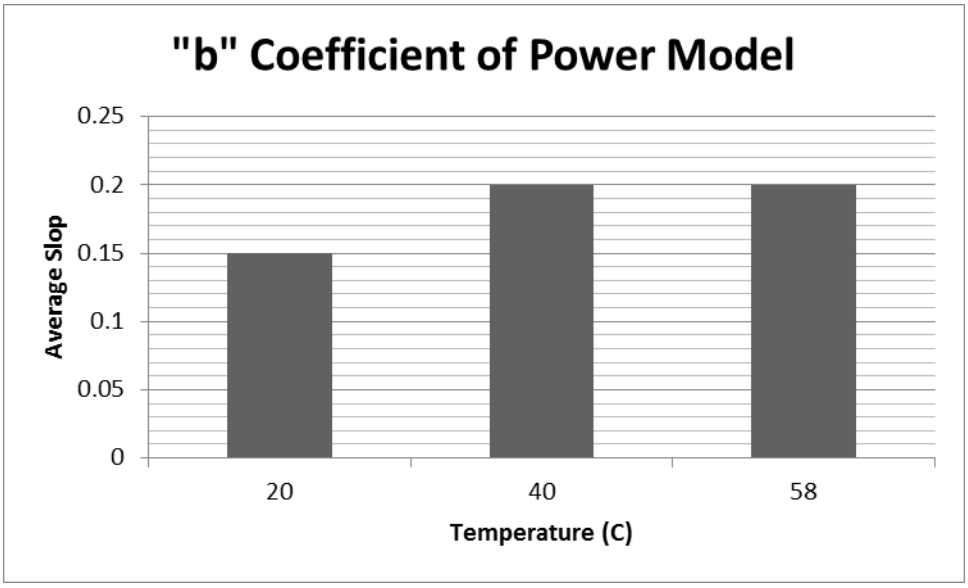

Figure 26: Average Slope of the Secondary Portion of the Permanent Deformation Response

4.2 Calibration of MEPDG Rut Model

The MEPDG utilizes an incremental approach to predict the total rut depth in a pavement structure. Rutting is predicted at the mid-depth of each sublayer of the pavement system. Total rut depth is calculated as the summation of the rut depths accumulated in all unbound and bound sublayers. Equation 8 shows the rut model currently incorporated in the MEPDG for asphalt concrete layers.

$$\frac{\epsilon_p}{\epsilon_r} = K_z B_1 10^{K_1}(T)^{K_2 B_2}(N)^{K_3 B_3} \quad \text{Equation (8)}$$

in which

ϵ_r = resilient strain at the middle of the sublayer

ϵ_p = plastic strain at the middle of the sublayer

T = temperature at the middle of the sublayer

N = number of axle loads

B_1, B_2, B_3 = global calibration coefficient (default values equal to 1)

K_1 = material constant (default value = -3.35412 in MEPDG)

K_2 = material constant (default value = 1.5606 in MEPDG)

K_3 = material constant (default value of 0.4791 in MEPDG)

K_z = depth function defined as:

$$K_z = (C_1 + C_2 D)(0.328196)^D$$

in which

$$C_1 = -0.1039 H_{HMA}^2 + 2.4868 H_{HMA} - 17.342$$

$$C_1 = 0.0172 H_{HMA}^2 - 1.733 H_{HMA} + 27.428$$

D = depth below the surface in inches

H_{HMA} = total HMA thickness in inches

For calibration of MEPDG rut model based on laboratory RLPD data, the Equation 8 has been simplified by setting B1, B_2, B_3 = 1. These factors can be changed during the field calibration process. The depth factor (K_z) is considered constant and equal to 1 for the purposes of analyzing laboratory test data. This yields Equation 9:

$$\frac{\epsilon_p}{\epsilon_r} = 10^{K_1}(T)^{K_2}(N)^{K_3} \quad \text{Equation (9)}$$

By taking the base 10 logarithm on both sides, the Equation 10 can be written as follow

$$\text{Log}\left(\epsilon_p \mid \epsilon_r\right) = K_1 + K_2 \text{LogT} + K_3 \text{ Log N} \quad \text{Equation (10)}$$

The AMPT measures permanent strain (ϵ_p) at each cycle of loading in the RLPD test. The resilient strain (ϵ_r) remains constant throughout the RLPD test (Von Quintus et al., 2011) and can be calculated from the corresponding E* values at 20^{o}C at 10Hz, 40^{o}C at 10Hz, and 58 ^{o}C at 10Hz. The dynamic modulus tests were performed under unconfined conditions while the RLPD tests were performed under confined conditions so it was necessary to convert the unconfined E* values into confined E* values. The effect of confinement has been found to be significant at low reduced frequencies, i.e., high temperature and/or low loading frequency (Pellinen et al., 2002, Zhao et al., 2013). At higher temperatures the contribution of the asphalt binder is reduced and the mix behavior is governed mostly by the aggregate, which explains why confinement has a larger effect under these conditions.

According to Zhao et al. (2013), vertical shift factors for E* can be calculated from the following formula.

$$\ln \lambda(P, \omega_r) = \frac{C_1(e^{-C_2 P_o} - e^{-C_2 P})}{1 + e^{C_3 + C_4 ln(\omega_r)}} \quad \text{Equation (11)}$$

in which

$\ln \lambda (P, \omega_r)$ = vertical shift factor

$C_1 = 3.181$, $C_2 = 8.395$, $C_3 = 1.602$, $C_4 = 0.479$

$\ln (\omega_r)$ = reduced frequency

P = confining pressure (MPa)

P_o = reference pressure

The vertical shift factors were added to the unconfined ln(E*) values at reduced frequencies corresponding to 20°C-10Hz, 40°C-10Hz and 58°C-10Hz for all mixtures to estimate the equivalent confined E* values for the RLPD test conditions. The resilient strains were then calculated using the following formula.

$$\epsilon_r = \frac{Deviator\ Stress}{Confined\ E^*@\ 10Hz} \quad \text{Equation (12)}$$

For each asphalt mixture, RLPD testing was performed on a minimum two replicate specimens at 20°C, 40°C, and 58°C for 10,000 cycles. The values of $\frac{\epsilon_p}{\epsilon_r}$, temperature, T, and number of loading cycles, N, for each specimen were converted into log values and the Regression data analysis tool in Microsoft Excel was used to find the coefficients K_1, K_2, and K_3 in Equation 8 for each asphalt mixture. These coefficients are tabulated in Table 11.

Table 11: Recalibrated Coefficients of the MEPDG Rut Model

Mix No	Asphalt Mixtures	K_1 (Intercept)	K_2 (Temperature Coeff)	K_3 (Loading Cycles Coeff)	R^2
1	H040A12R2C12	-0.4738	0.8493	0.2125	0.85
2	H051A12B4F01	-0.9173	1.1447	0.1826	0.82
3	H077A09A2C03	-0.2408	0.6259	0.2125	0.73
4	H077A09C2C01	-2.5466	2.0596	0.2646	0.98
5	H083A12C2C02	-0.0810	0.5955	0.1813	0.76
6	H083A19C2C02	0.4012	0.3402	0.1826	0.52
7	H116C09A2F02	-0.4716	0.8591	0.1654	0.90
8	H127A12R2C02	-0.0681	0.6078	0.1835	0.52
9	H128A12B4F02	-0.0503	0.5755	0.1975	0.36
10	H131A09A4C01	0.7998	0.0901	0.1594	0.59
11	H135A12G4F01	-1.9407	1.5915	0.1954	0.91
12	H135A12H2C02	-0.5006	0.7948	0.1764	0.95
13	H135A19G4F01	-0.5434	0.8729	0.2052	0.82
14	H138A12G4F05	-0.6581	0.8609	0.2115	0.85
15	H138B12R2C05	-0.2206	0.7784	0.1933	0.91
16	H151B19R2C02	-0.8652	1.1622	0.1687	0.90
17	H158B09R2C60	-0.7580	1.0422	0.2075	0.97
18	H160A09R1C03	-0.6433	0.9944	0.1859	0.70
19	H160A12H2F01	-0.1890	0.6643	0.1928	0.85
20	H161A12R4F01	-0.9350	1.1163	0.2209	0.74
21	H168A09R2C02	1.0588	0.1128	0.1220	0.74
22	H168A12R2C02	-0.6022	0.8963	0.1917	0.73
23	H169A12B4F03	-0.2489	0.8064	0.1925	0.89
24	H176A09R2C01	0.4939	0.2632	0.1866	0.42
25	H176A19R2C02	-0.2575	0.6263	0.2100	0.71
26	H177A12R2C50	-0.7826	0.9524	0.2133	0.97
27	H186D12B4F01	-0.5294	0.8580	0.2062	0.98
28	H187A19C2C02	-1.2111	1.1810	0.2330	0.92

The five highlighted R^2 values in Table 11 are below 0.7, which indicates less accuracy of prediction. More variability in permanent deformation among the specimens of these five mixtures may result in low R^2 values.

The predicted $\frac{\epsilon_p}{\epsilon_r}$ values were calculated by using the recalibrated coefficients K_1, K_2, and K_3 values in Equation 8 at 5000 and 10000 cycles of loading and compared against measured values, as shown in Figure 27. The R^2 and slope values of the best fit regression lines are 0.86 and 0.91, respectively, which indicate good accuracy of prediction.

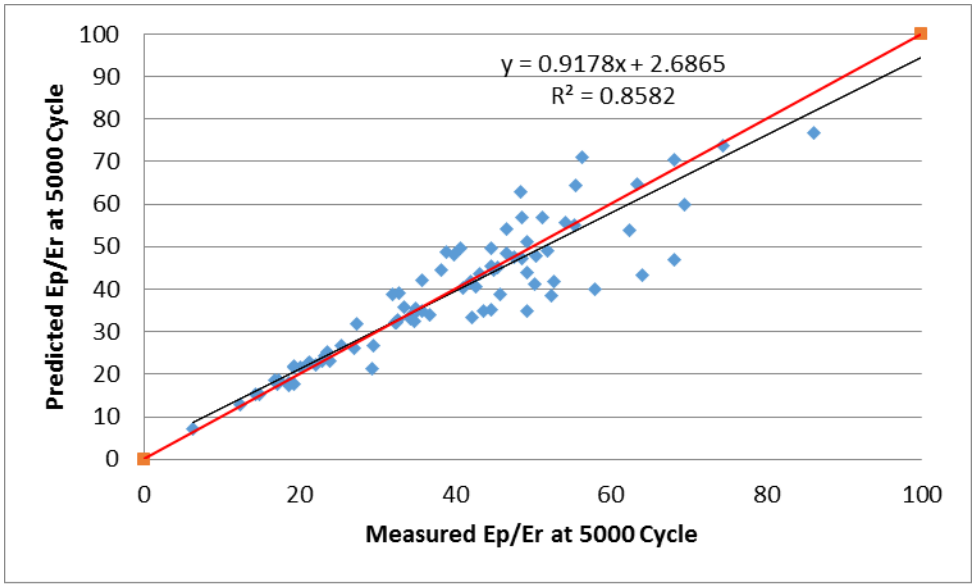

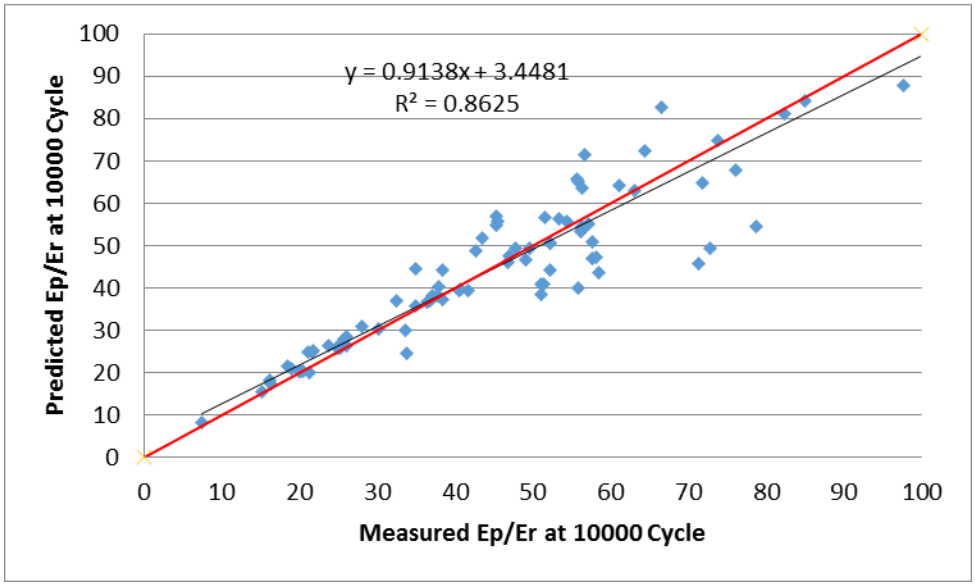

Figure 27: Predicted vs. Measured $\frac{\epsilon_p}{\epsilon_r}$ Values

4.3 RLPD Test Data from NCHRP Project 9-30A

For comparison purpose in addition to the RLPD data collected for the 28 Maryland mixtures, RLPD data for 18 asphalt mixtures tested in NCHRP Project 9-30A (Von Quintus et al., 2011) were also obtained. The MEPDG rut model (Equation 8) was calibrated to these additional mixtures to get the coefficients K_1, K_2, and K_3. These coefficients are tabulated in Table 12 and comparisons of the data are provided in the box and whisker plots shown in Figure 28. It can be noticed from Figure 28 that the variations in the coefficients of the rut model for the Maryland data is comparatively less that for the NCHRP Project 9-30A data. One reason for this is that the RLPD tests from NCHRP Project 9-30A were performed at air voids ranging from 3.6% to 8.6% while all of the Maryland tests were performed at 7% ± 0.5% air voids. The volumetric properties and RLPD test temperatures of the asphalt mixtures from NCHRP Project 9-30A are tabulated in Table 13.

Table 12: Coefficients of MEPDG Rut Model Based on NCHRP 9-30A RLPD Data

Mix No	Asphalt Mixtures	K1 (Intercept)	K 2 (Temperature Coeff)	K3 (Loading Cycles Coeff)	R^2
1	Alabama; HMA overlay	-0.5799	1.1706	0.0765	0.80
2	California; CA 47 mix	0.1081	0.2664	0.1378	0.92
3	California; CA 47M mix	-1.6256	1.1315	0.2383	0.68
4	California; CA 52 mix	-1.1699	0.7618	0.2363	0.49
5	Florida base neat mix	-0.9672	0.6695	0.2378	0.65
6	Florida N1	-1.8391	1.2346	0.2840	0.95
7	Florida N2	-1.0240	0.8369	0.1916	0.85
8	Indiana HMA mix 7A	-1.3083	1.1880	0.1853	0.90
9	Indiana HMA mix 7B	-1.6453	1.3683	0.2077	0.98
10	Indiana HMA mix 8B	-1.2238	0.9648	0.2408	0.91
11	Missouri virgin binder	0.8473	0.0453	0.1558	0.37
12	Missouri RAP binder	0.4705	0.2932	0.1659	0.60
13	Missouri surface	0.5181	0.1651	0.1805	0.61
14	Mississippi	0.7237	0.1686	0.1830	0.46
15	Montana	-0.5374	0.8903	0.2351	0.83
16	Wisconsin HMA surface mix	-0.2577	0.8404	0.1414	0.48
17	Wisconsin ATB base	0.2722	0.3736	0.2526	0.78
18	Wisconsin HMA binder mix	0.1272	0.4943	0.1326	0.77

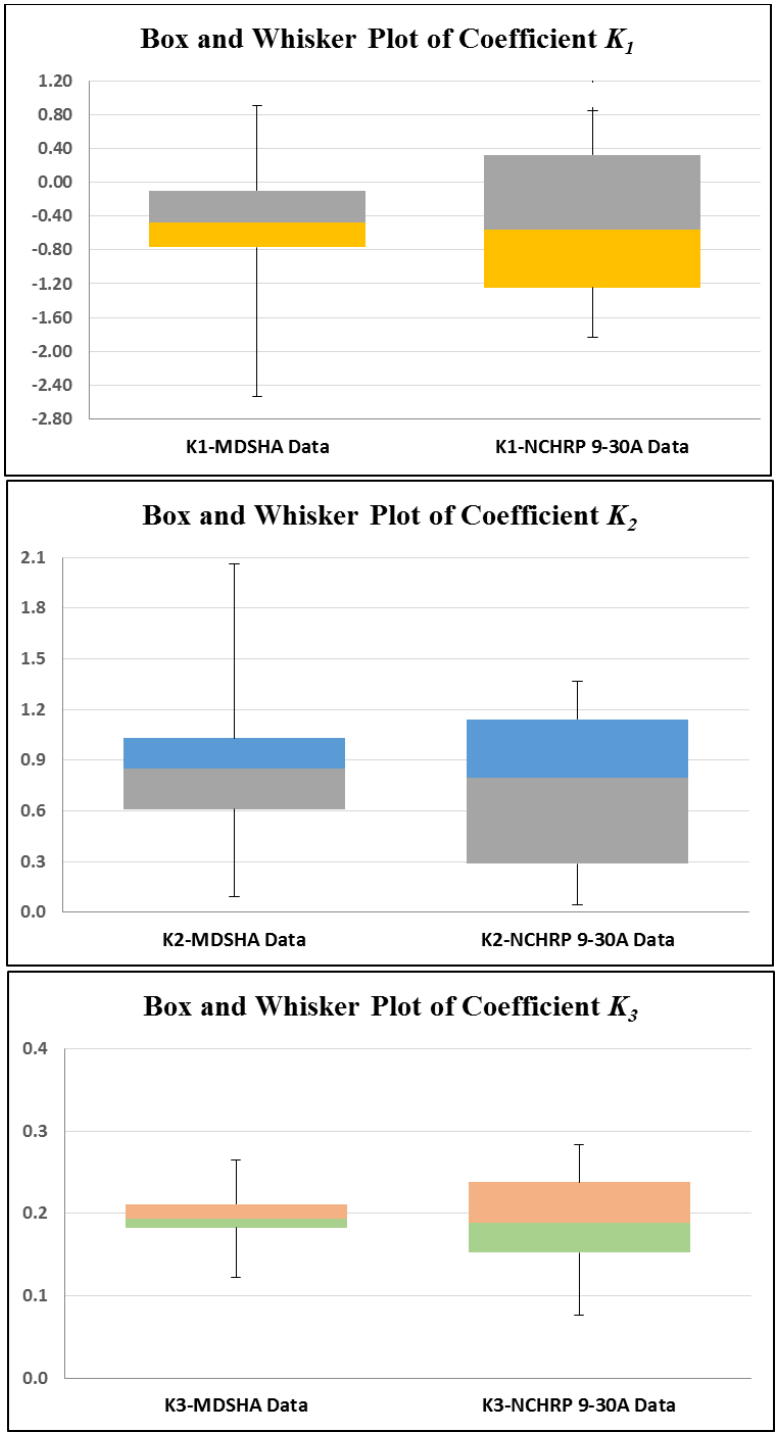

Figure 28: Comparison of Coefficients Obtained by MDSHA Lab Data and NCHRP 9-30A Data

Table 13: Volumetric Properties and RLPD Test Temperatures of Asphalt Mixtures of NCHRP 9-30A Project

Mix #	Mix ID	Mix type	VMA (%)	VFA (%)	Air Voids %	RLPD Test Temperatur (°C)
1	Alabama; HMA overlay	SPS-6, overlay binder, polymer modified	14.7	66.0	5.0	20, 40, 60
2	California; CA 47 mix	I-710 perpetual pavement, CA 47	16.0	64.3	5.8	20, 35, 50
3	California; CA 47M mix	I-710 perpetual pavement, CA 47M	16.3	63.1	5.5	20,35, 50
4	California; CA 52 mix	I-710 perpetual pavement, CA 52	14.4	81.8	2.5	20, 35, 50
5	Florida base neat mix	NCAT, HMA base	16.7	65.8	5.7	20, 37, 55
6	Florida N1	NCAT N1 section, PMA mix	18.3	59.0	7.6	20, 37, 55
7	Florida N2	NCAT N2 section, neat mix	16.3	64.2	5.8	20, 37, 55
8	Indiana HMA mix 7A	NCAT section 7A, HMA low void mix	18.0	71.3	5.2	20, 37, 55
9	Indiana HMA mix 7B	NCAT section 7B, HMA low void mix	18.4	70.1	5.6	20, 37, 55
10	Indiana HMA mix 8B	NCAT section 8B, HMA wearing surface	17.1	79.2	3.6	20, 37, 55
11	Missouri RAP binder	SPS-5, binder mix with RAP	16.4	50.7	8.1	20, 34, 47
12	Missouri virgin binder	SPS-5, binder mix without RAP (virgin)	19.0	54.9	8.6	20, 34, 47
13	Missouri surface	SPS-5, wearing surface	20.3	57.3	8.7	20,34, 47
14	Mississippi	Mississippi road	15.0	75.0	4.0	20,40,60
15	Montana	Montana road	14.9	75.0	3.6	20,38,55
16	Wisconsin ATB base	SPS-1, HMA base, ATB mix	14.9	56.9	6.3	20, 35, 50
17	Wisconsin HMA surface mix	SPS-1, HMA wearing surface	18.3	53.3	8.6	20, 35, 50
18	Wisconsin HMA binder mix	SPS-1, HMA binder mix	18.1	63.1	6.4	20, 35, 50

CHAPTER 5: EXPEDITED TESTING PROGRAM

In the past two decades, there has been a significant effort to standardize a series of simplified test methods to characterize the performance of asphalt mixtures using the Asphalt Mixtures Performance Tester (AMPT). During NCHRP Projects 9-19 and 9-29, the dynamic modulus and repeated load permanent deformation (RLPD) tests were selected as the preferred methods for mixture evaluation, structural design, and rutting performance prediction of asphalt mixtures (Witczak et al. 2002, Bonaquist, 2011). The outcome of these studies resulted in development of three provisional AASHTO standards for the AMPT equipment: specimen preparation (AASHTO PP 60), dynamic modulus and repeated load permanent deformation testing (AASHTP TP 79), and development of dynamic modulus master curve (AASHTO PP 61). While the refined test methods specified for the AMPT are faster and easier to perform than their preceding research grade test procedures, there is still reluctance among highway agencies and industry to conduct routine performance testing using the AMPT. A principal reason for this is the lengthy process of specimen preparation and test execution for DM and RLPD tests. In order to expedite the asphalt mixture characterization testing program, three investigations have been performed as part of the current study.

In the first investigation, the possibility of abbreviating the unconfined DM testing procedure was examined by replacing testing at 40°C with testing at an additional frequency of 0.01 Hz at 20°C. The goal here is to obtain a similar dynamic modulus master curve without the need to equilibrate to a new temperature and then run another complete set of frequencies.

In the second investigation, the possibility of reducing the total number of required specimens was evaluated. Specimen preparation is one of the most time and labor consuming steps in the testing program. Since dynamic modulus is considered to be non-destructive test, it should conceptually be possible to reuse these specimens for subsequent tests. The potential for reusing specimens was first evaluated by examining the changes in the dynamic modulus under repetitive testing—i.e., performing a second full dynamic modulus test on specimens that had already been tested once. Second, RLPD tests were performed on specimens that had already been subjected to dynamic modulus testing and the test results were compared with those from freshly made specimens. Reusing dynamic modulus test specimens reduces the total number of specimens required to characterize an asphalt mixture per AASHTO TP 79 from 12 to 9.

In the third investigation, the time-temperature superposition principal was extended to the RLPD test results and RLPD master curves were developed using the same shift factors determined during the development of DM master curves. This approach has the potential to reduce the total numbers of specimens required to completely characterize an asphalt mixture from 9 to 3. This provides substantial time savings in the preparation of specimens for RLPD testing and may motivate state agencies to perform this test on a more routine basis.

5.1 First Approach: Reduction in Dynamic Modulus Testing Time

The dynamic modulus (E*) is the primary material input for flexible pavement structural design in the MEPDG. Dynamic modulus values are measured over a range of temperatures and loading frequencies and are then shifted into a master curve for characterizing asphalt mixtures for pavement structural design. According to AASHTO PP 61, testing is performed at the three temperatures of 4^{o}C, 20^{o}C, and 40^{o}C and the three frequencies of 10, 1, and 0.1 Hz at each temperature, with an additional frequency of 0.01 Hz at the highest temperature. These are reduced sets of temperatures and loading frequencies as compared to standard research-grade testing using a Universal Testing Machine (UTM) as specified in AASHTO PP 62–09," Standard Practice for Developing Dynamic Modulus Master Curves for Hot Mix Asphalt (HMA)".

While the new test methods specified for the AMPT are faster and easier to perform than their preceding research grade test protocols, specimen preparation and conditioning can take several days. In addition, testing at 0.01 Hz at the highest temperature adds about 40 minutes to the duration of the test. This lengthy specimen preparation and testing time is considered by many highways agencies as unfeasible for routine testing. The 0.01 Hz low frequency loading at 40^{o}C for providing supplementary data for the prediction of the lower shelf of the master curve also has the highest specimen to specimen variability. Excluding this low frequency from the dynamic modulus test program would expedite the test. Even better would be excluding all of the 40°C testing because of the significant time saving from specimen conditioning.

In order to evaluate this expedited testing process for DM testing, twelve (12) asphalt mixtures out of the total 28 mixtures were selected. These selected mixtures

spanned a range of NMAS, gradation type (dense vs. gap graded), binder types, RAP content, and hot vs. warm mixes. In addition to the requirements of the AASHTO PP 61 protocol for DM testing, all three specimens of each mixture were tested at an additional frequency of 0.01Hz at 20^{o}C.

For comparison purpose, master curves were developed using only measured E* values at two temperatures (4^{o}C, 20^{o}C) and three frequencies (0.1, 1 and 10Hz), with an additional frequency of 0.01Hz at 20^{o}C. These new master curves were compared with the original master curves using the full set of data from the AASHTO PP 61 protocol.

Two scenarios were observed in this comparison. Eight out of twelve master curves overlap with each other while the other four curves deviated at the lower shelf. Examples for both scenarios are shown in Figure 29. All DM master curves developed from testing at two and three temperatures are included in APPENDIX C (Figure C-55 a to e).

Since the master curves are plotted in log-log space, it is hard to appreciate the real differences in E* values at different reduced frequencies. Box and whisker plots of percentage difference in arithmetic space are shown in Figure 30 at different reduced frequencies. These plots show the percentage difference in E* values predicted by master curves developed using data at three temperatures (3T) and at two temperatures (2T).

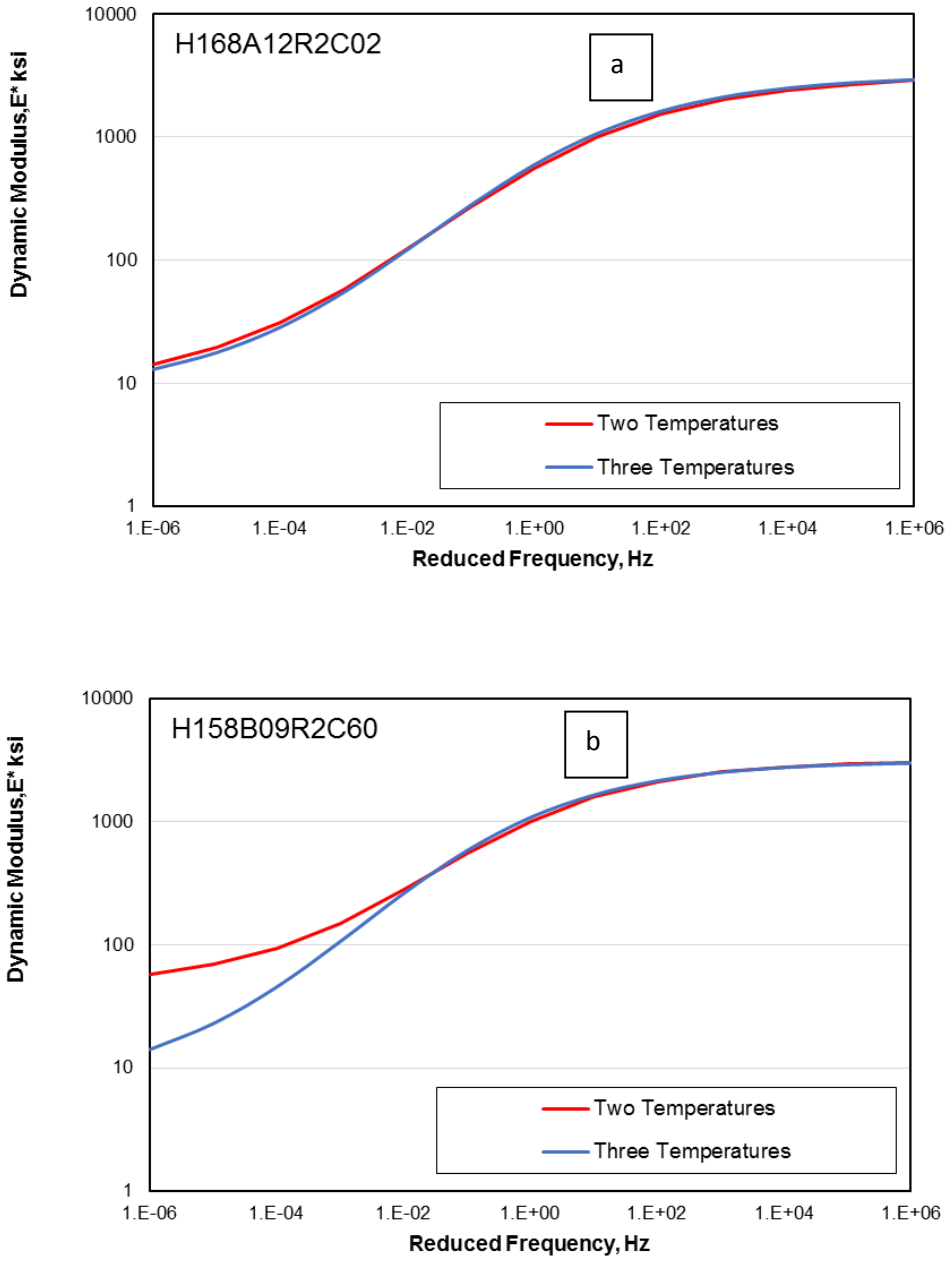

Figure 29: Master Curves Developed by E* Data Obtained at Two and Three Temperature a) Overlapping Scenario b) Non-Overlapping Scenario

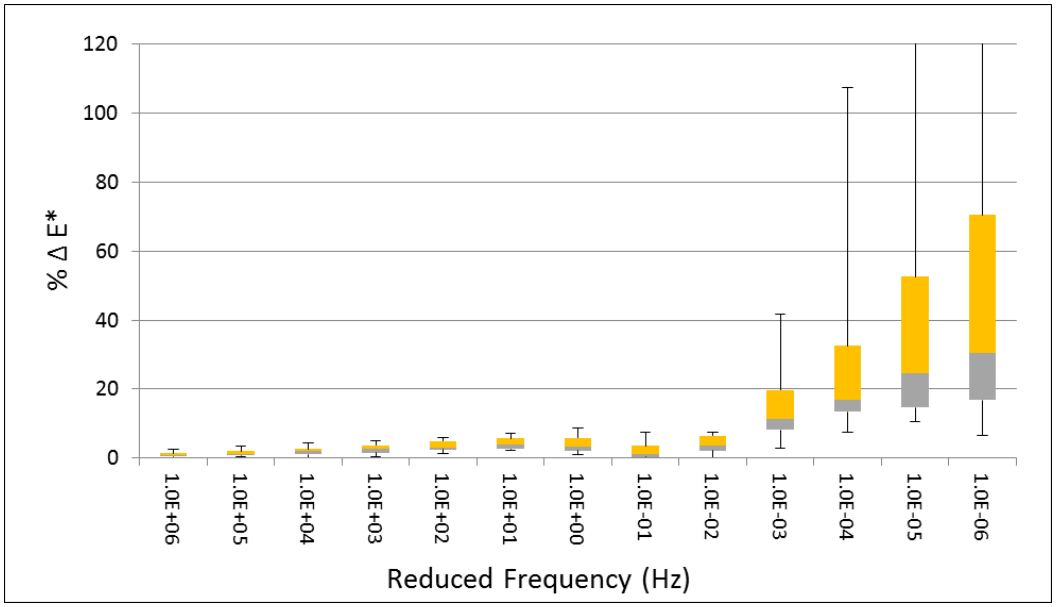

Figure 30: Variation in % Difference of E* Values of Twelve Asphalt Mixtures Obtained by 3T and 2T Master Curves

It can be seen from Figure 30 that the variation in percentage differences of E* values obtained by 3T and 2T master curves of all mixtures is comparatively very high at low reduced frequencies / high temperatures. This observation is consistent with the visual observations in Figure 29b.

In order to see whether the difference in the E* values obtained from 2T and 3T master curves for individual mixture are statistically significantly, t-tests were performed on E* values of lower shelfs (Reduced frequency < 0.01) for three mixtures which have the most differences in 2T and 3T master curves. The results are tabulated in Table 14. The null hypothesis (mean values of two samples are equal) is accepted in all mixtures. This leads to conclusion that the E* values obtained from 3T and 2T master curves are not statistically different from each other in all mixtures at the 5% significance level.

Table 14: T-Tests for E* Values (Lower Shelf , Reduced Frequency < 0.01) Obtained by 2T and 3T Master Curves of Mixtures

Statistic/Mixtures	H083A19C2C02	H158B09R2C60	H177A12R2C50
t Stat	1.11	1.56	0.63
P(T<=t) two-tail	0.31	0.17	0.55
t Critical two-tail@0.05	2.45	2.45	2.45
Null Hypothesis ($\mu_1 = \mu_2$)	Pass	Pass	Pass

In order to see the effect of E* values predicted by master curves developed by two and three temperatures to the predicted distresses (International Roughness index (IRI), Total Permanent Deformation (PD_t), Bottom Up Fatigue Cracking (BU-FC), Top Down Fatigue Cracking (TD-FC) and Permanent Deformation Asphalt Concrete (PD_{ac})), three mixtures out of twelve mixtures which had more differences in 2T and 3T E * values were selected for sensitive analysis in MEPDG software. Three traffic levels; low (3 million EASL), medium (10 million EASL) and heavy (30 EASL), one climate condition, three pavement structures; for low traffic (Asphalt Concrete (AC) = 7 inch, Unbound Base (UB) = 10 inch), for medium traffic (AC=9 inch, UB=12 inch), for heavy traffic (AC=14 inch, UB=12 inch) were selected for sensitive analysis. The E* predicted by master curves developed by two and three temperatures were used in MEPDG software for three selected mixtures and all other inputs (default values) in the software were kept constant. The predicted distresses obtained using 2T and 3T E* values of three mixtures at three traffic levels are compared and shown in Figure 31 . It can be seen from Figure 31 that there are no significant differences in predicted distresses using E* data obtained by 2T and 3T master curves. The percentage differences in predicted distresses using E* data obtained by 2T and 3T master curves of three mixtures are also shown in Figure 32. It can be seen from the Figure 32 that percentage difference in any of predicted distress is not more than 15% except PD_{ac} of one mixture at the end of design life of 20 years. It can be concluded

that E* values predicted by 2T master curves does not significantly affect the predicted distresses when compared with distresses predicted by using 3T master curve E* values.

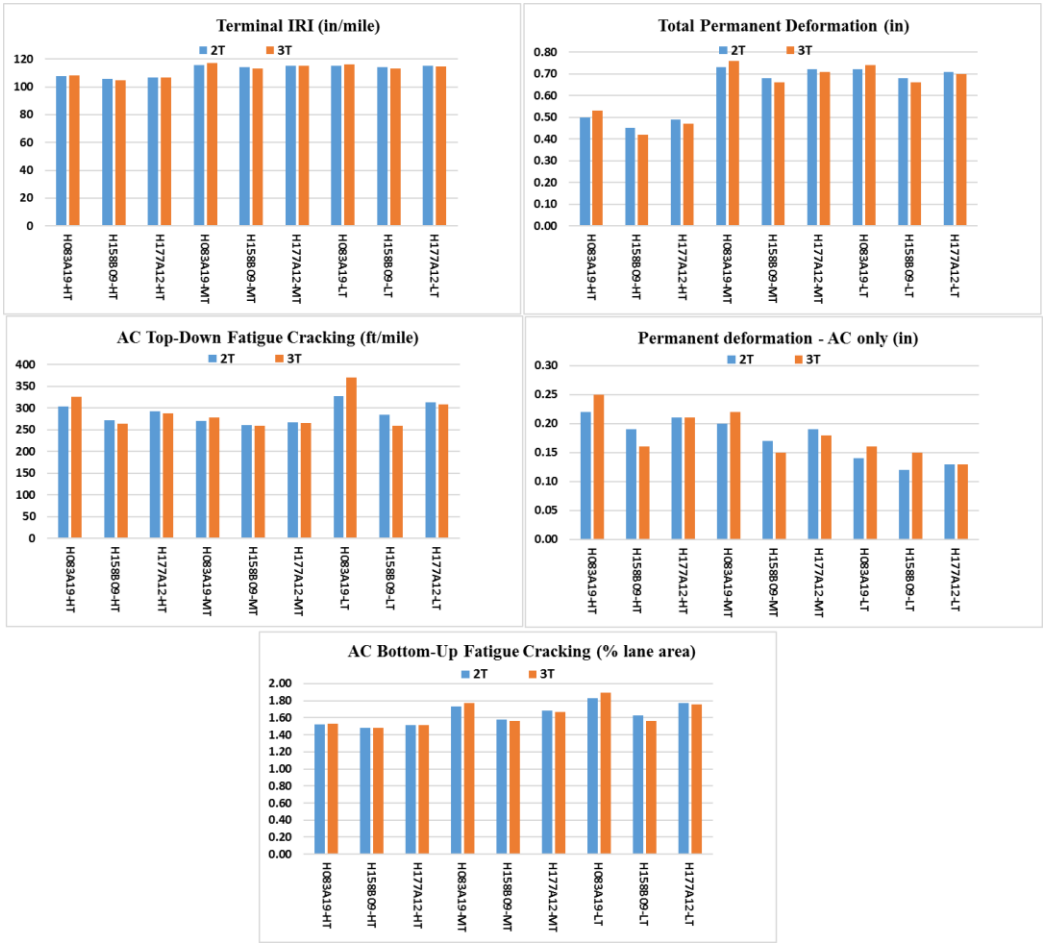

Figure 31: Predicted Distresses using E* Data Obtained from 2T and 3T Master Curves at Low Traffic (LT), Medium Traffic (MT) and Heavy Traffic (HT)

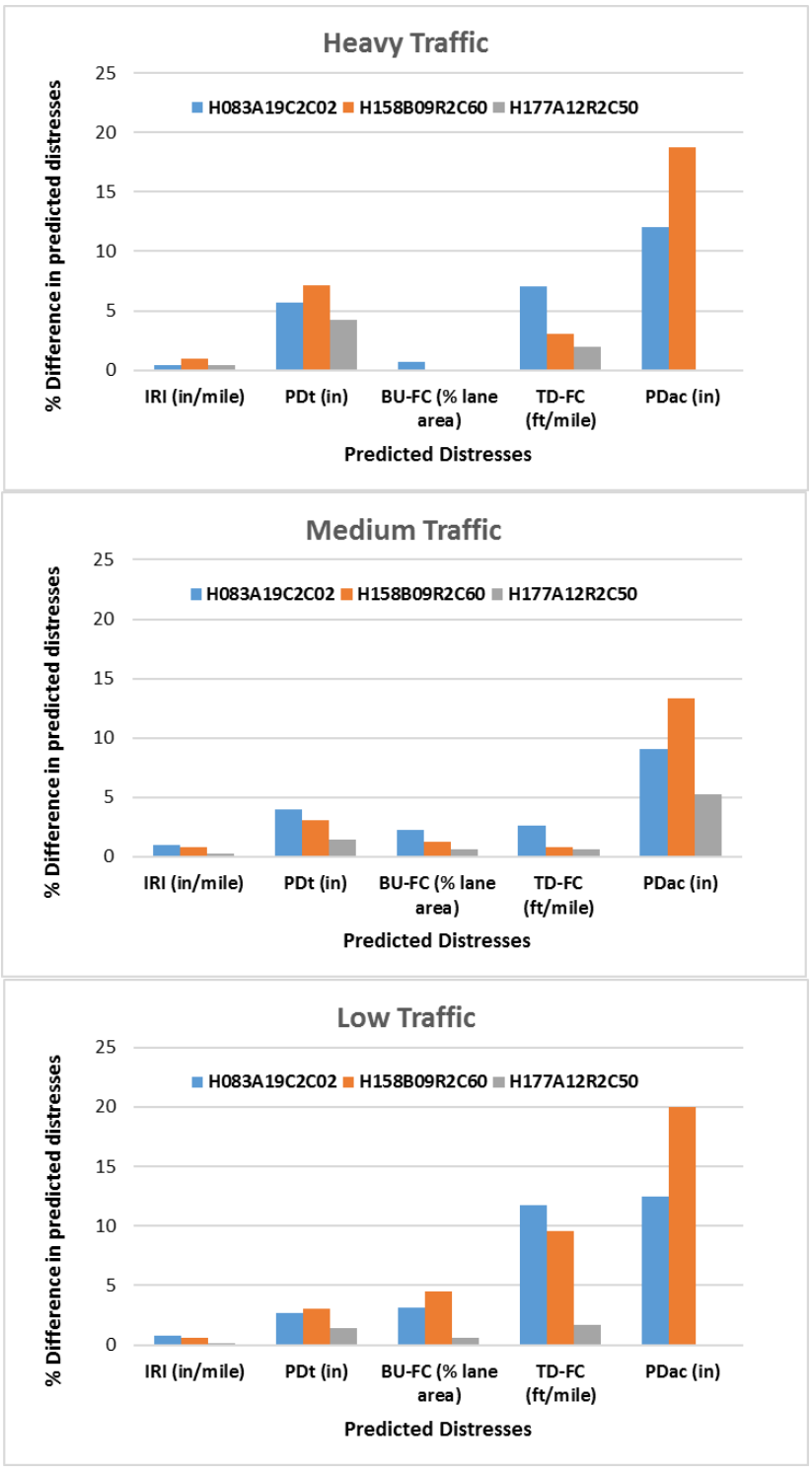

Figure 32: Percentage Differences in Predicted Distresses using E* Values Predicted by 2T and 3T Master Curves at Low Traffic (LT), Medium Traffic (MT) and Heavy Traffic (HT)

These results suggest that the AASHTO PP 61 protocol can be modified by adding an additional frequency of 0.01Hz at 20^{o}C and removing all testing at 40^{o}C. The DM master curves obtained by testing at two temperatures with one additional frequency of 0.01Hz at 20^{o}C are not significantly different from the master curves developed according to standard AASHTO PP 61 protocol.

5.2 Second Approach: Reduction in RLPD Specimens

The current protocol of AASHTO TP 79 requires a minimum of three replicate specimens for each test or a total 12 high-quality specimens for the combined DM and RLPD tests for a single asphalt mixture. The high-quality specimens should meet the specimen fabrication criteria (e.g. target air void content) and data quality statistics requirements for the two tests as defined in Table 3 (Chapter 2). Considering that specimen preparation can be a tedious process and that the specimen acceptance rate can be as low as 50% for certain mixtures (Bonaquist, 2010), there are clear benefits from reducing the required number of specimens.

Although the dynamic modulus test is considered to be non-destructive, some researchers have been skeptical about reusing the specimens in other tests and instead require fresh specimens. Consequently, this study explored whether DM specimens can be reused without significantly affecting the test results. First, the variation in dynamic modulus values under repeated testing was examined. Second, RLPD tests performed on specimens that had been previously used for dynamic modulus testing were compared with RLPD tests on freshly made specimens. Statistical evaluations were performed to assess whether any densification or damage was caused by the dynamic modulus testing.

In the first experiment, three replicate specimens from Mixture H161A12R4F01 were tested following the procedure depicted in Figure 33. Information about this mixture is provided in Table 4 and Table 5 (Chapter 3). As shown in Figure 33, each replicate was initially tested for dynamic modulus at 4^{o}C and 10, 1 & 0.1 Hz (Test A). Next, dynamic modulus test at 4^{o}C (Test B-0T) were performed on the same specimen with no delay. Test C-5T was performed following Test B-0T after a 5-minute rest period and Test D-15T was performed 15 minutes after Test C-5T to assess whether the rest time between consecutive tests had any effect on the response. After testing at 4^{o}C, the process was repeated at 20^{o}C and 40^{o}C, respectively. The Test C-5T was not performed at 40^{o}C temperature due to the long testing time. After the testing at 40°C was completed, the dynamic modulus frequency sweep was repeated again on the same specimen for a final time at 20^{0}C (Test E). This testing sequence was performed for all three replicate specimens for the mixture.

The dynamic moduli of re-tested specimens are plotted in Figure 34. The results show only a slight modulus increase of about 8% after the initial Test A at all temperatures and frequencies. This is likely due to densification of the specimens during the initial Test A series. The highest percentage modulus increase was about 13% in the high temperature testing.

The results in Figure 34 suggest that the variation of dynamic moduli among replicates is more significant than the variation within one replicate under repeated testing. The coefficients of variation (CV) within one specimen due to the repeated testing and among the three replicate specimens were calculated across the 10 different temperature-frequency combinations. As shown in Figure 35, the range of coefficients of variation between replicates is higher than within one specimen under repeated testing.

In order to see if the repeatedly tested specimen E* values are statistically different from mean E* values of the mixture, one sample t-tests were performed at all temperatures and frequencies combinations. All t-tests are passed as shown in Table 15, which indicates that mean E* values of repeatedly tested specimen at all temperatures and frequencies combinations are not statistically different from mean E* values of a mixture at the same temperature and frequencies combinations.

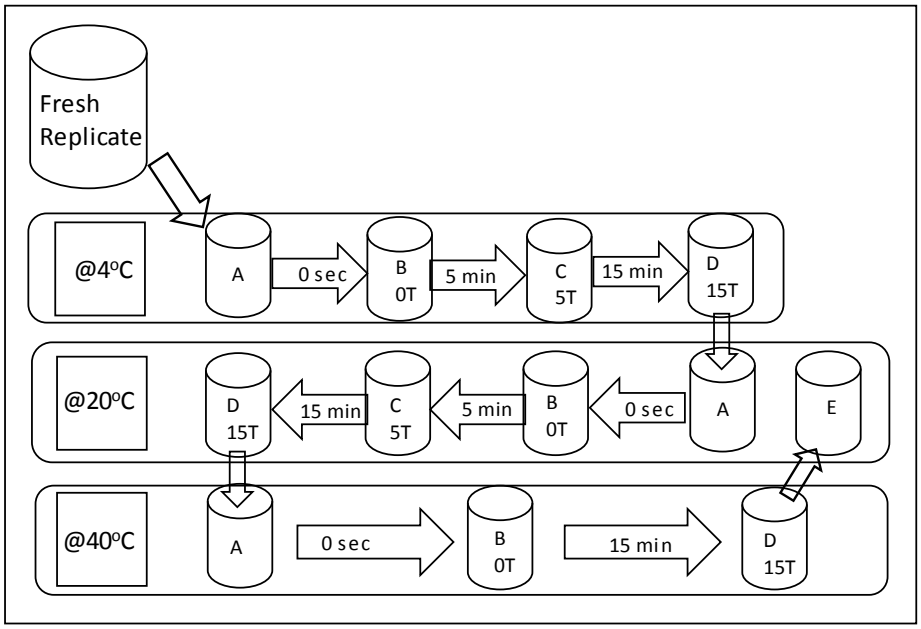

Figure 33: Sequence of Repeated DM Testing on a Specimen

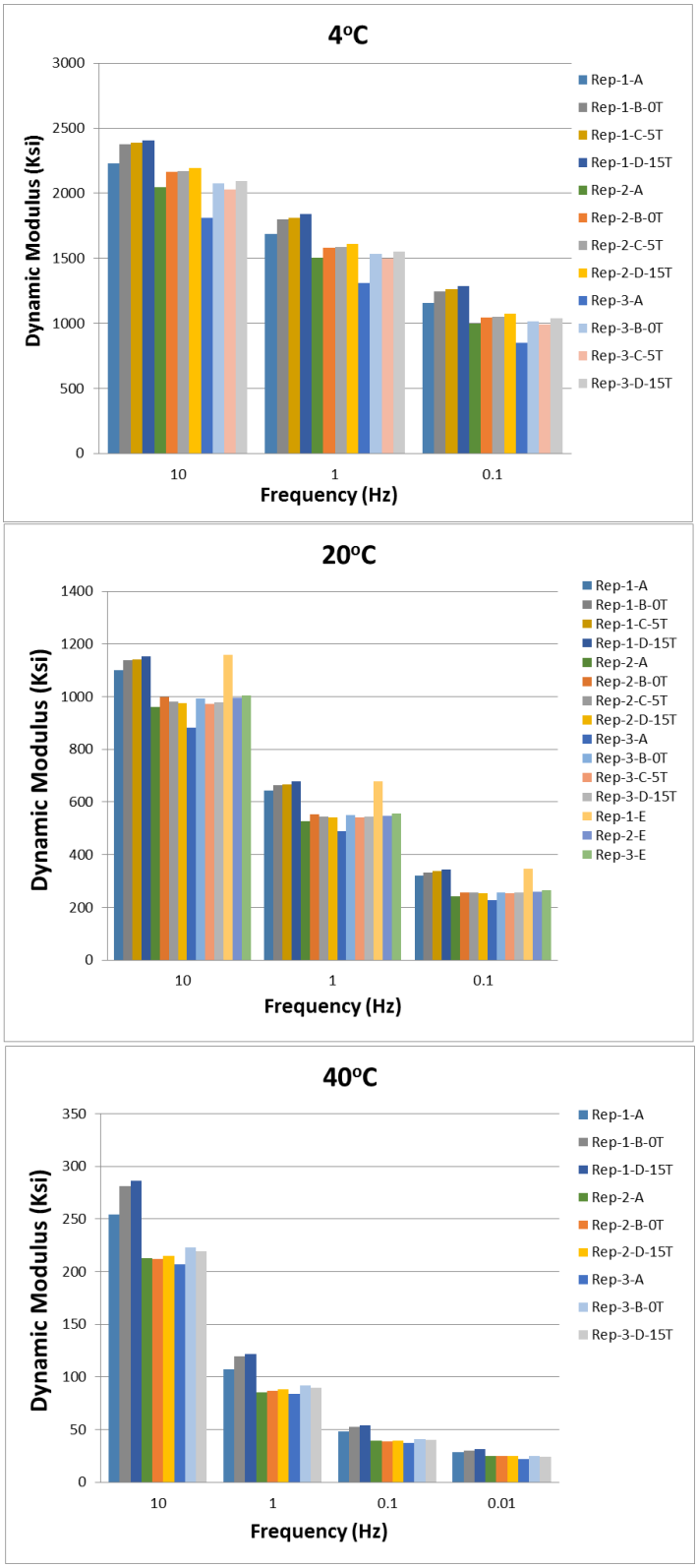

Figure 34: Dynamic Moduli of Re-Tested Specimens of H161A12R4F01 Mixture at 4^0C, 20^0C, and 40^0C

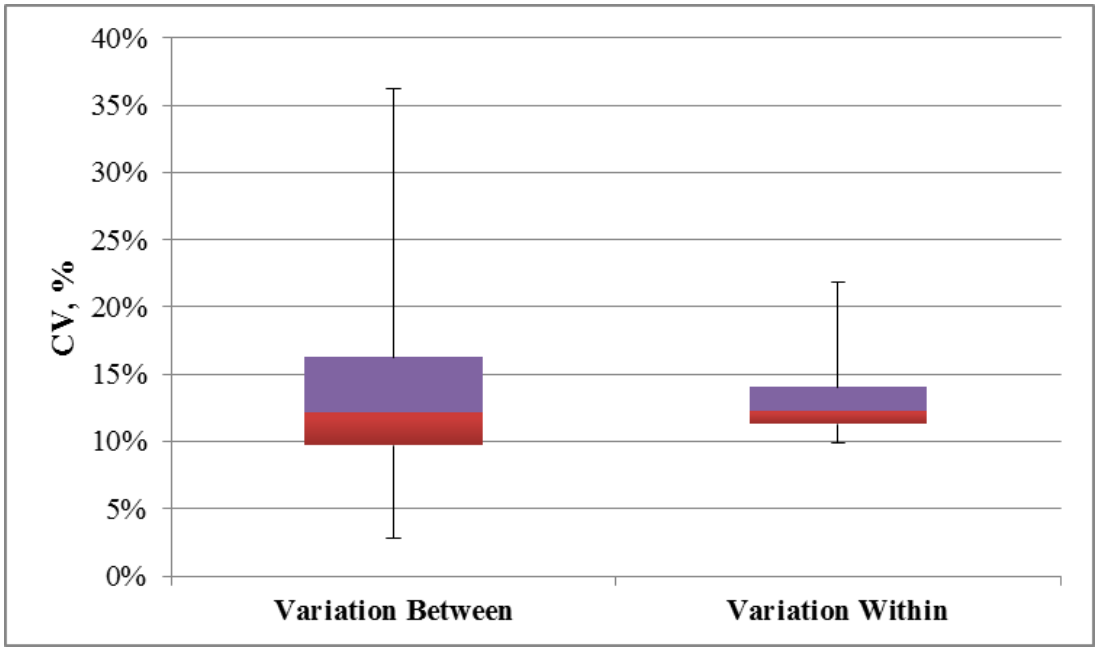

Figure 35: Variation in CV Between and Within the DM Tested Specimens

Table 15: t-Test on E* Values of Repeatedly Tested Specimens of a Mixture

Temperature (C)	4			20			40			
Frequency (Hz)	10	1	0.1	10	1	0.1	10	1	0.1	0.01
Specimen 1										
t Stat	2.24	2.33	2.41	2.37	2.39	2.39	2.74	2.72	2.64	2.61
P(T<=t) two-tail	0.15	0.14	0.14	0.14	0.14	0.14	0.11	0.11	0.12	0.12
t Critical two-tail	4.30	4.30	4.30	4.30	4.30	4.30	4.30	4.30	4.30	4.30
Null Hypothesis ($\mu_1 = \mu_2$)	Pass	Pass	Pass	Pass	Pass	Pass	Pass	Pass	Pass	Pass
Specimen 2										
t Stat	0.12	0.18	0.37	0.74	0.85	0.90	1.17	1.14	1.15	0.77
P(T<=t) two-tail	0.92	0.87	0.75	0.54	0.48	0.46	0.36	0.37	0.37	0.52
t Critical two-tail	4.30	4.30	4.30	4.30	4.30	4.30	4.30	4.30	4.30	4.30
Null Hypothesis ($\mu_1 = \mu_2$)	Pass	Pass	Pass	Pass	Pass	Pass	Pass	Pass	Pass	Pass
Specimen 3										
t Stat	1.00	2.19	0.92	0.82	3.79	0.92	0.75	3.57	0.78	0.89
P(T<=t) two-tail	0.42	0.16	0.45	0.50	0.06	0.46	0.53	0.07	0.52	0.47
t Critical two-tail	4.30	4.30	4.30	4.30	4.30	4.30	4.30	4.30	4.30	4.30
Null Hypothesis ($\mu_1 = \mu_2$)	Pass	Pass	Pass	Pass	Pass	Pass	Pass	Pass	Pass	Pass

As another approach to examine any potential damage caused by dynamic modulus testing, RLPD testing was conducted on freshly made specimens as well as specimens which had already been tested for dynamic modulus. The triaxial RLPD tests were conducted according to AASHTO TP 79 and at the NCHRP 9-30A recommended low, intermediate, and high temperatures of 20°C, 40°C, and 58°C, respectively. A minimum of two replicate specimens were tested at each temperature for each specimen condition (fresh or re-used). A cyclic haversine pulse with 0.1 second loading duration and 0.9 second rest period was applied for 10,000 cycles or until a 5% cumulative axial plastic strain was reached. The test stress state was a constant 10 psi confining pressure and a cyclic 70 psi deviator stress. Three asphalt mixtures were tested: H176A09R2C01, H138B12R2C05, and H138A12G4F05. Information about these mixtures is provided in Table 4 and Table 5 (Chapter 3).

Figure 36 shows the cumulative permanent microstrain versus number of loading cycles for tests on fresh (solid lines) and reused (dashed lines) specimens. The permanent deformation behavior for both types of specimens is very similar.

The average cumulative permanent microstrains in the reused and fresh specimens at 1,000 and 10,000 cycles at the three test temperatures are shown in Figure 37. The accumulated permanent microstrains in the reused and fresh specimens show only slight differences, and there are no systematic trends in these differences.

Figure 38 illustrates the average slope and intercepts of the secondary phase of the RLPD test for the reused and fresh specimens at the three test temperatures. Again, there are only small differences between reused and fresh specimens, and there are no systematic trends in these differences.

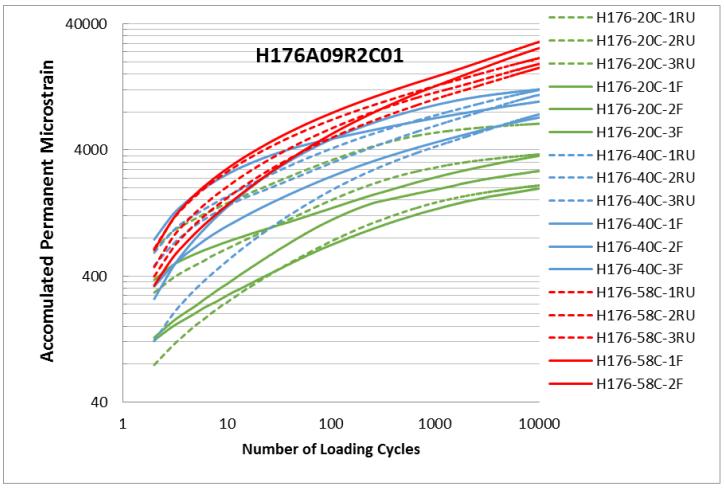

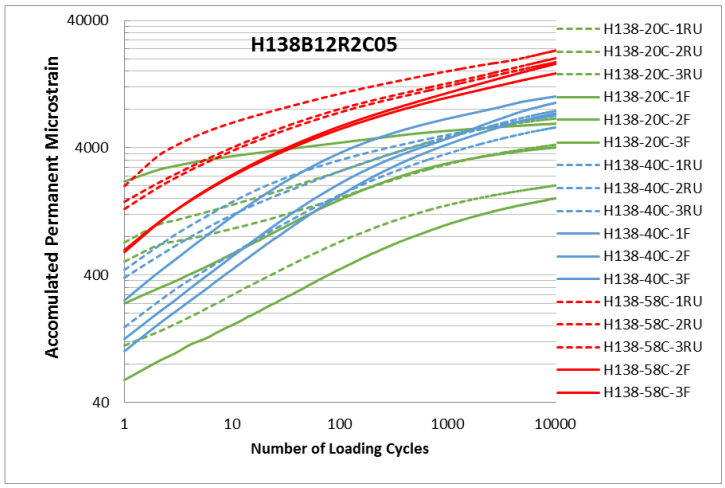

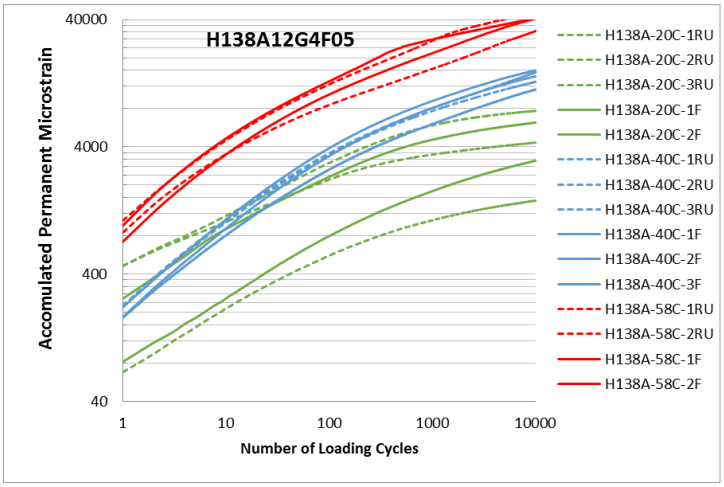

Figure 36: RLPD Test Results of Fresh and Reused Specimens

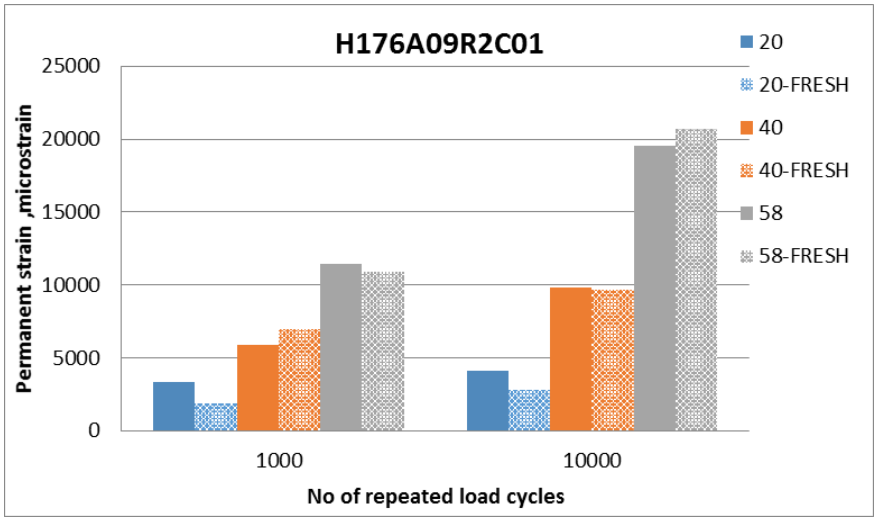

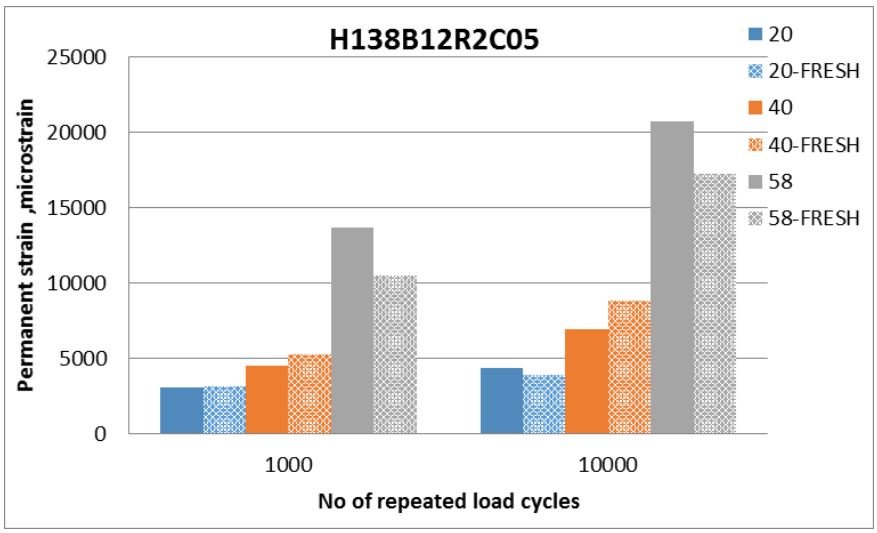

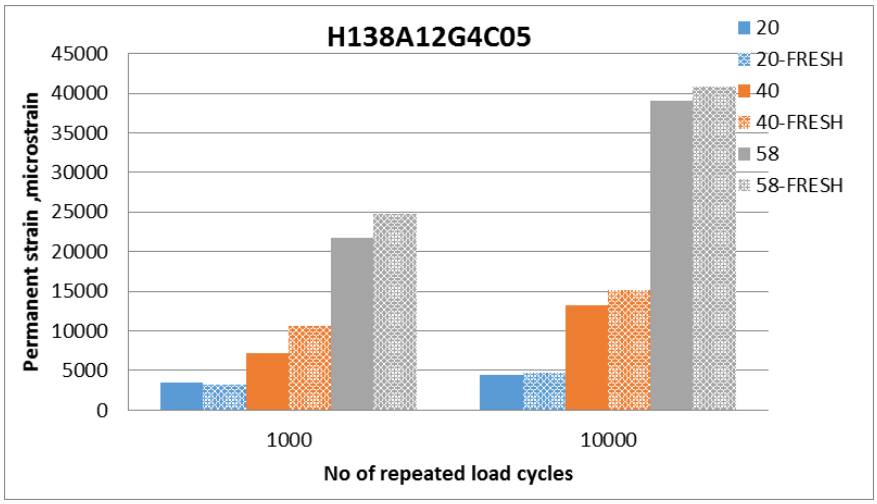

Figure 37: Comparison of Cumulative Strains of Fresh and Reused Specimens at 1000 and 10000 Cycles of Loading at Three Temperatures (20ºC, 40ºC and 58ºC)

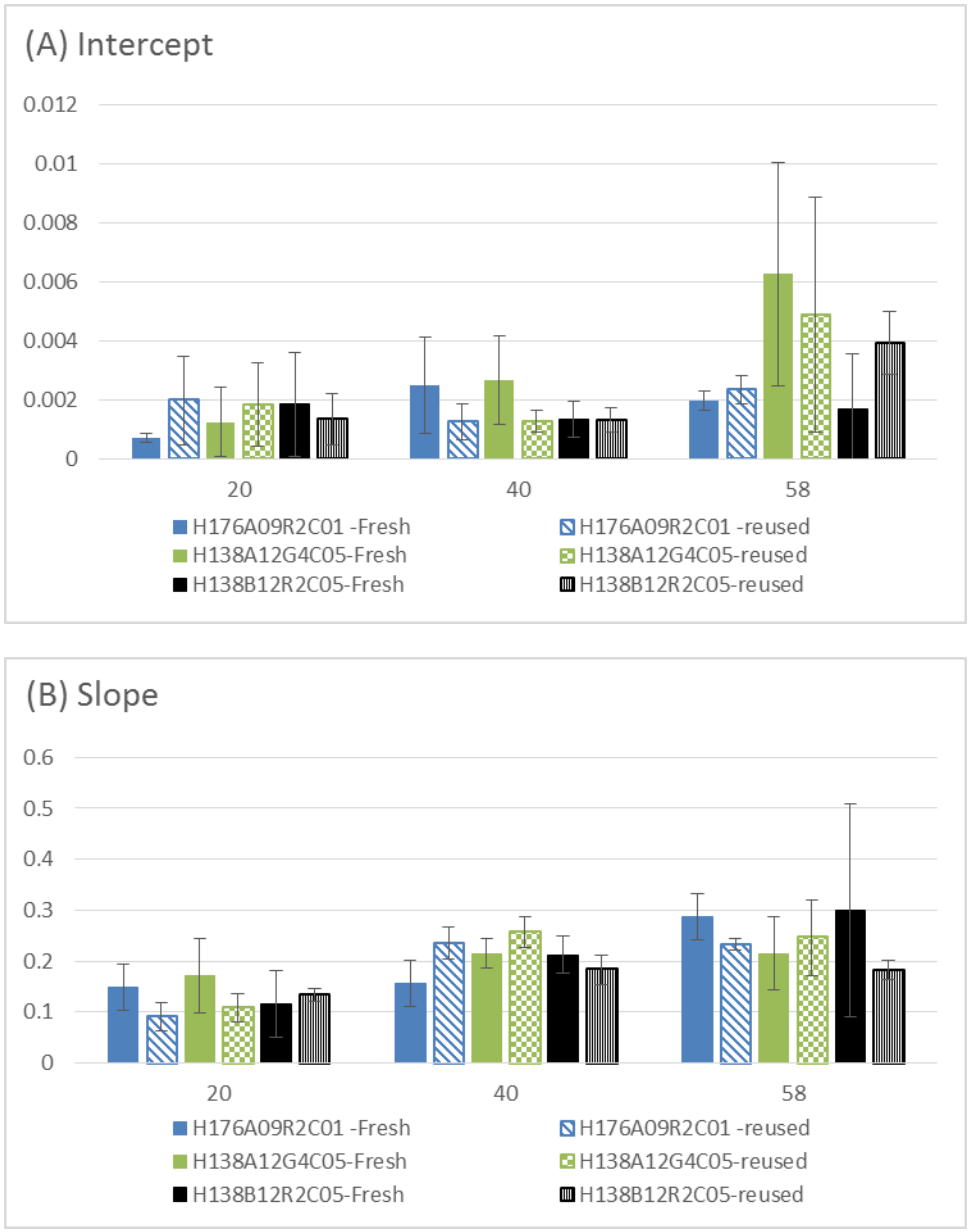

Figure 38: The Average (A) Intercept and (B) Slope of the Line of the Secondary Phase of RLPD Tests. The Error Bars Represent One Standard Deviation.

In order to substantiate the insignificant differences in the RLPD response of reused versus fresh specimens, two-tailed t-tests were performed for cumulative permanent microstrains in each mixture at 1,000 and 10,000 load cycles and the three test temperatures. The results summarized in Table 16 confirm that the differences in the RLPD responses of reused and fresh specimens are not statistically significant—i.e., any densification or damage caused by the dynamic modulus testing is insignificant. This confirms that specimens previously used for DM testing can be reused for RLPD testing, reducing the required total number of specimens from 12 to 9.

Table 16: Two Tailed t-Test to Evaluate the Differences Between Fresh and Reused RLPD Specimens

Mixture	Statistic	20@1000 Cycles	40@1000 Cycles	58@1000 Cycles	20@10000 Cycles	40@10000 Cycles	58@10000 Cycles
H176A09R2C01	t Stat	1.17	0.58	0.18	0.97	0.27	0.17
	P(T<=t) two-tail	0.36	0.59	0.88	0.40	0.80	0.88
	t Critical two-tail	4.30	2.78	4.30	3.18	2.78	4.30
	Null Hypothesis ($\mu_1 = \mu_2$)	**Accepted**	**Accepted**	**Accepted**	**Accepted**	**Accepted**	**Accepted**
H138B12R2C05	t Stat	0.04	0.85	2.65	0.22	1.99	2.03
	P(T<=t) two-tail	0.97	0.46	0.12	0.84	0.12	0.18
	t Critical two-tail	2.78	3.18	4.30	2.78	2.78	4.30
	Null Hypothesis ($\mu_1 = \mu_2$)	**Accepted**	**Accepted**	**Accepted**	**Accepted**	**Accepted**	**Accepted**
H138A12G4C05	t Stat	-0.48	1.60	0.16	0.22	-1.99	2.03
	P(T<=t) two-tail	0.68	0.25	0.89	0.84	0.12	0.18
	t Critical two-tail	4.30	4.30	3.18	2.78	2.78	4.30
	Null Hypothesis ($\mu_1 = \mu_2$)	**Accepted**	**Accepted**	**Accepted**	**Accepted**	**Accepted**	**Accepted**

5.3 Third Approach: Time-Temperature Superposition for RLPD Testing

In order to obtain a full characterization of permanent deformation properties of asphalt mixtures, NCHRP Project 9-30A (Von Quintus et al., 2011) recommends performing the RLPD test at three temperatures—high, intermediate, and low—to determine the inputs to the enhanced rutting models for structural design. However, conducting the full set of the RLPD tests is very time and labour intensive. The time-temperature superposition (TTS) principal commonly used to interpret viscoelastic response in dynamic modulus tests could greatly reduce testing time if it can be demonstrated that it also applies to the viscoplastic response in the RLPD test.

Previous research has shown that asphalt mixtures are thermorheologically simple in the linear viscoelastic region (Goodrich., 1991, Kim and Lee., 1995). This means that time and temperature are interchangeable in terms of the viscoelastic response; e.g., the material response at a long duration load at a low temperature is the same as the response to a short duration load at a high temperature. The time-temperature superposition principal (TTS) for thermorheologically simple materials applies horizontal shifting of the material response at different temperatures along the time or frequency horizontal axis to form a single master curve representing the response versus a "reduced" time or frequency. The reduced time or frequency incorporates both effects of time and temperature.

In addition, it has been theoretically demonstrated (Park and Schapery, 1997; Schapery, 1999) and verified through a number of laboratory studies (Schwartz et al., 2002; Chehab et al., 2002; Zhao and Kim, 2003) that asphalt mixtures remain thermorheologically simple beyond the linear viscoelastic region and well into the microstructural damage and viscoplastic domains approaching failure. Park and Schapery

(1997) and Schapery (1999) theoretically explained the validity of the time-temperature superposition in the linear viscoelastic state as well as the nonlinear damaged state in the context of a solid rocket propellant. Schwartz et al. (2002) showed the validity of the time-temperature superposition at large compressive strains via a series of uniaxial constant strain rate tests at various loading rates and temperatures. Chehab et al. (2002) in a similar study proved that asphalt mixtures remain thermorheologically simple in tension with growing damage approaching failure. Zhao and Kim (2003) confirmed the validity of TTS for asphalt mixtures with growing damage and permanent deformations via constant crosshead rate compression tests, repeated creep and recovery tests, and the cyclic sinusoidal loading tests in compression.

RLPD data for twenty three (23) different asphalt mixtures including different binder grades, different aggregates (virgin, RAP, RAS), and different gradations and aggregate sizes were obtained from NCHRP Project 9-30A and the present study. The activation energy factors, RLPD test temperatures, volumetric properties, and other characteristics of the 18 asphalt mixtures selected from the NCHRP Project 9-30A database are shown in Table 17. The mixtures selected from the present study are H168A09R2C02, H138B12R2C05, H176A09R2C01, H083A12C2C02, and H138A12G4F05. Their characteristics are given in Table 4 and Table 5 (Chapter 3).

The triaxial RLPD tests were conducted according to the NCHRP Project 9-30A recommendations for asphalt mixtures at low, intermediate, and high temperatures. A minimum of two replicate specimens were tested at each temperature. A cyclic deviator stress of 70 psi was applied for 10,000 cycles at a constant confining pressure of 10 psi. As

usual, each load cycle consisted of a 0.1 second loading duration followed by the 0.9 second rest period.

Table 17: NCHRP 9-30A Asphalt Mixture Properties

Mix #	Mix ID	Mix type	VMA%	VFA%	e%	ΔE	RLPD Test Temperatur (C^0)
1	Alabama; HMA overlay	SPS-6, overlay binder, polymer modified	14.7	66.0	5.0	213,992.3	20, 40, 60
2	California; CA 47 mix	I-710 perpetual pavement, CA 47	16.0	64.3	5.8	223,247.8	20, 35, 50
3	California; CA 47M mix	I-710 perpetual pavement, CA 47M	16.3	63.1	5.5	161,125.0	20,35, 50
4	California; CA 52 mix	I-710 perpetual pavement, CA 52	14.4	81.8	2.5	211,089.5	20, 35, 50
5	Colorado 1918 16.2 65.9 5.6	SPS-5, binder layer with rap	16.2	65.9	5.6	205,347.9	20, 35, 50
6	Colorado 1938	SPS-5, binder layer without rap (virgin)	16.3	68.5	5.1	223,377.0	20, 35, 50
7	Florida base neat mix	NCAT, HMA base	16.7	65.8	5.7	194,469.2	20, 37, 55
8	Florida N1	NCAT N1 section, PMA mix	18.3	59.0	7.6	204,455.5	20, 37, 55
9	Florida N2	NCAT N2 section, neat mix	16.3	64.2	5.8	203,096.9	20, 37, 55
10	Indiana HMA mix 7A	NCAT section 7A, HMA low void mix	18.0	71.3	5.2	192,529.3	20, 37, 55
11	Indiana HMA mix 7B	NCAT section 7B, HMA low void mix	18.4	70.1	5.6	190,761.3	20, 37, 55
12	Indiana HMA mix 8B	NCAT section 8B, HMA wearing surface	17.1	79.2	3.6	186,620.5	20, 37, 55
13	Missouri RAP binder	SPS-5, binder mix with RAP	16.4	50.7	8.1	226,800.1	20, 34, 47
14	Missouri virgin binder	SPS-5, binder mix without RAP (virgin)	19.0	54.9	8.6	191,982.1	20, 34, 47
15	Missouri surface	SPS-5, wearing surface	20.3	57.3	8.7	206,275.0	20,34, 47
16	Wisconsin ATB base	SPS-1, HMA base, ATB mix	14.9	56.9	6.3	200,750.5	20, 35, 50
17	Wisconsin HMA surface mix	SPS-1, HMA wearing surface	18.3	53.3	8.6	206,744.9	20, 35, 50
18	Wisconsin HMA binder mix	SPS-1, HMA binder mix	18.1	63.1	6.4	217,114.0	20, 35, 50

VMA:oids in Mineral Aggregates, VFA: Voids Filled With Asphalt, e: Air Voids, ΔE: Activation Energy

As per Section 4.1, the secondary portion of the RLPD test response is the most relevant for pavement performance prediction. A power model given in Equation 7 is typically used to represent the secondary stage of permanent deformation. A power law plots as a straight line in log-log space with log (a) as the intercept and b as the slope. The higher the slope and intercept of the secondary stage, the higher is the potential for rutting.

Figure 39 explains the shifting process for RLPD data. The cumulative plastic strain in the secondary stage of the RLPD test at different temperatures are shifted horizontally by the appropriate temperature shift factor $\alpha(T)$ taken from the DM testing:

$$\log(RN) = \log(N) + \log[\alpha(T)] \quad \text{Equation (13)}$$

in which

RN = Reduced number of loading cycles

The temperature shift factors here are the same as obtained from the DM test (Equation 3). Substituting N with RN in Equation 7 in log-log space, the new intercept of the shifted power law in log-log scale is:

$$\log \varepsilon_P = \log(a) + b \log (N) \quad \text{Equation (14)}$$

$$\log\varepsilon_P = \log (a) + b\ (log\ (N) + log[\alpha(T)]) \quad \text{Equation (15)}$$

$$\log\varepsilon_P = \log(a) + b\ log[\alpha(T)] + b \log(N) \quad \text{Equaiton (16)}$$

in which

$$\log a' = \log a + b \log a(T) \quad \text{Equation (17)}$$

a' = Intercept of the master RLPD curve at the reference temperature.

The master RLPD power law model in arithmetic space at the reference temperature will follow the following equation:

$$\varepsilon_P = \mathrm{a}\times\alpha(T)^b(RN)^b \qquad \text{Equation (18)}$$

The RLPD master curve function implicitly assumes that there are no significant differences in the slopes of the power law model at the different temperatures. This assumption is consistent with the findings of the comprehensive NCHRP 9-30A study (Von Quintus et al., 2011) and with many other conventional models for permanent deformations (Leahy, 1989; Kaloush and Witczak, 2000). More specifically, the NCHRP 9-30A methodology obtains the representative slope for a mixture by averaging all the slopes from the tests at various temperatures. If there is significant difference in the slopes at various temperatures, the representative slope of the mixture can be obtained from RLPD tests at the equivalent annual temperature (Von Quintus et al., 2011).

The NCHRP 9-30A methodology does include the temperature (T) dependency of the intercept (a) of the secondary stage power law model via an explicit global temperature term:

$$\mathrm{a} = \mathrm{d}T^n \qquad \text{Equation (19)}$$

in which

d = intercept

n = slope

By replacing intercept (a) in Equation 7

$$\varepsilon_p = \mathrm{d}T^n\times N^b \qquad \text{Equation (20)}$$

In the NCHRP 9-30A procedure, the value of log (a) for each temperature is taken as the average of the intercepts from the test replicates at that temperature. The coefficients *d* and *n* in Equation 20 are then determined from the intercept (a) vs. temperature (T) values via power law regression. Several other permanent deformation models also contain a similar global temperature term that influences only the intercept of the secondary stage (Leahy, 1989; Kaloush and Witczak, 2000).

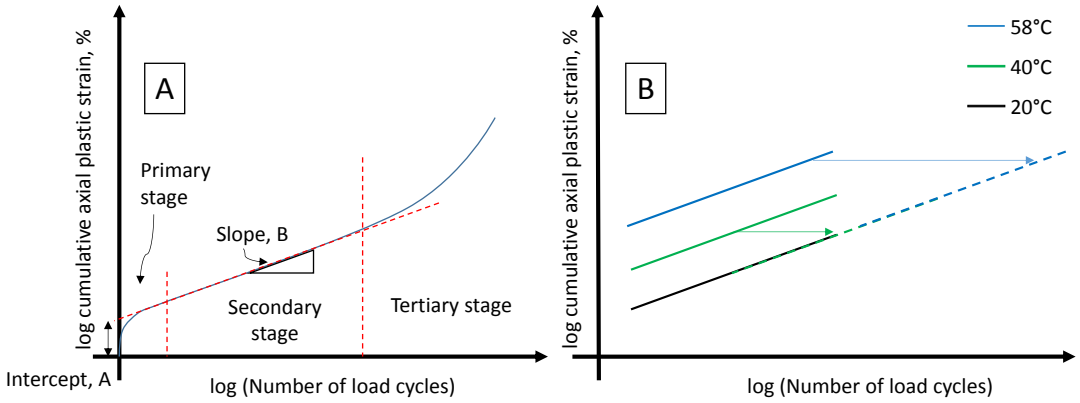

Figure 39: (A) Schematic of the Three Main Stages of the RLPD Behavior and the Slope and Intercept of the Secondary Stage; (B) The Process of Shifting the RLPD Data at Different Temperatures to Obtain the RLPD Master Curve at the Reference Temperature.

Figure 40 presents the secondary stage of the RLPD test results at the three test temperatures for the five evaluated mixtures from the current study. None of the specimens entered the tertiary stage. The first 2000 cycles were trimmed before fitting the power law model to eliminate the primary stage. The dashed lines in Figure 40 present the average prediction of the secondary stage at each temperature obtained by averaging the slopes (b) and intercepts ($log\ a$) of the test replicates at that temperature.

As explained in the test methodology, the temperature shift functions from the dynamic modulus master curve fitting were used to horizontally shift the cumulative plastic

axial strain of each replicate at each temperature to form the RLPD master curve at the reference temperature of 20°C. Figure 40 depicts the cumulative plastic axial strain versus reduced number of load cycles (RN) in log-log space. The cumulative plastic axial strain at different temperatures collapse relatively well to form a single cumulative strain versus reduced number of loading cycles (RN), confirming the validity of TTS in the viscoplastic domain in repeated load permanent deformation tests.

While it is not valid to take the average of all intercepts at different temperatures in physical load cycle space (N), it is justified to do so in reduced time domain (RN) since all the data are shifted to a same reference temperature of 20°C. The solid red line in Figure 40b is the representative RLPD power law master curve fit based on all test replicates after shifting obtained by averaging the slopes (b) and shifted intercepts ($log\ a'$) of all test replicates. The dashed lines in Figure 40b present the representative RLPD lines in reduced N domain for the data at each temperature.

Table 18 summarizes the coefficients of the RLPD power law relations before and after the shifting process at each temperature (i.e. the slopes and intercepts of the dashed lines in Figure 40a) and the coefficients of the RLPD master curve (solid red line in Figure 40b). The average slope at the low temperature of 20°C was slightly lower than the other two temperatures, but this discrepancy was statistically insignificant. The NCHRP 9-30A study also reported some differences in the average slope at the lowest temperature as compared to the other temperatures and suggests using the slope at the higher temperatures in case of a significant difference. As summarized in

Table 18, the coefficients of the RLPD master curve are in closest agreement in most cases with those of the 40°C shifted to the reference temperature, suggesting that the testing program can be reduced to this single temperature.

H168A09R2C02F

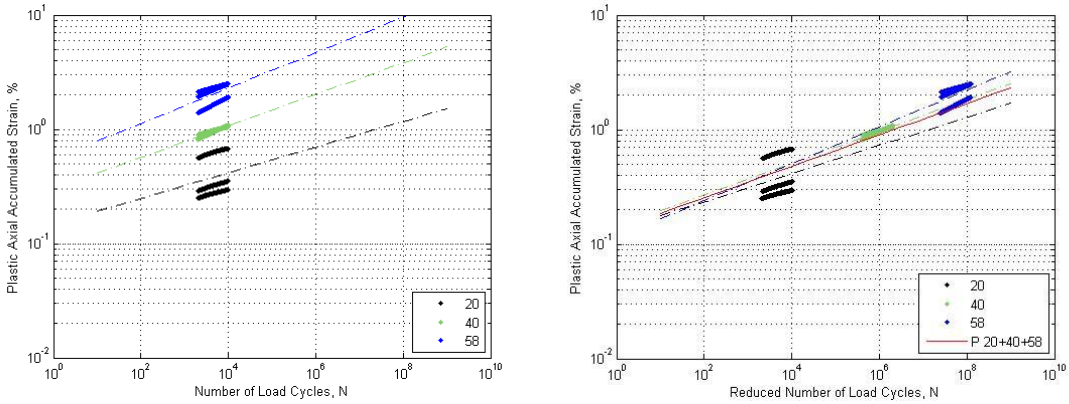

H138B12R2C05

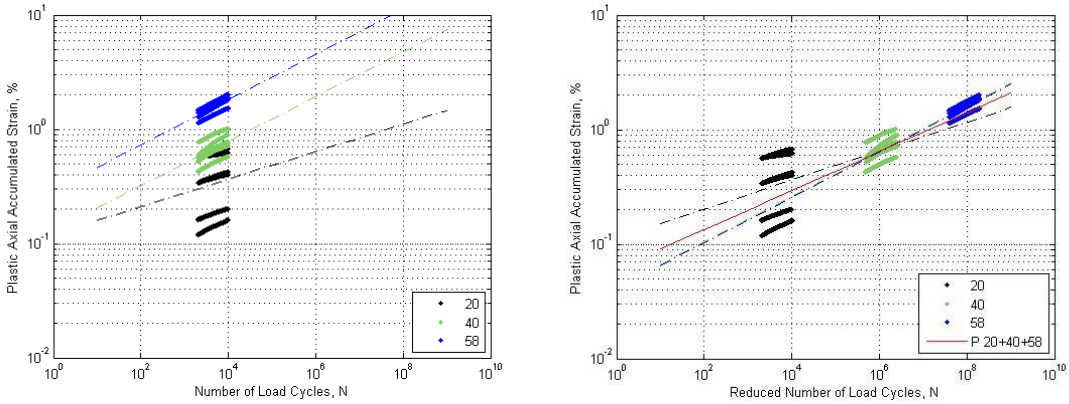

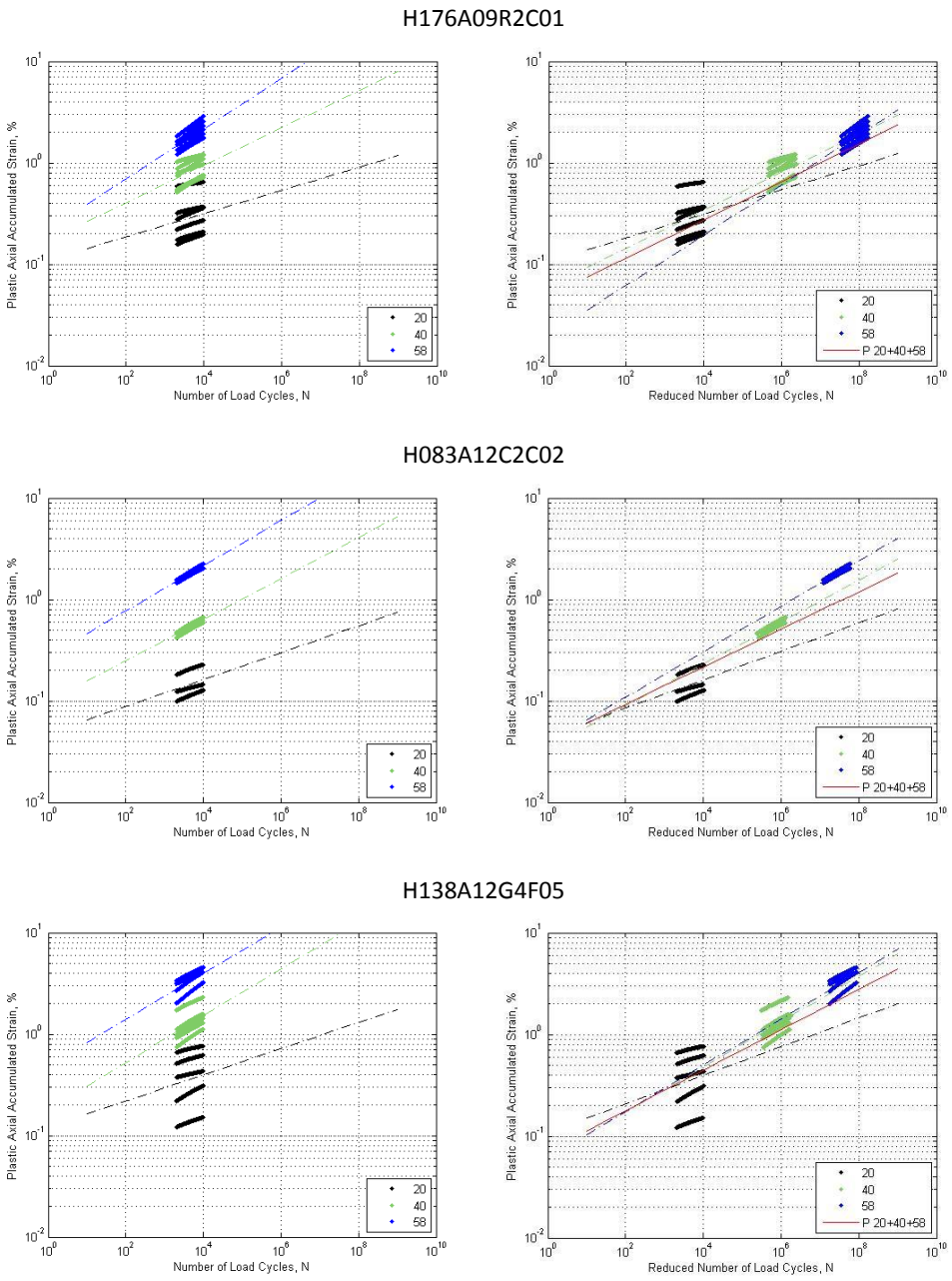

A (before shifting) B (after shifting)

Figure 40: The RLPD Test Results at Three Different Temperatures (A) Before Shifting and (B) After Shifting

Table 18: Average Coefficients of RLPD Power Law Model before and after Shifting

		Before shifting		*After shifting*		
Mixture ID	Temperature °C	Intercept (A)	Slope (B)	Intercept A.[a(T)]^B	Slope B	Number of Replicates
H176A09R2C01	20	0.0011	0.12	0.0011	0.12	6
	40	0.0017	0.19	**0.0006***	**0.19**	7
	58	0.0022	0.25	0.0002	0.25	7
	All	----	----	0.0005	0.19	20
H138A12G4F05	20	0.0012	0.13	0.0012	0.13	5
	40	0.0018	0.23	**0.0006**	**0.23**	6
	58	0.0048	0.23	**0.0006**	**0.23**	4
	All	----	----	0.0007	0.20	15
H138B12R2C05	20	0.0012	0.12	0.0012	0.12	6
	40	0.0013	0.20	**0.0004**	**0.20**	6
	58	0.0029	0.20	**0.0004**	**0.20**	4
	All	----	----	0.0006	0.17	16
H083A12C2C02	20	0.0005	0.14	0.0005	0.14	3
	40	0.0009	0.21	0.0003	**0.21**	3
	58	0.0027	0.22	**0.0004**	0.22	2
	All	----	----	0.0004	0.19	8
H168A09R2C02F	20	0.0014	0.12	0.0014	0.12	3
	40	0.0030	0.14	**0.0014**	**0.14**	2
	58	0.0055	0.15	0.0011	0.15	3
	All	----	----	0.0014	0.14	8

*** Bolded numbers denote the A' and B values closest to the average master curve for each mixture.**

In order to take practical advantage of TTS to reduce the testing requirements for permanent deformation characterization of asphalt mixtures, it is important to effectively predict the cumulative strain at any temperature using the RLPD test results from a single temperature. To validate this, the master curve obtained at a single temperature testing was used to predict the cumulative strain at the other temperatures at 5000 cycles.

Figure 41 shows the average relative errors of the predicted permanent strains at different numbers of cycles over all data. The RLPD master curves were developed by using all data at all three temperatures for all 23 asphalt mixtures.

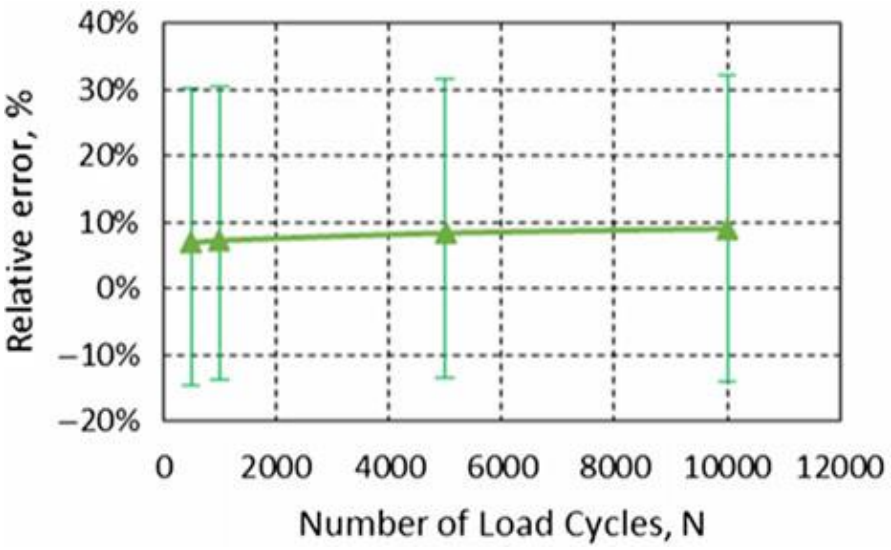

Figure 41: Average Prediction Errors for All Temperatures using the RLPD Master Curve (MC_{all}); Error Bars Show One Standard Deviation

Figure 42 (A)–(D) summarizes the predicted cumulative plastic axial strain based on RLPD master curves constructed using data at all temperatures (MCa_{ll}), at the low temperature only (MC_{low}), at the intermediate temperature only (MC_{intmed}), and at the high temperature only (MC_{high}), respectively, versus measured cumulative plastic strain at 5000 physical cycles. There is a fairly good correlation between the predicted and measured cumulative plastic strain using all of the different master curve models (MC_{all}, MC_{low}, MC_{intmed} and MC_{high}). However, the MC_{high} generally provided the most accurate predictions overall. The average relative prediction errors from the four master curve models (MC_{all}, MC_{low}, MC_{intmed} and MC_{high}) are presented in Table 19 for all test temperatures together and separately for low, intermediate and high test temperatures.

There is less than 10% relative error on average associated with MC_{high} predictions for the 23 evaluated mixtures. Moreover, the R^2 value of 0.98 confirms the high level of correlation between the MC_{high} predicted strains and the measured strains.

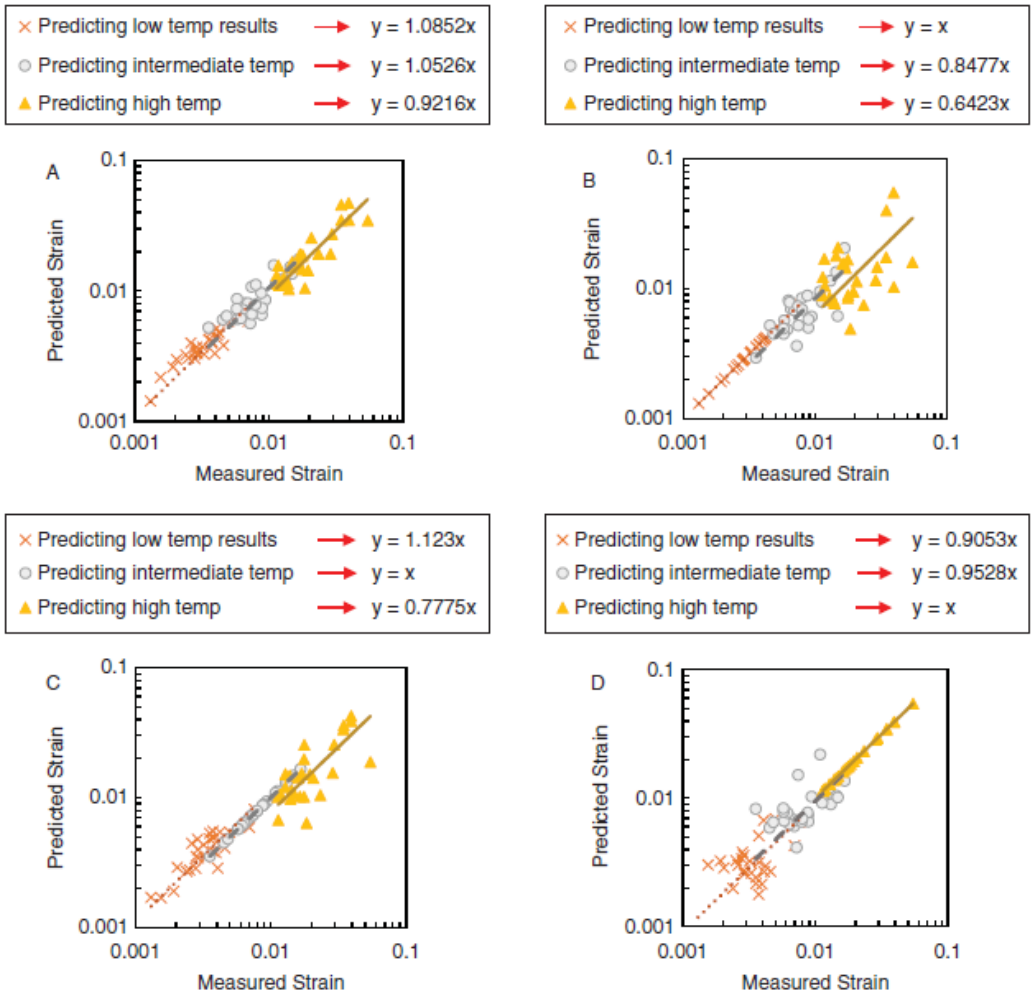

Figure 42: Predicted Versus Measured Plastic Axial Cumulative Strains at Various Temperatures at 5000 Cycles. Prediction Master Curve Coefficients Obtained using: (A) Data at All Temperatures; (B) Low Temperature Data Only; (C) Intermediate Temperature Data Only; (D) High Temperature Data Only

Table 19: Average Relative Error from Each Master Curve Model

Measure	Model	MC_{all}	MC_{low}	MC_{inter}	MC_{high}
	Prediction	%	%	%	%
Relative Error (%)	All Temperatures	8	-13	1	4
	Low Temperature	17	0	20	1
	Intermediate Temperature	12	-12	0	10
	High Temperature	-4	-25	-17	0
R^2		0.94	0.71	0.87	0.98

Figure 43 demonstrates the distribution of relative errors at low and intermediate temperatures as predicted using MC_{high}. There is a generally uniform distribution of relative errors with no significant local or global bias. In theory, the master curve obtained at any temperature should be able to predict the strain at any other temperature based on TTS. Nevertheless, the results from 23 mixtures with different binder and aggregate types suggest that MC_{high} obtained using the high temperature test data only provides the most accurate and least biased predictions over the range of temperatures. Moreover, since the asphalt layer is most susceptible to permanent deformations in high temperatures, it is arguably preferable to capture its performance at high temperature through direct testing and use the TTS principle to predict the permanent deformation at lower temperatures of interest.

Each RLPD test takes around three hours to run not including the specimen preparation time. The proposed scheme of performing RLPD testing only at the high temperature and using TTS with the temperature shift function derived from DM testing can practically reduce the number of required specimens from 9 to 3 and the testing duration from 27 h (three replicates at each of three temperatures) to 9 h (three replicates at high temperature only), excluding specimen preparation time. This will greatly facilitate the adoption of routine RLPD testing by agencies.

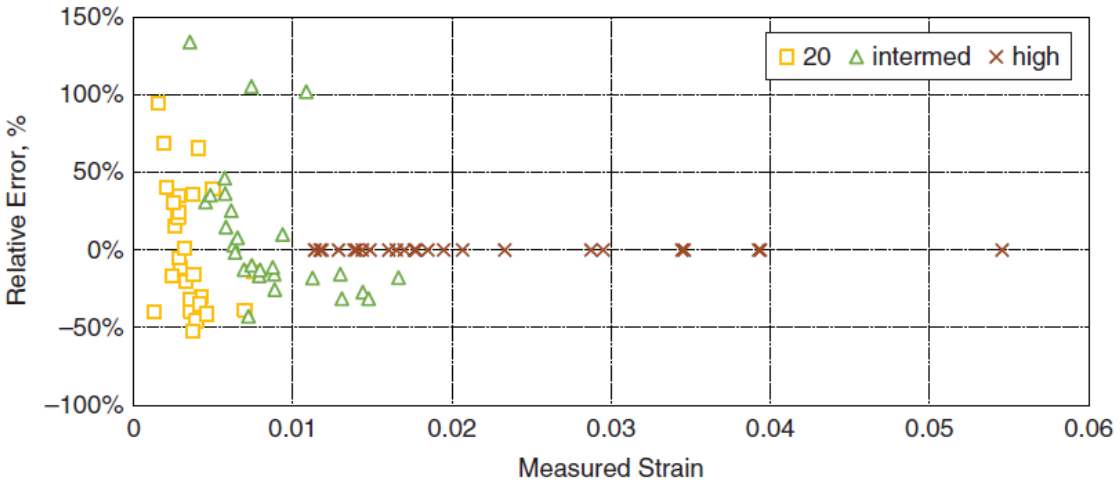

Figure 43: Distribution of MC_{high} Relative Error of Prediction in Low and Intermediate Temperatures

SUMMARY AND CONCLUSIONS

NCHRP Projects 9-19 and 9-29 developed the DM and RLPD tests as performed in the AMPT as routine tests for asphalt mixture evaluation, structural design, and rutting performance prediction of asphalt mixtures. While the refined test methods specified for AMPT are faster and easier to perform than their preceding research grade test protocols, there is still reluctance among highway agencies and industry to conduct these tests on a routine basis. A main reason for this is the lengthy process of specimen preparation and testing program for DM and RLPD tests.

To expedite the asphalt mixtures characterization testing program three investigations were performed to evaluate elimination of high temperature testing in the DM test, reuse of DM test specimens for RLPD testing, and using time-temperature superposition to reduce the number of temperatures in the RLPD test. The findings from these investigations are as follows:

(1) Testing time can be saved by completely eliminating the testing at 40°C and adding a frequency of 0.01Hz at 20C with no statistically significant impact on the computed dynamic modulus master curves.

(2) Reusing the DM specimens in RLPD test reduces time and labor by reducing the total number of specimens from 12 to 9. Reuse of DM specimens has no statistically significant influence on the computed RLPD properties.

(3) Applying the time-temperature superposition (TTS) concept to RLPD testing reduces time and labor by reducing the number of test temperatures from three to one and the total number of RLPD specimens from nine to three (for three replicates per test condition). TTS, when performed based on tests performed

at the highest temperature, introduces very little error into the permanent deformation characterization.

The overall consequences of all three of these findings is a reduction in the total number of test specimens from 12 to 3, a reduction in total specimen preparation time from 60 to 15 hours, and a reduction in total testing time (including temperature equilibration) from 30 to 10 hours. These represent substantial economies in the structural characterization of asphalt mixtures.

CHAPTER 6: SENSITIVE ANALYSIS OF DM AND RLPD PROPERTIES IN MEPDG

Previous studies (Khazanovich et al., 2008; Thyagarajan et al., 2010; Li, 2013) on the sensitivity of predicted pavement performance to the MEPDG design inputs found that predicted permanent deformation (total and asphalt rutting) and cracking (top-down and bottom up fatigue cracking) are very sensitive to the E* values of asphalt layers. Due to this high sensitivity, sensitivity analyses were performed to evaluate the influence of of measured (Level 1 input) versus predicted E* (Level 3) values on predicted distress for Maryland mixtures. These sensitivity analyses will answer two questions: What is the sensitivity of predicted performance to the differences in measured E* values for different mixtures? and What is the senstitivity of predicted performance to Level 1 versus Level 3 E* inputs?

In addition to E* values, another factor, the coefficients of the MEPDG rutting model, was added in the senstivity analysis. The RLPD tests data was used to calibrate the MEPDG rut model as explained in Chapter 4, with the obtained coefficients tabulated in Table 20.

6.1 Variables and Fixed Inputs Used in Sensitivity Analyses

The latest vesion 2.1 of the AASHTOWare Pavement ME Design was used in the sensitivity analyses. The Maryland State Highway Administration Pavement and Geotechnical Design Guide (MDSHA PGDG) was used as a reference for traffic levels, climate conditions, material properties inputs, and design limits for distresses. The fixed and variable inputs used in the sensitivity analyses are shown in Table 21 and Table 22

respectively. The distesses limits defined by the MDSHA PAGD for flexible pavement in Maryland are tabulated in Table 23 .

The sensitivity analyses were performed for three scenarios: 1) Level 3 E* data of E* and default K_1, K_2 and K_3 rut model coefficients (L-3 inputs), 2) Level 1 E* data and default K_1, K_2 and K_3 rut model coefficients (L-1-A inputs), and 3) Level 1 E*data and re-calibrated K_1, K_2 and K_3 rut model coefficients from the RLPD measurements (L-1 inputs). Low, medium and high traffic levels and one climate condition were considered in the sensitivity analyses. Overall, 252 runs (28 mixtures x 3 traffic levels x 3 scenarios of inputs) of the Pavement ME Design software were performed. Each run requires about 5 to 10 minutes of execution time.

When using Level 1 E* input to the Pavement ME Design software, Level 1 binder shear modulus (G*) inputs are also required. Therefore, Level 1 G* data were required for the two binders (PG 64-22 and PG 76-22) used in the Maryland mixtures. Typical Level 1 G* data for PG 64-22 and PG 76-22 binders were obtained from the FHWA Turner-Fairbank Highway Research Center. Subsequent analyses proved that the predicted pavement distresses were largely insensitive to the Level 1 G* binder inputs as compared to the Level 1 E* mixture inputs.

Table 20: Recalibrated Coefficients of the MEPDG Rut Model

No	HMA Mixtures	K1 (Intercept)	K 2 (Temperature Coeff)	K3 (Loading Cycles Coeff)
1	H040A12R2C12	-0.4738	0.8493	0.2125
2	H051A12B4F01	-0.9173	1.1447	0.1826
3	H077A09A2C03	-0.2408	0.6259	0.2125
4	H077A09C2C01	-2.5466	2.0596	0.2646
5	H083A12C2C02	-0.0810	0.5955	0.1813
6	H083A19C2C02	0.4012	0.3402	0.1826
7	H116C09A2F02	-0.4716	0.8591	0.1654
8	H127A12R2C02	-0.0681	0.6078	0.1835
9	H128A12B4F02	-0.0503	0.5755	0.1975
10	H131A09A4C01	0.7998	0.0901	0.1594
11	H135A12G4F01	-1.9407	1.5915	0.1954
12	H135A12H2C02	-0.5006	0.7948	0.1764
13	H135A19G4F01	-0.5434	0.8729	0.2052
14	H138A12G4F05	-0.6581	0.8609	0.2115
15	H138B12R2C05	-0.2206	0.7784	0.1933
16	H151B19R2C02	-0.8652	1.1622	0.1687
17	H158B09R2C60	-0.7580	1.0422	0.2075
18	H160A09R1C03	-0.6433	0.9944	0.1859
19	H160A12H2F01	-0.1890	0.6643	0.1928
20	H161A12R4F01	-0.9350	1.1163	0.2209
21	H168A09R2C02	1.0588	0.1128	0.1220
22	H168A12R2C02	-0.6022	0.8963	0.1917
23	H169A12B4F03	-0.2489	0.8064	0.1925
24	H176A09R2C01	0.4939	0.2632	0.1866
25	H176A19R2C02	-0.2575	0.6263	0.2100
26	H177A12R2C50	-0.7826	0.9524	0.2133
27	H186D12B4F01	-0.5294	0.8580	0.2062
28	H187A19C2C02	-1.2111	1.1810	0.2330

Table 21: Fixed Inputs Used in MEPDG Software for Sensitivity Analyses

Desing Life (Years)	20
Traffic Data	
Number of lanes in design direction:	2
Percent of trucks in design direction (%):	50
Percent of trucks in design lane (%):	95
Operational speed (mph)	60
Mean wheel location (in)	18
Traffic wander standard deviation (in)	10
Design lane width (ft)	12
Average axle width (ft)	8.5
Dual tire spacing (in)	12
Tire pressure (psi)	120
Tandem axle spacing (in)	51.6
Tridem axle spacing (in)	49.2
Quad axle spacing (in)	49.2
Climate Data	
Climate Station Cities:	HAGERSTOWN, MD
Mean annual air temperature (ºF)	53.65
Mean annual precipitation (in)	34.58
Freezing index (ºF - days)	344.56
Average annual number of freeze/thaw cycles:	57.96
Material Properties	
Asphalt Layer	
Air Voids (%)	**7**
Unit weight of asphalt layer (psi)	150
Poisson's Ratio of asphalt layer	0.35
Reference temperature (ºF)	70
Thermal conductivity (BTU/hr-ft-ºF)	0.67
Heat capacity (BTU/lb-ºF)	0.23
Base and Subgrade	
Granulare Base	Default values of A-1-a Soil
Subgrade	Default values of A-4 Soil
Depth of Subgrade	Semi Infinite
Water table depth(ft)	10

Table 22: Input Values for Sensitivity Analyses

Traffic Level	EASLs (Millions)	AADTT	Functional Class	Pavemetn Structure		Speed (mph)	Dynamic Modulus of Asphalt layer (E*)	Coefficients of Rut Model (k1,k2,k3)	Effective Binder Contents and Gradations	G* values of Binder
				AC Thick (In)	Granular Base (in)					
Low traffic	3	300	17 (urban)	7	10	60	Measured and Predicted Values of 28 mixtures	Default and Re-Calibrated Values	Data of 28 mixtures	PG-64-22 and PG 76-22
Medium traffic	10	800	6 (Rural)	9	12	60				
Heavy traffic	30	3400	12 (Urban)	14	12	45				

Table 23: Design Distress Limits as per MDSHA PAGD

Design Distress Limit						
IRI (in/mile) Initial = 60	PD (t) (in)	BU FC (%)	Therm.C (ft/mile)	TD-FC (ft/mile)	PD (ac) in	Reliability
175	0.75	5	7500	500	0.2	50% (IRI)
158	0.75	5	6500	500		90%
115	0.75	5	5000	500		

The predicted distresses considered in the sensitivity analyses were the International Rough Index (IRI), Total Permanent Deformation (PD_t), Permanent Derformation of the Asphalt Concrete Layers (PDac), Top-Down Fatigue Cracking (TD-FC), and Bottom-Up Fatigue Cracking (BU-FC). The obtained distresses after running 252 runs of Pavement ME Design are normalized by the design limits given in Table 23. The variations in these normalized distressess with respect to the three traffic scenarios for the 28 mixtures are summarized in the box and whisker plots shown in Figure 44.

Table 24 and Figure 45 summarize the average percentage differences in the predicted distresses between L-3 versus L-1, L-3 versus L-1-A, and L-1-A versus L-1 asphalt inputs. Asphalt rutting is most impacted by the different input levels, followed by total rutting. As would be intuitively expected, the differences between L-3 versus L-1 inputs are the largest of the three scenarios.

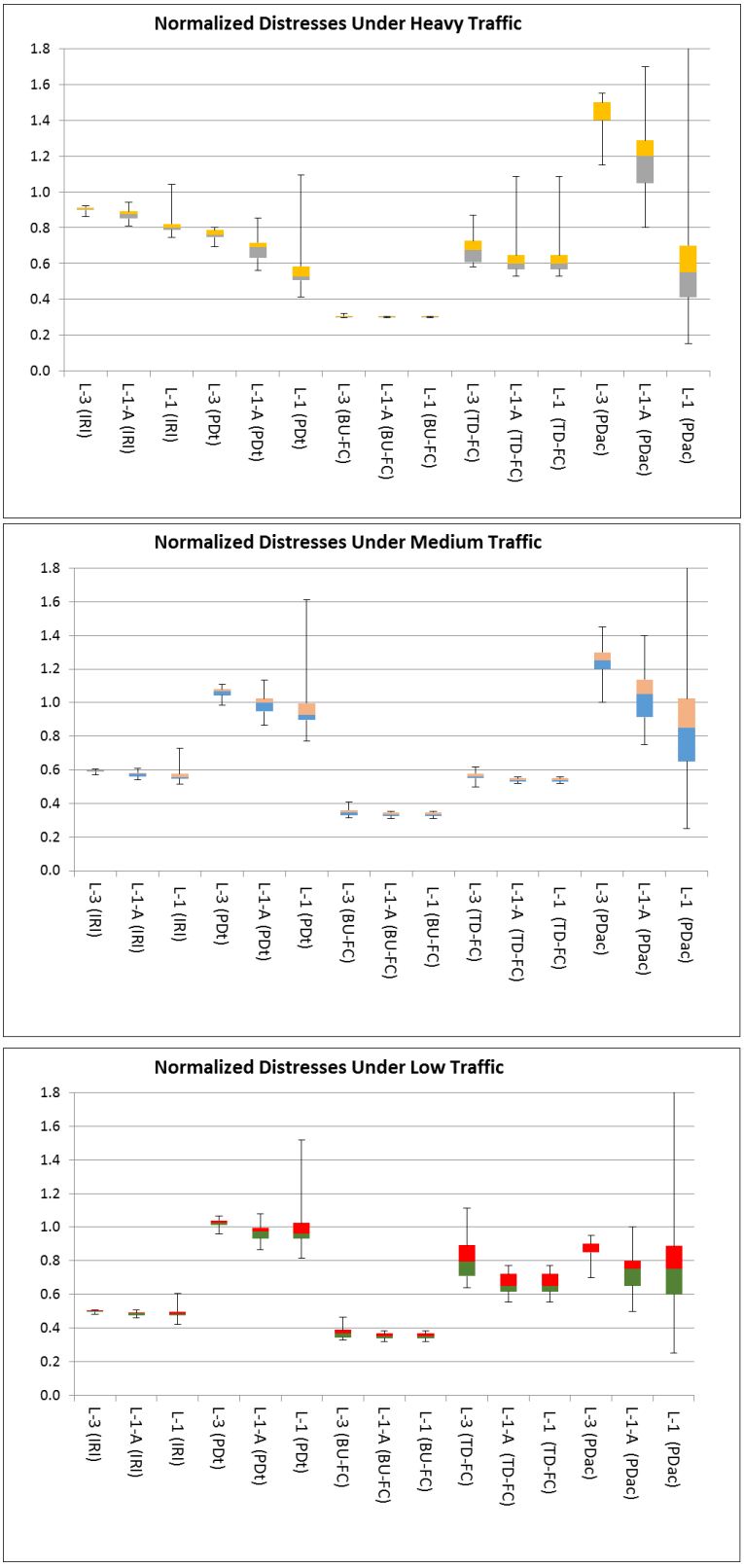

Figure 44: Variations in Predicted Distresses due to L-1, L-1-A, and L-1 Input Levels

Table 24: Percentage Differences of Predicted Distresses Due to L-3, L-1-A, and L-1 Input Levels at Three Volumes of Traffic

Distress Type			Terminal IRI (in/mile)	PD - Total pavement (in)	AC-BU (% lane area)	AC-TD (ft/mile)	PD - AC only (in)
Heavy Traffic	Normalized Average Values	L-3	0.90	0.76	0.30	0.68	1.41
		L-1-A	0.87	0.69	0.30	0.62	1.19
		L-1	0.80	0.54	0.30	0.62	0.56
	Average % Difference	L-3 & L-1-A	3.13	7.67	0.28	5.75	21.96
		L-3 & L-1	10.04	22.49	0.28	5.64	85.27
		L-1 & L-1A	6.91	14.82	0.00	-0.11	63.31
Medium Traffic	Normalized Average Values	L-3	0.59	1.06	0.35	0.56	1.24
		L-1-A	0.57	0.99	0.33	0.54	1.04
		L1	0.56	0.94	0.33	0.54	0.81
	Average % Difference	L-3 & L-1-A	1.87	6.99	1.23	2.16	19.46
		L-3 & L-1	3.28	12.39	1.26	2.17	42.80
		L-1 & L-1A	1.41	5.41	0.03	0.01	23.34
Low Traffic	Normalized Average Values	L-3	0.50	1.02	0.37	0.81	0.85
		L-1-A	0.48	0.97	0.35	0.66	0.72
		L-1	0.48	0.97	0.35	0.66	0.72
	Average % Difference	L-3 & L-1-A	1.32	5.62	1.79	14.55	12.86
		L-3 & L-1	1.43	5.66	1.83	14.54	12.87
		L-1 & L-1A	0.10	0.04	0.04	-0.01	0.01

PD: Permanent Deformation, AC-BU: Asphalt Concrete-bottom up fatigue cracking, AC-TD: Asphalt Concrete-top down fatigue

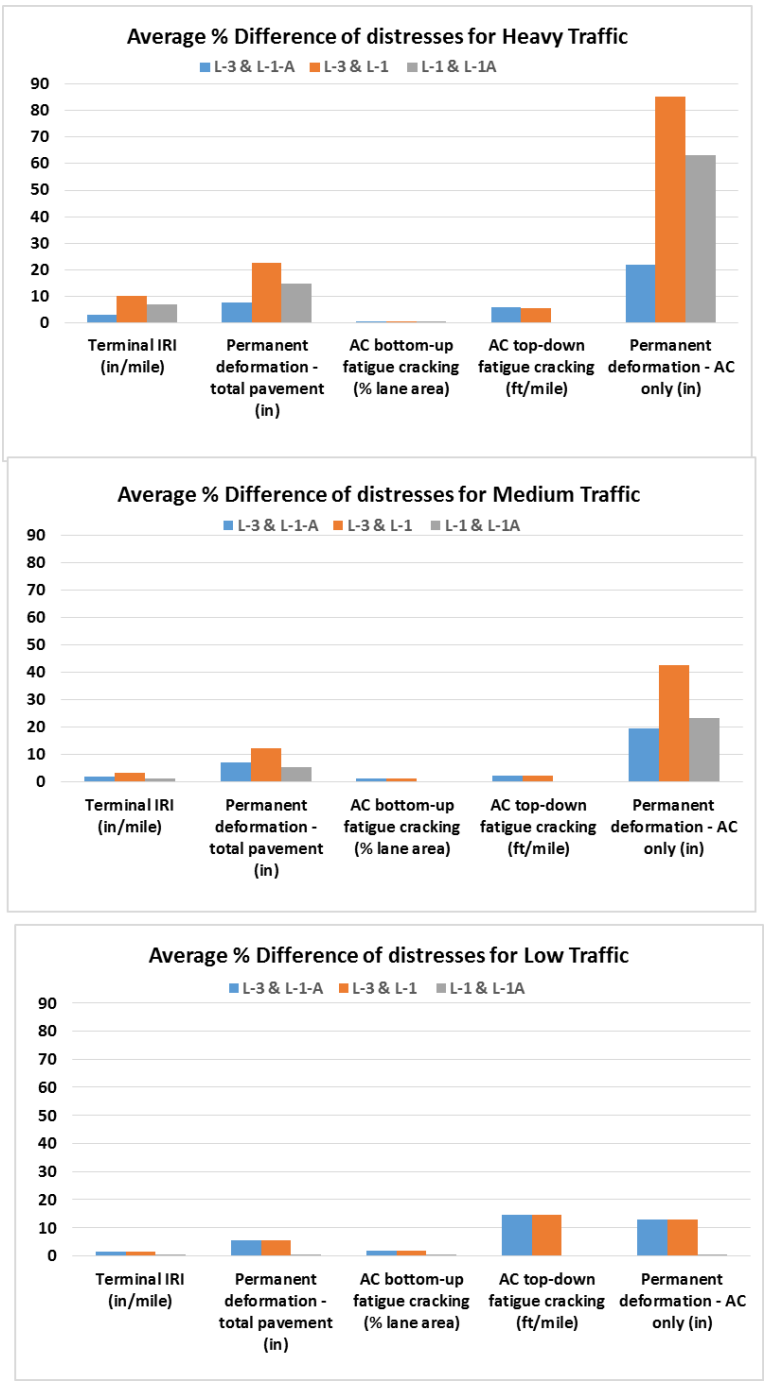

Figure 45: Average Percentage Differences from L-3 versus L-1-A, L-3 versus L-1, and L-1 versus L-1-A Inputs

6.2 Insights from the Sensitivity Analyses

Insights from the sensitivity analyses include the following:

1. Predicted distresses are sensitive to the DM and RLPD properties of asphalt mixtures. The predicted distresses using default values for E* and rut model coefficients do not adequately differentiate the effects of different types of asphalt mixtures. More differentiation in predicted distresses was found when using L-1 inputs (measured E* and recalibrated K_1, $K2$, and K_3 rut model coefficients) as compared to L-1A (measured E* and default rut model coefficients) and L-3 (predicted E* values and default rut model coefficients) inputs.
2. The sensitivity of predicted distresses to L-3, L-1-A and L-1 inputs at three levels of traffic can be ranked in the following order: rutting of the apshalt layers, total rutting, top down fatigue cracking (except for the medium traffic level), International Roughness Index, and bottom up fatigue cracking.
3. The average percentage differences in asphalt rutting due to L-1, L-1-A and L-3 inputs is significantly higher than for the other distresses at all traffic levels (Figure 45).
4. The average percentage differences for each predicted distress at all levels of traffic are highest for L-1 versus L-3 inputs and lowest for L-3 versus L-1-A inputs (Figure 45).

CHAPTER 7: RECALIBRATION OF WITCZAK E* PREDICTIVE MODEL

7.1 Recalibration of Witczak E* Predictive Model

The measured dynamic modulus values are defined as Level 1 inputs in the MEPDG software. In the absence of Level 1 E* inputs, Level 3 inputs consisting of predicted E* values calculated using the Witczak E* prediction model (Witczak and Fonseca, 1996) can be used in MEPDG design. The Witczak E* prediction model is given in Equation 6 and reproduced here.

$$\log E^* = 3.750063 + 0.029\rho_{200} - 0.0018{\rho_{200}}^2 - 0.0028\rho_4 - 0.058V_a - 0.822\frac{V_{eff}}{V_{eff}+V_a} + \frac{3.872-0.0021\rho_4+0.004\rho_{38}-0.000017({\rho_{38}}^2)+0.0055\rho_{34}}{1+e^{(-0.603313-0.313351\log(f)-0.393532\log(\eta)}}$$

in which

E* = Dynamic modulus of mix, psi

η = Viscosity of binder, 10^6 Poise

f = Loading frequency, Hz

ρ_{200} = % passing #200 (0.075mm) sieve

ρ_4 = Cumulative % retained on #4 (4.75mm) sieve

ρ_{38} = Cumulative % retained on 3/8 inch (9.5mm) sieve

$\rho_{3/4}$ = Cumulative % retained on 3/4 inch (19mm) sieve

V_a = Air void, % by volume

V_{beff} = Effective binder content, % by volume.

Equation 6 was used to calculate the predicted E* values for all asphalt mixtures tested in this study. Figure 46 plots the predicted (MEDPG Level 3) vs. measured (MEDPG Level 1) E* values for all mixtures. It is clear from Figure 46 that the Witczak E* prediction model tends to underpredict the E* values, as most of the data points are either on or below the line of equality (red line). This underprediction of E* may result in over or under predictions of the distresses in the pavement structure over its design life.

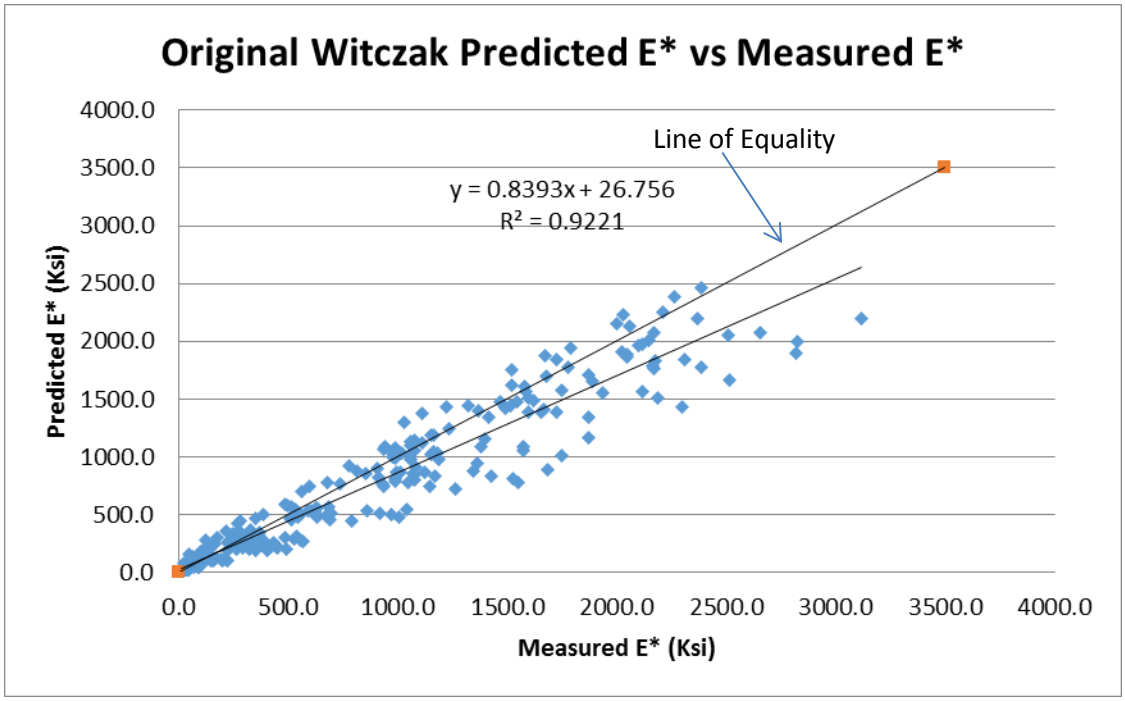

Figure 46: Comparison of Level 3 (Predicted using Original Witczak Model) versus Level 1 (Measured) Dynamic Moduli

It is possible to recalibrate the Witczak E* model based on the measured E* values of 28 Maryland asphalt mixtures to provide better predictions. In order to recalibrate the nonlinear Witczak E* regression equation, the measured E* data of 28 mixtures and the "Solver" data analysis tool in Microsoft Excel was used. The Solver tool uses the generalized reduced gradient (GRG) nonlinear algorithm to optimize the coefficients of the model to minimize the sum of the squared errors. The recalibration of Witczak's model was performed in log-log space. The new coefficients of the Witczak model obtained from this recalibration process replace the coefficients of the original Witczak model. The Equation 6 is rewritten with new coefficients as Equation 21.

$$\log E^* = 5.036758 + 0.002831\rho_{200} - 0.001219{\rho_{200}}^2 - 0.004033\rho_4 - 0.039516V_a - 1.513365\frac{V_{eff}}{V_{eff}+V_a} + \frac{2.961695 - 0.000001\rho_4 + 0.000001\rho_{38} - 0.000045({\rho_{38}}^2) + 0.038446\rho_{34}}{1+e^{(-0.352259 - 0.469202\log(f) - 0.486493\log(\eta))}}$$

Equation (21)

The Equation 21 is used to make new predictions of the E* values for the mixtures. The predicted E* values are compared with the measured E* values in Figure 47. It can be seen from the Figure 47 that the recalibrated Witczak model gives better predictions as compared to original Witczak model (Figure 46). The R^2 values of best-fit regression lines in Figure 46 and Figure 47 are not significantly different from each other; however, the slopes of the lines have been improved from 0.83 to 0.96. The bias toward underprediction in the original Witczak model has been largely removed by the recalibration. The recalibrated E* predicted values are evenly distributed around the line of equality as shown in Figure 47.

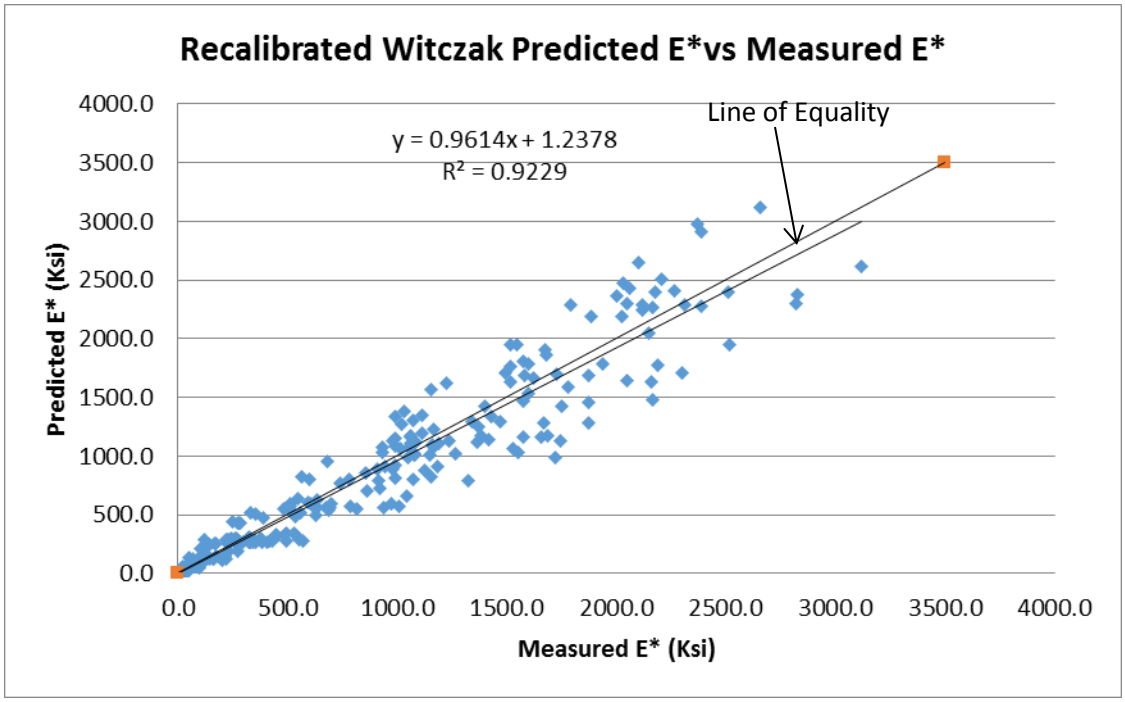

Figure 47: Comparison of Level 3 (Predicted using Recalibrated Witczak Model) versus Level 1 (Measured) Dynamic Moduli

The errors (predicted E* - measured E*) were significantly reduced after recalibration. The box and whisker plots of absolute values of errors produced by the original versus the recalibrated Witczak models are shown in Figure 48, where it can be observed that the ranges of errors at all temperatures and loading frequencies are significantly reduced. The use of the recalibrated Witczak model for Maryland asphalt mixtures can significantly improve the E* prediction and consequently, the accuracy of predicted distresses.

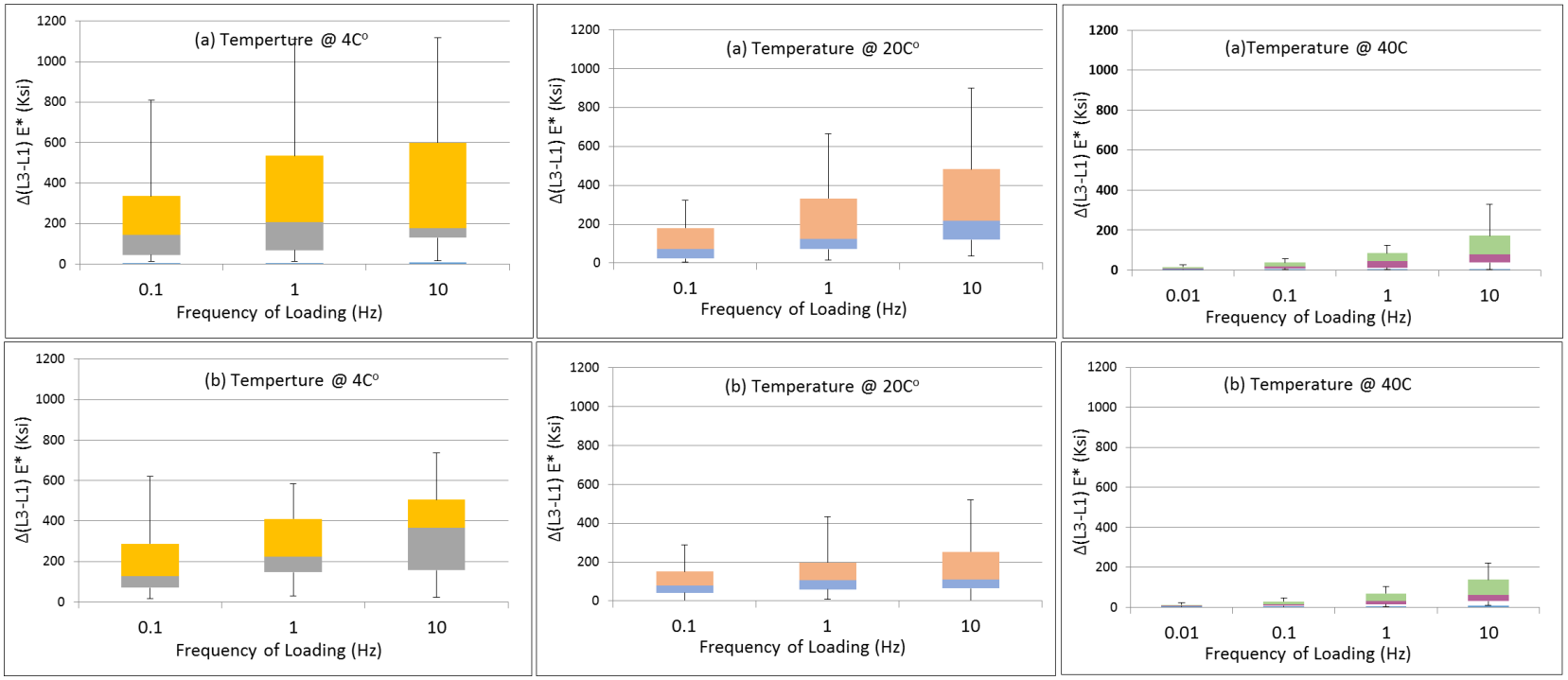

Figure 48: Ranges of Errors for Predicted versus Measured E* Values at Different Temperatures and Loading Frequencies. (A) Original Witczak Model (B) Recalibrated Witczak Model

7.2 MEPDG Sensitivity Analyses of Recalibrated E* Predicted Model

Five asphalt mixtures (H083A19C2C02, H131A09A4C01, H138B12R2C05, H158B09R2C60, H187A19C2C02) were selected to evaluate the impact of the recalibrated Level 3 E* values on predicted performance using the MEPDG software. Level 3 E* master curves generated using the recalibrated Witczak model (CWM) were developed and compared with master curves generated using the E* values from the original Witczak model and from Level 1 measured E* values. The comparison of master curves is shown in Figure 49. The master curves developed using the recalibrated Witczak model (Level 3 CWM) are generally closer to the master curves developed using the measured E* values for all five mixtures considered.

Sensitivity analyses were performed to evaluate the impact on predicted performance using E* values predicted by the recalibrated Witczak model. The recalibrated E* values used in the sensitivity analyses were extracted from the Level 3 (CWM) master curves for the five asphalt mixtures as shown in Figure 49 . The predicted distresses obtained using the recalibrated E* inputs (L-3 CWM) are compared with predicted distresses obtained using Level 1 and Level 3 (original Witczak model) E* inputs. The pavement structures, fixed inputs, traffic levels, climate conditions, and design limits used in these sensitivity analyses are the same as used in Chapter 6. The scenarios considered in the sensitivity analyses were: L-3 (Level 3 E* inputs predicted using the original Witczak model and default K_1, K_2, and K_3 rut model coefficients); L-3 CWM (Level 3 E* inputs predicted using the recalibrated Witczak model and default K_1, K_2, and K_3 rut model coefficients); L-1-A (Level E* 1 inputs and default K_1, K_2, and K_3 rut model coefficients); and L-1 (Level 1 E* inputs and Level 1 K_1, K_2, and K_3 rut model coefficients).

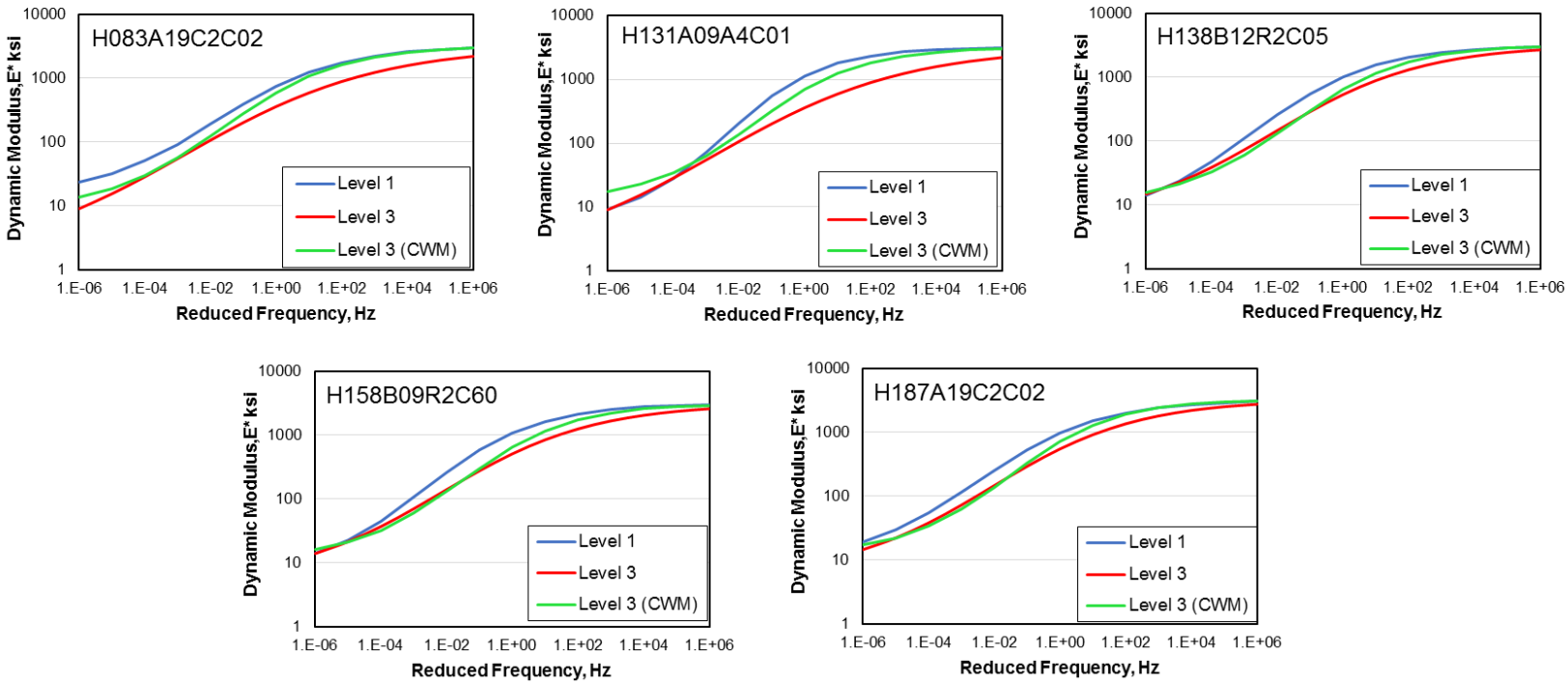

Figure 49: Master Curves Developed using E* Values Predicted by Original Witczak Model (Level 3), Recalibrated Witczak Model (Level 3 CWM), and Measured Level 1 Values.

The predicted distresses obtained from these sensitivity analyses were normalized by the design limits of the distresses (given in Chapter 6) and converted into percentages. The normalized percentages of each distress obtained by different input scenarios for the five asphalt mixtures analyzed are compared to each other in Figure 50 and Figure 51. The average percentage differences in distresses due to the different input scenarios are shown Figure 52 . The following observations are made from Figures 47 through 49.

1. The differences in predicted IRI (International Roughness Index) and Bottom Up Fatigue Cracking (BU-FC) for all five mixtures for the various input scenarios are minimal, with maximum differences of only about 5%. Top Down Fatigue Cracking (TD-FC) predicted using the original Witczak model Level 3 E* values are 5% to 30% higher than from the other input level scenarios (L-1, L-1-A, and L-3 CWM) at low and high traffic levels. TD-FC distress also varied significantly among the five asphalt mixtures.
2. Predicted asphalt concrete permanent deformation (PD_{AC}) varied the most with the different input scenarios (L-1, L-1-A, L-3, L-3 CWM). It can be seen from Figure 51 that the PD_{AC} values predicted using the original Level 3 inputs are significantly higher than from the other input scenarios. The differences in PD_{AC} between L-3 and L-3 CWM are quite large, varying from 10% to 50%.
3. As shown in Figure 52, the average percentage differences for predicted distresses for the L-3 versus L-1 scenario are significantly higher than for the L-3 CWM versus L-1 scenario. In other words, the distresses predicted using L-3 CWM inputs are closest to the distresses predicted using the measured L-1 inputs.

The overall conclusion from these sensitivity analysis is that the L-3 (CWM) E* inputs are the best to use for pavement design and performance prediction in absence of measured L-1 E* values.

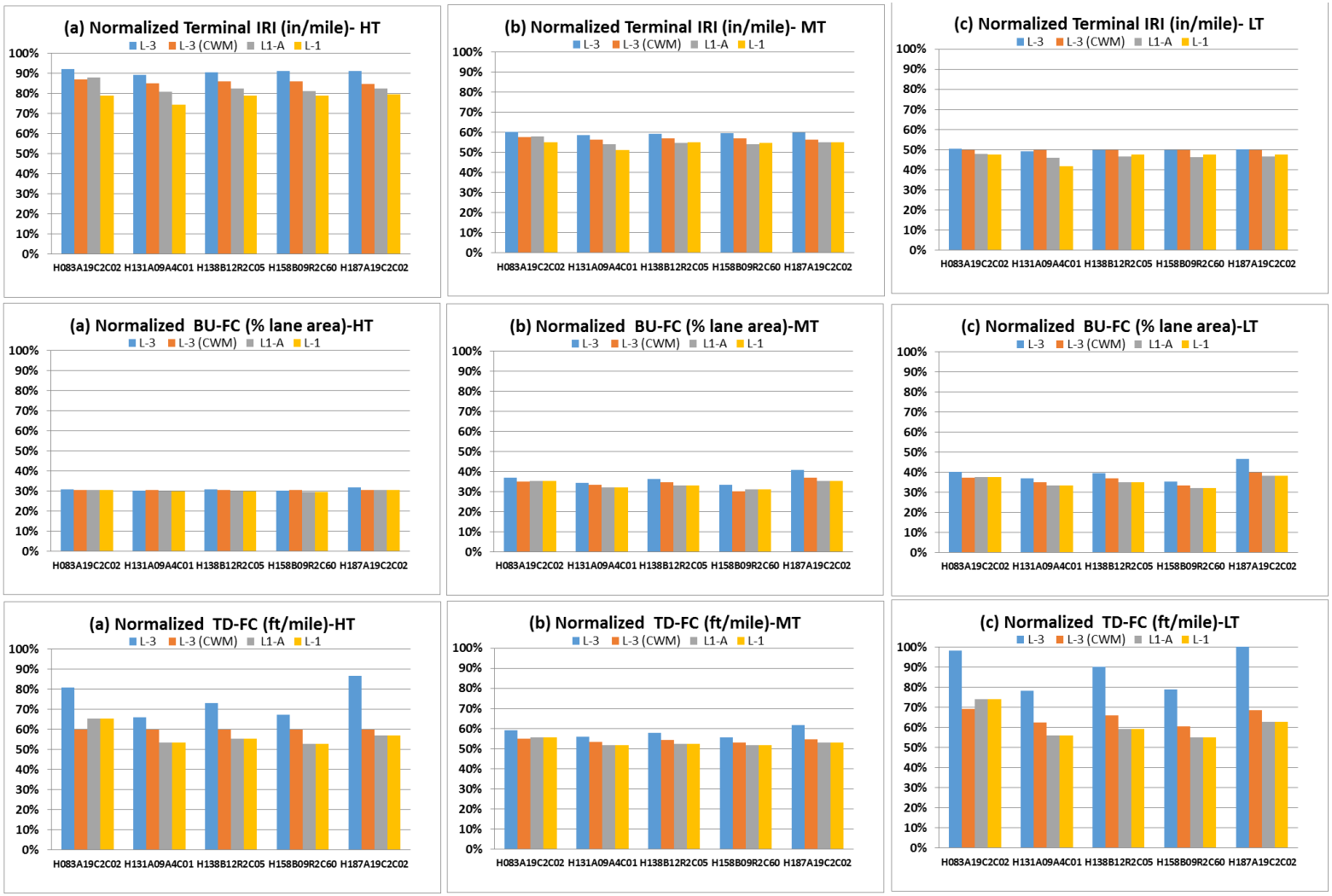

Figure 50: Predicted Distresses for Different MEPDG Input Scenarios for Five Asphalt Mixtures. (A) Heavy Traffic (HT), (B) Medium Traffic (MT), (C) Low Traffic (LT).

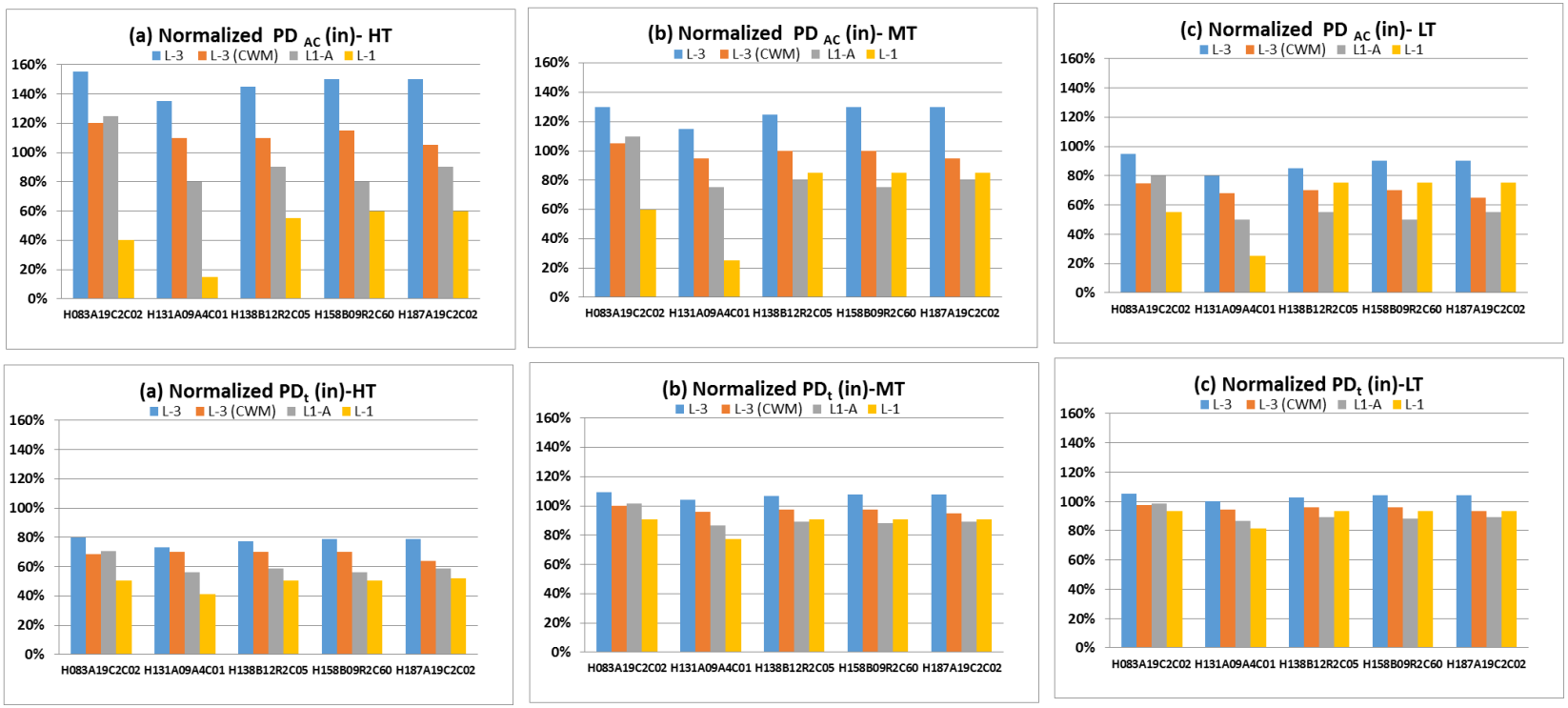

Figure 51: Predicted Distresses for Different MEPDG Input Scenarios for Five Asphalt Mixtures. (A) Heavy Traffic (HT), (B) Medium Traffic (MT), (C) Low Traffic (LT).

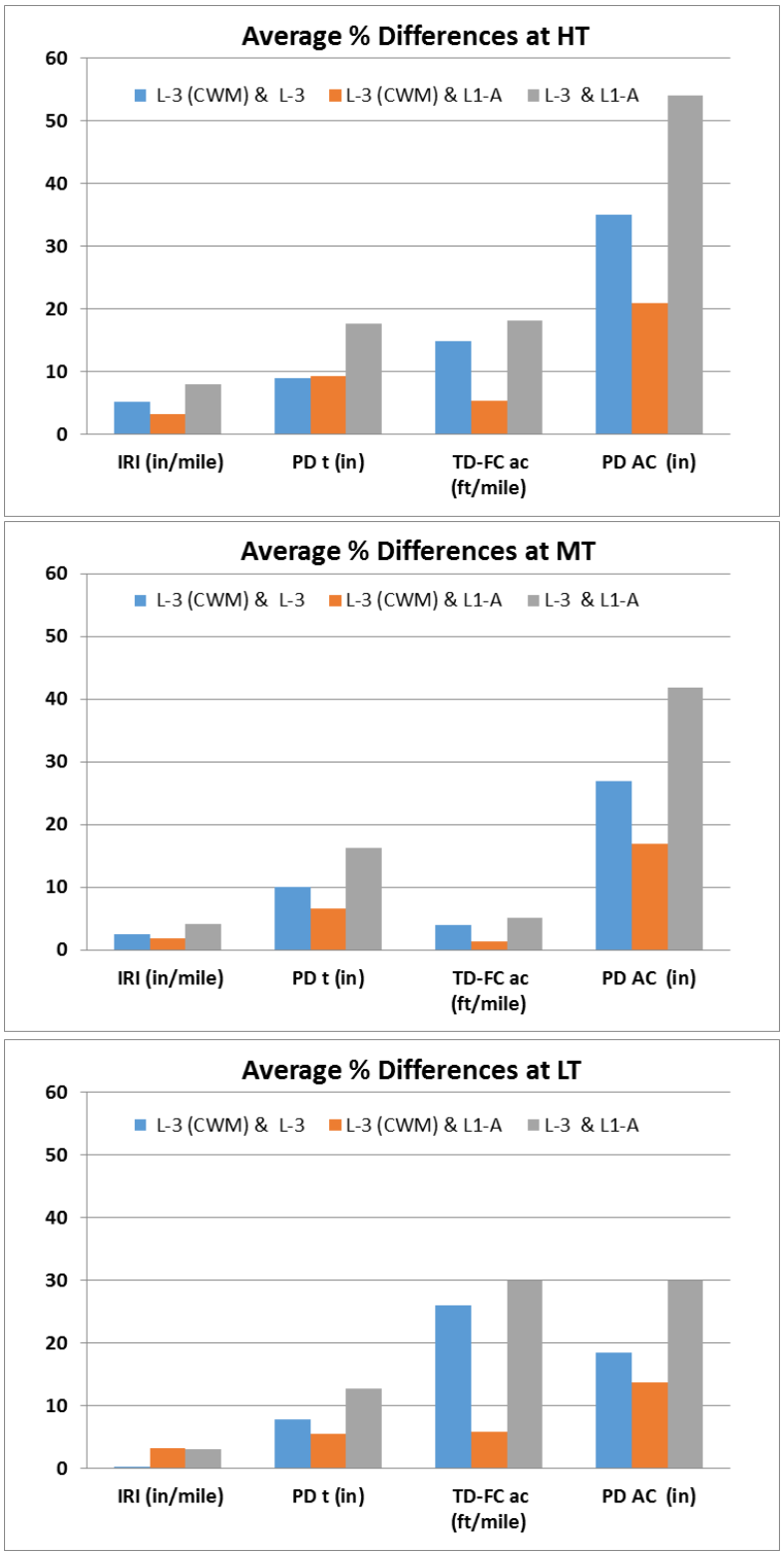

Figure 52: Percentage Differences for Different Input Scenarios at Low, Medium, and Heavy Traffic.

CHAPTER 8: PREDICTIVE MODELS FOR RLPD PROPERTIES

8.1 Predictive Models for RLPD Properties

The RLPD test is a very time consuming and labor intensive test. It would be beneficial to have Level 3 predictive models to predict the K_1, K_2 and K_3 rut model coefficients. This would complement the Level 3 predictive models for E*. The model would relate the rut model coefficients to mixture properties such as gradation, volumetric properties, and binder grade. This chapter describes an attempt to develop these models.

The model used in the MEPDG software to calculate the permanent deformation (rutting) of an asphalt layer is given in Equation 8 (Chapter 4) and reproduced here:

$$\frac{\epsilon_p}{\epsilon_r} = K_z B_1 10^{K_1} (T)^{K_2 B_2} (N)^{K_3 B_3}$$

In which

ϵ_r = resilient strain at middle of layer

ϵ_p = plastic strain at middle of the layer

T = temperature at middle of layer

N = number of axle load for a time period

B_1, B_2, B_3 = global calibration coefficient (set equal to 1)

K_1 = -3.35412 (default value in MEPDG)

K_2 = 1.5606 (default value in MEPDG)

K_3 = 0.4791 (default value in MEPDG)

K_z = depth function given as:

$$K_z = (C_1 + C_2 D)(0.328196)^D$$

in which

$$C_1 = -0.1039 H_{HMA}^2 + 2.4868 H_{HMA} - 17.342$$

$$C_1 = 0.0172 H_{HMA}^2 - 1.733 H_{HMA} + 27.428$$

D = total thickness of the asphalt layer

H_{HMA} = total HMA thickness, inch

The coefficients K_1 and K_3, should depend primarily on gradation and volumetric properties while K_2 should be a function of binder grade. Values for the K_1, K_2 and K_3 coefficients were obtained by recalibrating the MEPDG rut model (Equation 8) using the laboratory RLPD test data for the 28 Maryland asphalt mixtures evaluated in this study and the additional 18 asphalt mixtures from NCHRP Project 9-30A (Von Quintus et al., 2011). These coefficients are tabulated in Table 11 and Table 12 of Chapter 4. The 28 Maryland mixtures had air voids of 7% ± 0.5% while the NCHRP 9-30A mixtures had air voids varying from 2.5% to 8.7%.

Four different sets of data were used to develop predictive models for the K_1, K_2 and K_3 coefficients of the MEPDG rutting model:

1) Maryland (MDSHA) data only
2) NCHRP Project 9-30A data only

3) All data (MDSHA and NCHRP 9-30A). The gradation data for eight of the NCHRP 9-30A mixtures were not available, so gradation in this data set is expressed only in terms of the nominal maximum aggregate size (NMAS).
4) A combined data set of all asphalt mixtures having complete gradation data (28 MDSHA mixtures plus 10 NCHRP 9-30A mixtures).

8.2 Data Set 1 - MDSHA Mixtures Only

8.2.1 Correlation Matrices

As a first step of statistical modeling, the correlations of K_1, K_2 and K_3 with gradation parameters, and mixture volumetric properties were examined. The specific mixture properties included in the correlation analyses were:

G_{mm} = maximum specific gravity

G_{mb} = bulk specific gravity

P_b = asphalt content by weight

G_{sb} = combined bulk specific gravity of aggregates

VMA = voids in mineral aggregates

VFA = voids filled by asphalt

Percent passing 3/8 inch, #4, #8, #16, #30, #50, and #200 sieves

The correlation matrices are shown in Table 25. The following observations are drawn from these correlations:

1. The K_1 coefficient is not strongly correlated with any independent variable. However, it is somewhat correlated with G_{sb}, VMA, VFA, and the percentage passing the 3/8 inch, #4, #8, #16, #30 and #50 sieves. The correlation coefficient (R) values between these variables and K_1 range from 0.11 to 0.25. These

correlation coefficients are highlighted in blue in Table 25 . VFA and VMA are strongly intercorrelated, as are the 3/8 inch, #4, #8, #16, and #30 sieves. These high intercorrelation values (R>0.7) are highlighted in yellow in Table 25. Because of this, only one of these sieves (#8) and VMA was used in modeling to minimize the effect of intercorrelation on the modeling. The K_1 coefficient is negatively correlated with #200 sieve, which is not rational. Based on all of this, the independent variables G_{sb}, VMA, #8, and #50 sieves were selected for modeling K_1.

2. The K_2 coefficient, which captures the temperature influence on rutting, is not strongly correlated with any independent variable. This is rational; K_2 is a function of binder characteristics such as viscosity and complex shear moduli, but variations in these properties are not considered in this study since only PG 64-22 or PG 76-22 virgin binder grades were included. The true binder grade, viscosity, and complex shear moduli of the combined virgin and RAP binders were not measured in this study. The K_2 coefficient was slightly correlated with G_{sb}, VMA, VFA, and percentage passing the 3/8 inch, #4, #8, #16, #30, and #50 sieves, where R values ranged from 0.13 to 0.23. These are highlighted in blue in Table 25. VFA and VMA are strongly intercorrelated as are the 3/8 inch, #4, #8, #16, and #30 sieves. These high inter-correlation values (R>0.7) are highlighted in yellow in Table 25. Because of this, only one of these sieves (#8) and VMA was used for modeling to minimize the effect of intercorrelation on the modeling. Based on all of this, the independent variables G_{sb}, VMA, #8, and #50 sieves were selected for modeling K_2.

3. The K_3 coefficient is not strongly correlated with any independent variable. However, it is somewhat correlated with G_{sb}, VMA, and percentage passing the 3/8 inch, #4, #8, and #50 sieves, where R values range from 0.13 to 0.26. These are highlighted by blue shading. VFA and VMA are strongly intercorrelated, as are the percent passing the 3/8 inch, #4, and #8 sieves. These high intercorrelation values (R>0.7) are highlighted in yellow color in Table 25. Because of this, only one of these sieves (#4) and VMA was used in modeling to minimize the effect of intercorrelation on the modeling. The K_3 coefficient is negatively correlated with the #200 sieve, which is not rational. Based on all of this, the independent variables G_{sb}, VMA, #4 and #50 sieves were selected for modeling K_3.

In addition to intercorrelation of independent variables, the limited range of values for the independent variables could be one of the reasons for the low correlation coefficients.

Table 25: Correlation Coefficient (R Values) Matrices of Dependent and Independent Variables (MDSHA Data)

	K_1	G_{mm}	G_{mb}	P_b	G_{sb}	VMA	VFA	3/8	#4	#8	#16	#30	#50	#200
K_1	1.00													
G_{mm}	0.06	1.00												
G_{mb}	0.06	1.00	1.00											
P_b	-0.03	-0.35	-0.34	1.00										
G_{sb}	-0.11	0.81	0.80	0.10	1.00									
VMA	-0.19	-0.25	-0.25	0.88	0.34	1.00								
VFA	-0.12	-0.25	-0.25	0.88	0.31	0.95	1.00							
3/8	0.15	0.16	0.19	-0.06	0.02	-0.17	-0.05	1.00						
#4	0.24	-0.07	-0.05	-0.31	-0.35	-0.45	-0.35	0.77	1.00					
#8	0.25	-0.07	-0.05	-0.39	-0.40	-0.53	-0.44	0.69	0.96	1.00				
#16	0.19	0.03	0.04	-0.45	-0.30	-0.54	-0.46	0.72	0.88	0.94	1.00			
#30	0.12	0.12	0.13	-0.28	-0.09	-0.33	-0.25	0.72	0.69	0.73	0.88	1.00		
#50	0.18	0.10	0.11	0.36	0.19	0.27	0.32	0.30	0.08	0.06	0.15	0.45	1.00	
#200	-0.02	-0.19	-0.20	0.80	0.19	0.73	0.72	-0.25	-0.48	-0.52	-0.54	-0.34	0.53	1

	K_2	G_{mm}	G_{mb}	P_b	G_{sb}	VMA	VFA	3/8	#4	#8	#16	#30	#50	#200
K_2	1.00													
G_{mm}	-0.04	1.00												
G_{mb}	-0.04	1.00	1.00											
P_b	0.02	-0.35	-0.34	1.00										
G_{sb}	0.12	0.81	0.80	0.10	1.00									
VMA	0.19	-0.25	-0.25	0.88	0.34	1.00								
VFA	0.13	-0.25	-0.25	0.88	0.31	0.95	1.00							
3/8	-0.13	0.16	0.19	-0.06	0.02	-0.17	-0.05	1.00						
#4	-0.21	-0.07	-0.05	-0.31	-0.35	-0.45	-0.35	0.77	1.00					
#8	-0.23	-0.07	-0.05	-0.39	-0.40	-0.53	-0.44	0.69	0.96	1.00				
#16	-0.17	0.03	0.04	-0.45	-0.30	-0.54	-0.46	0.72	0.88	0.94	1.00			
#30	-0.10	0.12	0.13	-0.28	-0.09	-0.33	-0.25	0.72	0.69	0.73	0.88	1.00		
#50	-0.15	0.10	0.11	0.36	0.19	0.27	0.32	0.30	0.08	0.06	0.15	0.45	1.00	
#200	0.04	-0.19	-0.20	0.80	0.19	0.73	0.72	-0.25	-0.48	-0.52	-0.54	-0.34	0.53	1.00

	K_3	G_{mm}	G_{mb}	P_b	G_{sb}	VMA	VFA	3/8	#4	#8	#16	#30	#50	#200
K_3	1.00													
G_{mm}	0.12	1.00												
G_{mb}	0.12	1.00	1.00											
P_b	-0.04	-0.35	-0.34	1.00										
G_{sb}	0.24	0.81	0.80	0.10	1.00									
VMA	0.13	-0.25	-0.25	0.88	0.34	1.00								
VFA	0.07	-0.25	-0.25	0.88	0.31	0.95	1.00							
3/8	-0.13	0.16	0.19	-0.06	0.02	-0.17	-0.05	1.00						
#4	-0.26	-0.07	-0.05	-0.31	-0.35	-0.45	-0.35	0.77	1.00					
#8	-0.16	-0.07	-0.05	-0.39	-0.40	-0.53	-0.44	0.69	0.96	1.00				
#16	-0.08	0.03	0.04	-0.45	-0.30	-0.54	-0.46	0.72	0.88	0.94	1.00			
#30	-0.03	0.12	0.13	-0.28	-0.09	-0.33	-0.25	0.72	0.69	0.73	0.88	1.00		
#50	-0.21	0.10	0.11	0.36	0.19	0.27	0.32	0.30	0.08	0.06	0.15	0.45	1.00	
#200	-0.05	-0.19	-0.20	0.80	0.19	0.73	0.72	-0.25	-0.48	-0.52	-0.54	-0.34	0.53	1.00

Multiple linear regression approach was used to develop models for the K_1, K_2 and K_3 rut model coefficients. ANOVA and t-tests were performed to quantify the quality of the predictions. The Regression tool in Microsoft Excel was used to perform the multiple linear regressions and statistical tests.

The regression statistics of the predictive models for the K_1, K_2 and K_3 coefficients are shown in Table 26.. The F and t tests failed in all models. The goodness of fit statistics for models (R^2 and the ratio of the standard error S_e to the standard deviation of the dependent variable S_y) are also very poor for all models shown in Table 26. In other words, the multiple linear regression models relating the coefficients K_1, K_2 and K_3 to volumetric properties and gradation parameters are not good predictive models.

Table 26: Regression Statistics for the Predictive Models for the Rut Model Coefficients (MDSHA Data)

Regression Statistic for Coefficient K_1			
Multiple R	0.33	$F_{cr\ @\ \alpha = 0.05}$	2.80
R Square	0.11	$t_{cr\ @\ \alpha = 0.05}$	*2.069*
Se	0.74	**Null Hypothesis (β=0) Accepted.**	
Se/Sy	1.02	**F and t- Tests Failed**	
Observations	28	**Not Good Model**	
ANOVA	*df*	*F*	*Significance F*
Regression	4	0.72	0.59
Residual	23		
Total	27		
t.Test	*Coefficients*	*t Stat*	*P-value*
Intercept	0.721		
G_{sb}	-0.472	-0.172	0.865
VMA	-0.074	-0.666	0.512
#8	0.012	0.541	0.593
#50	0.092	1.045	0.307
Regression Statistic for Coefficient K_2			
Multiple R	0.31	$F_{cr\ @\ \alpha = 0.05}$	2.80
R Square	0.10	$t_{cr\ @\ \alpha = 0.05}$	*2.069*
Se	0.42	**Null Hypothesis (β=0) Accepted.**	
Se/Sy	1.03	**F and t- Tests Failed**	
Observations	28	**Not Good Model**	
ANOVA	*df*	*F*	*Significance F*
Regression	4	0.62	0.65
Residual	23		
Total	27		
t.Test	*Coefficients*	*t Stat*	*P-value*
Intercept	-0.520		
G_{sb}	0.459	0.296	0.770
VMA	0.045	0.704	0.489
#8	-0.010	-0.382	0.706
#50	-0.048	-0.962	0.346
Regression Statistic for Coefficient K_3			
Multiple R	0.39	$F_{cr\ @\ \alpha = 0.05}$	2.80
R Square	0.15	$t_{cr\ @\ \alpha = 0.05}$	*2.069*
Se	0.03	**Null Hypothesis (β=0) Accepted.**	
Se/Sy	1.00	**F and t- Tests Failed**	
Observations	28	**Not Good Model**	
ANOVA	*df*	*F*	*Significance F*
Regression	4	1.00	0.43
Residual	23		
Total	27		
t.Test	*Coefficients*	*t Stat*	*P-value*
Intercept	-0.041		
G_{sb}	0.099	1.057	0.302
VMA	0.001	0.283	0.780
#8	-0.001	-0.545	0.591
#50	-0.001	-1.227	0.232

Some nonlinear models, including power, semi-log, and log-log, were also considered for modeling. The summary of all models along with their regression statistics are shown in Table 27. It can be seen from Table 27 that the goodness of fit statistics, R^2 and S_e/S_y, for all of the models are very poor, which means very low accuracy of prediction. F and t-tests in all models also failed.

Table 27: Summary of Predictive Models along with Their Regression Statistics (MDSHA Data)

No	Model Type	Model	Goodness of Fitness		Rationality	F-Test	t-Test
			R^2	S_e/S_y			
MDSHA Data Only							
K_1 - Models							
1	Linear	$K_1 = 0.721-0.472G_{sb-0.074}VMA+0.012$ (% Passing (#8)+0.092 (Percentage % (#50))	0.11	1.02	Yes	Fail	Fail
K_2 - Models							
2	Linear	$K_2 = -0.520+0.459G_{sb}$ -0.045VMA-0.01(% passing (#8))-0.048(%passing (#50))	0.10	1.03	Yes	Fail	Fail
3	Log-Log	$\text{Log } K_2 = -2.18 + 7.09 \text{ Log } G_{sb} + 0.58 \text{ Log VMA}-0.51 \text{ Log (\% passing (\#8))}-0.97 \text{ Log (\%passing (\#50))}$	0.18	1.02	Yes	Fail	Fail
4	Semi Log	$K_2 = -1.54 + 3.66 \text{ Log } G_{sb} + 2.10 \text{ Log VMA}-0.24 \text{ Log (\% passing (\#8))}-1.43 \text{ Log (\%passing (\#50))}$	0.10	1.03	Yes	Fail	Fail
5	Power	$K_2 = 10^{-1.54} \times G_{sb}^{3.66} \times VMA^{2.10} (\%\text{ passing \#8})^{-0.24} \times (\%\text{ passing \#50})^{-1.43}$	0.10	1.03	Yes	Fail	Fail
K_3 - Models							
6	Linear	$K_3 = -0.041+0.099G_{sb} + 0.001\text{VMA} - 0.001(\%\text{passing (\#8)}) - 0.001 (\%\text{passing (\#50)})$	0.15	1.00	Yes	Fail	Fail
7	Log-Log	$Log\ K_3 = -1.237+ 1.565 \text{ Log } G_{sb} + 0.151 \text{ Log VMA} - 0.053 \text{ Log (\%passing (\#8))} - 0.247 \text{ Log (\%passing (\#50))}$	0.16	1.01	Yes	Fail	Fail
8	Semi Log	$K_3 = -0.038+ 0.671 \text{ Log } G_{sb} + 0.068 \text{ Log VMA} - 0.015 \text{ Log (\%passing (\#8))} - 0.113 \text{ Log (\%passing (\#50))}$	0.15	1.01	Yes	Fail	Fail
9	Power	$K_3 = -0.038 \times G_{sb}^{0.671} \times VMA^{0.068} \times (\%\text{ passing \#8})^{-0.015} \times (\%\text{ passing \#50})^{-0.113}$	0.15	1.01	Yes	Fail	Fail

8.3 Second Set of Data (NCHRP 9-30A Project)

Only data from the NCHRP 9-30A project were used in this data set. This data set consisted of 18 different mixtures. Unlike the Maryland data, the air voids of the asphalt mixtures were not constant.

8.3.1 Correlation Matrices

As mentioned previously, detailed gradation information was not available for all eighteen NCHRP 9-30A mixtures so nominal maximum aggregate size (NMAS) was used for the correlation analyses. The correlation matrices are shown in Table 28 . Information about binder grades of some of NCHRP 9-30A mixtures was available and some mixtures do not have binder grade information, so binder grade was not used as a predictive variable in the modeling due to partial information. The following observations are drawn from Table 28.

1. The K_1 (intercept) and K_2 (temperature) coefficients are somewhat correlated with all the independent variables. The correlation coefficient varies from 0.29 to 0.75. The G_{sb} is intercorrelated with G_{mm} and V_A is intercorrelated with G_{mb} and VFA so G_{mm} and V_A were not included in the model. The independent variables G_{mb}, P_b, Gsb, VMA, VFA, and NMAS were selected for modeling the K_1 and K_2 coefficients.
2. The K_3 (loading cycle) coefficient is somewhat correlated with G_{mb}, P_b, G_{sb}, VMA, and VFA. The negative correlation of K_3 with P_b is not rational so P_b was not included as an independent variable (predictor) in the model. The air voids (V_A) is negatively correlated with K_3 and intercorrelated with G_{mb} and VFA so it was also

eliminated as a predictor in the model. The independent variables G_{mb}, G_{sb}, VMA, and VFA were selected for modeling the K_3 coefficient.

All high intercorrelation are highlighted in yellow and independent variables included in the models are highlighted in blue in Table 28.

Table 28: Correlation Coefficient (R Values) Matrices of Dependent and Independent Variables (NCHRP 9-30A Data)

	K_1	G_{mm}	G_{mb}	P_b	G_{sb}	VMA	VFA	V_A	NMAS
K_1	1.00								
G_{mm}	-0.44	1.00							
G_{mb}	-0.59	0.52	1.00						
P_b	-0.31	-0.52	0.00	1.00					
G_{sb}	-0.75	0.74	0.61	0.03	1.00				
VMA	-0.35	0.17	-0.30	0.32	0.54	1.00			
VFA	-0.45	-0.24	0.65	0.60	0.27	-0.16	1.00		
V_A	0.38	0.03	-0.81	-0.28	-0.17	0.52	-0.85	1.00	
NMAS	0.55	-0.18	-0.21	-0.60	-0.56	-0.59	-0.32	0.11	1.00

	K_2	G_{mm}	G_{mb}	P_b	G_{sb}	VMA	VFA	V_A	NMAS
K_2	1.00								
G_{mm}	0.31	1.00							
G_{mb}	0.46	0.52	1.00						
P_b	0.44	-0.52	0.00	1.00					
G_{sb}	0.55	0.74	0.61	0.03	1.00				
VMA	0.29	0.17	-0.30	0.32	0.54	1.00			
VFA	0.37	-0.24	0.65	0.60	0.27	-0.16	1.00		
V_A	-0.32	0.03	-0.81	-0.28	-0.17	0.52	-0.85	1.00	
NMAS	-0.49	-0.18	-0.21	-0.60	-0.56	-0.59	-0.32	0.11	1.00

	K_3	G_{mm}	G_{mb}	P_b	G_{sb}	VMA	VFA	V_A	NMAS
K_3	1.00								
G_{mm}	0.17	1.00							
G_{mb}	0.32	0.52	1.00						
P_b	-0.12	-0.52	0.00	1.00					
G_{sb}	0.43	0.74	0.61	0.03	1.00				
VMA	0.13	0.17	-0.30	0.32	0.54	1.00			
VFA	0.32	-0.24	0.65	0.60	0.27	-0.16	1.00		
V_A	-0.24	0.03	-0.81	-0.28	-0.17	0.52	-0.85	1.00	
NMAS	0.07	-0.18	-0.21	-0.60	-0.56	-0.59	-0.32	0.11	1.00

The regression statistics of the multivariate linear models are shown in Table 29 . The goodness of fitness, R^2 and S_e/S_y, for all three models in Table 29 indicate reasonable prediction accuracy. However, the models are not rational because the signs of some of the regression terms are opposite of the correlation coefficients in Table 28 . The predictors variables for which the signs reversed are highlighted in Table 29 . The increase in goodness of fit could be due to the reduction in degrees of freedom of models. There are only 18 observations and four to six predictors in the models.

Another multivariate linear regression analysis was performed after excluding all irrational predictor variables. The regression statistics for the new models are shown in Table 30. The goodness of fit statistics R^2 and S_e/S_y of the K_1 and K_2 models are 0.65, 0.48 and 0.63, 0.76, respectively, which can be considered reasonable. However, for K_3 model, these statistics are very poor (R^2=0.23, S_e/S_y=0.93). The models for K_1 and K_2 pass their F- and t-tests, meaning that the predictor variables have a significant effect on the response variable. Unfortunately, the goodness of fit statistics for the K_3 model are very poor and the model fails the F- and t-tests, all indicating that this is not a good model.

Nonlinear power law, semi-log, and log-log models were also considered for modeling. Summaries of these models along with their regression statistics are shown in Table 31 . Model numbers 2 and 4 pass the F and t-tests. Although the R^2 for model 2 is good, the R^2 for model 4 is low which means low prediction accuracy. There is no good model for K_3 coefficient. The models numbers 1, 7, and 12 are more accurate predictive models but these models are not rational due to reversed signs of the correlation coefficients in the models.

Table 29: Regression Statistics of Predictive Models for Rut Model Coefficients (NCHPR 9-30A Data)

Regression Statistics of K_1			
Multiple R	0.85	$F_{cr\ @\ \alpha = 0.05}$	3.09
R Square	0.72	$t_{cr\ @\ \alpha = 0.05}$	*2.20*
Se	0.58	**F-Test Pass and t-Test Fail**	
Se/Sy	0.65	**Accurate but Irrational Model**	
Observations	18		
ANOVA	*df*	*F*	*Significance F*
Regression	6	4.81	0.01
Residual	11		
Total	17		
t.Test	*Coefficients*	*t Stat*	*P-value*
Intercept	9.12		
G_{mb}	111.91	1.14	0.28
P_b	-3.72	-1.49	0.17
G_{sb}	-116.10	-1.32	0.21
VMA	3.33	1.22	0.25
VFA	0.03	0.76	0.46
NMAS	-0.03	-0.58	0.57
Regression Statistics of K_2			
Multiple R	0.85	$F_{cr\ @\ \alpha = 0.05}$	3.09
R Square	0.72	$t_{cr\ @\ \alpha = 0.05}$	*2.20*
Se	0.28	**F-Test Pass and t-Test Fail except P_b**	
Se/Sy	0.65	**Accurate but Irrational Model**	
Observations	18		
ANOVA	*df*	*F*	*Significance F*
Regression	6	4.81	0.01
Residual	11		
Total	17		
t.Test	*Coefficients*	*t Stat*	*P-value*
Intercept	-8.93		
G_{mb}	-61.09	-1.30	0.22
P_b	2.63	2.19	0.05
G_{sb}	65.23	1.55	0.15
VMA	-1.93	-1.48	0.17
VFA	-0.05	-2.62	0.02
NMAS	0.04	1.57	0.14
Regression Statistics of K_3			
Multiple R	0.72	$F_{cr\ @\ \alpha = 0.05}$	3.18
R Square	0.52	$t_{cr\ @\ \alpha = 0.05}$	*2.16*
Se	0.04	**F and t-Tests Pass**	
Se/Sy	0.76	**Not Accurate and Irrational Model**	
Observations	18		
ANOVA	*df*	*F*	*Significance F*
Regression	4	3.59	0.04
Residual	13		
Total	17		
t.Test	*Coefficients*	*t Stat*	*P-value*
Intercept	2.13		
G_{mb}	-4.53	-2.85	0.01
G_{sb}	3.69	3.09	0.01
VMA	-0.10	-2.82	0.01
VFA	0.01	2.95	0.01

Table 30: Regression Statistics of Modified Predictive Models for Rut Model Coefficients (NCHRP 9-30A Data)

Regression Statistics of K_1			
Multiple R	0.80	$F_{cr\ @\ \alpha = 0.05}$	3.68
R Square	0.65	$t_{cr\ @\ \alpha = 0.05}$	*2.13*
Se	0.56	**F and t-Tests Pass**	
Se/Sy	0.63	**Rational-Accurate Model**	
Observations	18		
ANOVA	*df*	*F*	*Significance F*
Regression	2	13.73	0.00
Residual	15		
Total	17		
t.Test	*Coefficients*	*t Stat*	*P-value*
Intercept	29.89		
P_b	-0.42	-1.86	0.08
G_{sb}	-10.61	-4.84	0.00
Regression Statistics of K_2			
Multiple R	0.70	$F_{cr\ @\ \alpha = 0.05}$	3.68
R Square	0.48	$t_{cr\ @\ \alpha = 0.05}$	*2.13*
Se	0.32	**F and t-Tests Pass**	
Se/Sy	0.76	**Rational but Not Accurate**	
Observations	18	**Model**	
ANOVA	*df*	*F*	*Significance F*
Regression	2	7.04	0.01
Residual	15		
Total	17		
t.Test	*Coefficients*	*t Stat*	*P-value*
Intercept	-10.60		
P_b	0.30	2.30	0.04
G_{sb}	3.67	2.89	0.01
Regression Statistics of K_3			
Multiple R	0.48	$F_{cr\ @\ \alpha = 0.05}$	3.68
R Square	0.23	$t_{cr\ @\ \alpha = 0.05}$	*2.13*
Se	0.05	**F and t-Tests Fail**	
Se/Sy	0.93	**Rational but Not Accurate**	
Observations	18	**Model**	
ANOVA	*df*	*F*	*Significance F*
Regression	2	2.20	0.15
Residual	15		
Total	17		
t.Test	*Coefficients*	*t Stat*	*P-value*
Intercept	-0.72		
Gsb	0.32	1.56	0.14
VFA	0.001	0.91	0.38

Table 31: Summary of Predictive Models and Their Regression Statistics (NCHRP 9-30A Data)

No	Model Type	Model	Goodness of Fitness		Rationality	F-Test	t-Test
			R^2	S_e/S_y			
Only NCHRP 9-30A Data							
K_1 - Models							
1	Linear	$K_1 = 9.12+111.91G_{mb}-3.72P_b-116.10G_{sb}+3.33VMA+0.03VFA-0.03NMAS$	0.72	0.65	No	Pass	Fail
2	Linear	$K_1 = 29.89-0.42P_b - 10.61G_{sb}$	0.65	0.63	Yes	Pass	Pass
K_2 - Models							
3	Linear	$K_2 = -8.93-61.09G_{mb}+2.63P_b+65.23G_{sb}-1.93VMA-0.05VFA+0.04NMAS$	0.72	0.65	No	Pass	Fail
4	Linear	$K_2 = -10.60+0.30P_b+3.67G_{sb}$	0.48	0.76	Yes	Pass	Pass
5	Log-Log	$\text{Log } K_2 = 4.67-140.9 \text{ Log } G_{mb}+15.6 \text{ Log } P_{b+}187.6 \text{ Log } G_{sb}-31.8 \text{ Log VMA}-3.10 \text{ Log VFA}+0.6 \text{ Log NMAS}$	0.60	0.83	No	Fail	Fail
6	Log-Log	$\text{Log } K_2 = -11.03+3.48 \text{ Log } P_b+19.5 \text{ Log } G_{sb}$	0.44	0.84	Yes	Pass	Pass
7	Semi Log	$K_2 = 16.95-268.81 \text{ Log } G_{mb}+25.93_{\text{Log}} P_b+333.44 \text{ Log } G_{sb}-56.53 \text{ Log VMA}-5.52 \text{ Log VFA}+1.5 \text{ Log NMAS}$	0.75	0.60	No	Pass	Pass
8	Semi Log	$K_2 = -11.27+3.7 \text{ Log } P_b+22 \text{ Log } G_{sb}$	0.49	0.76	Yes	Pass	Pass
9	Power	$K_2 = 10^{-11} \text{ x } P_b^{3.7} \text{ x } G_{sb}^{22}$	0.49	0.76	Yes	Pass	Pass
K_3 - Models							
10	Linear	$K_3 = 2.13-4.53G_{mb}+3.69G_{sb}-0.10VMA+0.01VFA$	0.52	0.76	No	Pass	Pass
11	Linear	$K_3 = -0.72+0.32G_{sb+}0.001VFA$	0.23	0.93	Yes	Fail	Fail
12	Log-Log	$\text{Log } K_3 = 6.41-84.84 \text{ Log } G_{mb} + 76.74 \text{ Log } G_{sb}-12.14 \text{ Log VMA}+ 3.53 \text{ Log VFA}$	0.68	0.64	No	Pass	Pass
13	Log-Log	$\text{Log } K_3 = -3.65 + 4.83 \text{ Log } G_{sb} + 0.48 \text{ Log VFA}$	0.40	0.76	Yes	Fail	Fail
14	Semi Log	$K_3 = 2.5-28.7 \text{ Log } G_{mb} + 26.6 \text{ Log } G_{sb}-4.2 \text{ Log VMA}+ 1.2 \text{ Log VFA}$	0.58	0.70	No	Pass	Pass
15	Semi Log	$K_3 = -9.19 + 1.89 \text{ Log } G_{sb} + 0.17 \text{ Log VFA}$	0.20	0.90	Yes	Fail	Fail
16	Power	$K_3 = 10^{-9.19} \text{ x } G_{sb}^{1.89} \text{ x VFA}^{0.17}$	0.20	0.90	Yes	Fail	Fail

8.4 Combined Data Set (MDSHA and NCHRP 9-30A Project Data – Set 1)

In this set of data, the MDSHA and NCHRP 9-30A data (28+18 = 46 mixtures) are combined and used for modeling.

8.4.1 Correlation Matrices

The correlation matrices are shown in Table 32 . The following observations are taken from Table 32 .

1) The K_1 (intercept) coefficient is not strongly correlated with any independent variable. However, it is somewhat correlated with G_{sb}, P_b, G_{sb}, VMA, VFA, V_A, and NMAS. The R values range from 0.12 to 0.33. Both G_{sb} and G_{mb} are strongly intercorrelated with G_{mm}, VMA is intercorrelated with P_b and G_{sb}, and V_A is intercorrelated with VFA. The independent variables G_{mb}, P_b, G_{sb}, VFA, and NMAS were selected or modeling of the K_1 coefficient. Due to high intercorrelations of independent variables, the independent variables (predictors) G_{mb}, P_b, G_{sb}, VFA, and NMAS were selected for modeling the K_2 coefficient. The high intercorrelations and selected predictors for modeling of K_1 and K_2 coefficients are highlighted in yellow and blue respectively in Table 32.
2) Due to strong intercorrelation of independent variables, only G_{mb}, G_{sb} and VFA were selected for modeling of K_3. The intercorrelations (yellow) and selected predicted variables (blue) are highlighted in Table 32.

Table 32: Correlation Coefficient (R Values) Matrices of Dependent and Independent Variables (Combined MDSHA and NCHRP 9-30A Data – Set 1)

	K_1	G_{mm}	G_{mb}	P_b	G_{sb}	VMA	VFA	V_A	NMAS
K_1	1								
G_{mm}	-0.09	1.00							
G_{mb}	-0.22	0.78	1.00						
P_b	-0.12	-0.24	-0.19	1.00					
G_{sb}	-0.31	0.84	0.68	0.16	1.00				
VMA	-0.21	0.21	-0.14	0.66	0.60	1.00			
VFA	-0.32	-0.30	0.25	0.51	0.06	0.01	1.00		
V_A	0.25	0.24	-0.39	-0.06	0.16	0.49	-0.79	1.00	
NMAS	0.33	-0.12	-0.13	-0.40	-0.30	-0.38	-0.24	0.01	1.00

	K_2	G_{mm}	G_{mb}	P_b	G_{sb}	VMA	VFA	V_A	NMAS
K_2	1.00								
G_{mm}	0.14	1.00							
G_{mb}	0.18	0.78	1.00						
P_b	0.17	-0.24	-0.19	1.00					
G_{sb}	0.32	0.84	0.68	0.16	1.00				
VMA	0.27	0.21	-0.14	0.66	0.60	1.00			
VFA	0.21	-0.30	0.25	0.51	0.06	0.01	1.00		
V_A	-0.12	0.24	-0.39	-0.06	0.16	0.49	-0.79	1.00	
NMAS	-0.30	-0.12	-0.13	-0.40	-0.30	-0.38	-0.24	0.01	1.00

	K_3	G_{mm}	G_{mb}	P_b	G_{sb}	VMA	VFA	V_A	NMAS
K_3	1.00								
G_{mm}	0.12	1.00							
G_{mb}	0.22	0.78	1.00						
P_b	-0.07	-0.24	-0.19	1.00					
G_{sb}	0.28	0.84	0.68	0.16	1.00				
VMA	0.12	0.21	-0.14	0.66	0.60	1.00			
VFA	0.25	-0.30	0.25	0.51	0.06	0.01	1.00		
V_A	-0.17	0.24	-0.39	-0.06	0.16	0.49	-0.79	1.00	
NMAS	-0.01	-0.12	-0.13	-0.40	-0.30	-0.38	-0.24	0.01	1.00

Multivariate linear regression analyses were performed to develop the models. The regression statistics of the models are given in Table 33. The highlighted variables in Table 33 are reversed in sign as compared to the correlation coefficients (Table 32), which indicates irrationality. A multivariate linear regression analysis was thus performed using only the rational variables. The regression statistics for these models are shown in Table 34.

The goodness of fit statistics R^2 and S_e/S_y for all three models in Table 34 are very poor. Although all three models passed the F-test, the individual variables failed the t-test, which means that no one predictor in these models can significantly predict the response variable with level of significance of 5%. Overall, these linear models are not good predictors for K_1, K_2, and K_3.

Table 33: Regression Statistics of Models for Rut Model Coefficients (Combined MDSHA and NCHRP 9-30A Data – Set 1)

Regression Statistics of K_1			
Multiple R	0.53	Fcr @ α = 0.05	2.45
R Square	0.28	tcr @ α = 0.05	*2.02*
Se	0.70	**F-Test Pass and t-Test Fail**	
Se/Sy	0.90	**except G_{sb} and VFA**	
Observations	46	**Irrational-Not Accurate Model**	
ANOVA	*df*	*F*	*Significance F*
Regression	5	3.10	0.02
Residual	40		
Total	45		
t Test	*Coefficients*	*t Stat*	*P-value*
Intercept	0.96		
G_{mb}	6.32	1.43	0.16
P_b	0.44	1.83	0.08
G_{sb}	-5.66	-2.16	0.04
VFA	-0.06	-2.59	0.01
NMAS	0.05	1.68	0.10
Regression Statistics of K_2			
Multiple R	0.43	Fcr @ α = 0.05	2.45
R Square	0.19	tcr @ α = 0.05	*2.02*
Se	0.40	**F and t-Tests Fail**	
Se/Sy	0.96	**Irrational-Not Accurate Model**	
Observations	46		
ANOVA	*df*	*F*	*Significance F*
Regression	5	1.84	0.13
Residual	40		
Total	45		
t Test	*Coefficients*	*t Stat*	*P-value*
Intercept	-1.25		
G_{mb}	-2.19	-0.89	0.38
P_b	-0.09	-0.70	0.49
G_{sb}	2.53	1.72	0.09
VFA	0.02	1.29	0.20
NMAS	-0.02	-1.25	0.22
Regression Statistics of K_3			
Multiple R	0.37	Fcr @ α = 0.05	2.83
R Square	0.14	tcr @ α = 0.05	*2.02*
Se	0.04	**F and t-Tests Fail**	
Se/Sy	0.96	**Irrational-Not Accurate Model**	
Observations	46		
ANOVA	*df*	*F*	*Significance F*
Regression	3	2.20	0.10
Residual	42		
Total	45		
t Test	*Coefficients*	*t Stat*	*P-value*
Intercept	-0.24		
G_{mb}	-0.04	-0.23	0.82
G_{sb}	0.16	1.51	0.14
VFA	0.0014	1.63	0.11

Table 34: Regression Statistics of Modified Predictive Models for Rut Model Coefficients (Combined MDSHA and NCHRP 9-30A Data – Set 1)

Regression Statistics of K_1			
Multiple R	0.47	Fcr @ α = 0.05	2.83
R Square	0.22	tcr @ α = 0.05	*2.02*
Se	0.72	**F-Test Pass and t-Tests Fail Rational-Not Accurate Model**	
Se/Sy	0.92		
Observations	46		
ANOVA	*df*	*F*	*Significance F*
Regression	3	3.90	0.02
Residual	42		
Total	45		
t Test	*Coefficients*	*t Stat*	*P-value*
Intercept	7.79	1.73	0.09
G_{sb}	-2.52	-1.62	0.11
VFA	-0.03	-1.82	0.08
NMAS	0.04	1.35	0.18
Regression Statistics of K_2			
Multiple R	0.41	Fcr @ α = 0.05	2.83
R Square	0.17	tcr @ α = 0.05	*2.02*
Se	0.39	**F-Test Pass and t-Tests Fail Rational-Not Accurate Model**	
Se/Sy	0.94		
Observations	46		
ANOVA	*df*	*F*	*Significance F*
Regression	3	2.89	0.05
Residual	42		
Total	45		
t Test	*Coefficients*	*t Stat*	*P-value*
Intercept	-3.52	-1.44	0.16
G_{sb}	1.47	1.73	0.09
VFA	0.01	1.01	0.32
NMAS	-0.02	-1.27	0.21
Regression Statistics of K_3			
Multiple R	0.37	Fcr @ α = 0.05	3.21
R Square	0.13	tcr @ α = 0.05	*2.02*
Se	0.04	**F-Test Pass and t-Tests Fail Rational-Not Accurate Model**	
Se/Sy	0.95		
Observations	46		
ANOVA	*df*	*F*	*Significance F*
Regression	2	3.35	0.04
Residual	43		
Total	45		
t Test	*Coefficients*	*t Stat*	*P-value*
Intercept	-0.28	-1.34	0.19
G_{sb}	0.14	1.89	0.07
VFA	0.00	1.66	0.10

Nonlinear power law, semi-log, and log-log models were also evaluated. Summaries of these models along with their regression statistics are shown in Table 35. None of the models in Table 35 had sufficient goodness of fit statistics or rational coefficients.

Table 35: Summary of Predictive Models with Regression Statistics (Combined MDSHA and NCHRP 9-30A Data)

No	Model Type	Model	Goodness of Fitness		Rationality	F-Test	t-Test
			R^2	S_e/S_y			
Total Data: MDSHA + NCHRP 9-30A Project Data							
K_1 - Models							
1	Linear	$K_1 = 0.96+6.32G_{mb}-0.44P_b-5.66G_{sb}-0.06VFA+0.05NMAS$	0.28	0.9	No	Pass	Fail
2	Linear	$K_1 = 7.79-2.52G_{sb}-0.03VFA+0.04NMAS$	0.22	0.92	Yes	Pass	Fail
K_2 - Models							
3	Linear	$K_2 = -1.25-2.19G_{mb}-0.09P_b+2.53G_{sb}+0.02VFA-0.02NMAS$	0.19	0.96	No	Fail	Fail
4	Linear	$K_2 = -3.52+1.47G_{sb}+0.01VFA-0.02NMAS$	0.17	0.94	Yes	Pass	Fail
5	Log-Log	$LogK_2 = -8.91+10.88 \text{ Log } G_{sb}+1.96 \text{ Log VFA}-0.23 \text{ Log NMAS}$	0.25	0.96	Yes	Pass	Fail
6	Semi Log	$K_2 = -5.26+9.46 \text{ Log } G_{sb}+1.44 \text{ Log VFA}-0.58 \text{ Log NMAS}$	0.17	0.96	Yes	Pass	Fail
7	Power	$K_2 = 10^{-5.26} \times G_{sb}^{9.46} \times VFA^{+1.44} \times (NMAS)^{-0.58}$	0.17	0.96	Yes	Pass	Fail
K_3 - Models							
8	Linear	$K_3 = -0.24-0.04G_{mb}+0.16G_{sb}+0.001VFA$	0.14	0.96	No	Fail	Fail
9	Linear	$K_3 = -0.28+0.14G_{sb}+0.001VFA$	0.13	0.95	Yes	Pass	Fail
10	Log-Log	$Log\ K_3 = -2.72+2.57 \text{ Log } G_{sb}+0.49 \text{ Log VFA}$	0.16	0.95	Yes	Pass	Fail
11	Semi Log	$K_3 = -0.53+0.87 \text{ Log } G_{sb}+0.19 \text{ Log VFA}$	0.13	0.96	Yes	Pass	Fail
12	Power	$K_3 = 10^{-0.53} \times G_{sb}^{0.87} \times VFA^{0.19}$	0.13	0.96	Yes	Pass	Fail

8.5 Combined Data (MDSHA and NCHRP 9-30A Project Data – Set 2)

The modeling technique used in above data sets could not give accurate and rational predictive models for the rutting coefficients. In order to see the effect of each independent variable on the predictive models of coefficients, a stepwise multiple linear regression (SMLR) technique is used in this section. In this set of data, the thirty-eight (38) asphalt mixtures having complete gradation information are combined. These mixtures include MDSHA and NCHRP Project 9-30A data.

8.5.1 Stepwise Multiple Linear Regression Models.

The regression statistics of SMLR are shown in Table 36. The same issue of change in signs of correlation coefficients of predictors was encountered in this analysis. The predictors which cause irrationality in the models are highlighted in the Table 36. The exclusion of these predictors from the models reduces the accuracy of prediction of models as found in previous sections; however, the models become rational.

8.6 Summary of Modeling

No one set of models was found to provide accurate and rational predictions for K_1, K_2 and K_3. To find better trends between each variable and the rut model coefficients, more testing may be needed on different types of mixtures with a wider range of binder grades, gradations and volumetric properties. The index and/or engineering properties of the binder such as complex shear modulus and viscosity (virgin, modified or combined RAP and virgin binders) should be measured and used in the models as predictors. This may result in accurate and rational models.

Table 36: Regression Statistics of Stepwise Multivariate Linear Regression Analyses

Stepwise Regression of K_1						
S_y=0.88, Intercept = -12.2						
Variable	CoR	Increase in R^2	R^2	S_e	S_e/S_y	Slop (β)
#200	-0.15	0.00	0.02	0.88	1.00	-0.35
#50	0.03	0.06	0.06	0.87	0.99	0.25
#30	-0.10	0.13	0.20	0.82	0.93	-0.14
VFA	0.10	0.04	0.25	0.80	0.91	0.24
V_A	0.13	0.03	0.28	0.80	0.90	0.47
VMA	-0.06	0.11	0.39	0.74	0.84	-0.78
P_b	0.05	0.02	0.42	0.74	0.84	0.64
G_{mm}	0.02	0.01	0.42	0.75	0.85	51.50
G_{mb}	0.04	0.04	0.46	0.73	0.83	-52.8
Stepwise Regression of K_2						
S_y=0.43, Intercept = 10.05						
#200	0.22	0.00	0.05	0.43	0.98	0.18
#50	0.03	0.06	0.12	0.43	0.96	-0.10
#30	-0.04	0.06	0.18	0.41	0.94	0.02
G_{sb}	0.18	0.04	0.22	0.40	0.93	8.15
P_b	0.06	0.02	0.24	0.40	0.93	-0.23
G_{mm}	0.10	0.01	0.25	0.41	0.94	-34.05
3/8	0.04	0.01	0.27	0.41	0.94	0.01
Va	-0.14	0.01	0.28	0.41	0.95	-0.15
VFA	0.05	0.09	0.37	0.39	0.90	-0.12
G_{mb}	0.10	0.03	0.41	0.39	0.89	25.70
VMA	0.15	0.01	0.41	0.39	0.91	0.18
Stepwise Regression of K_3						
S_y=0.10, Intercept = 2.12						
#30	0.36	0.00	0.11	0.10	0.96	1.20
3/8	-0.19	0.15	0.25	0.09	0.88	-0.31
#4	-0.12	-0.01	0.24	0.09	0.90	-0.32
#8	0.02	0.06	0.30	0.09	0.88	0.28
VFA	-0.21	0.06	0.37	0.08	0.85	-7.57
#200	0.08	0.02	0.39	0.08	0.85	0.46
#50	0.08	0.05	0.44	0.07	0.82	-0.39
VMA	-0.09	-0.01	0.43	0.08	0.84	-0.19
V_A	-0.07	0.16	0.60	0.07	0.72	-0.10
P_b	-0.30	-0.02	0.57	0.08	0.76	0.11
G_{mm}	-0.10	0.05	0.63	0.07	0.72	-87.60
G_{mb}	-0.14	0.06	0.69	0.07	0.66	48.53
G_{sb}	-0.09	0.08	0.78	0.06	0.58	35.42

CHAPTER 9: SUMMARY AND CONCLUSIONS

In order to further implementation of the mechanistic-empirical pavement design guide (MEPDG) in Maryland, typical Level 1 (measured) material properties are required to characterize asphalt mixtures commonly used in the state. Specifically, these proprieties are the dynamic modulus (DM) and the repeated load permanent deformation (RLPD) properties. To achieve this goal, 28 asphalt mixtures were collected from construction sites/asphalt plants and tested in the Maryland State Highway Administration Office of Materials Technology Asphalt Technology Division laboratory. The DM and RLPD testing was performed on all 28 asphalt mixtures following the AASHTO PP 60, AASHTO PP 61 and AASHTO TP 79 protocols. In addition to the 28 asphalt mixtures from Maryland, DM and RLPD data for 18 asphalt mixtures tested in NCHRP Project 9-30A were also included in parts of this study.

Specific objectives of this research included:

- Creating a catalog of Level 1 (measured) asphalt mixture DM and RLPD properties for input into the Pavement ME Design MEPDG software.
- Development of procedures for expediting the time consuming DM and RLPD testing as required by the current AASHTO protocols for characterizing a mixture.
- Comparisons of measured Level 1 and predicted Level 3 DM values of mixtures.
- Recalibration of the Level 3 DM predictive model for asphalt mixtures in Maryland.
- Evaluation of the sensitivity of pavement performance as predicted by the Pavement ME Design software to the DM and RLPD material property input values.

The principal conclusions from this study are described in the subsequent subsections.

9.1 Dynamic Modulus Data

1. High RAP and Warm Mix asphalt mixtures have comparatively high DM values regardless of virgin binder grade (C/PG 64-22) or F/PG 76-22) of the mixtures and ranked as first and second respectively among all other asphalt mixtures based on their DM values.
2. 19mm NMAS mixtures have more variability in DM values as compared to the 9mm and 12mm mixtures at all temperatures and frequencies. The 12mm NMAS mixtures have the lowest variability in DM values as compared to 9mm and 19mm NMAS mixtures. Within each NMAS category, the variability in DM decreases with decreasing frequency and increasing temperature. At high temperatures and low frequencies, almost all mixtures behave similar to granular materials because the viscosity of the binder becomes negligibly small.
3. Comparisons of predicted pavement distress using measured Level 1 (L-1) DM versus predicted Level 3 (L-3) E* inputs to the Pavement ME Design software found that the prediction discrepancies (absolute values of L-1 – L-3 E*) increase as the frequency of loading increases and decrease as the temperature increases. The magnitude of these discrepancies is high in the 9mm NMAS mixtures at all three temperatures/loading rate combinations as compared to the 12mm and 19mm NMAS mixtures. The range of discrepancies in the 12mm NMAS mixtures is the smallest among the three types of mixtures. The difference between L-1 and L-3 E* inputs to the Pavement ME Design software can have a significant effect on the pavement distress predictions.

9.2 Repeated Load Permanent Deformation Data

1. High RAP and Warm Mix asphalt mixtures have comparatively low accumulated permanent microstrains at 1000, 5000 and 10000 loading cycles regardless of virgin binder grade (C/PG 64-22 or F/PG 76-22).
2. The gradations and volumetric properties have insignificant effect on the permanent deformation of the mixtures included in this research study. The type of mix—e.g., high RAP or low RAP, hot mix or warm mix—has significant effect on the permanent deformations of the mixture.
3. The accumulated permanent microstrains of the mixtures are more variable at 40^{o}C as compared to 20^{o}C and 58^{o}C.
4. The 19mm mixtures exhibited less accumulated permanent microstrains at all temperatures than did the 12mm and 9mm mixtures. The 9mm mixtures have higher variability in accumulated permanent microstrains at 20^{o}C as compared to 12mm and 19mm mixtures at the same temperature. The variability in accumulated permanent microstrains of 19mm mixtures was also less than that for the 9mm and 12mm mixtures at 58^{o}C.
5. The average slope of the accumulated permanent strain vs. number of loading cycles (in log-log space) in the RLPD tests at 20^{o}C was twenty-five percent less than that average slope at 40^{o}C and 58^{o}C. The average slope of the mixtures at 40^{o}C was the same as at 58^{o}C.

9.3 Expedited Testing

1. Testing time can be saved by completely eliminating the DM testing at 40°C and adding a frequency of 0.01Hz at 20°C. This change in testing protocol was found to have no statistically significant impact on the computed dynamic modulus master curves.
2. Reusing the DM specimens in the RLPD tests reduces the time and labor in preparing specimens by reducing the total number of specimens from 12 to 9. Reuse of DM specimens was found to have no statistically significant influence on the computed RLPD properties.
3. Applying the time-temperature superposition (TTS) concept to RLPD testing reduces time and labor required for preparing, conditioning, and testing specimens by reducing the number of test temperatures from three to one and the total number of RLPD specimens from 9 to 3 (for three replicates per test condition). TTS, when performed based on tests performed at the highest temperature, introduces very little error into the permanent deformation characterization.
4. By combining the findings of these expedited testing approaches, the number of samples required for complete characterization of one asphalt mixtures per AASHTO PP 61 and AASHTO TP 79 can be reduced from 12 to 3. These savings in time and labor could motivate state agencies to perform DM and RLPD testing on a routine basis. It could also lead to the development of new performance based specification for asphalt mixtures.

9.4 Predicted Pavement Performance Using MEPDG

1. Predicted distresses (Asphalt Rutting, Total Rutting, Top Down Fatigue Cracking, Bottom Up Fatigue Cracking, and International Roughness Index) are sensitive to the DM and RLPD properties of the asphalt mixture. Predicted distresses using default values of E* and rut model coefficients do not significantly differentiate the effect of different types of asphalt mixtures. More differentiation in predicted distresses among mixtures was found using L-1 inputs (measured E* recalibrated rut model coefficients K_1, K_2, K_3) versus L-1-A inputs (measured E* and default rut model coefficients) versus L-3 (predicted E* values and default rut model coefficients) inputs. This finding clearly indicates that measured E* and rut model coefficients are important to accurate and economical pavement designs.
2. The sensitivity of predicted distresses to all levels (L-1, L-1-A and L-3) of inputs at all three traffic levels ranked in order as asphalt rutting, total rutting, top down fatigue cracking, International Roughness Index, and bottom up fatigue cracking.
3. The average differences in predicted asphalt rutting using L-1, L1-A, and L-3 inputs were significantly higher than the other distresses at all traffic levels. The significant difference in predicted asphalt rutting using L-1 vs. L-3 inputs at all traffic levels clearly indicates the importance of measured DM and RLPD data.
4. The average differences for each distress predicted using L-3 versus L-1 inputs was higher at all traffic levels as compared to the average differences using L-3 versus L-1-A or L-1-A versus L-1 inputs.

5. The differences in predicted asphalt rutting using L-3 inputs based on the original Witczak model versus those from the model recalibrated on Maryland mixtures (L-3 CWM) varied from 10% to 50%.
6. The average differences among predicted distresses using L-3 versus L-1 inputs are significantly higher than for L-3 (CWM) versus L-1 inputs.
7. An attempt was made to develop predictive equations for the coefficients of the MEPDG rut model based on the gradation and volumetric properties of the mixtures. Due to very weak correlations among the rut model coefficients and the mixture properties, no sufficiently accurate and rational predictive model could be found. A larger data set with a larger variety of mixtures and the addition of binder characterization data may make such a model possible in the future.

APPENDIX A

Table A-37: JMF and Verification Data of Asphalt Mixtures

Data	AMPTMixList	P_b	G_{mm}	G_{mb}	G_{sb}	V_A	VMA	VFA	TSR	Percentage Passing of Sieve Sizes in mm									
										19	12.5	9.5	4.75	2.36	1.18	0.6	0.3	0.15	0.1
JMF	H040A12R2C12	4.80	2.558	2.456	2.751	4.0	15.0	73.4	98.7	100	97	90	61	40	26	17	13	10	6.3
Verification Data		4.83	2.566	2.463		4.4	15.1	71.4		100.0	98.1	92.1	60.1	37.5	23.6	16.9	13.0	9.8	7.1
JMF	H051A12B4F01	6.50	2.512	2.425	2.766	3.5	18.0	80.8	94.8	100	98	84	39	19	14	12	11	10	8.3
Verification Data		6.42	2.528	2.419		3.5	17.6	79.7		100.0	97.3	83.7	39.7	20.0	14.4	12.6	11.3	10.2	8.8
JMF	H077A09A2C03	5.20	2.558	2.455	2.741	4.0	15.1	73.3	95.8	100	100	97	57	34	26	18	10	7	5.3
Verification Data		5.19	2.567	2.458		4.0	15.0	73.6		100.0	100.0	95.9	56.2	35.0	26.2	18.5	9.7	6.4	5.3
JMF	H077A09C2C01	5.30	2.541	2.439	2.742	4.0	15.8	74.5	91.5	100	100	96	63	41	29	20	11	8	6.2
Verification Data		5.47	2.539	2.453		3.1	15.2	79.7		100.0	100.0	96.1	61.2	39.5	28.7	20.1	11.5	8.4	6.8
JMF	H083A12C2C02	4.80	2.583	2.480	2.764	4.0	14.6	72.7	89.0	100	98	83	50	33	24	18	12	8	5.7
Verification Data		4.82	2.583	2.491		3.6	14.2	74.8		100.0	98.0	87.8	48.1	31.0	23.2	17.8	13.0	9.3	6.5
JMF	H083A19C2C02	4.30	2.590	2.486	2.765	4.0	14.0	71.2	92.1	98	86	77	39	25	20	15	11	8	6.2
Verification Data		4.34	2.579	2.480		3.9	13.9	71.7		97.2	89.5	76.8	39.4	25.5	19.9	16.0	12.0	8.9	6.4
JMF	H116C09A2F02	5.30	2.573	2.472	2.780	3.9	15.8	75.1	94.0	100	100	95	71	38	24	17	12	8	5.5
Verification Data		5.36	2.589	2.503		3.2	15.5	79.5		100.0	100.0	95.9	65.4	38.4	26.1	19.4	13.8	10.1	6.8
JMF	H127A12R2C02	5.10	2.554	2.452	2.760	4.0	15.7	74.5	91.1	100	98	90	62	34	22	15	12	10	7.5
Verification Data		5.09	2.578	2.466		4.0	15.2	74.1		100.0	97.9	91.3	60.5	34.8	22.6	16.9	13.1	9.9	7.4
JMF	H128A12B4F02	6.50	2.610	2.505	2.848	4.0	17.8	77.3	90.6	100	98	81	27	20	16	14	12	10	8.0
Verification Data		6.39	2.589	2.485		4.9	18.3	73.9		100.0	96.9	82.5	28.4	18.9	15.7	13.9	12.0	10.4	8.2
JMF	H131A09A4C01	5.20	2.490	2.390	2.668	4.0	15.1	73.4	86.3	100	100	95	71	44	28	19	13	9	6.8
Verification Data		5.30	2.496	2.386		3.9	15.3	84.1		100.0	100.0	94.9	70.0	44.0	28.4	20.2	14.3	10.2	7.3
JMF	H135A12G4F01	6.70	2.424	2.339	2.666	3.5	18.1	80.7	0.9	100	97	82	37	20	16	14	12	11	8.5
Verification Data		6.65	2.445	2.333		4.0	18.4	78.4		100.0	97.0	83.9	35.4	19.8	15.7	13.9	12.3	10.7	8.1
JMF	H135A12H2C02	5.00	2.490	2.390	2.650	4.0	14.3	72.0	0.9	100	98	82	53	38	28	20	14	9	6.3
Verification Data		5.01	2.492	2.383		4.7	14.5	68.6		100.0	96.5	82.8	56.7	38.8	27.1	19.0	13.4	9.3	6.6
JMF	H135A19G4F01	6.50	2.432	2.347	2.680	3.5	18.1	80.7	90.0	100	82	43	22	16	13	12	11	10	9.0
Verification Data		6.42	2.435	2.377		2.6	17.0	84.7		100.0	82.3	46.8	23.6	17.4	14.2	12.7	11.6	10.4	8.8
JMF	H138A12G4F05	6.50	2.552	2.462	2.806	3.5	18.0	80.4	94.4	100	95	76	30	22	18	17	15	13	9.5
Verification Data		6.41	2.624	2.551		2.0	15.4	87.6		100.0	96.2	78.8	37.0	22.7	17.3	14.9	13.2	10.9	7.8
JMF	H138B12R2C05	4.40	2.605	2.500	2.792	4.0	14.4	72.0	89.8	100	99	90	56	34	24	20	14	10	6.5
Verification Data		4.26	2.609	2.488		4.3	14.7	70.6		100.0	99.0	89.5	51.3	32.0	24.3	20.0	14.8	10.5	6.7
JMF	H151B19R2C02	4.00	2.572	2.469	2.731	4.0	13.2	69.7	87.3	95	74	60	39	25	18	13	9	7	5.3
Verification Data		4.29	2.570	2.470		3.3	13.7	76.6		95.5	80.5	69.5	43.0	27.5	19.5	15.5	11.5	9.0	6.9
JMF	H158B09R2C60	5.20	2.550	2.449	2.766	4.0	16.1	75.3	92.0	100	100	95	66	41	31	21	11	7	5.2
Verification Data		5.18	2.548	2.450		3.7	15.8	76.7		100.0	100.0	94.8	61.9	35.5	26.4	19.4	10.4	7.2	5.6
JMF	H160A09R1C03	5.20	2.534	2.433	2.717	4.0	15.1	73.6	88.1	100	100	96	63	38	27	21	14	9	6.0
Verification Data		5.14	2.530	2.443		3.7	14.7	75.4		100.0	100.0	95.9	60.5	36.2	26.0	20.0	14.4	9.9	7.2
JMF	H160A12H2F01	5.20	2.548	2.446	2.721	4.0	14.8	72.9	100.5	100	97	86	53	35	25	19	13	8	6.0
Verification Data		5.22	2.545	2.450		3.6	15.4	77.6		100.0	97.0	85.8	51.4	33.1	23.8	18.2	13.2	8.7	6.4
JMF	H161A12R4F01	5.00	2.557	2.455	2.716	4.0	14.1	71.8	96.5	100	92	77	54	37	23	16	10	7	5.8
Verification Data		4.71	2.532	2.476		3.2	13.1	75.1		100.0	92.4	72.5	50.8	35.2	21.6	14.2	10.0	7.5	6.1
JMF	H168A09R2C02	5.90	2.515	2.415	2.684	4.0	15.3	74.1	0.9	100	100	92	70	44	27	18	12	10	7.4
Verification Data		5.92	2.530	2.413		4.3	15.5	72.6		100.0	100.0	93.9	66.2	40.1	23.7	15.3	10.8	8.6	7.2
JMF	H168A12R2C02	5.60	2.534	2.432	2.708	4.0	15.2	73.6	0.9	100	92	82	56	35	22	14	11	9	6.9
Verification Data		5.51	2.520	2.424		4.3	15.5	71.4		100.0	94.2	80.5	52.9	32.8	19.9	13.5	9.9	8.0	6.7
JMF	H169A12B4F03	6.50	2.495	2.408	2.755	3.5	18.2	80.9	92.5	100	97	81	36	22	19	16	14	12	8.8
Verification Data		6.57	2.549	2.431		4.3	18.1	37.7		100.0	95.5	77.6	31.2	20.0	16.9	15.2	14.1	12.6	10.0
JMF	H176A09R2C01	6.10	2.456	2.357	2.645	4.0	16.3	75.3	85.5	100	100	96	70	44	27	18	12	9	7.1
Verification Data		5.94	2.480	2.363		4.5	16.0	72.1		100.0	100.0	97.0	68.2	42.7	26.1	17.1	11.8	9.1	7.5
JMF	H176A19R2C02	5.30	2.505	2.385	2.668	4.0	14.0	69.0	85.5	95.0	74.0	67		47	31		13	9	5.4
Verification Data		5.3	2.503	2.382		4.2	13.9	68.5		94.0	74.2	67.5		46.5	39.0		12.0	9.0	5.0
JMF	H177A12R2C50	4.90	2.531	2.431	2.722	4.0	15.1	73.8	87.6	100	99	90	54	33	23	17	9	6	4.7
Verification Data		4.96	2.542	2.430		4.4	15.4	71.5		100.0	98.7	91.6	55.7	34.3	25.4	19.2	10.5	7.1	5.4
JMF	H186D12B4F01	6.50	2.592	2.501	2.891	3.5	19.1	81.6	91.6	100	94	79	39	23	17	15	13	10	8.3
Verification Data		6.34	2.590	2.535		2.7	17.9	85.1		100.0	92.3	76.3	39.8	22.7	16.5	14.5	12.5	11.5	8.8
JMF	H187A19C2C02	4.20	2.582	2.478	2.755	4.0	13.8	70.9	87.7	95	83	69	34	24	19	14	9	7	6.1
Verification Data		4.39	2.611	2.510		3.7	13.1	79.5		95.1	80.4	67.6	35.0	23.9	18.8	15.0	11.1	8.9	6.4

APPENDIX B

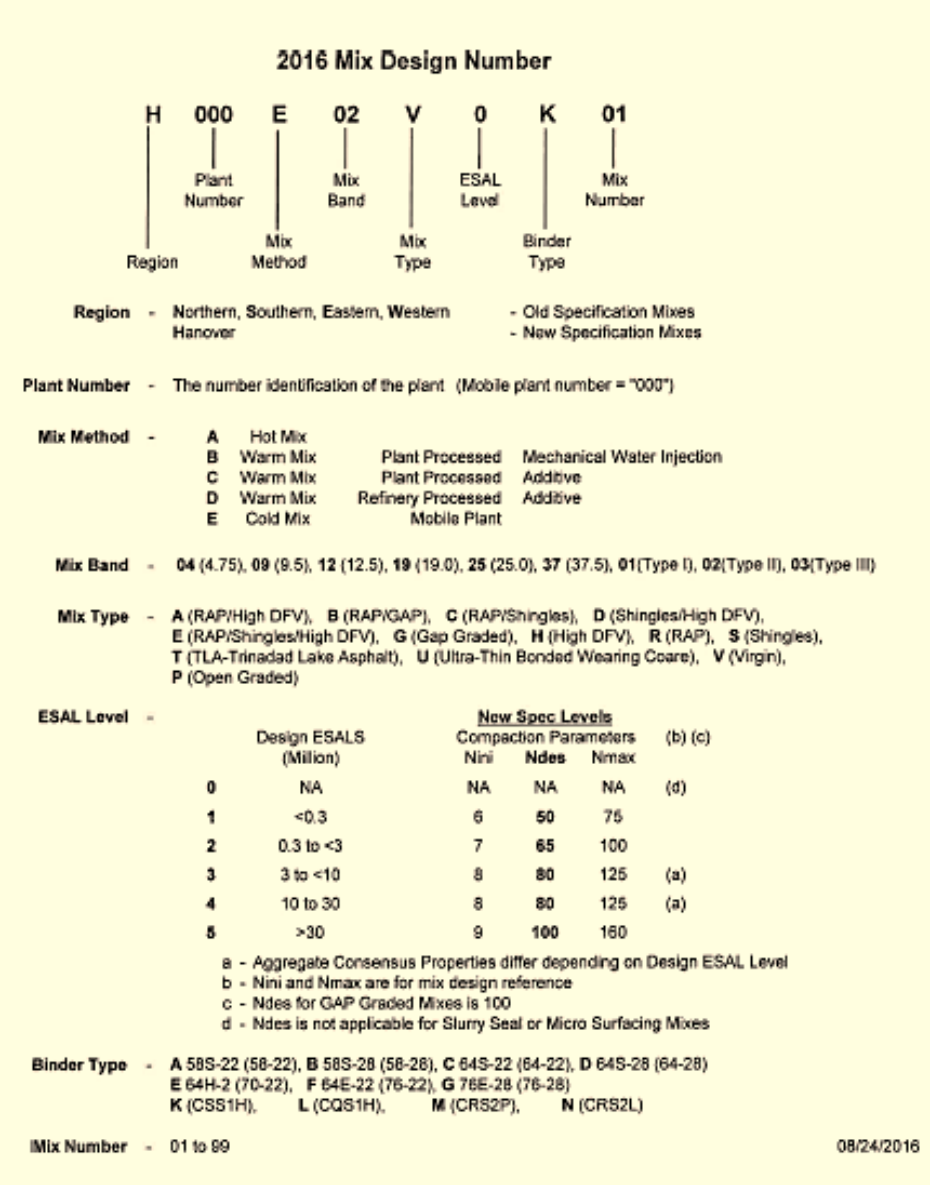

Figure B-53: Naming Convention for MDSHA Asphalt Mixtures

Table B-38: Predicted E* Values from Master Curves of Asphalt Mixtures

No.	Mixtures	Dynamic Modulus (Ksi) Calculated Values from Master Curve												
		1.0E+06	1.0E+05	1.0E+04	1.0E+03	1.0E+02	1.0E+01	1.0E+00	1.0E-01	1.0E-02	1.0E-03	1.0E-04	1.0E-05	1.0E-06
1	H040A12R2C12	3002.2	2868.8	2650.6	2315.0	1848.7	1294.8	767.7	385.9	175.9	81.8	43.3	27.2	20.0
2	H051A12B4F01	2822.1	2670.1	2436.6	2099.9	1660.2	1164.1	704.6	368.8	175.6	83.4	43.4	26.1	18.2
3	H077A09A2C03	2930.4	2762.3	2494.6	2099.7	1583.7	1022.3	546.7	246.0	101.9	44.3	22.6	13.9	10.1
4	H077A09C2C01	2787.9	2610.4	2355.9	2012.4	1588.7	1128.5	705.0	385.6	189.9	89.7	44.0	23.9	14.8
5	H083A12C2C02	2797.6	2604.3	2333.4	1975.7	1543.0	1079.8	658.5	344.7	156.8	65.2	26.9	12.0	6.1
6	H083A19C2C02	2968.3	2816.9	2579.8	2231.7	1769.8	1242.5	751.9	394.4	190.2	93.0	50.5	31.9	23.2
7	H116C09A2F02	2937.1	2795.7	2569.9	2231.1	1770.7	1233.2	726.4	359.8	158.2	69.0	33.5	19.3	13.2
8	H127A12R2C02	2879.4	2707.4	2447.9	2081.8	1615.4	1103.8	645.0	321.9	143.9	63.3	30.3	16.9	11.0
9	H128A12B4F02	2711.6	2508.3	2201.0	1777.3	1270.1	773.3	395.8	177.6	77.3	36.7	20.4	13.5	10.3
10	H131A09A4C01	3098.8	3035.9	2917.4	2701.9	2336.5	1790.4	1130.4	550.8	209.8	72.5	28.3	14.3	9.3
11	H135A12G4F01	2626.8	2410.1	2112.7	1734.8	1303.9	878.4	525.9	284.7	146.3	76.2	42.9	27.0	19.1
12	H135A12H2C02	2813.6	2615.6	2333.2	1956.9	1502.5	1025.0	606.6	310.7	142.6	63.1	29.4	15.4	9.4
13	H135A19G4F01	2593.1	2376.5	2080.0	1704.3	1276.9	855.9	508.4	271.8	137.1	69.9	38.4	23.6	16.3
14	H138A12G4F05	2851.9	2676.0	2399.9	1999.2	1486.8	943.3	495.5	219.8	90.2	39.1	19.9	12.2	8.8
15	H138B12R2C05	3045.7	2931.4	2747.6	2465.7	2064.5	1556.5	1014.9	556.2	259.1	110.3	48.2	23.9	14.1
16	H151B19R2C02	2973.5	2831.8	2615.6	2302.4	1884.0	1388.3	891.9	490.6	235.3	105.1	48.2	24.7	14.7
17	H158B09R2C60	3003.5	2917.4	2770.2	2528.4	2158.8	1656.3	1086.6	585.9	262.3	106.7	45.6	23.0	14.2
18	H160A09R1C03	2917.5	2751.5	2483.8	2085.7	1565.7	1006.3	541.6	253.0	114.0	56.2	32.7	22.6	18.0
19	H160A12H2F01	2898.6	2717.3	2439.3	2044.3	1545.5	1015.2	565.9	272.5	122.3	57.1	30.3	19.0	13.8
20	H161A12R4F01	2978.5	2840.3	2607.5	2242.1	1733.3	1145.4	623.6	285.3	121.8	56.2	31.0	20.7	16.1
21	H168A09R2C02	2887.3	2712.2	2451.6	2087.7	1626.3	1118.5	657.3	326.5	141.6	58.3	25.4	12.6	7.5
22	H168A12R2C02	2925.6	2762.2	2503.3	2121.9	1621.9	1071.4	593.3	279.2	121.1	54.7	28.5	17.8	13.0
23	H169A12B4F03	2682.1	2484.7	2204.5	1833.9	1392.0	935.8	544.7	275.0	125.4	55.7	26.4	14.1	8.8
24	H176A09R2C01	2800.7	2609.6	2334.8	1965.5	1515.9	1039.8	619.8	320.8	149.7	67.9	32.7	17.7	11.1
25	H176A19R2C02	2933.3	2768.1	2502.3	2106.7	1587.9	1025.3	552.6	256.0	112.8	53.7	30.2	20.2	15.7
26	H177A12R2C50	2963.0	2821.8	2600.8	2274.4	1833.9	1315.7	812.4	427.4	199.2	90.0	43.9	24.7	16.4
27	H186D12B4F01	2791.6	2649.2	2422.9	2086.1	1635.3	1121.2	651.1	321.7	144.5	66.1	34.2	21.0	15.0
28	H187A19C2C02	3067.2	2942.7	2744.6	2444.9	2026.5	1509.8	975.5	536.0	256.6	115.9	55.0	29.8	19.0

Table B-39: Phase Angles and Shift Factors of Asphalt Mixtures

Temp (C°)	Reduced Freq (wr)	Phase Angle (deg) ϕ	Shift Factor Log a (T)	Reduced Freq (wr)	Phase Angle (deg) ϕ	Shift Factor Log a (T)	Reduced Freq (wr)	Phase Angle (deg) ϕ	Shift Factor Log a (T)	Reduced Freq (wr)	Phase Angle (deg) ϕ	Shift Factor Log a (T)	Reduced Freq (wr)	Phase Angle (deg) ϕ	Shift Factor Log a (T)	Reduced Freq (wr)	Phase Angle (deg) ϕ	Shift Factor Log a (T)	Reduced Freq (wr)	Phase Angle (deg) ϕ	Shift Factor Log a (T)
	H040A12R2C12			H051A12B4F01			H077A09A2C03			H077A09C2C01			H083A12C2C02			H083A19C2C02			H116C09A2F02		
4	9.4407	16.03	1.98	10.3623	16.26	2.02	9.2334	19.61	1.97	10.7190	19.61	2.03	7.8501	17.89	1.89	6.0457	17.89	1.78	8.3238	17.92	1.92
4	94.4066	11.98	1.98	103.6231	12.34	2.02	92.3343	14.74	1.97	107.1905	14.74	2.03	78.5012	13.81	1.89	60.4573	13.81	1.78	83.2383	13.53	1.92
4	944.0658	9.24	1.98	1036.2312	9.49	2.02	923.3426	11.12	1.97	1071.9049	11.12	2.03	785.0118	10.75	1.89	604.5734	10.67	1.78	832.3827	10.30	1.92
20	0.1000	29.09	0.00	0.1000	27.72	0.00	0.1000	33.66	0.00	0.1000	33.66	0.00	0.1000	28.50	0.00	0.1000	27.77	0.00	0.1000	29.23	0.00
20	1.0000	24.62	0.00	1.0000	23.27	0.00	1.0000	29.11	0.00	1.0000	29.11	0.00	1.0000	24.33	0.00	1.0000	24.10	0.00	1.0000	24.90	0.00
20	10.0000	19.44	0.00	10.0000	18.27	0.00	10.0000	22.81	0.00	10.0000	22.81	0.00	10.0000	19.57	0.00	10.0000	19.71	0.00	10.0000	19.63	0.00
40	0.0001	21.04	-2.18	0.0001	23.55	-2.23	0.0001	17.85	-2.17	0.0001	17.85	-2.25	0.0001	27.83	-2.10	0.0001	24.32	-1.97	0.0001	25.33	-2.12
40	0.0007	27.73	-2.18	0.0006	28.25	-2.23	0.0007	27.59	-2.17	0.0006	27.59	-2.25	0.0008	31.61	-2.10	0.0011	28.26	-1.97	0.0008	30.77	-2.12
40	0.0065	31.77	-2.18	0.0059	31.12	-2.23	0.0067	34.27	-2.17	0.0057	34.27	-2.25	0.0080	32.43	-2.10	0.0107	30.06	-1.97	0.0075	33.74	-2.12
40	0.0653	32.12	-2.18	0.0589	31.00	-2.23	0.0669	36.70	-2.17	0.0568	36.70	-2.25	0.0801	33.43	-2.10	0.1069	29.73	-1.97	0.0751	33.41	-2.12
	H127A12R2C02			H128A12B4F02			H131A09A4C01			H135A12G4F01			H135A12H2C02			H135A19G4F01			H138A12G4F05		
4	8.5345	19.28	1.93	8.7158	21.90	1.94	10.16	14.01	2.01	10.0109	16.27	2.00	11.9124	17.61	2.08	12.6078	16.73	2.10	9.3820	21.10	1.97
4	85.3455	14.62	1.93	87.1585	16.64	1.94	101.62	9.94	2.01	100.1087	12.51	2.00	119.1237	13.01	2.08	126.0782	12.68	2.10	93.8199	15.60	1.97
4	853.4546	11.27	1.93	871.5845	12.50	1.94	1016.22	7.24	2.01	1001.0874	9.81	2.00	1191.2372	9.98	2.08	1260.7824	9.80	2.10	938.1985	11.50	1.97
20	0.1000	30.83	0.00	0.1000	32.73	0.00	0.10	31.22	0.00	0.1000	28.13	0.00	0.1000	30.95	0.00	0.1000	28.46	0.00	0.1000	33.80	0.00
20	1.0000	25.86	0.00	1.0000	29.64	0.00	1.00	23.20	0.00	1.0000	24.14	0.00	1.0000	25.58	0.00	1.0000	24.32	0.00	1.0000	29.30	0.00
20	11.0000	20.37	0.00	10.0000	24.23	0.00	10.00	16.57	0.00	11.0000	19.51	0.00	10.0000	19.75	0.00	10.0000	19.39	0.00	10.0000	23.00	0.00
40	0.0001	19.67	-2.14	0.0001	19.13	-2.15	0.00	27.98	-2.22	0.0001	23.55	-2.21	0.0001	18.90	-2.30	0.0000	20.03	-2.32	0.0000	22.00	-2.68
40	0.0007	27.37	-2.14	0.0007	25.14	-2.15	0.00	35.35	-2.22	0.0006	28.02	-2.21	0.0005	27.98	-2.30	0.0005	27.16	-2.32	0.0002	27.10	-2.68
40	0.0073	32.02	-2.14	0.0071	31.46	-2.15	0.01	38.27	-2.22	0.0061	30.61	-2.21	0.0050	33.36	-2.30	0.0047	31.28	-2.32	0.0021	33.40	-2.68
40	0.0730	33.12	-2.14	0.0713	35.05	-2.15	0.06	35.40	-2.22	0.0612	30.99	-2.21	0.0505	34.72	-2.30	0.0474	32.14	-2.32	0.0207	38.70	-2.68
	H138B12R2C05			H151B19R2C02			H158B09R2C60			H160A09R1C03			H160A12H2F01			H161A12R4F01			H168A09R2C02		
4	13.3822	15.94	2.13	9.0698	15.11	1.96	10.2332	13.07	2.01	6.60	20.39	1.82	9.39	19.56	1.97	7.4724	20.07	1.87	11.4895	17.50	2.06
4	133.8217	11.88	2.13	90.6984	11.14	1.96	102.3317	9.79	2.01	66.04	15.23	1.82	93.92	14.24	1.97	74.7236	14.65	1.87	114.8954	12.90	2.06
4	1338.2171	9.11	2.13	906.9842	8.51	1.96	1023.3173	7.47	2.01	660.36	11.36	1.82	939.23	10.51	1.97	747.2364	10.75	1.87	1148.9535	9.80	2.06
20	0.1000	27.65	0.00	0.1000	28.22	0.00	0.1000	27.26	0.00	0.10	31.39	0.00	0.10	32.50	0.00	0.1000	33.49	0.00	0.1000	31.20	0.00
20	1.0000	22.34	0.00	1.0000	22.43	0.00	1.0000	20.97	0.00	1.00	28.04	0.00	1.00	27.72	0.00	1.0000	28.34	0.00	1.0000	25.70	0.00
20	10.0000	17.28	0.00	10.0000	16.83	0.00	10.0000	15.60	0.00	10.00	22.40	0.00	10.00	21.46	0.00	10.0000	21.96	0.00	10.0000	19.80	0.00
40	0.0000	28.21	-2.35	0.0001	24.19	-2.17	0.0001	28.01	-2.22	0.00	17.45	-2.01	0.00	21.63	-2.18	0.0001	18.20	-2.07	0.0001	26.20	-2.28
40	0.0004	31.94	-2.35	0.0007	31.10	-2.17	0.0006	33.12	-2.22	0.00	24.81	-2.01	0.00	28.13	-2.18	0.0008	27.13	-2.07	0.0005	31.60	-2.28
40	0.0044	34.35	-2.35	0.0068	33.49	-2.17	0.0060	34.20	-2.22	0.01	30.73	-2.01	0.01	33.58	-2.18	0.0085	33.60	-2.07	0.0053	35.70	-2.28
40	0.0444	33.05	-2.35	0.0683	31.34	-2.17	0.0597	30.90	-2.22	0.10	33.44	-2.01	0.07	35.56	-2.18	0.0846	35.46	-2.07	0.0526	35.70	-2.28
	H168A12R2C02			H169A12B4F03			H176A09R2C01			H176A19R2C02			H177A12R2C50			H186D12B4F01			H187A19C2C02		
4	7.8288	19.01	1.89	12.2698	16.91	2.09	12.0694	16.59	2.08	8.9864	20.29	1.95	11.5708	15.35	2.06	10.4120	17.24	2.02	10.8386	14.55	2.03
4	78.2883	14.05	1.89	122.6978	12.83	2.09	120.6937	12.31	2.08	89.8641	14.91	1.95	115.7077	11.37	2.06	104.1202	12.80	2.02	108.3865	10.90	2.03
4	782.8827	10.57	1.89	1226.9783	9.84	2.09	1206.9374	9.52	2.08	898.6408	10.93	1.95	1157.0769	8.71	2.06	1041.2023	9.56	2.02	1083.8648	8.45	2.03
20	0.1000	31.74	0.00	0.1000	29.66	0.00	0.1000	29.66	0.00	0.1000	31.41	0.00	0.1000	28.37	0.00	0.1000	29.73	0.00	0.1000	26.91	0.00
20	1.0000	27.50	0.00	1.0000	25.00	0.00	1.0000	24.84	0.00	1.0000	27.93	0.00	1.0000	22.88	0.00	1.0000	25.15	0.00	1.0000	21.81	0.00
20	10.0000	21.74	0.00	10.0000	19.58	0.00	10.0000	19.45	0.00	10.0000	22.25	0.00	10.0000	17.38	0.00	10.0000	19.60	0.00	10.0000	16.94	0.00
40	0.0001	18.85	-2.10	0.0000	25.87	-2.31	0.0000	25.05	-2.30	0.0001	17.49	-2.16	0.0001	23.87	-2.28	0.0001	22.76	-2.23	0.0001	26.39	-2.25
40	0.0008	26.56	-2.10	0.0005	30.54	-2.31	0.0005	30.52	-2.30	0.0007	24.24	-2.16	0.0005	29.81	-2.28	0.0006	28.07	-2.23	0.0006	30.63	-2.25
40	0.0080	32.14	-2.10	0.0049	34.05	-2.31	0.0050	33.59	-2.30	0.0069	30.54	-2.16	0.0052	32.97	-2.28	0.0059	32.28	-2.23	0.0056	32.01	-2.25
40	0.0803	34.04	-2.10	0.0489	34.24	-2.31	0.0498	33.73	-2.30	0.0690	34.11	-2.16	0.0522	32.18	-2.28	0.0586	33.49	-2.23	0.0561	30.33	-2.25

Table B-40: Measured E* Values for All Mixtures

No	Mixtures	Dynamic Modulus (Ksi) Measured Values									
		4C@ 0.1 Hz	4C@1 Hz	4C@10 Hz	20C@0.1 Hz	20C@1 Hz	20C@10 Hz	40C@0.01 Hz	40C@0.1 Hz	40C@1Hz	40C@10Hz
1	H040A12R2C12	1380.8	1938.5	2510.3	375.9	699.0	1169.2	38.3	72.5	159.4	346.2
2	H051A12B4F01	1183.3	1667.4	2162.8	373.4	689.6	1127.4	38.5	69.6	147.3	320.5
3	H077A09A2C03	1063.0	1598.1	2178.8	245.4	514.6	936.3	20.8	37.1	89.6	223.5
4	H077A09C2C01	1164.1	1622.2	2119.1	386.5	677.4	1078.7	37.2	74.9	159.3	331.8
5	H083A12C2C02	1057.6	1519.0	2026.1	341.8	631.8	1050.2	24.5	60.9	146.4	324.6
6	H083A19C2C02	1189.1	1727.3	2313.1	382.2	694.6	1149.9	49.6	98.5	202.8	407.5
7	H116C09A2F02	1227.4	1790.0	2390.3	356.0	682.5	1153.7	30.3	64.2	145.8	330.7
8	H127A12R2C02	1063.4	1584.2	2169.6	329.0	628.5	1078.2	28.0	55.4	130.3	294.3
9	H128A12B4F02	780.2	1237.0	1749.5	176.5	387.3	737.8	19.5	32.0	68.1	165.7
10	H131A09A4C01	1875.1	2515.4	3118.8	539.3	1045.5	1689.1	23.3	59.3	172.9	449.2
11	H135A12G4F01	979.3	1369.2	1782.1	281.0	518.4	857.3	39.3	65.9	130.1	269.6
12	H135A12H2C02	1060.9	1519.8	2002.7	319.3	604.2	1012.6	24.7	46.7	111.5	258.3
13	H135A19G4F01	937.6	1322.9	1724.5	271.7	496.9	817.4	33.4	53.6	109.0	232.0
14	H138A12G4F05	943.0	1472.8	2050.3	221.8	485.9	907.8	14.1	23.7	49.6	123.4
15	H138B12R2C05	1577.1	2191.1	2825.3	555.8	973.8	1530.7	36.2	84.5	195.8	419.9
16	H151B19R2C02	1399.9	1888.5	2370.4	486.9	863.0	1344.5	42.8	91.1	209.3	446.6
17	H158B09R2C60	1748.2	2298.7	2821.8	569.3	1009.3	1553.7	37.4	90.3	222.3	495.2
18	H160A09R1C03	979.4	1493.4	2050.6	245.6	511.5	935.0	32.5	55.0	115.5	263.1
19	H160A12H2F01	1030.9	1520.0	2031.4	273.3	562.5	993.0	28.2	48.3	104.1	247.5
20	H161A12R4F01	1114.2	1674.0	2267.2	285.5	599.8	1076.3	30.3	51.6	116.2	279.5
21	H168A09R2C02	1168.6	1681.6	2209.5	327.0	637.0	1085.6	20.5	45.5	112.1	265.8
22	H168A12R2C02	1079.8	1600.0	2148.4	275.4	559.0	989.5	27.2	49.8	114.3	271.3
23	H169A12B4F03	993.0	1419.9	1872.0	278.7	536.3	913.7	21.8	42.3	95.9	225.5
24	H176A09R2C01	1114.6	1579.2	2059.7	318.7	595.1	994.8	26.6	53.9	119.3	262.1
25	H176A19R2C02	1019.5	1545.6	2101.1	259.1	546.2	993.1	28.8	46.1	98.4	232.9
26	H177A12R2C50	1363.9	1874.6	2390.2	432.5	789.4	1267.2	36.9	71.4	159.8	354.8
27	H186D12B4F01	1155.1	1656.9	2169.7	323.7	630.0	1072.7	30.2	55.0	120.5	275.9
28	H187A19C2C02	1574.6	2118.9	2656.9	529.6	922.1	1427.9	45.5	97.3	216.3	451.2

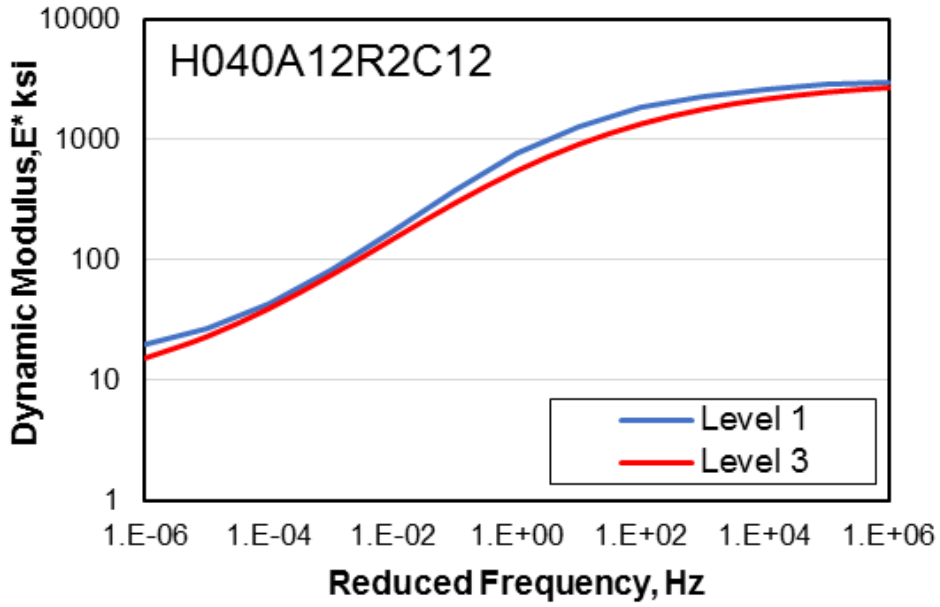

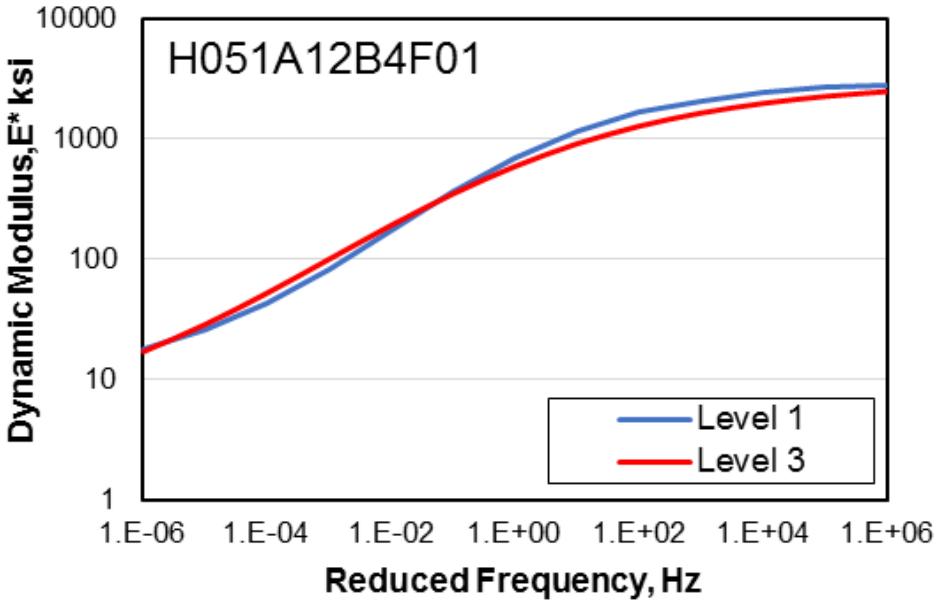

Figure B-54a: Master Curves Developed using Level 1 and Level 3 E* Values

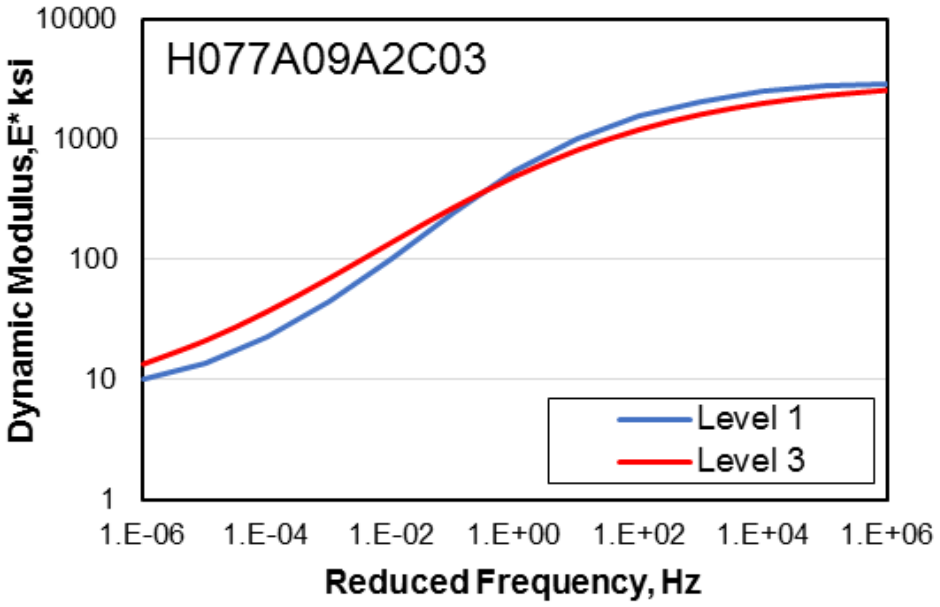

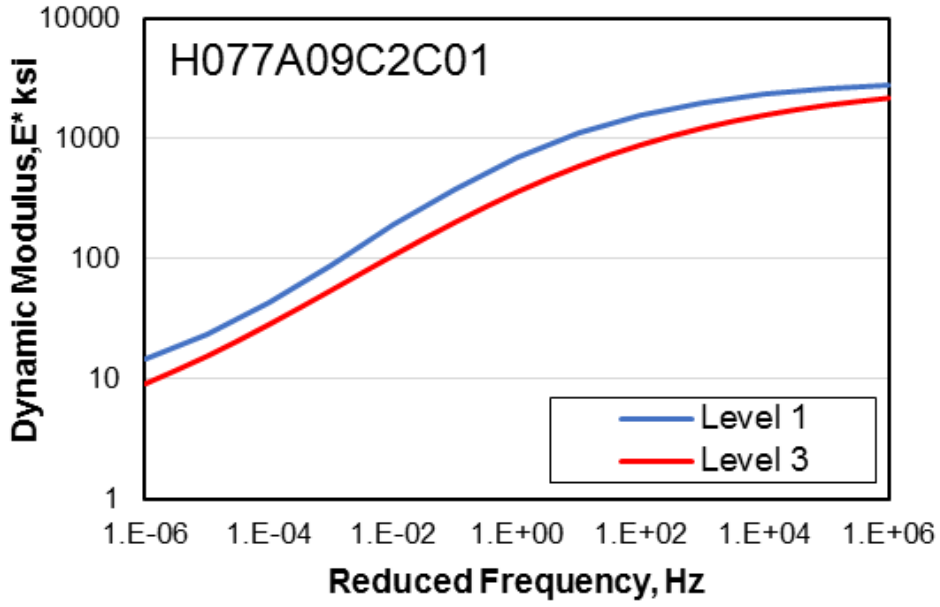

Figure B-54b: Master Curves Developed using Level 1 and Level 3 E* Values

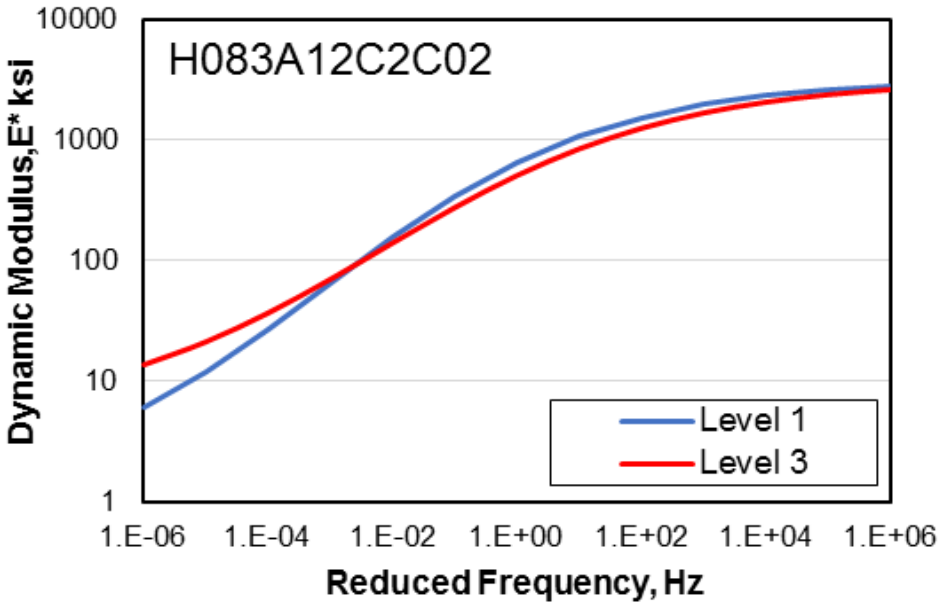

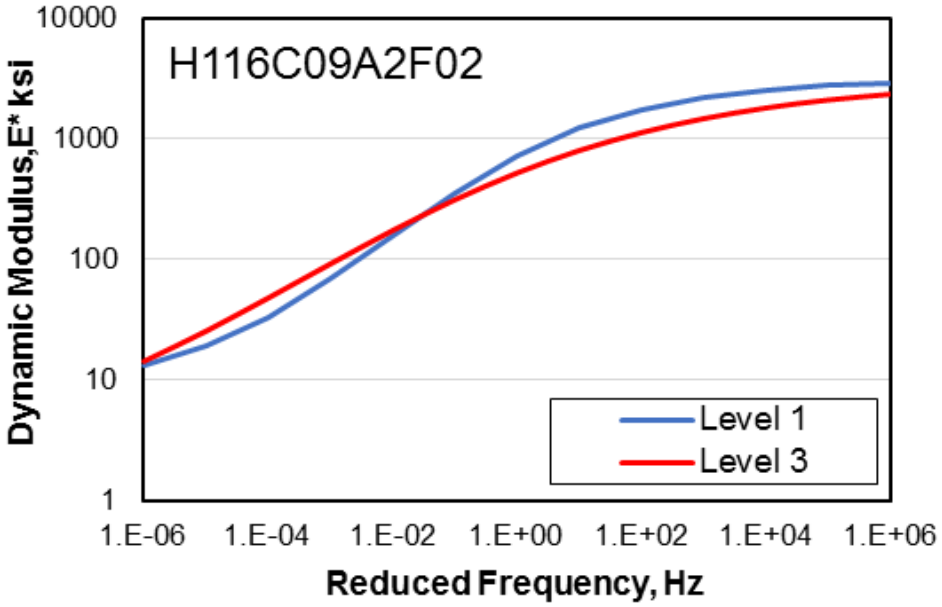

Figure B-54c: Master Curves Developed using Level 1 and Level 3 E* Values

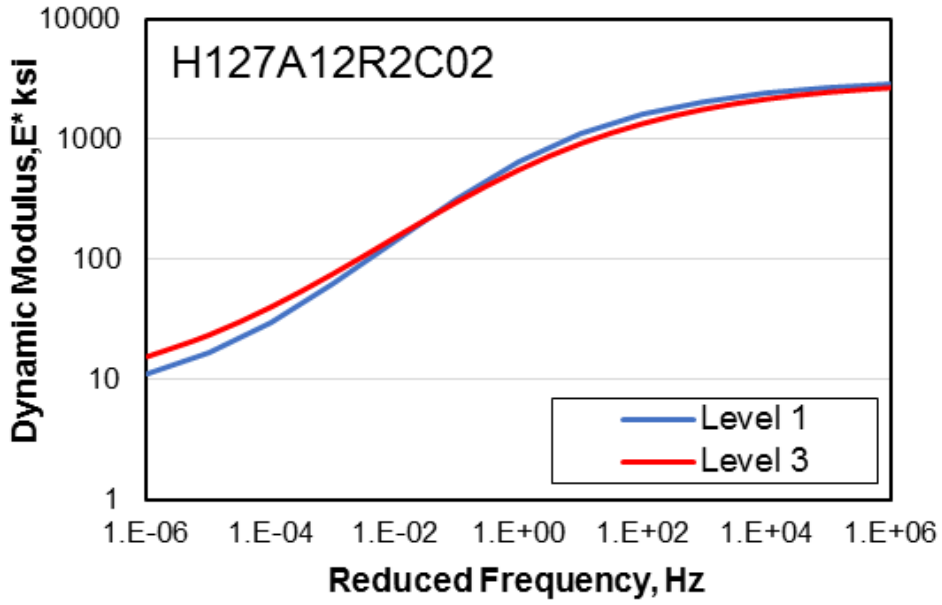

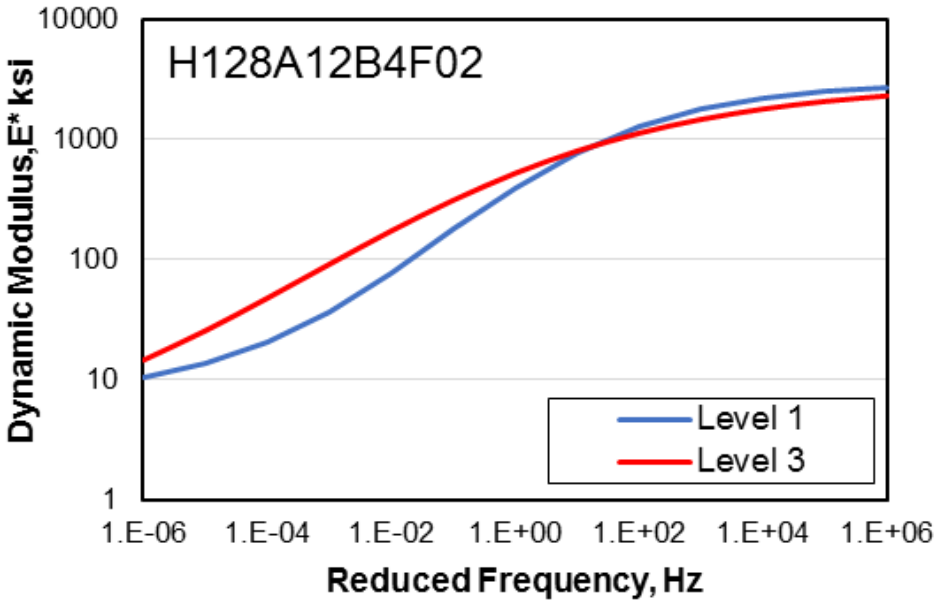

Figure B-54d: Master Curves Developed using Level 1 and Level 3 E* Values

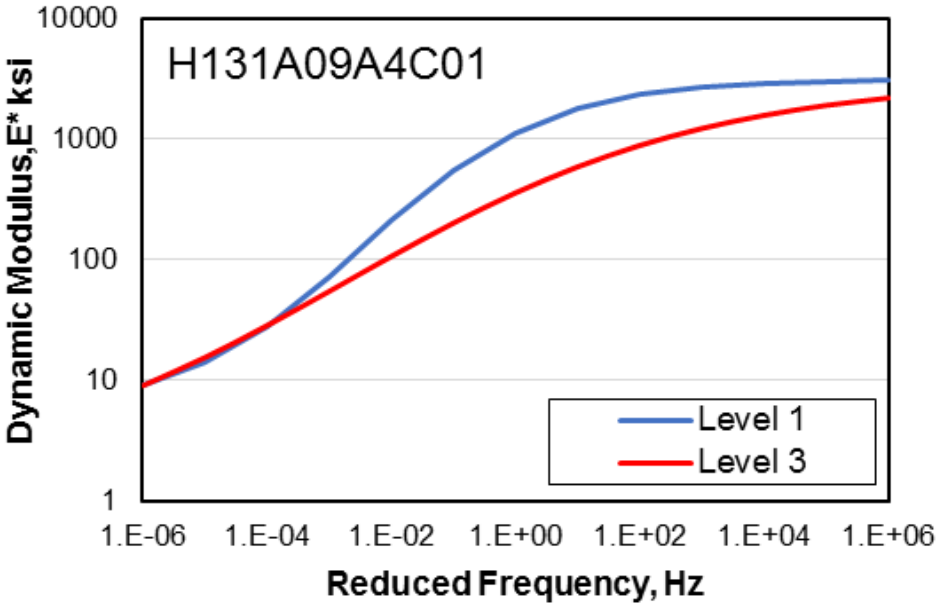

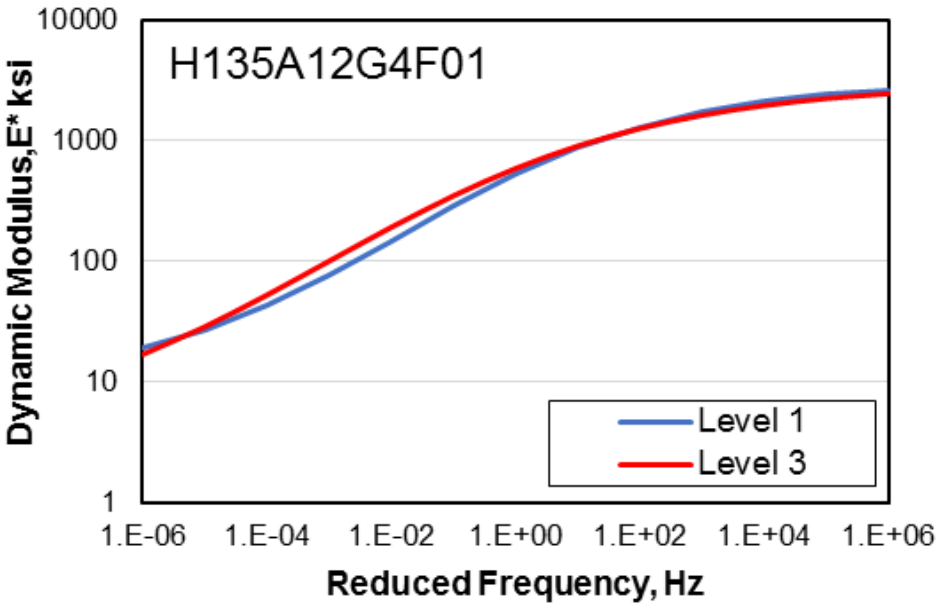

Figure B-54e: Master Curves Developed Using Level 1 and Level 3 E* Values

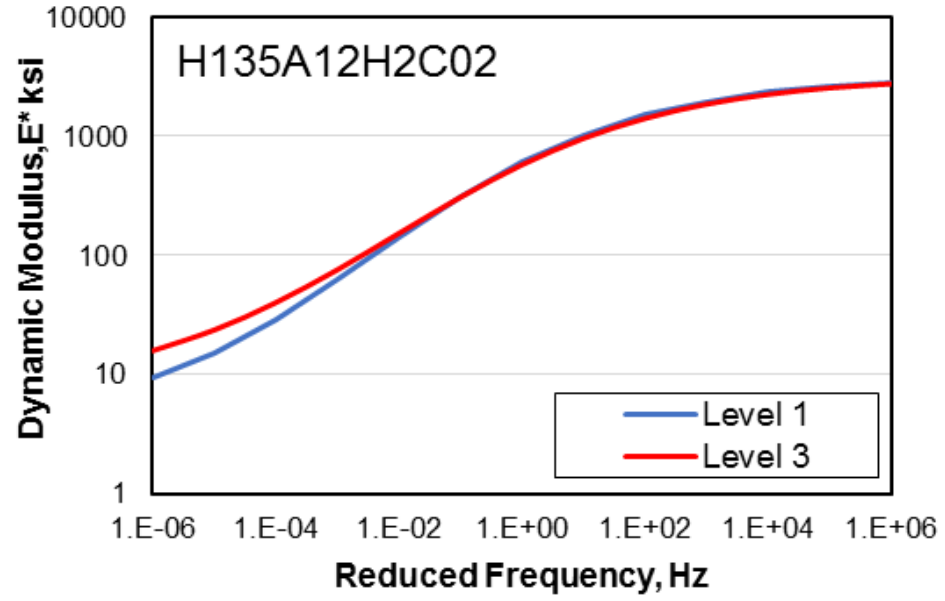

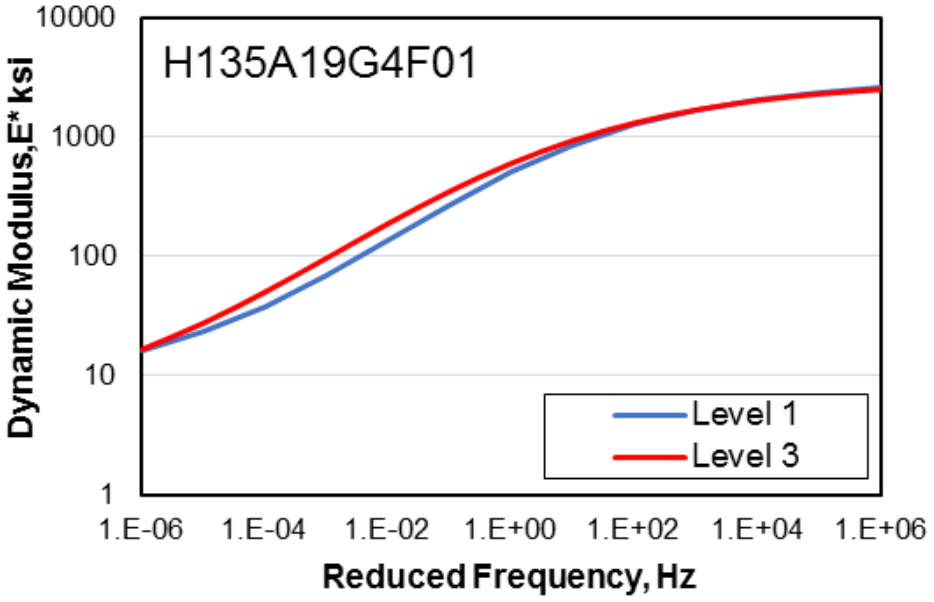

Figure B-54f: Master Curves Developed using Level 1 and Level 3 E* Values

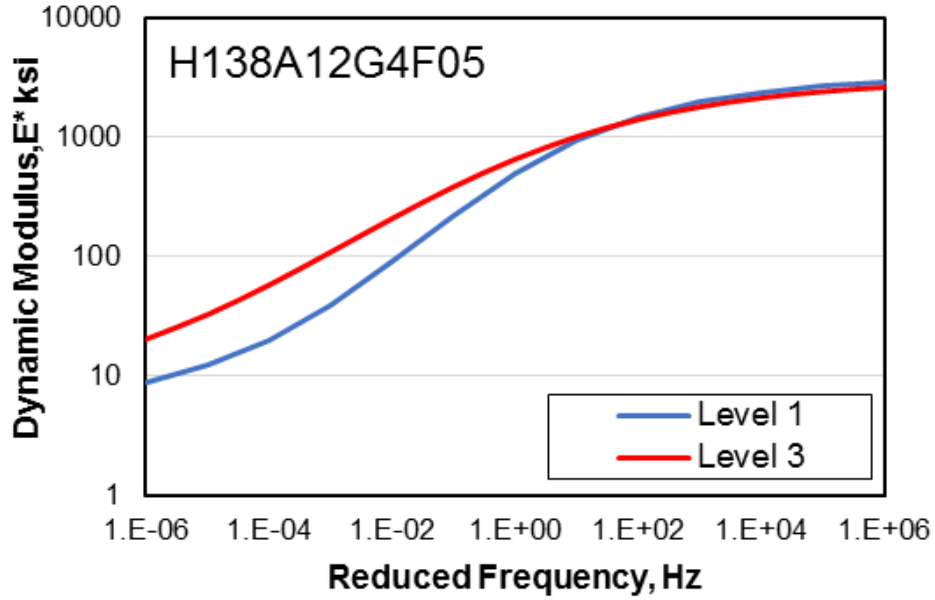

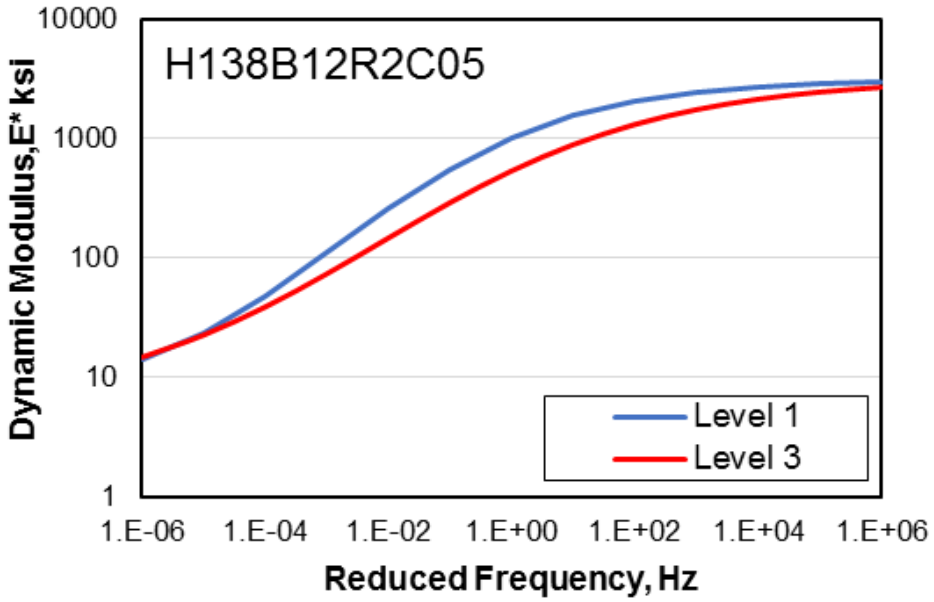

Figure B-54g: Master Curves Developed using Level 1 and Level 3 E* Values

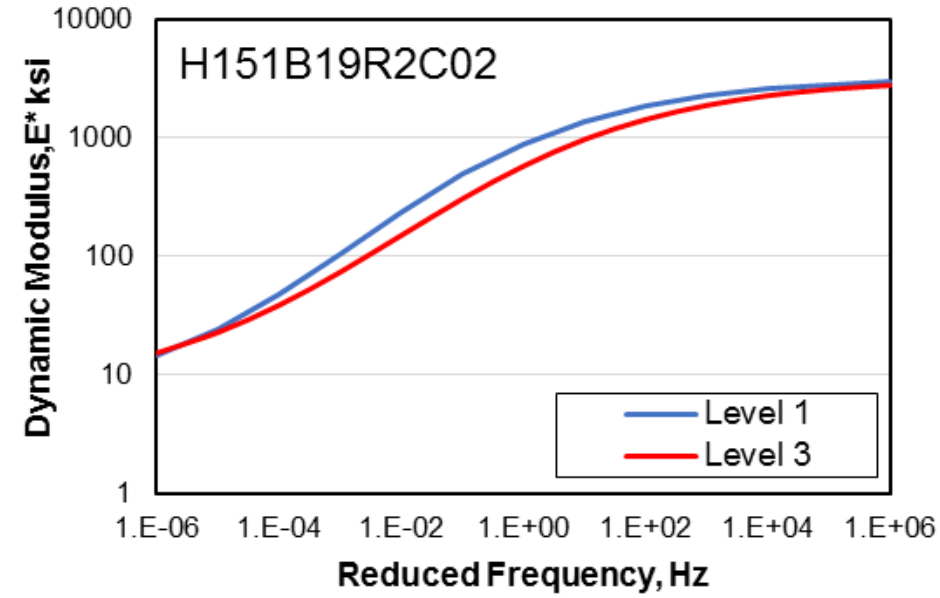

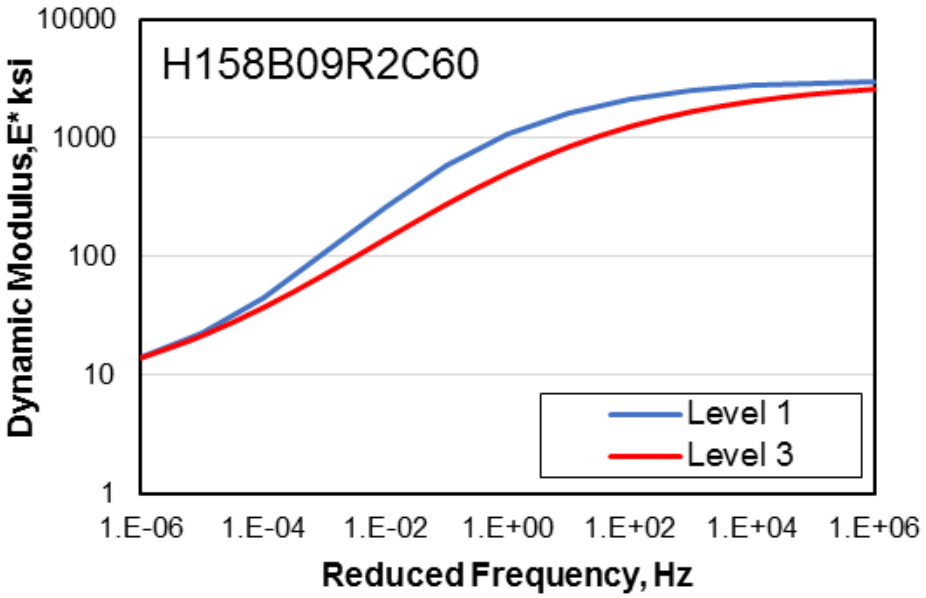

Figure B-54h: Master Curves Developed using Level 1 and Level 3 E* Values

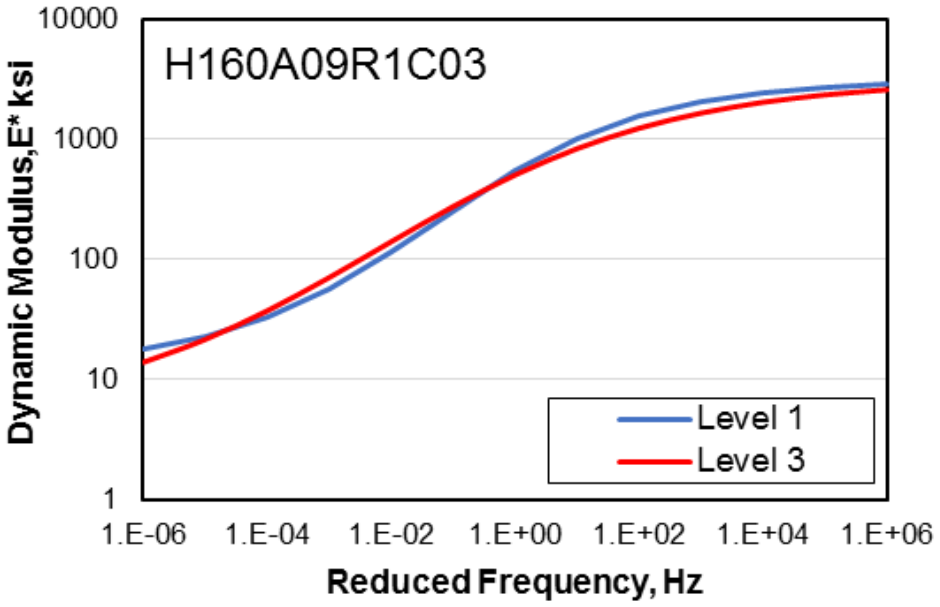

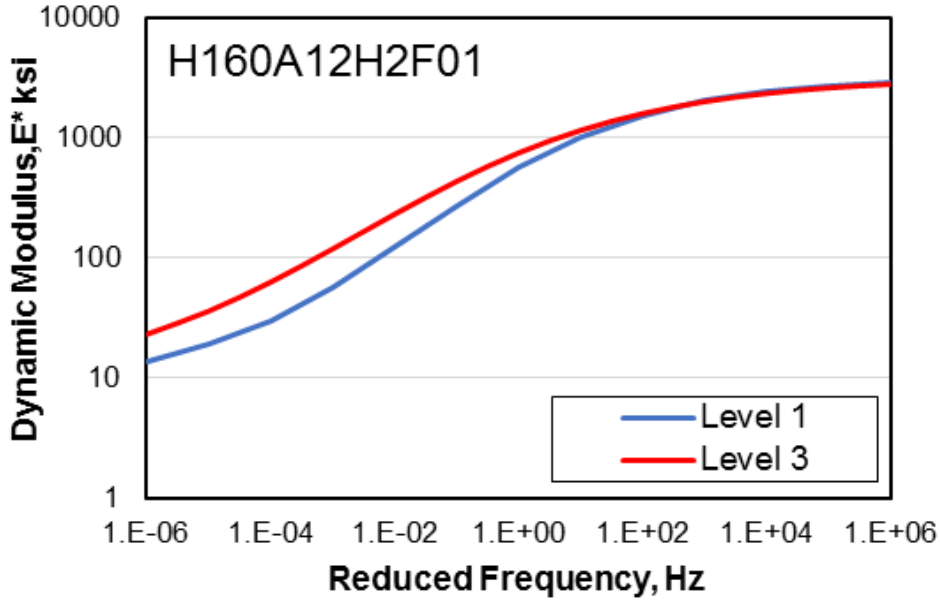

Figure B-54i: Master Curves Developed using Level 1 and Level 3 E* Values

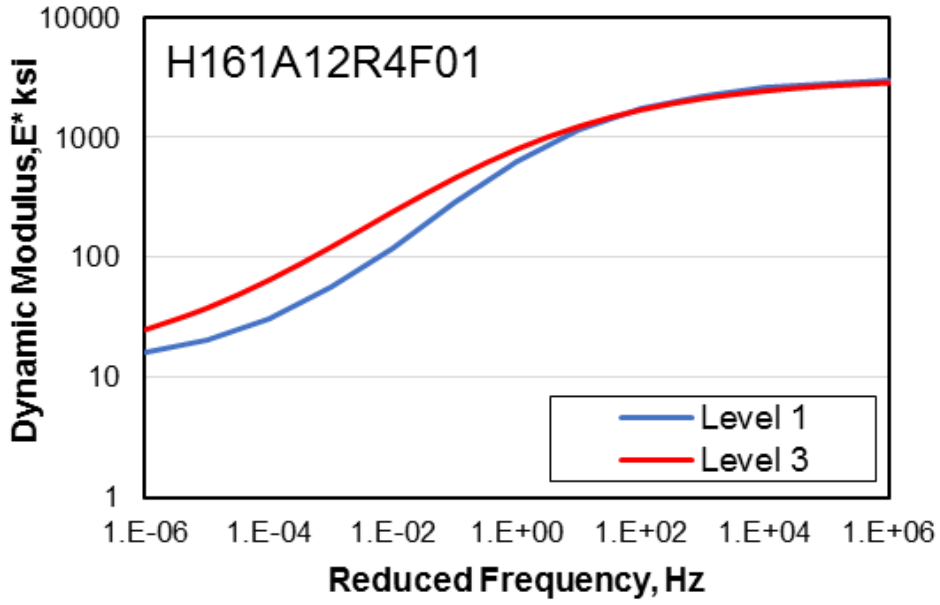

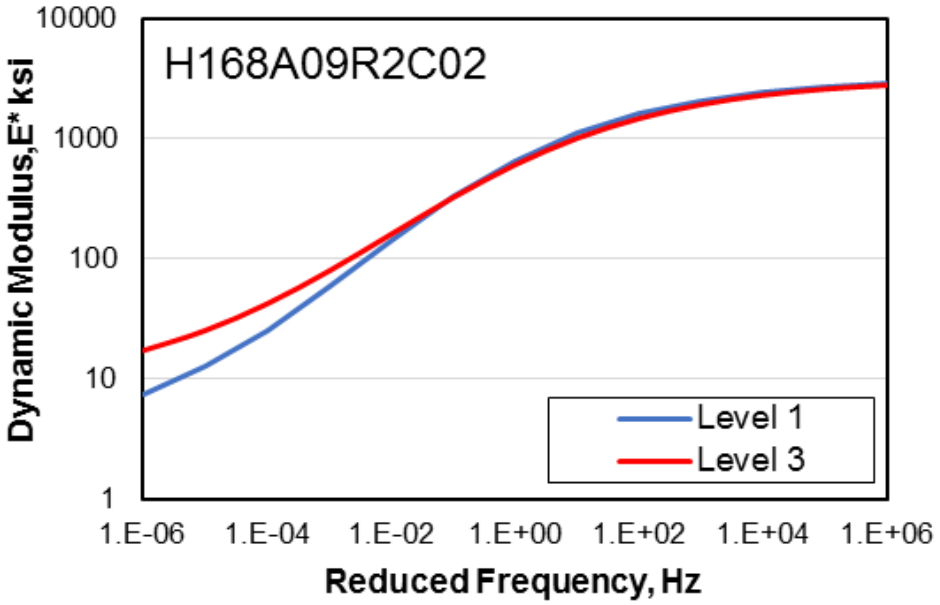

Figure B-54j: Master Curves Developed using Level 1 and Level 3 E* Values

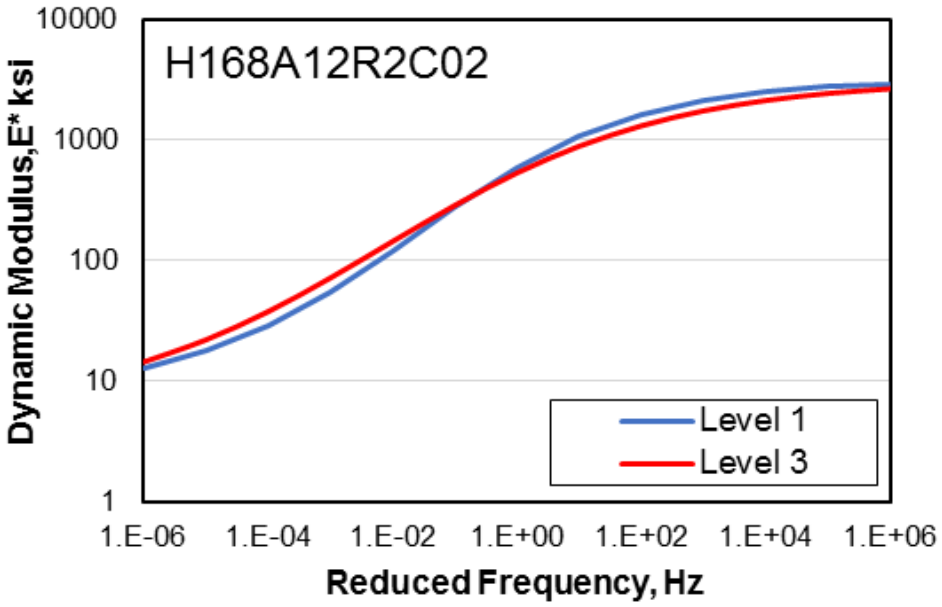

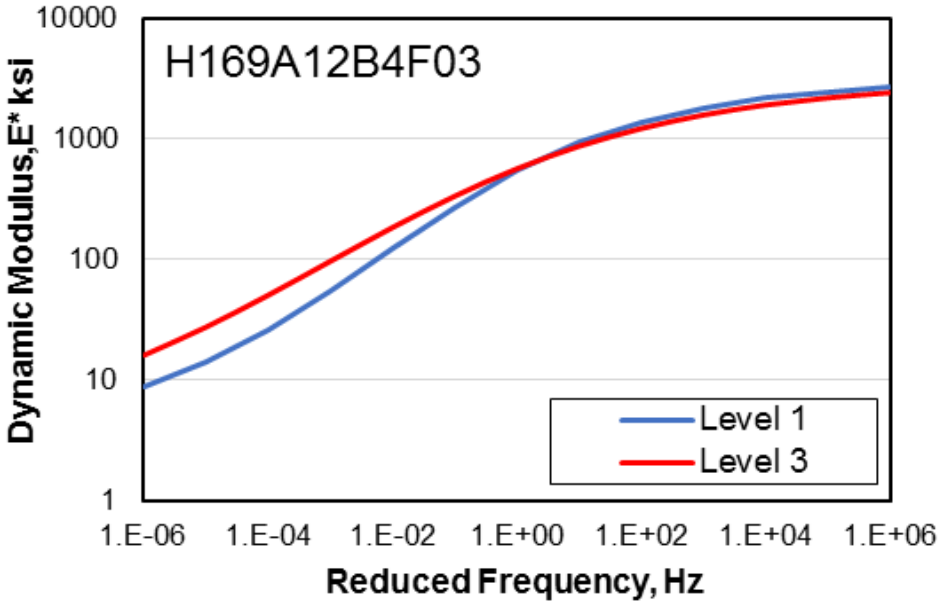

Figure B-54k: Master Curves Developed using Level 1 and Level 3 E* Values

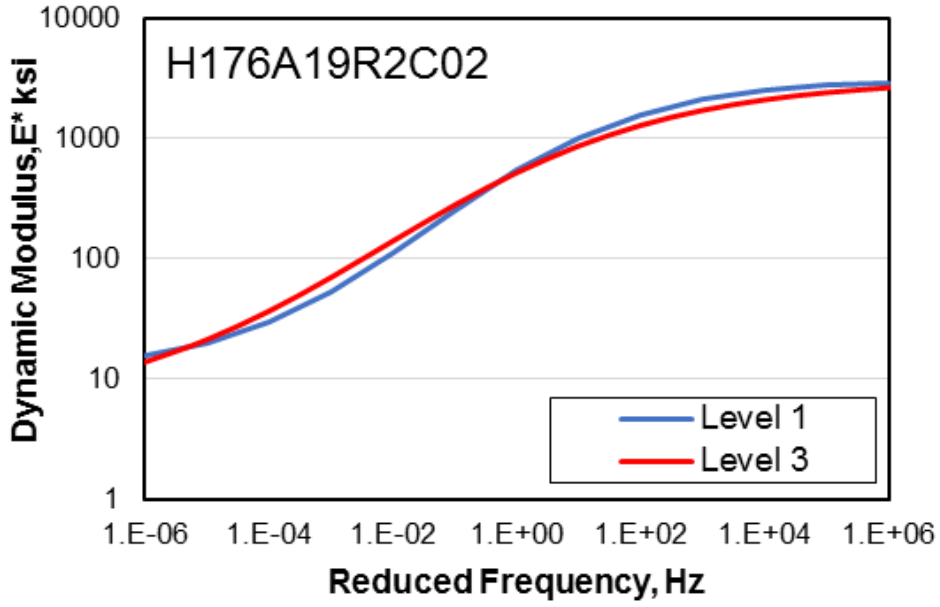

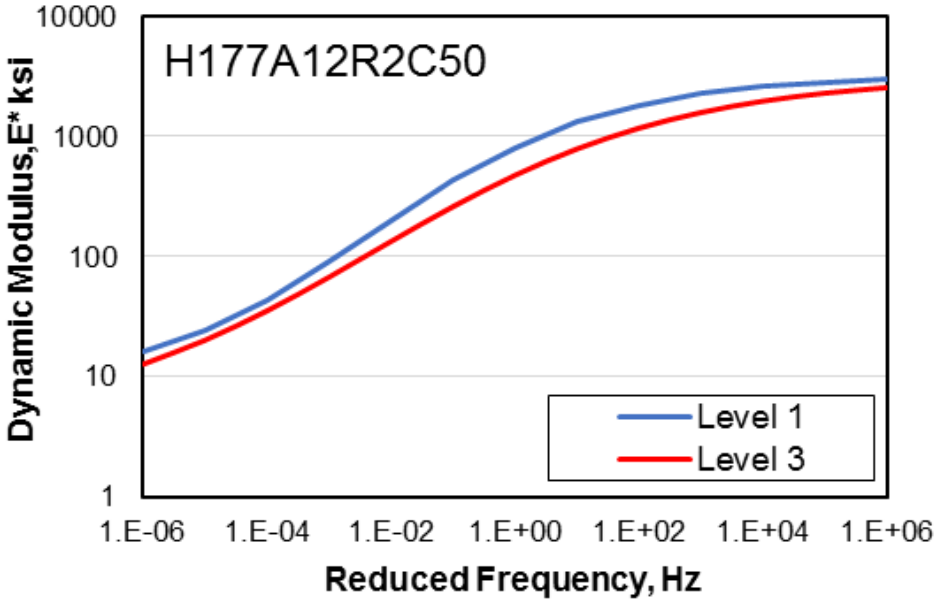

Figure B-54l: Master Curves Developed using Level 1 and Level 3 E* Values

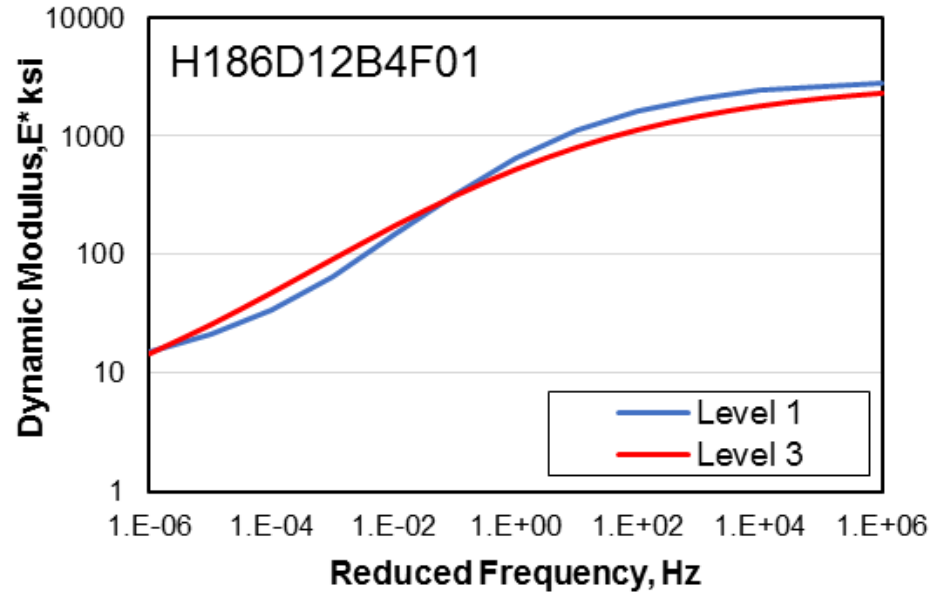

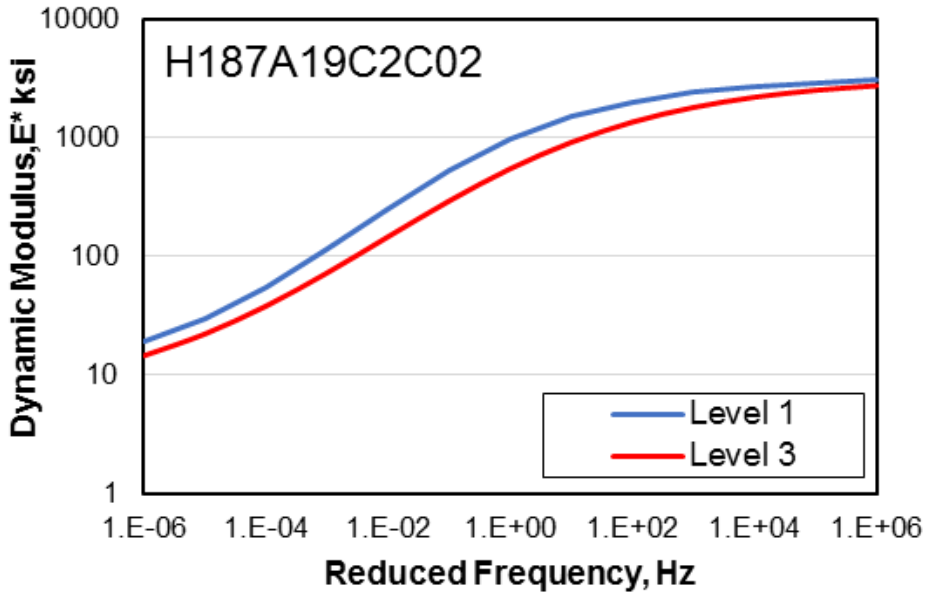

Figure B-54m: Master Curves Developed using Level 1 and Level 3 E* Values

APPENDIX C

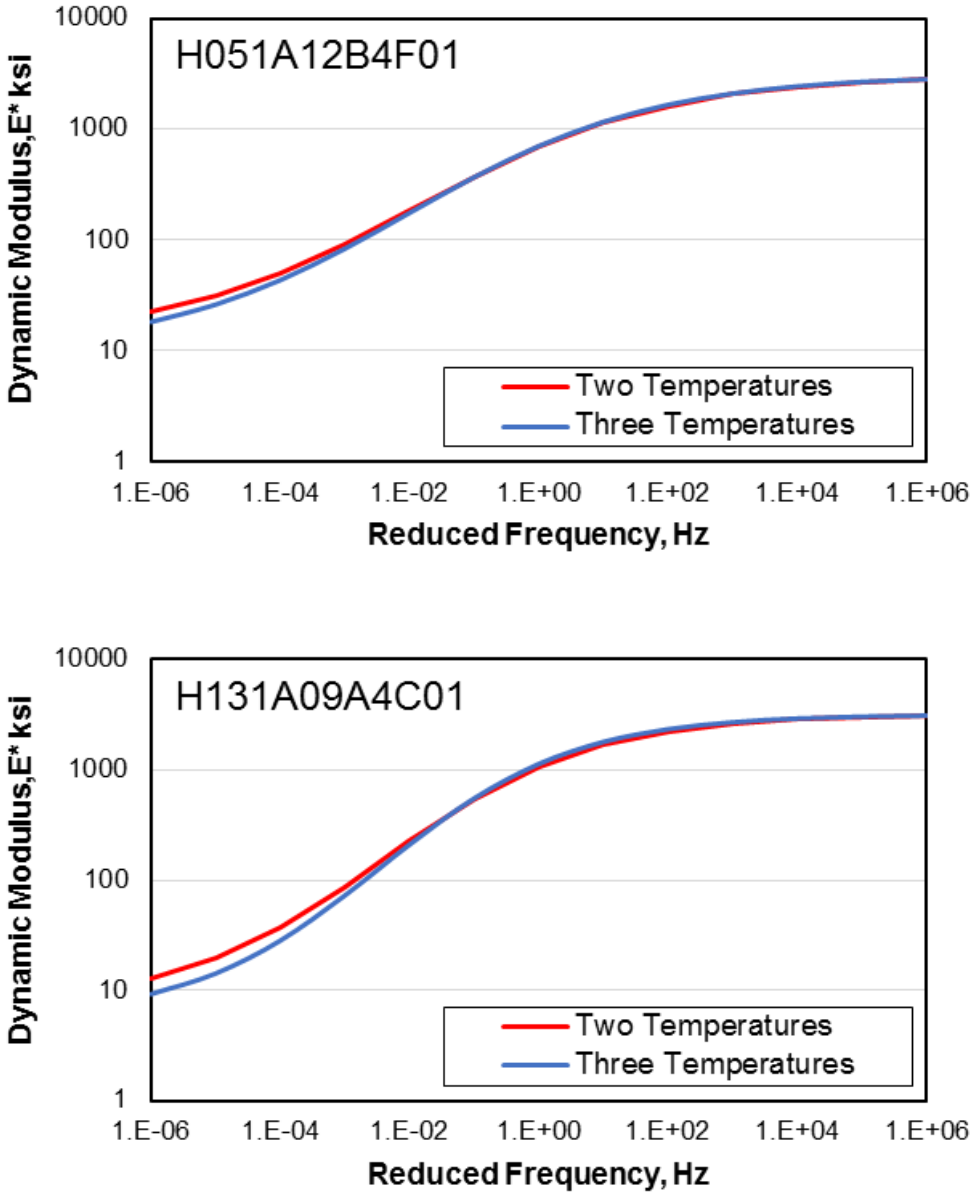

Figure C-55a: Master Curves Developed from Tests at Two and Three Temperatures

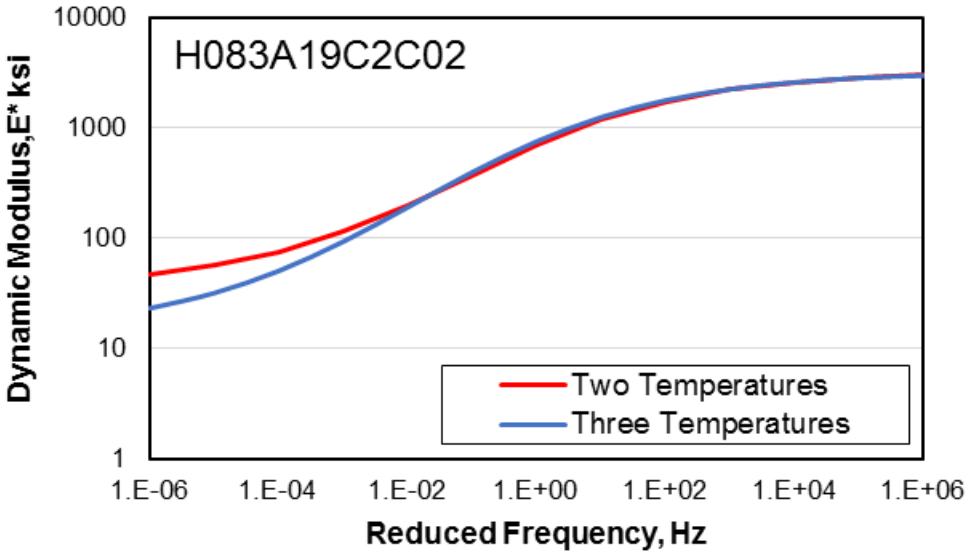

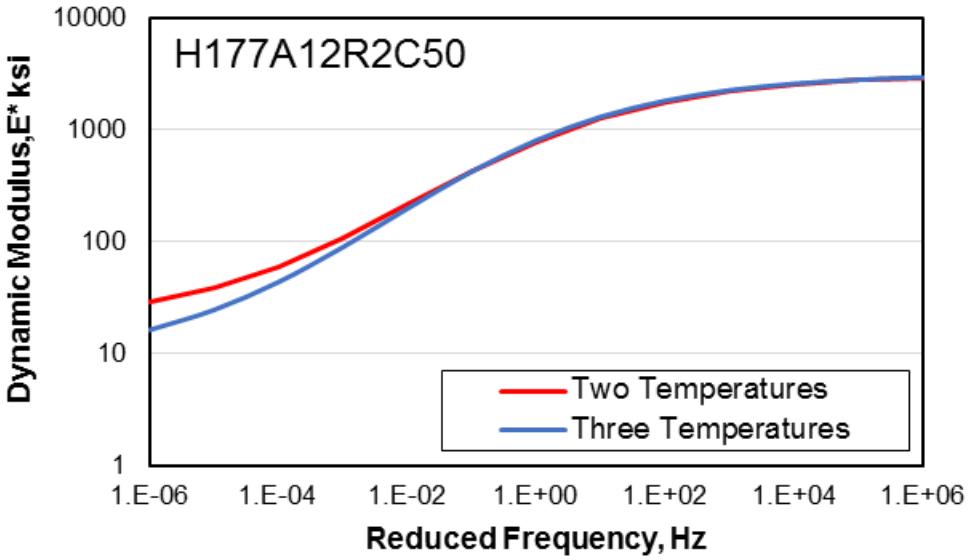

Figure C-55b: Master Curves Developed from Tests at Two and Three Temperatures

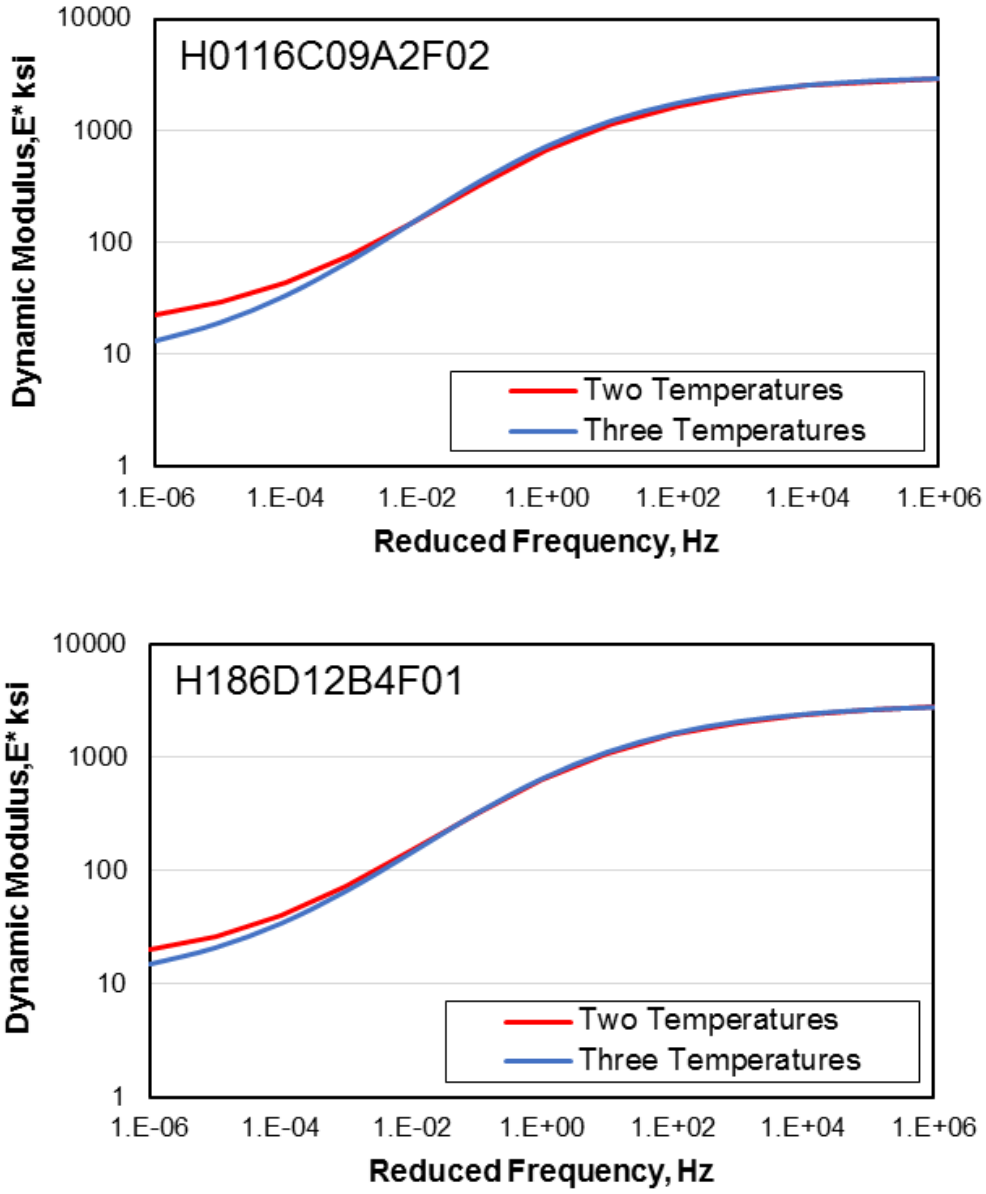

Figure C-55c: Master Curves Developed from Tests at Two and Three Temperatures

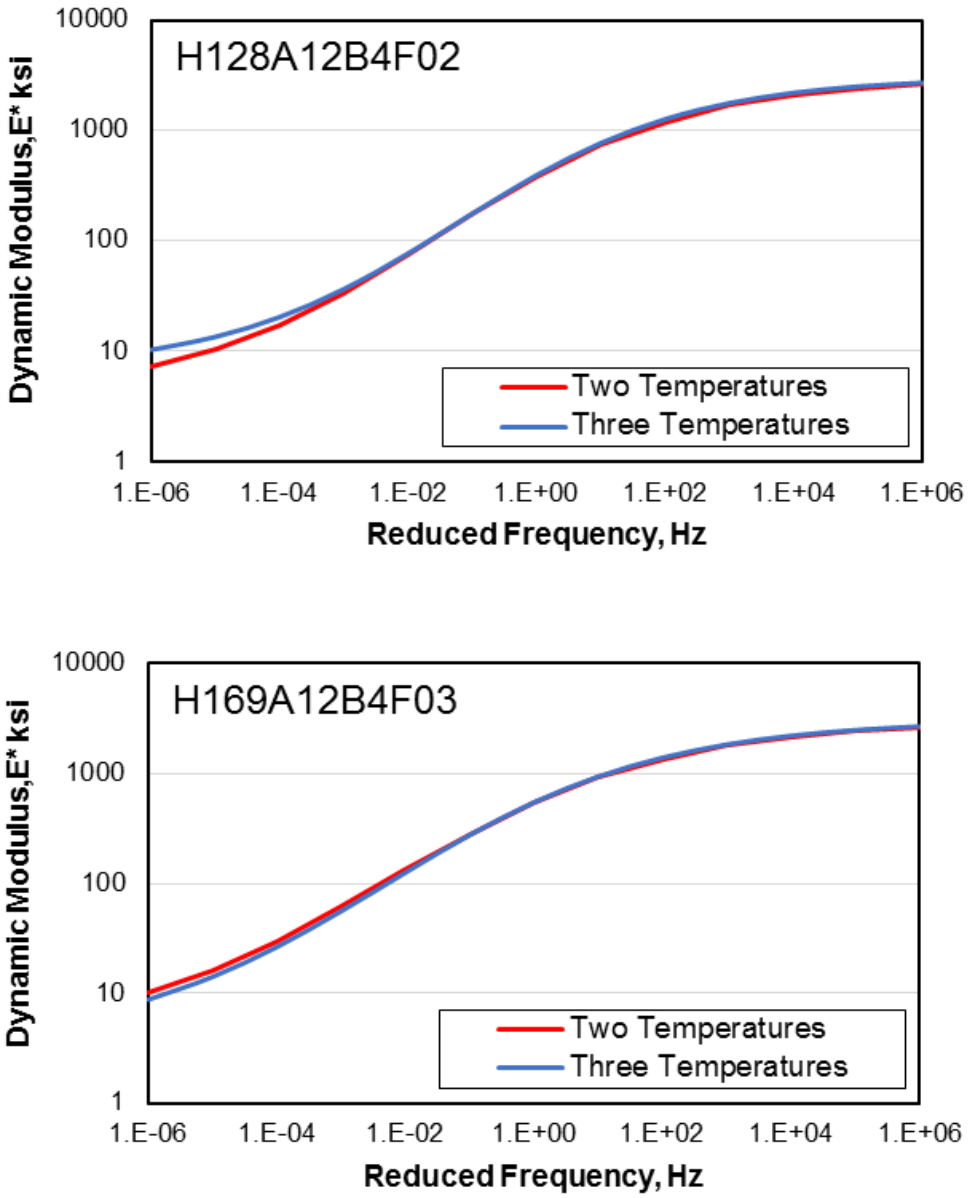

Figure C-55d: Master Curves Developed from Tests at Two and Three Temperatures

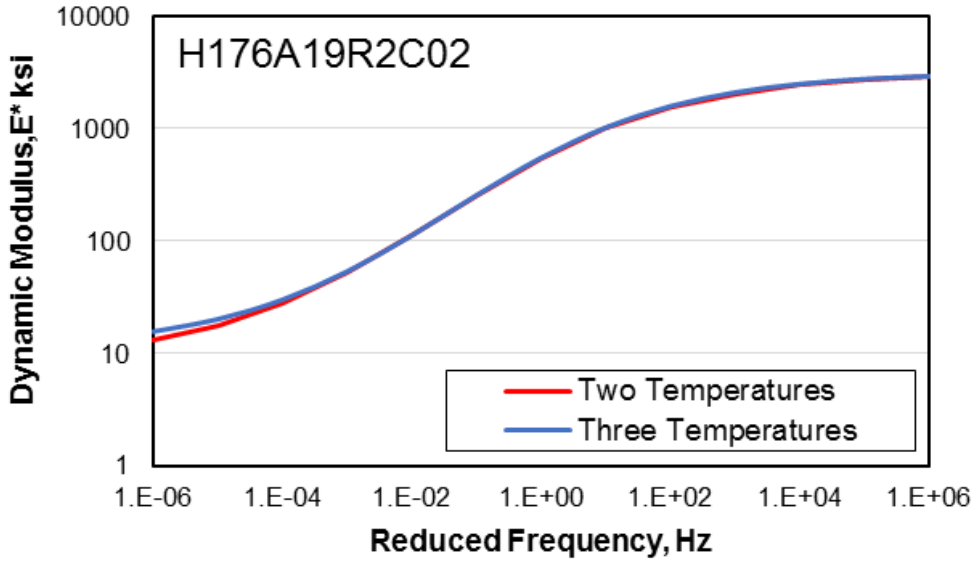

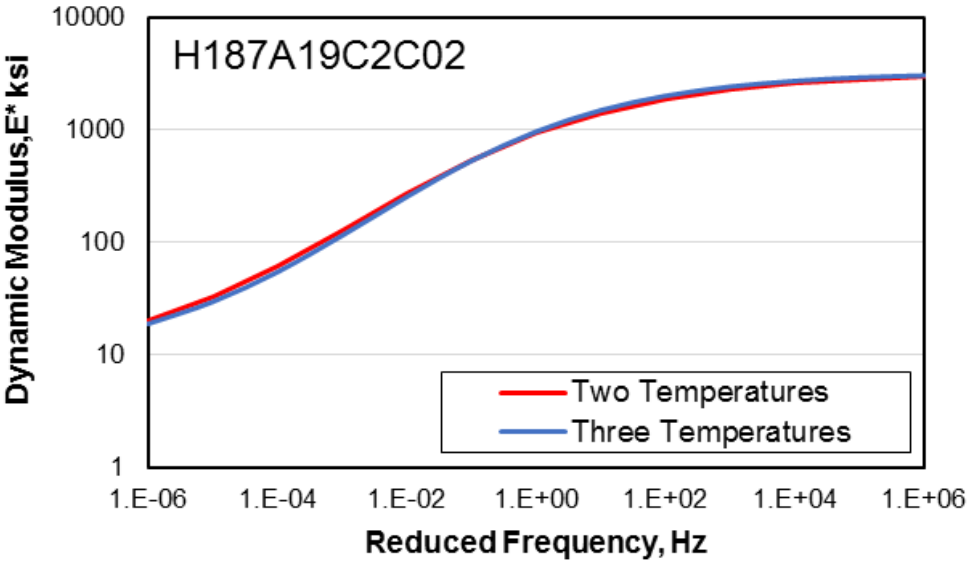

Figure C-55e: Master Curves Developed from Tests at Two and Three Temperatures

REFERENCES

AASHTO, T. 166, 2013, "Standard Practice for Bulk Specific Gravity of Compacted Asphalt Mixtures using Saturated Surface Dry Specimens," *American Association of State Highway Transportation Officials (AASHTO)*, Washington, D.C.

AASHTO, T. 209, 2012, "Standard Practice for Theoretical Maximum Specific Gravity and Density of Hot Mix Asphalt," *American Association of State Highway Transportation Officials (AASHTO)*, Washington, D.C.

AASHTO, T. 27, 2011, "Standard Practice for Sieve Analysis of Fine and Coarse Aggregates," *American Association of State Highway Transportation Officials (AASHTO)*, Washington, D.C.

AASHTO, T. 308, 2010, "Standard Practice for Determining the Asphalt Binder Content of Hot Mix Asphalt by the Ignition Method," *American Association of State Highway Transportation Officials (AASHTO)*, Washington, D.C.

AASHTO, PP. 60, 2009, "Standard Practice for Preparation of Cylindrical Performance Test Specimens using the Superpave Gyratory Compactor (SGC)," *American Association of State Highway Transportation Officials (AASHTO)*, Washington, D.C.

AASHTO, PP. 61, 2009, "Standard Practice for Developing Dynamic Modulus Master Curves for Hot Mix Asphalt (HMA) using the Asphalt Mixture Performance Tester (AMPT)," *American Association of State Highway Transportation Officials (AASHTO)*, Washington, D.C.

AASHTO PP. 62, 2009, "Standard Practice for Developing Dynamic Modulus Master Curves for Hot Mix Asphalt (HMA)," *American Association of State Highway Transportation Officials (AASHTO)*, Washington, D.C.

AASHTO TP. 79 2009, "Standard Method of Test for Determining the Dynamic Modulus and Flow Number for Hot Mix Asphalt (HMA) using the Asphalt Mixture Performance Tester (AMPT)," *American Association of State Highway Transportation Officials (AASHTO)*, Washington, D.C.

AASHTO (1986). "Guide for Design of Pavements Structures," *American Association of State Highway and Transportation Officials (AASHTO)*, Washington, D.C.

Andrei, D., Witczak, M.W., and Mirza, M.W. (1999). "Development of a Revised Predictive Model for the Dynamic (Complex) Modulus of Asphalt Mixtures." NCHRP 1-37, An Interim Report, *National Cooperation Highway Research Program*, University of Maryland, College Park, MD.

ARA, Inc., ERES Consultants Division (2004). "Guide for Mechanistic–Empirical Design of New and Rehabilitated Pavement Structures." NCHRP 1-37A, Final Report, *Transportation Research Board of the National Academies*, Washington, D.C.

ASTM, D. 6752, 2009, "Standard Test Method for Bulk Specific Gravity and Density of Compacted Bituminous Mixtures using Automatic Vacuum Sealing Method," *American Society for Testing and Materials (ASTM)*, West Conshohocken, PA.

Bari, J. and Witczak, M.W. (2006). "Development of a New Revised Version of the Witczak E* Predictive Model for Hot Mix Asphalt Mixtures," *Journal of the Association of Asphalt Paving Technologists*, Vol. 75, pp. 381- 423.

Bonaquist, R. and Christensen, D.W. (2011). "Precision of the Dynamic Modulus and Flow Number Tests Conducted with the Asphalt Mixture Performance Tester," NCHRP 9-29, Report 702: *Transportation Research Board, National Research Council*, Washington, D.C.

Bonaquist, R. (2010). "Asphalt Mixture Performance Tester, Participant Workbook," Course No. 32, FHWA-NHI-131118, *Federal Highway National Highway Institute*, US Department of Transportation, Arlington, VA.

Ceylan, H., Kim, S., and Gopalakrishnan, K. (2007). "Hot Mix Asphalt Dynamic Modulus Prediction Models using Neural Network Approach." ANNIE 2007, *ANNs in Engineering Conference*, St. Louis, Missouri.

Chehab, G.R., O'Quinn E., Kim, Y.R. (2000). "Specimen Geometry Study for Direct Tension Test Based on Mechanical Tests and Air Void Variation in SGC-Compacted Asphalt Concrete Specimens." *Transportation Research Record*, 1723, pp. 125-132.

Chehab, G.R., Kim, Y.R., Schapery, R.A., Witczak, M.W., and Bonaquist, R. (2002). "Time–Temperature Superposition Principle for Asphalt Concrete with Growing Damage in Tension State." *Journal of the Association of Asphalt Paving Technologists*, Vol. 71, pp. 559–593.

Christensen, D.W., Jr. Pellinen, T., and Bonaquist, R.F. (2003). "Hirsch Model for Estimating the Modulus of Asphalt Concrete." *Journal of Association of Asphalt Paving Technologists*, Vol. 72, pp. 97-121.

Claussen, A. I. M., Edwards, J.M., Sommer, P., Ugé, P. (1977). "Asphalt Pavement Design - The Shell Method," *Proceedings of the 4th International Conference on the Structural Design of Asphalt Pavements*, Vol. 1 pp. 39-74.

Goodrich, J.L. (1991). "Asphaltic Binder Rheology, Asphalt Concrete Rheology and Asphalt Concrete Mix Properties," *Journal of the Association of Asphalt Paving Technologists,* Vol. 60. pp. 80-120.

Kaloush, K. E. and Witczak, M. W. (2000). "Development of a Permanent to Elastic Strain Ratio Model for Asphalt Mixtures." Inter-Team Technical Report for Development of the 2002 Guide for the Design of New and Rehabilitated Pavement Structures, NCHRP 1-37A, *ERES Consultants, Inc.*

Khazanovich, L.I., Yut, S.H., Turgeon, C., and Burnham, T. R. (2008). "Adaption of MEPDG for Design of Minnesota Low-Volume Portland Cement Concrete Pavements." *Journal of the Transportation Research Board*, Vol. 2087, pp. 57–67.

Kim, Y.R. and Lee, Y.C. (1995). "Interrelationships among Stiffnesses of Asphalt-Aggregate Mixtures." *Journal of the Association of Asphalt Paving Technologists*, Vol. 64, pp. 575-606

King, M., Momen, M. and Kim, Y.R. (2005) "Typical Dynamic Moduli Values of Hot Mix Asphalt in North Carolina and their Production." *84th Annual Meeting of Transportation Research Board, National Research Council*, Washington, D.C.

Leahy, R.B. (1989). "Permanent Deformation Characteristics of Asphalt Concrete," Ph.D. dissertation, University of Maryland, College Park, MD (USA).

Li, R. (2013). "Sensitivity Evaluation of the Mechanistic-Empirical Pavement Design Guide (MEPDG) for Flexible Pavement Performance Prediction." Ph.D. Dissertation, University of Maryland, College Park, Maryland.

NCHRP (1992). "Calibrated Mechanistic Structural Analysis Procedure for Pavements," NCHRP 1-26, Final Report, Phase 2. *National Cooperative Highway Research Program*, Washington, D.C.

Brown, S. F., Darter, M., Larson, G., Witczak, M., & El-Basyouny, M. M. (2006). "Independent Review of the" Mechanistic-Empirical Pavement Design Guide" and Software," *National Cooperative Highway Research Program (NCHRP) research results digest*, (307).

Park, S.W. and Schapery, R.A. (1997). "A Viscoelastic Constitutive Model for Particulate Composites with Growing Damage," *International Journal of Solids and Structures*, Vol. 34 (8), pp. 931–947.

Pellinen, T.K., and Witczak, M. W. (2002). "Stress Dependent Master Curve Construction for Dynamic (Complex) Modulus (with discussion)," *Journal of the Association of Asphalt Paving Technologists,* Vol. 71, pp. 281-309.

SHELL (1978). "Pavements and Overlays for Road Traffic," *Shell International Petroleum,* London.

Schapery, R.A. (1999). "Nonlinear Viscoelastic and Viscoplastic Constitutive Equations with Growing Damage," *International Journal of Fracture,* Vol. 97 (1-4), pp. 33–66.

Schwartz, C.W., Gibson, N., and Schapery, R.A. (2002). "Time– Temperature Superposition for Asphalt Concrete at Large Compressive Strains," *Journal of the Transportation Research Board*, Vol. 1789 (1), pp. 101–112.

Thyagarajan, S., Sivaneswaran, N., Muhunthan, B., & Petros, K. (2010). "Statistical Analysis of Critical Input Parameters in Mechanistic Empirical Pavement Design Guide," *Journal of the Association of Asphalt Paving Technologists*, Vol. 79, pp. 635- 662.

Tran, N.H. and Kevin D.H. (2005). "Evaluating the Predictive Equation in Determining Dynamic Moduli of Typical Asphalt Mixtures Used in Arkansas," *Electronic Journal of the Association of Asphalt Paving Technologists*, Vol. 74E.

Von Quintus, H.L., Mallea, J., Bonaquist, R., Schwartz, C. W., & Carvalho, R. L. (2011) "Calibration of Rutting Models for HMA Structural and Mixture Design," NCHRP report 719, NCHRP Project 9-30A, *National Cooperative Highway Research Program,* Washington, D.C.

Witczak, M. W., Kaloush, K., Pellinen, T., El-Basyouny, M., & Von Quintus, H. (2002), "Simple Performance Test for Superpave Mix Design," NCHRP 9-19, Report 465, *Transportation Research Board, National Cooperative Highway Research Program,* Washington, D.C.

Witczak, M.W. and Fonseca, O.A. (1996). "Revised Predictive Model for Dynamic Modulus of Asphalt Mixtures." *Journal of the Transportation Research Board,* Washington, D.C. Vol. 1540, pp 15-23.

Zhao, Y. and Kim, Y.R. (2003). "Time Temperature Superposition for Asphalt Mixtures with Growing Damage and Permanent Deformation in Compression," *Journal of the Transportation Research Board*, Vol. 1832 (1), pp. 161–172.

Zhao, Y., Liu, Hui., Liu, W. (2013). “Characterization of Linear Viscoelastic Properties of Asphalt Concrete Subjected to Confining Pressure,” Journal of Mechanics of Time Dependent Materials, Issue 3 (17), pp. 449-469.